AUG 8 1960

BULLETIN

OF THE

CHEMICAL SOCIETY OF JAPAN

Vol. 33 No. 6 June 1960

CONTENTS

General and Physical

M. Ōki and H. Iwamura: Intramolecular Interaction between Hydroxyl Group and π-Electrons. VIII. Energetics of the Interaction 717

Y. Kotera and K. Naraoka: Electrophotoluminescence of Zinc Sulfide Phosphors 721

Y. Kubokawa: An Interpretation of the Elovich Equation for the Rate of Chemisorption on the Basis of Surface Heterogeneity 734

Y. Kubokawa: Effect of Hydrogen and Carbon Monoxide on the Electrical Conductivity of Zinc Oxide 739

Y. Kubokawa. Effect of Oxygen Pretreatment on Hydrogen and Carbon Monoxide Chemisorption on Zinc Oxide 743

Y. Kubokawa: Hydrogen Chemisorption on $ZnO \cdot Cr_2O_3$, $ZnO \cdot MoO_3$ and Cr_2O_3 747

S. Ikeda and T. Isemura: Monolayers of Some Cyclic Peptides. Fungisporin and Gramicidin J_1. 753

S. Hasegawa and N. Nishimura: Studies on Organic Peroxides. V. Decomposition of Benzoyl Peroxide by Iron(II) 775

H. Yamada: Molecular Complexes between Ketones and Alkali Salts 780

Y. Iida and K. Shimada: Hydrogen Reduction of a Single Crystal of Nickel Oxide 790

K. Nakanishi: Partial Molal Volumes of Butyl Alcohols and of Related Compounds in Aqueous Solution 793

M. Takahasi: Pyrolysis of Organic Compounds. I. Kinetic Study of the Pyrolysis of Toluene . 801

M. Takahasi: Pyrolysis of Organic Compounds. II. Pyrolysis of Toluene-3-d and Toluene-4-d . 808

A. Wada: Dielectric Properties of Polypeptide Solutions. Measurement of the Dielectric Properties of the α-Helix by the Low Frequency Bridge Method 822

H. Hosoya, J. Tanaka and S. Nagakura: Ultraviolet Absorption Spectra of Aqueous Solutions and Single Crystals of Thioacetamide and Thiourea 850

Analytical and Inorganic

H. Nagai: Separation of Lanthanons by Paper Precipitation Chromatography with 8-Quinolinol. I. Separation and Detection of Lanthanum, Cerium and Praseodymium (Part 1) 715

S. Hikime: Spectrophotometric Determination of Tellurium(IV) by Extraction with Tributylphosphate. 761

H. Tsubota and Y. Kitano: A Rapid Method for Determining Fission Products Contained in Waters Using an Ion Exchanger 765

H. Tsubota and Y. Kitano: A Rapid Method for Determining Alkali and Alkaline Earth Elements Using an Ion Exchanger 770

(Continued on inside cover)

Published by the Chemical Society of Japan

THE CHEMICAL SOCIETY OF JAPAN
(NIPPON KAGAKUKAI)

Founded in 1948

Successor to the former Chemical Society of Japan founded in 1878 and to the Society of Chemical Industry, Japan founded in 1898.

OFFICERS

Shoichiro NAGAI, *President*, Nihon University, Tokyo
Eiichi IWASE, *Vice-President*, Institute of Physical and Chemical Research, Tokyo
Wasaburo KIMURA, *Vice-President*, Nagoya University
Sojiro OKA, *Vice-President*, The University of Tokyo
Ichiro SAKURADA, *Vice-President*, Kyoto University
Hiroshi SOBUE, *Vice-President*, The University of Tokyo

BULLETIN OF THE CHEMICAL SOCIETY OF JAPAN

Editor: Yoshiyuki URUSHIBARA, The University of Tokyo, Tokyo
Assistant Editor: Saburo NAGAKURA, The University of Tokyo, Tokyo
Editorial Board:

Toshio ANDO	Ichiro MIYAGAWA	Tadashi SUEHIRO
Yoshié BANSHO	Masazumi NAKAGAWA	Kenzi TAMARU
Hidehiro GOTÔ	Koji NAKANISHI	Takeo WATASE
Yoshimasa HIRATA	Shigeo OKUMURA	Iwao YASUMORI
Kenichi HONDA	Kazuo SAITO	Tsuneo YOSHINO
Sunao IMANISHI	Naoyasu SATA	Koshiro YOSHIOKA

(*Continued from outside cover*)

T. KIBA, S. OHASHI and T. MAEDA: Systematic Separation of Fission Products by Solvent Extraction Method 818

H. ONISHI, N. ISHIWATARI and H. NAGAI: Spectrophotometric Determination of Traces of Boron in Uranium 830

S. MISUMI and Y. IDE: Polarographic Studies on the Rare Earths. III. Yttrium. 836

M. MORI and R. TSUCHIYA: Thermodynamic Studies on Cobalt Complexes. V. On the Solubility and the Thermal Dissociation of Aquopentamminecobalt(III) Nitrate and Bromide, and on the Thermodynamic Stability of Monoacidopentamminecobalt(III) Complexes 841

J. HIDAKA, Y. SHIMURA and R. TSUCHIDA: Rotatory Dispersion of Metallic Co-ordination Compounds. II. Absorption Spectra and Rotatory Dispersion of Cobalt(III) Complexes of EDTA 847

Organic and Biological

S. ISHIDA: Polyethers. I. Stereospecific Polymerization of Epihalohydrins 727

S. ISHIDA: Polyethers. II. Copolymerizations of Propylene Oxide with Epihalohydrins 731

M. ŌKI and K. MUTAI: Intramolecular Interaction between N-H Group and π-Electrons in *N*-Benzylanilines 784

M. ABO: On the Hydrolysis Products of Abietic Acid-Maleic Anhydride Adduct 798

S. SAKAKIBARA: Studies on Dehydroalanine Derivatives. II. Synthesis of Polydehydroalanine. . 814

Short Communications

S. OOI, T. KAWASE, K. NAKATSU and H. KUROYA: The Crystal Structure of Tetra-thiourea-palladium(II) Chloride, $[Pd(SCN_2H_4)_4]Cl_2$. 861

T. MATSUMOTO and A. SUZUKI: The Structure and a Nobel Type Rearrangement of a Ketol Produced by the Robinson Annelation Reaction 862

M. OKUDA and T. TACHIBANA: The Existence of Acid Centers of Lewis Type on Silica-Alumina Surface 863

M. FUJIMOTO: Ein Beitrag zur Entwicklung der Harztüpfelmethode mittels Zentrifugierens der fein zerriebenen Ionenaustauscherteilchen 864

Separation of Lanthanons by Paper Precipitation Chromatography with 8-Quinolinol. I. Separation and Detection of Lanthanum, Cerium and Praseodymium (Part 1)

By Hideo NAGAI

(Received September 30, 1959)

The separation of lanthanons by paper chromatography and its analogous column method was studied by Lederer[1-4] and Pollard et al.[5,6], and the separation was effective to some extent. However, the separation of adjacent elements was very difficult, although a few elements have been separated. The difficulties were principally caused by considerable tailing and the close R_f values of the elements. On the other hand, precipitation chromatography with 8-quinolinol (oxine), which the author has studied[7-12], involved fundamentalf actors to reduce these difficulties. The procedure of precipitation chromatography is as follows. One drop of the test solution is applied at the center of a circular filter paper, previously impregnated with oxine, and developed with an adequate developing solvent. As the developing solvent penetrates into the filter paper, the oxine contained in the filter paper dissolves and reacts with the cations in the test solutions; the phenomenon can be compared with the dropwise addition of the precipitating agent to the test solution in the precipitation titration. Accordingly, from the analogous deduction of the precipitation titration, the cation which forms the most stable metal complex with oxine precipitates at the central part of the filter paper. By the precipitation the reaction product is removed from the reaction system. Therefore the reaction proceeds in such a way as to cause the predominant precipitation of the same kind of complex salt to continue, until the greater part of this cation was consumed. Then the deposition of the next stable complex salt in the test solution follows. Such a course of precipitation prevents the overlapping of the bands corresponding to each cation in the test solution.

In addition to the advantage described above, this chromatographic procedure scarcely ever causes any tailing. This phenomenon is probably due to the following reason: when the test solution is applied on the filter paper, nuclei of the precipitate of the cations are formed and grow smoothly during the entire development. On the other hand, the difficulties caused by the coprecipitation are encountered in this procedure, especially, when the lanthanons are treated. Accordingly, an improved procedure was devised so as to utilize the advantages of precipitation chromatography and to avoid as much as possible the coprecipitation of the elements.

Experimental

Apparatus.—The apparatus used for developing the chromatogram is illustrated in Fig. 1.

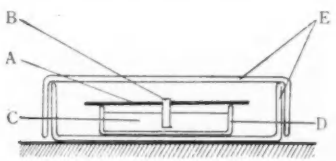

Fig. 1

A is a sheet of filter paper impregnated with oxine, which was prepared as follows. One hundred sheets of circular filter paper 9 cm. in diameter (Toyo filter paper No. 5B) were dipped in an ethanolic solution of oxine containing ca. 1g. oxine in 80 ml. of ethanol (95%). After about 10 min. the paper was taken out, and dried in the open air. When the paper was almost dry, it was placed in an electric drier and completely dried. After storage for a few days in a closed vessel, the paper was used for the experiment. B is a narrow strip of untreated filter paper, 1~1.5 mm. in width, inserted in a slit cut at the center of the oxine-treated filter paper where one drop of the test solution, saturated with isobutanol, had been spotted. C is the developing solvent. D is a small Petri dish (the container for the developing solvent). E is a large Petri dish (12~13 cm. in diameter).

Preparation of Test Solutions.—The available

1) M. Lederer, *Compt. rend.*, **236**, 1557 (1953).
2) M. Lederer, *Nature*, **176**, 462 (1955).
3) M. Lederer, *Anal. Chim. Acta*, **15**, 46 (1956).
4) M. Lederer, ibid., **15**, 122 (1956).
5) F. H. Pollard, J. F. W. McOmie and H. M. Stevens, *J. Chem. Soc.*, **1952**, 4730.
6) F. H. Pollard, J. F. W. McOmie and H. M. Stevens, ibid., **1954**, 3435.
7) H. Nagai, *J. Chem. Soc. Japan, Pure Chem. Sec.* (*Nippon Kagaku Zasshi*), **76**, 1246 (1955).
8) H. Nagai, ibid., **77**, 1267 (1956).
9) H. Nagai, ibid., **77**, 1794 (1956).
10) H. Nagai, ibid., **78**, 285 (1957).
11) H. Nagai, ibid., **78**, 840 (1957).
12) H. Nagai, ibid., **78**, 1334 (1957).

lanthanon material consisted of lanthanum oxide, praseodymium oxide, and cerous nitrate. Aqueous nitrate solutions were prepared by evaporating to dryness ca. 10 mg. of the required oxide or nitrate with a few drops of 2 N nitric acid, and dissolving the residue in water to produce the test solution containing ca. 10 mg. cation in 1 ml. solution. The following binary mixtures were prepared similarly: La–Ce, La–Pr and Ce–Pr.

Development. — Acetic acid-butanol system has been successfully used in a number of cases as the developing solvent for precipitation chromatography in the separation of many metallic cations, but it seemed to show insufficient separability in the case of lanthanons, though identification of each element in binary systems was possible with some difficulty. The lanthanum-cerium system developed with 0.5% acetic acid (by volume) saturated with isobutanol, and the cerium-praseodymium system developed with ca. 0.01% acetic acid and isobutanol (saturation) gave bare identification of the cations. In the separation of lanthanum and praseodymium, 0.01% acetic acid (saturated with isobutanol) was the most suitable solvent for the identification of praseodymium, while ca. 0.5% acetic acid (saturated with isobutanol) was the most suitable for the identification of lanthanum. The use of a solution more concentrated than 2% acetic acid (saturated with isobutanol) as the developing solvent caused irregular deformation of the chromatogram early in the development and then the bands of the chromatogram completely dissolved; thus the identification of the components of the test solution was scarcely ever possible.

Solution of *n*-butyric acid saturated with isobutanol showed far better results in the separation of lanthanons. Solutions of 0.005, 0.01, 0.05, 0.1, 0.5, 1, 2, 3, 5 and 10% *n*-butyric acid (by volume) saturated with isobutanol were used as developing solvent. The results were as follows. When the test solution was developed with 0.005 or 0.01% solution the innermost band was formed without leaving any blank space at the center of the chromatogram, and the bands showed practically no migration during the development. By the use of the solutions of 0.05 and 0.1% *n*-butyric acid, a blank area appeared at the central portion of the chromatogram, and, although the bands migrated a little on development, the results resembled the foregoing two cases. In the development with more than 1% *n*-butyric acid, the appearance of the bands resembled rather the chromatograms of the perfectly dissolved type than the precipitation chromatogram. When solutions of 1, 2 and 3% were used, the patterns of the chromatograms resembed one another, and the most desirable results were obtained generally in these cases (Fig. 2).

When 5% *n*-butyric acid (saturated with isobutanol) was used, the bands mixed together appreciably. And when 10% *n*-butyric acid (saturated with isobutanol) was used, the confusion of the bands became more marked, but the deformation of the chromatogram, which was observed at a higher concentration of acetic acid, was not observed in the *n*-butyric acid system.

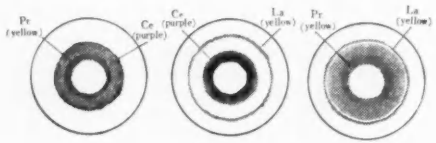

Fig. 2.

The temperature of the developing solvents was $20 \pm 1^{\circ}$C. After the development was finished, the chromatogram was subjected to reaction with ammonia vapor so as to stabilize the metal oxinates, and investigated under both visible and ultraviolet light.

Discussion

When the acetic acid system (saturated with isobutanol) was used as the developing solvent, cerium and praseodymium were identified most readily by the use of 0.01% acid. Since the R_f values of cerium and praseodymium hitherto reported have been the same, this can be regarded as an improvement, though their complete separation has met with little success. On the other hand, lanthanum-praseodymium and lanthanum-cerium whose R_f values were reported to be somewhat different from each other (but the real separation was very difficult owing to their considerable tailing), showed rather better separation at a higher concentration of acetic acid (ca. 0.5% acetic acid).

When the *n*-butyric acid system (saturated with isobutanol) was used as the developing solvent, the separation of cations was achieved at a higher concentration than in the case of the acetic acid system. Accordingly, the chromatogram appeared to be somewhat soluble rather than of complete precipitation but a distinct difference was observed from the perfectly dissolved chromatogram. It was far superior to that of the acetic acid system described above.

These phenomena might be explained as follows. Precipitation chromatography inherently possesses the characteristic of exaggerating the separation factor among the cations, but the coprecipitation is apt to compensate for the advantage of the precipitation chromatography, as the author pointed out at the beginning of this paper. One way to minimize the influence of coprecipitation was to increase the acidity of the developing solvent. When the acidity reached a concentration adequate to prevent coprecipitation and to maintain the ability to form complex salts, the best separability could be expected. Even if the complex salts thus formed do not precipitate completely, their diffusion (migration) velocities in the filter paper decrease so markedly by complex formation that they can not migrate together with the developing front where the reaction between the complexing agent and the cation is predominantly taking place. Accordingly, it would

be reasonable to say that the reaction product (the complex salt formed) was taken out of the reaction system as in the case of precipitation. Thus, the advantages of precipitation chromatography are still retained while its minor disadvantage, coprecipitation, is avoided.

The author wishes to thank Professor T. Sasaki, Tokyo Metropolitan University, Professor N. Saito, the University of Tokyo, Professor J. Yoshimura, Kyushu University, Professor R. Matuura, Kyushu University, Professor K. Ochiai, Kumamoto University, and Assistant Professor H. Kimizuka, Fukuoka Gakugei University, for their encouragement and numerous suggestions throughout the investigation. Also the author expresses hearty thanks to Professor S. Misumi for the gift of lanthanons. The cost of this research was defrayed from the Scientific Research Fund of the Ministry of Education.

Department of Chemistry
Faculty of Science
Kumamoto University
Kurokami-machi, Kumamoto

Intramolecular Interaction between Hydroxyl Group and π-Electrons. VIII[1]. *Energetics of the Interaction*

By Michinori Ōki and Hiizu Iwamura

(Received December 11, 1959)

Little is known of the energy of the intramolecular interation between the hydroxyl group and π-electrons in spite of many studies on this phenomenon in a number of compounds. In the first paper[2] of the present series, the authors reported briefly that the energies of the intramolecular interaction in 2-hydroxy-4- and -4′-nitrobiphenyls are 2.5 and 0.93 kcal./mol., respectively. Goldman and Crisler[3] suggested that the strengths of this kind of interaction in 2-phenylethanol and 2-(*p*-methoxyphenyl)-ethanol are 0.88 and 0.98 kcal./mol., respectively, assuming that Badger's postulation, that 70 cm^{-1} shift of the wave number of the hydroxyl stretching bands caused by the hydrogen bond formation corresponds to one kcal./mol. in the energy[4], is operative in this interaction. Necessity of elucidating the true nature of the interaction prompted the authors to examine the energy difference between the free and the interacting forms, since the results would be very useful for the discussion of the relation between band properties and the energy difference and consequently for the discussion of the nature. The present paper deals with some detailed procedures used in the measurement of the energies, which were omitted in the former short communication[2], and reports some data added recently in this laboratory. The materials include 2-allylphenol[1], 2-benzylphenol[1], 2-isopropenylphenol[5] and 2-hydroxybiphenyl[1]. The variation with the temperature of the infrared absorption spectra due to free and interacting hydroxyl groups was measured. These phenols were chosen out of many which possess the internal interaction by considering not only the fundamental structure representing each series, but also some technical advantages. The relative intensities of the free and the interacting O H stretching absorption bands (ν_{O-H}) at various temperatures can be measured most accurately when the intensities of the two bands are nearly equal. Otherwise, when the most favorable absorbance of one band is secured, the other will be either so weak that it may be affected by the noise of the recording system or so strong that it may exceed saturation. 2-Hydroxybiphenyl does not necessarily fulfill this requirement but the duplicate measurement under the best condition of the spectrometer gave reasonable data, although the probable error was fairly large in this case. To cover all the types of the intramolecular interaction, further combinations of the alcoholic hydroxyl group and the π-electrons of olefins and aromatic rings must be considered. The alcohol, however, as pointed out previously[6], shows rather complicated ν_{O-H} consisting

1) Part VII: This Bulletin, **33**, 681 (1960).
2) M. Ōki, H. Iwamura and Y. Urushibara, ibid., **31**, 770 (1958).
3) I. M. Goldman and R. O. Crisler, *J. Org. Chem.*, **23**, 751 (1958).
4) R. M. Badger, *J. Chem. Phys.*, **8**, 288 (1940).
5) M. Ōki and H. Iwamura, Presented at the Symposium on the Electronic State of Molecules, Tokyo, Sept. 8, 1959.
6) M. Ōki and H. Iwamura, **32**, 567 (1959).

of two free ν_{O-H}'s of rotational isomers and one interacting ν_{O-H} and thus obliges some discretion in dividing the apparent curve into absorptions due to free and interacting forms. This phenomenon caused the authors to give up the study of energy in the alcoholic series in the present work.

Experimental

Measurement.—A Perkin Elmer Model 112 G Double Pass High Precision Grating Infrared Spectrometer was used as previous[6], the spectral slit width being 1.0 cm^{-1} in this region. In a quartz absorption cell of 2 cm. length, having a window of 2.5 cm. diameter and protected with a heating coil covered with asbestos, about 20 ml. of the solution of the sample ($c \sim 0.001$ mol./l.) in carbon tetrachloride was placed, and the temperature was controlled by varying the current through the heating coil, kept at each equilibrated temperature within ± 0.2 °C and read by a thermometer dipped in the solution. The spectrometer being of a single beam type, a background trace was recorded every time immediately before the spectral measurement of the solution and the latter was always referred to the former, which also changed a little with the varying temperature.

Calculation.—Separation of the apparent curve and calculation of the integrated intensities of the two bands were made according to Ramsay's first method[6,7] for each of the absorption curves at different temperatures.

$$\text{Free form} \rightleftarrows \text{Interacting form}$$

Then the integrated form of the well-known van't Hoff equation (1) can be applied to obtain the energy difference between the two forms.

$$\ln K = -\frac{\Delta H}{RT} + \frac{\Delta S}{R} \qquad (1)$$

K can be given by

$$K = \frac{C_i}{C_f} = \frac{A_i/a_i}{A_f/a_f} = a\frac{A_i}{A_f} \qquad (2)$$

where a_i and a_f represent intensities per molecule with a free hydroxyl group and an interacting one, respectively, and A's integrated intensities. Combination of Eq. 1 with Eq. 2 gives

$$\ln \frac{A_i}{A_f} = \frac{-\Delta H}{RT} + \left(\frac{\Delta S}{R} - \ln a\right) \qquad (3)$$

The slope of the line obtained by taking $\ln(A_i/A_f)$ on the ordinate and $1/T$ on the abscissa gives the energy of the interaction ($-\Delta H$). Here it is assumed, that a_i and a_f, or at least their ratio a, should be independent of the temperature, since the temperature range is rather narrow (25~70 °C).

Materials.—Phenols used in the measurements are all known compounds and their physical constants were already reported previously[1,5].

Results and Discussion

Apparent absorption curves of 2-isopropenylphenol at various temperatures are shown in Fig. 1 and $\ln(A_i/A_f)$ and temperature relation in Fig. 2.

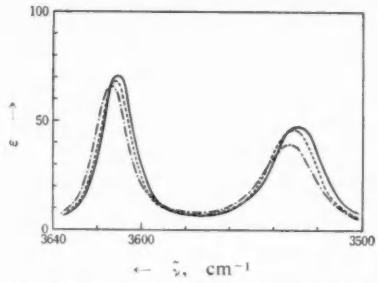

Fig. 1. ν_{O-H} absorptions of 2-isopropenylphenol at various temperatures.
28.1 °C —— 45.3 °C ------ 70.5 °C -·-·

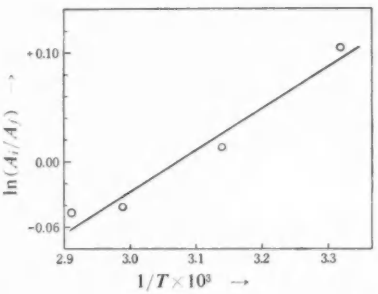

Fig. 2. Relation between $\ln(A_i/A_f)$ and temperature for 2-isopropenylphenol.

The effects of the temperature on the hydroxyl stretching frequencies and on the intensities are summarized in Tables I to IV.

There is always a slight but definite increase in absorption frequencies of both free and interacting ν_{O-H}, accompanied by a decrease in the total integrated intensities ($A_i + A_f$). These effects might be attributed to the rupture of the remaining hydrogen bonding, but, in concentration employed here ($c \sim 0.001$ mol./l.), the possibility of the bonding of two phenol molecules can be neglected with certainty. Liddel and Becker[8] already observed an appreciable decrease in the peak intensity and a slight increase in frequency (ca. 6 cm^{-1}) of the free ν_{O-H} of methanol in carbon tetrachloride in the temperature range between −10 and 50 °C, and suggested that these variations might be considered to be owing to a weak hydrogen bonding to the solvent. This possibility is apparently reasonable because this type of interaction may be very weak and the observed shift of the frequencies is only small, besides it can be ruptured easily with the rising temperature. Tables I to IV show, however, that

7) D. A. Ramsay, *J. Am. Chem. Soc.*, **74**, 72 (1952).

8) U. Liddel and E. D. Becker, *J. Chem. Phys.*, **25**, 173 (1956).

Table I. The effect of the temperature on ν_{O-H}'s of 2-allylphenol

Temperature $1/T\times10^3$(°K^{-1})	ν_{max} (cm^{-1})	$\Delta\nu^a_{1/2}$ (cm^{-1})	$A\times10^{-3}$ (mol^{-1}·l.·cm^{-2})	A_i/A_f	$\Delta\nu_{max}$ (cm^{-1})
3.31	3612.2	17.0	6.66	1.30	65.2
	3547.0	62.3	8.72		
3.14	3613.2	17.4	6.58	1.30	64.6
	3548.6	62.8	8.55		
3.03	3614.1	17.6	6.52	1.23	62.4
	3551.7	64.2	8.04		
2.92	3614.9	18.0	6.23	1.20	58.8
	3556.1	65.8	7.46		

Table II. The effect of the temperature on ν_{O-H}'s of 2-benzylphenol

Temperature $1/T\times10^3$(°K^{-1})	ν_{max} (cm^{-1})	$\Delta\nu^a_{1/2}$ (cm^{-1})	$A\times10^{-3}$ (mol^{-1}·l.·cm^{-2})	A_i/A_f	$\Delta\nu_{max}$ (cm^{-1})
3.31	3611.1	17.2	8.48	1.02	50.5
	3560.6	60.8	8.67		
3.14	3612.0	17.8	8.53	0.99	50.2
	3561.8	59.2	8.44		
3.04	3612.6	17.8	8.07	0.98	46.8
	3565.8	60.8	7.90		
2.91	3613.4	18.4	7.90	0.96	46.5
	3566.9	61.8	7.55		

Table III. The effect of the temperature on ν_{O-H}'s of 2-isopropenylphenol

Temperature $1/T\times10^3$(°K^{-1})	ν_{max} (cm^{-1})	$\Delta\nu^a_{1/2}$ (cm^{-1})	$A\times10^{-3}$ (mol^{-1}·l.·cm^{-2})	A_i/A_f	$\Delta\nu_{max}$ (cm^{-1})
3.32	3611.0	16.7	4.19	1.11	81.6
	3529.4	26.5	4.59		
3.14	3612.0	16.8	4.08	1.01	80.1
	3531.9	26.0	4.28		
2.99	3612.8	16.8	3.99	0.96	80.4
	3532.4	25.8	3.83		
2.91	3613.8	17.0	3.92	0.96	80.3
	3533.5	25.6	3.75		

Table IV. The effect of the temperature on ν_{O-H}'s of 2-hydroxybiphenyl

Temperature $1/T\times10^3$(°K^{-1})	ν_{max} (cm^{-1})	$\Delta\nu^a_{1/2}$ (cm^{-1})	$A\times10^{-3}$ (mol^{-1}·l.·cm^{-2})	A_i/A_f	$\Delta\nu_{max}$ (cm^{-1})
3.30	3606.9	15.5	1.39	9.44	42.0
	3564.9	15.0	13.11		
3.19	3607.3	15.8	1.48	8.77	42.0
	3565.3	15.2	12.99		
3.08	3607.7	16.0	1.63	7.72	41.8
	3565.9	15.2	12.57		
3.01	3607.9	16.2	1.59	8.10	41.6
	3566.3	15.6	12.84		
2.90	3608.3	17.0	1.80	6.92	41.5
	3566.8	15.8	12.48		

Table V

Phenols	$-\Delta H$ (kcal./mol.)	$\Delta S/R-\ln a$	$\Delta\nu_{max}$(cm^{-1})
2-Allylphenol	0.46±0.14	−0.49±0.22	65.5
2-Benzylphenol	0.33±0.05	−0.53±0.10	50.8
2-Isopropenylphenol	0.76±0.11	−1.17±0.20	82.0
2-Hydroxybiphenyl	1.45±0.27	−0.17±0.42	42.0

the frequencies of the internally interacting ν_{O-H} which has no available proton any longer also rise in the same way with the temperature and this fact may be explained from lessening of the dipole-dipole interaction between phenols and solvent molecules by their thermal motion, to which Cole and Macritchie[9] have recently alluded. About a half of the decrease in the total intensity can be attributed to the thermal expansion of the solvent, the volume expansion coefficient of carbon tetrachloride being 1.236×10^{-3}.

In Table V are listed the energies of the interaction ($-\Delta H$), together with constant $\Delta S/R - \ln a$, obtained by applying Eq. 3 to the above data in Tables I to IV. The shifts (for the room temperature) of the ν_{O-H} absorption maxima of the interacting form from that of the free one are listed in the last column for comparison of the shifts with the energy.

$-\Delta H$'s are all smaller than the weakest one of the ordinary hydrogen bonding which ranges from 2.3 (NH···N) to 7 (FH···F) kcal./mol.[10] Even the strongest interaction of this kind ever measured, 2.5 kcal./mol. for 2-hydroxy-4-nitrobiphenyl[2], lies at the lowest limit of the energy for the hydrogen bonding. This difference in energy may be the best criterion which differentiates this interaction from the ordinary hydrogen bonding. It seems that at least no simple relation exists between $\Delta\nu_{max}$ and $-\Delta H$. The rotational degree of freedom must be taken into account. In 2-allylphenol, 2-benzylphenol and 2-isopropenylphenol, a loss of energy may be caused by the formation of the internal interaction, because the molecule must take a structure, which is otherwise the sterically unfavored one. The apparent $-\Delta H$, therefore, does not necessarily mean the true energy difference of the interaction. These considerations lead to the reasonable explanation of the arbitrary relation between $\Delta\nu_{max}$ and the energy difference. Some relation may be expected between $\Delta\nu_{max}$ and $-\Delta H$ if the compounds are limited to a certain series, but, it is still clear that the relation is not so simple as a linear one, as is understood from the three compounds in the biphenyl series. Hence, it is dangerous to evaluate the energy of the interaction from the mere comparison of the two frequencies.

Although, for strict understanding of the entropy changes of the interaction (ΔS), another standard band common in frequency and in molecular absorption coefficient to both molecular types must be further used together with these two ν_{O-H}'s, as shown by Mizushima and his collaborators[11], constant $\Delta S/R - \ln a$ obtained by extrapolating T to infinity in the Eq. 3 can be assumed to be a measure of the entropy change, since roughly speaking it can be assumed that constant a in Eq. 2 is equal to unity, when $\ln a$ becomes zero. This assumption is partly supported by the speculation that the changes of the dipole moment accompanying the vibrational motion are much smaller, than in the case of the ordinary hydrogen bonding, and partly by the observation, that the total integrated intensities ($A_i + A_f$) in these phenols possessing different degrees of interaction are about equal to 1.5×10^4 except that of 2-isopropenylphenol which is rather sterically hindered. Entropy changes accompanying the intramolecular interaction consist of those of the vibrational motion and of the internal rotation, each being estimated to be a few entropy units, when they are perfectly restricted[11,12]. With weak intramolecular interaction between the hydroxyl group and π-electrons this effect is expected to be less and it is the case in three of the phenols presented above. On the contrary, 2-isopropenylphenol shows an extraordinary great entropy term which can not be explained from the above factors only. It can be well explained by assuming that this phenol exists in four rather stable conformations near coplanarity, and only one of them can be the molecular form favorable for the interaction. Then the ratio of the number of the conformation, 1/3, must be introduced into the entropy term in the form of ln 3 and subtraction of the latter from the former gives a reasonable value (-0.07) comparable to the other phenols. Almost equal $\Delta S/R - \ln a$ values in 2-allylphenol and 2-benzylphenol can be understood by considering that the interaction in both cases will occur with the π-electron at the "β" carbon atom in respect of the phenol nucleus as already suggested in the previous paper[1]. The small $\Delta S/R - \ln a$ value in 2-hydroxybiphenyl is rather unexpected. One of the most interesting internal motions in this molecule is that of rotation and/or vibration around the pivot bond. This will give rise to an appreciable entropy decrease if perfectly restricted. The observed small amount of the entropy term shows that the contribution of this effect is very small, and the moderate changes in the O-H force constants between free and interacting forms can be accomodated with almost no entropy changes.

The authors wish to express their hearty thanks to Professor Y. Urushibara and Professor

9) A. R. H. Cole and F. Macritchie, *Spectrochim. Acta*, **1959**, 6.
10) C. A. Coulson, *Research*, **10**, 149 (1957).
11) S. Mizushima, T. Shimanouchi, K. Kuratani and T. Miyazawa, *J. Am. Chem. Soc.*, **74**, 1378 (1952).
12) H. H. Jaffé, ibid., **79**, 2373 (1957).

T. Shimanouchi for their valuable suggestions and discussions. The authors are also indebted to the Ministry of Education for the Grant in Aid for Fundamental Scientific Research.

Department of Chemistry
Faculty of Science
The University of Tokyo
Hongo, Tokyo

Electrophotoluminescence of Zinc Sulfide Phosphors

By Yoshihide KOTERA and Kiyotaka NARAOKA

(Received October 13, 1959)

Various effects of electric fields on the light emission of zinc sulfide phosphors during or after excitation by ultraviolet or X-rays have been investigated by a number of authors[1-4]. The effects include a quenching or an enhancement of the luminescence under the electric field, a momentary stimulation of luminescence at application or removal of the electric field, and other miscellaneous effects.

If the observations on various phosphors, each having different kinds of activators or different chemical compositions of matrix, for example, hex.-ZnS:Cu, cub.-ZnS:Mn, (Zn, Cd)S:Ag and ZnS:Cu, Pb are carried out under the same conditions, then each phosphor has different influences. The purpose of this paper is to find how the influence of an alternating electric field on luminescence varies with the kinds of activator or chemical composition of the matrix.

Destriau[2] made extensive investigations of these effects, and he reported that it seems that the sulfides with a persistent phosphorescence are very sensitive to momentary stimulation and insensitive to the quenching effect, while the sulfides with brief phosphorescence show an appreciable quenching effect and a slight or even insignificant momentary stimulation. However, he[5] noted that although thermoluminescence and infrared stimulation can occur after the action of the field, application of the field after thermoluminescence or infrared stimulation, on the other hand, does not produce any emission. From this observation, it might be concluded that the electric field acts only on shallow traps but not on deep traps, but he thought that this conclusion is uncertain, because the field obviously has a directional character, whereas temperature or infrared radiation has not.

Matossi[4] has studied the electrophotoluminescence of various zinc sulfide phosphors, but he could not find any systematic dependence of the characteristics of stimulation or quenching on the method of preparation (kind of activator or flux) or on other luminescence properties, such as the time of afterglow.

It is explained by several authors that the momentary field stimulation might be caused by electron traps, from which the electron is released by electric field and returns to luminescent centers to cause emission. Further, phosphorescence, infrared stimulation and thermoluminescence are explained by the action of electron traps. Therefore it is expected that there might be a close relation between momentary stimulation and those characteristics. From this standpoint, we are going to discuss the relations between momentary field stimulation and phosphorescence, infrared stimulation, or thermoluminescence, respectively.

Experimental

The phosphors were synthesized from the pure zinc sulfide by adding appropriate aqueous solution of activator and two weight percent sodium chloride. The mixtures were stirred well, dried, transferred to a silica crucible and fired for crystallization from 750 to 1200°C in a temperature-controlled furnace in air for half an hour. After crystallization, the preparations were washed free of water-soluble chloride and were dried. The composition of phosphors and the condition of firing are shown in columns 2 and 3 of Table I.

All phosphors were embedded in Acrylite (Polymethylmethacrylate, produced by Mitsubishi Rayon Co.) and investigated in cells of the common construction of the electroluminescent cell with about 10 cm^2 area and about 0.5 mm. thickness of the layer. The phosphor-dielectrics layer was held between two electrodes, one of which was conductive glass coated with tin oxide layer, and the other was aluminum

1) G. Destriau, *Phil. Mag.*, **38**, 784 (1947).
2) G. Destriau, ibid., **38**, 880 (1947).
3) I. T. Steinberger, W. Low and E. Alexander, *Phys. Rev.*, **99**, 1219 (1955).
4) F. Matossi, *J. Electrochem. Soc.*, **103**, 122 (1956).
5) G. Destriau and H. F. Ivey, *Proceeding of the IRE*, **43**, 1911 (1955).

TABLE I. THE COMPOSITION OF PHOSPHORS AND THEIR LUMINESCENT CHARACTERISTICS

No.	Composition	Firing temp. °C	concn. of act. mol./1 mol. ZnS	P. L.	Phospho.	I. R. S.	M. F. S.	F. Q.	Notes
1	ZnS : Ag	1000	10^{-5}	b	S			+	
2	〃	1150	10^{-5}	〃	〃			+	
3	〃	〃	10^{-4}	〃	〃			+	
4	〃	〃	10^{-3}	〃	〃			+	
5	$(Zn_{0.80}, Cd_{0.20})S$: Ag	950	10^{-4}	g	〃			+	
6	$(Zn_{0.50}, Cd_{0.50})S$: Ag	〃	〃	y	〃			+	
7	$(Zn_{0.20}, Cd_{0.80})S$: Ag	〃	〃	r	〃			−	
8	$(Zn_{0.63}, Cd_{0.37})S$: Ag	1150	10^{-5}	g	L		+	+	
9	〃	〃	10^{-4}	〃	〃		+	+	
10	〃	〃	10^{-3}	〃	S			+	
11	(Zn, Cd)S : Ag	—	—	y	〃			+	(a)
12	ZnS : Zn	900	—	b	〃			+	
13	ZnS : Cu	〃	10^{-6}	g. b.	〃		+	+	
14	〃	〃	3×10^{-6}	g	〃		++	+	
15	〃	〃	10^{-5}	〃	M		++	+	
16	〃	〃	3×10^{-5}	〃	〃		++	+	
17	〃	〃	10^{-4}	〃	〃		+	+	
18	〃	〃	3×10^{-4}	〃	S			+	
19	〃	〃	10^{-3}	〃	〃			+	
20	〃	1000	10^{-5}	〃	M		++	+	(b)
21	〃	〃	10^{-4}	〃	S		+	+	(〃)
22	〃	〃	10^{-3}	〃	〃			+	(〃)
23	〃	1200	3×10^{-6}	〃	L			+	
24	〃	〃	10^{-5}	〃	V. L	+	+	−	
25	〃	〃	3×10^{-5}	〃	〃	+	+	−	
26	〃	〃	10^{-4}	〃	L			+	
27	〃	〃	3×10^{-4}	〃	〃			+	
28	〃	〃	10^{-3}	〃	S			+	
29	〃	—	—	〃	V. L			−	(c)
30	$(Zn_{0.80}, Cd_{0.20})S$: Cu	1050	10^{-4}	y	L			+	
31	$(Zn_{0.50}, Cd_{0.50})S$: Cu	〃	〃	r	S			−	
32	Zn(S, Se) : Cu	780	10^{-4}	y	〃			−	
33	ZnS : Cu, Fe	1200		g	〃			+	
34	ZnS : Cu, Pb	1150		〃	L	++		−	(d)
35	〃	—	—	〃	M		+	−	(e)
36	ZnS : Pb	900	—	〃	〃	+	+	+	
37	〃	1200	—	〃	L	+		−	
38	ZnS : Pb, Mn	1150		y	〃	+		−	
39	ZnS : Mn	1000	10^{-2}	o	S	+		−	
40	〃		〃	〃	〃		+	−	(f)
41	〃	1200	〃	〃	〃	+		−	
42	ZnS, ZnO : Mn	1000	〃	〃	〃		+	−	
43	$(Zn_{0.80}, Cd_{0.20})S$: Mn	〃	〃	〃	〃	+		+	
44	〃	〃	〃	〃	〃			+	(f)

(a) A commercial product for X-ray.
(b) Fired in nitrogen stream.
(c) A commercial product for phosphorescent paint.
(d) Fonda's phosphor.
(e) Electroluminescent phosphor.
(f) No flux.

TABLE I (continued)

P. L. :	Color of photoluminescence b=blue, g=green, y=yellow, r=red, g. b=greenish blue, o=orange.
Phospho. :	Phosphorescence S=short persistence, M=medium, L=long, V. L=very long.
I. R. S. :	Infrared stimulation +=weak i.r.s., ++=strong i.r.s.
M. F. S. :	Momentary field stimulation (the Gudden-Pohl effect) +=considerable m.f.s., ++=strong m.f.s.
F. Q. :	Quenching of luminescence by electric field application during excitation −=none or slight, +=considerable field quenching.

plate. A d-c operated black light lamp with a Corning glass filter 5840 transmitting from 3100 to 4200 Å served as the exciting ultraviolet source. The light emitted by phosphor was allowed to fall upon the cathode of the 1P21 photomultiplier, the anode current from the photomultiplier being measured by means of d-c amplifier and cathode ray oscillograph, and the oscillogram of transient phenomenon for emission at electric field application or removal was observed.

The applied electric field was obtained from 50 c. p. s a-c line, and field intensity was estimated to be about 10000 volts per centimeter. With this field intensity electroluminescence was not detected with the exception of zinc sulfide phosphors which contain 10^{-3} mol. or more of copper per 1 mol. ZnS.

Experimental Results and Discussion

On application of the alternating electric field during continuous ultraviolet excitation, the average brightness of luminescence increases for a moment. After these transitory phenomena the average brightness reaches a new equilibrium level, lower than the luminescent level before application of the filed. Some phosphors show no steady state quenching. The transient variation of emission is shown schematically as a function of time in Fig. 1. The field quenching lasts as long as the field is applied, and recovers gradually, then reaches a steady level.

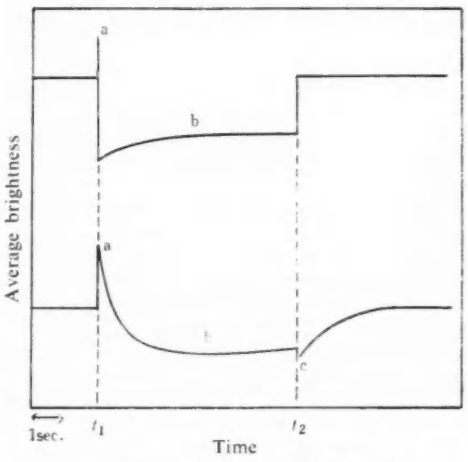

Fig. 1. Average brightness of luminescence when electric field is applied or removed.
t_1···field application, t_2···field removal,
a···momentary stimulation,
b···field quenching, c···cut-off dip.

The stimulated and quenched brightness were modulated by applied alternating electric field. A frequency of brightness wave was that of applied alternating field or twice this frequency. The modulated frequency for pure zinc sulfide phosphors was 100 c.p.s., while that of zinc-cadmium sulfide phosphors which contained 20 mol. percent cadmium sulfide or more was 50 c.p.s.. Fig. 2 shows the oscillogram of modulated wave for ZnS and (Zn, Cd)S phosphors. The (Zn, Cd)S phosphors which contain below 20 mol. percent cadmium sulfide was not studied.

When the electric field was removed, then the phosphors such as ZnS : Cu, Fe, (Zn, Cd)S : Ag (No. 11), and Zn(S, Se) : Cu (No. 32) had a short flash, while the phosphors such as ZnS : Cu and (Zn, Cd)S : Cu had a dip of brightness. On the other hand, the phosphors such as the many ZnS : Ag and (Zn, Cd)S : Ag phosphors recovered directly without flash or dip. The cut-off stimulation was found by Matossi for almost all phosphors to consist of two components, a very sharp peak and a tail of long duration. We found this cut-off

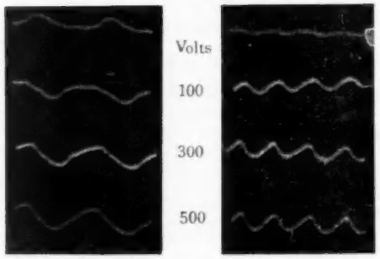

Fig. 2. Oscillogram of quenching brightness wave during 1/25 second at various voltage. The patterns of 'a' show quenching brightness waves of (Zn, Cd)S : Ag, and they are modulated to 50 c.p.s. The patterns of 'b' show the waves of ZnS : Cu, modulated to 100 c.p.s.

Fig. 3. Oscillogram of brightness at field application and removal. The luminescence of ultraviolet excited phosphors are affected by alternating electric field in following order, 1; steady luminescence, 2; field stimulation during excitation (the Gudden-Pohl effect), 3; field quenching during excitation, 4; cut-off stimulation or dip, 5; recovery.

stimulation only for ZnS : Cu, Fe, while (Zn, Cd)S : Ag (No. 11) and Zn(S, Se) : Cu (No. 32) showed a different kind of cut-off stimulation from Matossi's, and had no sharp peak, but the emission increased gradually with time, reaching a maximum at about one second after removal of the electric field, then decreased slowly to initial brightness. The increased emission at field removal was observed by the naked eye for the (Zn, Cd)S : Ag (No. 11). Their characteristics are shown in Fig. 3b. In Fig. 3 various typical brightness curves of luminescence which are influenced by the electric field are shown. In these figures the coordinate is brightness and the abscissa is time. Steady emission before the application of the electric field, momentary stimulation, field quenching, cut-off stimulation, and recovery are shown from left to right. During this period the phosphor was illuminated continuously by ultraviolet light.

The intensity of first stimulation depends on exciting ultraviolet intensity, the time interval between repeated field applications after first application and so on. The stimulated emission increased with the intensity of excitation and the time interval, and showed saturation. Fig. 4 shows stimulated emission as a function of the time interval at various exciting intensities.

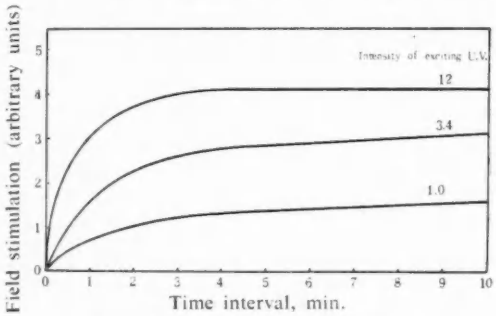

Fig. 4. Momentary field stimulation during excitation as a function of excited time interval at various intensity of ultraviolet. Phosphor ZnS : Cu (No. 17).

The time of application was about 10 sec. and in that time the momentary stimulation was over.

For the Gudden-Pohl effect after removal of the ultraviolet radiation the form of brightness pulse and dependence on kinds of activator and chemical composition of phosphors are similar to the first momentary stimulation during excitation.

The behavior under electric field, phosphorescence and infrared stimulation are shown in Table I. From this table, it is possible to compare the influence of electric field on the different phosphors. This is summarized as follows:

1. Many of the ZnS : Ag and (Zn, Cd)S : Ag phosphors with short persistent afterglow show appreciable field quenching during excitation, estimated to be 40% at a field intensity

of 10000 volts per cm., and have slight momentary stimulation. (Zn, Cd)S : Ag phosphors with longer afterglow show large momentary stimulation, but the quenching ratio does not decrease.

2. ZnS : Mn and (Zn, Cd)S : Mn which show considerable infrared stimulation have no field quenching, while ZnS : Mn which incorporates ZnO and also shows short afterglow and no infrared stimulation has a momentary stimulation whose duration is very short.

3. Cub.-ZnS : Pb with a short persistent phosphorescence and some infrared stimulation shows a strong field stimulation and a small field quenching, while hex.-ZnS : Pb with a long persistence and a strong infrared stimulation shows feeble field stimulation and no field quenching. ZnS : Cu, Pb (Fonda's phosphor) has a most remarkable infrared stimulation but shows feeble field stimulation and no field quenching.

4. The field sensitivity of ZnS : Cu and ZnS : Ag phosphors decreases by substitution of a large amount of cadmium for zinc, for example, $(Zn_{0.20}, Cd_{0.80})S : Ag$ (red) and $(Zn_{0.50}, Cd_{0.50})S : Cu$ (red) have no field stimulation and also no field quenching. But zinc-cadmium sulfide phosphors with medium substitution of cadmium for zinc still have considerable field sensitivity.

5. The influence on ZnS : Cu phosphors is very complicated. The zinc sulfide fired at 1020°C or higher is expected to have hexagonal structure, while sulfide fired below 1020°C is expected to have cubic structure. In this observation, the sulfide was fired at 1200°C for the hexagonal phosphor, and at 900°C for the cubic.

Their phosphorescence, infrared stimulation, and momentary stimulation during decay at field application are shown in Fig. 5 as a function of copper concentration. In this figure, the phosphorescence is plotted as an afterglow intensity after a lapse of one minute from removal of ultraviolet excitation, and the infrared stimulation as an initial flash-up intensity under infrared illumination also after one minute's decay, and the integral of light flash at field application (the area under the curve obtained in Fig. 6, in which the abscissa is time and the ordinate is the photocurrent from the photomultiplier) was taken as the measure of the Gudden-Pohl effect.

In hex.-ZnS : Cu, the phosphorescence is found to be increased by increasing the copper content and to reach a maximum at copper content of 3×10^{-5} mol. per one mol. of ZnS, and Gudden-Pohl stimulation is also increased by increasing the copper content and reaches a maximum at a copper content of 10^{-5} mol.

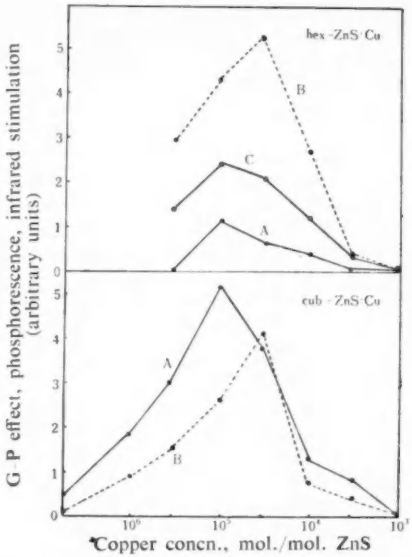

Fig. 5. The Gudden-Pohl effect during decay, phosphorescence and infrared stimulation as a function of copper concentration in hex. and cub. zinc sulfide phosphors.
A. The Gudden-Pohl effect,
B. phosphorescence, C. infrared stimulation.

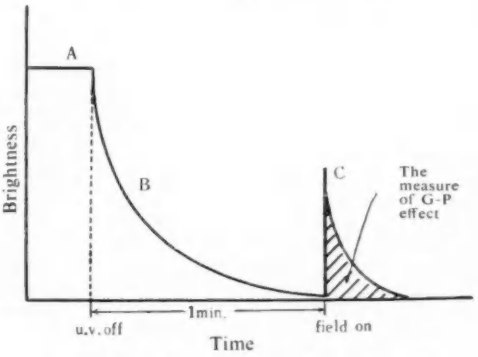

Fig. 6. The Gudden-Pohl effect (C) after removal of ultraviolet excitation.
A : steady state luminescence, B : decay.

The zinc sulfide with 3×10^{-5} mol. copper has a very long persistent phosphorescence and the strongest infrared stimulation among the zinc sulfide phosphors activated with copper, but it shows weak field stimulation. Independent of the copper content the momentary field stimulation of hex.-ZnS : Cu is weaker than that of cub.-ZnS : Cu. The field stimulation of cub.-ZnS : Cu phosphors as a function of copper concentration is similar to that of hexagonal phosphors, but infrared stimulation is so feeble

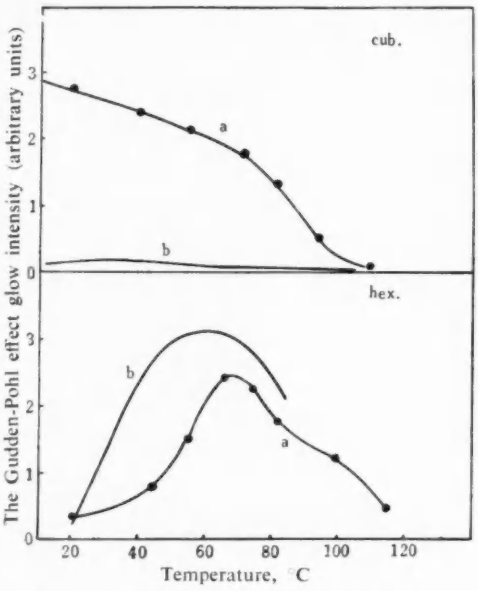

Fig. 7. The Gudden-Pohl stimulation as a function of temperature and glow curve. a: the Gudden-Pohl effect, b: glow intensity. Sample, cub.···ZnS:Cu(No. 16), hex.···ZnS:Cu (No. 24).

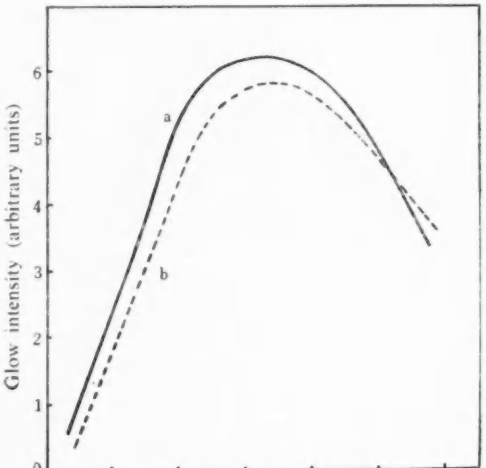

Fig. 8. Glow curves depending upon whether an electric field has been previously applied or not. Sample ZnS:Cu (No. 24).
a: previously applied, b: not applied.

that it can not be detected. The Gudden-Pohl effect of cub.-ZnS:Cu with a suitable amount of copper is strong and shows relatively long duration, and it takes about one second to fall from flash-up to quenching level, and also several seconds to recover to initial brightness.

The intensity and decay of the flash by the electric field depend on temperature, that is, at higher temperature momentary stimulation at field application is sharper and its decay is more rapid. In Fig. 7 field stimulation is plotted as a function of temperature, and glow curves of phosphors which were excited and caused to decay at room temperature are shown in the same figure. The heating rate of glow curves was 0.2°C per second. In cub.-ZnS:Cu, the higher the temperature is, the smaller is the field stimulation between 20° and 120°C, and there is no peak in this temperature range. The momentary stimulation of hex.-ZnS:Cu increases with temperature reaching a maximum at 70°C, while the glow curve has a peak at 55°C.

Some knowledge of traps has been obtained from glow curve measurements by Bube[6]. He proposed that a large number of traps are present in self-activated ZnS phosphors with no added copper impurity. The incorporation of copper up to 1.7×10^{-4} mol. (0.01%) causes the appearance of traps which are deeper than those present before the addition of copper. Incorporation of copper in amounts of more than 1.7×10^{-4} mol. causes disappearance of the deep traps due to copper.

Comparing our experimental results with the knowledge about traps, it could be considered that there is a maximum of momentary stimulation as a function of copper concentration at 10^{-5} mol. copper content and the number of deeper traps has a maximum value at 1.7×10^{-4} mol. copper content, that is, two maxima are uncoincident. So the deeper traps might not be contributing to the momentary stimulation.

Two glow curves of hex.-ZnS:Cu (24) depending upon whether or not the electric field has been previously are shown in Fig. 8. The application of the field was done after removal of excitation, and the time of application was ten seconds. A similar experiment was carried out by Destriau[5]. In our observation, it can be seen that the maxima of two glow curves have about the same height. From this observation, we might assume that the deeper trap which corresponds to the glow peak at 55°C does not contribute to momentary stimulation at room temperature. Rather the increase of momentary stimulation at higher temperature may be ascribed to the effect of emptying the deeper

6) R. H. Bube, *Phys. Rev.*, **80**, 655 (1950).

traps which can release their electron thermally at higher temperature.

Summary

The effects of the electric field on the luminescence of ultra-violet excited zinc sulfide phosphors are shown as a function of kinds of activator and chemical composition of matrix. All phosphors were measured in an electroluminescent cell of common construction. The electric field was obtained from 50 c.p.s. alternating line. The Gudden-Pohl effect of both hexagonal and cubic ZnS:Cu increased with increasing copper content and reached a maximum at a content of 10^{-5} mol. The effect of cubic ZnS:Cu (10^{-5}) is the strongest in the zinc sulfide phosphors at room temperature. Cubic sulfide phosphors activated by copper are sensitive to both momentary stimulation and field quenching.

Further, a relation between electron traps and the Gudden-Pohl effect was studied. From the temperature dependence of the Gudden-Pohl effect and glow curves, it might be assumed that the deeper trap which corresponds to a glow peak at 55°C does not produce the Gudden-Pohl effect at room temperature, rather the increase of the effect at higher temperature may be ascribed to the emptying of the deeper traps which can release their electrons thermally at higher temperature.

Government Chemical Industrial Research Institute
Hatagaya, Tokyo

Polyethers. I. Stereospecific Polymerization of Epihalohydrins†

By Shin'ichi ISHIDA*

(Received October 3, 1959)

Recenctly a number of publications have appeared which describe the polymerization of propylene oxide with different catalysts to give a product which contains crystalline polypropyleneoxide[1-5]. On the contrary, there has been no publication on stereospecific polymerization of epihalohydrins. In the earlier work[6] or epihalohydrin, using Friedel-Crafts catalysts such as stannic chloride, it was reported to produce only viscous liquid or pasty resins of low molecular weight.

In the present paper, the author wishes to report on the synthesis of crystalline polymers of epichlorohydrin and epifluorohydrin.

The attempted stereospecific polymerization of epiiodohydrin was unsuccessful.

Experimentals

Epichlorohydrin and Propylene Oxide.—Commercial materials were dried over a molecular sieve and fractionally distilled before use.

Epifluorohydrin.—It was prepared from epichlorohydrin and anhydrous potassium fluoride by Gryszkiewicz-Trochimowsky's method[7]. The yield was lower than that reported; only 7 g. of the product boiling at 85~86°C was obtained from 100 g. of epichlorohydrin and 100 g. of anhydrous potassium fluoride.

Epiiodohydrin.—It was prepared according to the direction given by E. Wedekind.[8] Epichlorohydrin (48.5 g.) was mixed with a solution of dry sodium iodide (78.5 g.) in acetone (530 ml.) and this mixture was refluxed for 30 hr. The yield of the product boiling at 62°C (24 mmHg) was 40% (37 g.). n_D^{20} 1.5418.

Ferric Chloride Complex Catalyst.—A complex of ferric chloride with propyleneoxide was prepared immediately before use according to the procedure of Price[1]. Analogous complexes of ferric chloride with epichlorohydrin and with epifluorohydrin were prepared in a similar manner. A pasty complex catalyst was weighed and dissolved into anhydrous acetone. (about 10% by weight.)

Polymerization by Ferric Chloride Complex

† Presented at the 8th Annual Meeting of the Society of Polymer Science, Tokyo. May, 1959.

* Present address: Textile Research Laboratory, Asahi Chem. Ind. Co. Ltd., 118, Ama, Takatsuki, Osaka.

1) C. C. Price and M. Osgan, *J. Am. Chem. Soc.* **78**, 4787 (1956).

2) S. Kambara and M. Hatano, *J. Polymer Sci.*, **27**, 586 (1958).

3) M. Osgan and C. C. Price, *J. Polymer Sci.*, **34**, 153 (1959).

4) R. O. Colclough, G. Gee, W. C. E. Higginson, J. B. Jackson and M. Litt, *J. Polymer Sci.*, **34**, 171 (1959).

5) J. Furukawa, T. Tsuruta, T. Saegusa and G. Kakogawa, *J. Polymer Sci.*, **36**, 541 (1959).

6) "Epichlorohydrin", Shell Chem. Corp. Technical Booklet (1949).

7) MM. E. Gryszkiewicz-Trochimowski, A. Spoizynski and J. Wnuk, *Rec. trav. chim.*, **66**, 413 (1947).

8) E. Wedekind and E. Bruch, *Ann.*, **471**, 97 (1929).

TABLE I. POLYMERIZATION OF EPICHLOROHYDRIN AND PROPYLENEOXIDE BY THE $FeCl_3$ COMPLEXES AT 80°C WITHOUT SOLVENT

No.	Catalyst	wt. %	Time hr.	Total conversion %	Fraction, % I	II	III	m. p. of of I, °C
Epichlorohydrin								
Ep-9	$FeCl_3$-PO	5	41	78.5	60.7	12.2	27.1	115
Ep-27	$FeCl_3$PO	5	48	61.0	55.0	10.7	34.3	108
Ep-101	$FeCl_3$-EpCl	10	68	46.0	38.0	nil*	62.0	104
Ep-104	$FeCl_3$-EpCl	5	68	31.7	41.3	nil*	58.7	111
Propyleneoxide								
Fp-22	$FeCl_3$-PO	5	68	34.6	28.2	nil†	71.8	—
PO-10	$FeCl_3$-PO	2.5	96	81.8	44.7	nil†	55.3	59
Ep-105	$FeCl_3$-EpCl	5	68	29.0	18.0	nil†	82.0	61

* No case of the complex with epichlorohydrin has been obtained fraction II.
† In the case of propylene oxide, there was found no fraction II.

Catalyst.—The general procedures were as follows: A catalyst solution of known concentration was injected into a glass tube and then the solvent was evaporated in vacuo at room temperature. In cooling, monomer was poured into tubes. The tubes were flushed with nitrogen and sealed and then placed in a constant temperature bath at 80±0.5°C.

Polymer Purification.—At the end of the reaction time the tube was cooled and opened. The polymer produced was fractionated into three parts by the following procedure.

Fraction I.—To the reaction mixture was added acidified (HCl) acetone. The insoluble material was collected, washed with dilute HCl-acetone and methanol successively, and then reprecipitated from tetrahydrofuran solution by adding methanol as precipitant.

Fraction II.—Acetone solution separated from fraction I was added dropwise with stirring to a large volume of methanol. A white powder, in some cases a pasty mass, separated out of the solution. The precipitate was further fractionated by washing with methanol in which it was partly soluble. The insoluble residue (Fraction II) was reprecipitated from acetone solution with metanol.

Fraction III.—The acetone-methanol solution separated from fraction II and methanol washing of fraction II, were combined, concentrated to a small volume and poured into a large excess of water, then centrifuged to give the third fraction III which was a viscous liquid or in some cases a paste.

Polymerization by Organometallic Compounds.—In all cases, the catalyst was added to the monomer or the solution of monomer in *n*-hexane or benzene, which was placed in the glass tube cooling in Dry-Ice acetone under nitrogen atmosphere, and then the tube was sealed and placed in a constant temperature bath. The polymers were isolated by an appropriate reprecipitation procedure.

Results and Discussion

Epichlorohydrin was polymerized using a complex catalyst of ferric chloride and propylene oxide ($FeCl_3$-PO) or an analogous complex catalyst of ferric chloride and epichlorohydrin ($FeCl_3$-EpCl) without solvent at 80±0.5°C. Some results were shown in Table I, in which the results of polymerization of propylene oxide by the same catalysts were compared.

The product was fractionated to three fractions, an acetone-insoluble (at room temperature) fraction (I), an acetone-soluble and methanol-insoluble fraction (II) and a methanol-soluble fraction (III).

Fraction I, a white and non-tacky solid, was insoluble in boiling methanol, ethanol, and diethyl ether and cold acetone, but soluble in boiling acetone, tetrahydrofuran and benzene. This fraction was shown by X-ray diagram to be crystalline. The melting point of the fraction I obtained from the different conditions varied from 109 to 115°C, but a purified sample showed the melting point of 119°C by capillary method. The molten polymer could be formed into a strong fiber and a tough film which showed a high degree of orientation after drawing. The drawn fiber had an identity period of 7.05±0.1 Å.

This value is nearly equal to the period of 7.16 Å on polypropyleneoxide[9].

Fraction II was a white solid, melting at

TABLE II. ELEMENTAL ANALYSIS OF THREE FRACTIONS AND LIQUID POLYMERS OBTAINED BY BF_3-ETHERATE

Fraction	C	H	Cl
I	38.85	5.44	38.06
II	38.39	5.13	37.35
III	40.17	5.86	36.54
liquid polymer	38.85	5.62	38.76
calcd. for $(-CH_2-\underset{\displaystyle CH_2Cl}{\underset{\vert}{CH}}-O-)$	38.94	5.45	38.32

9) G. Natta, *Angew. Chem.*, **68**, 393 (1956).

about 75°C, or in some case, a tacky semi-solid from which a strong film or fiber could not be obtained. Usually, it was possible to obtain an additional crystalline polymer from this fraction by redissolving it in acetone and chilling the solution to −30°C. The amorphous polymer was recovered by evaporation of the filtrate to dryness.

Fraction III was a viscous liquid or a paste and was not found to be crystalline.

All these fractions mentioned above were confirmed to be polyepichlorohydrin by the elemental analysis (Table II).

The infrared spectra of fraction I differ from those of fractions II and III and also from an amorphous liquid polymer which was obtained by a polymerization using BF_3-etherate as a catalyst, and the differences might well be attributed to the presence of crystalline-sensitive bands. As may be seen in Fig. 1, the spectral difference between the amorphous and crystalline polymers is striking, several bands at 1472(w), 1336(sh.w), 1277(s), 1232(s), 1173(s), 1036(m), 972(s) and 900(s) cm^{-1} were observed only in spectra of the crystalline fraction. A similar feature was found in the case of polypropyleneoxide: bands at 1480(s),1330(m),1240(s),1140(s), 1039(m) and 931(m) cm^{-1} were observed only

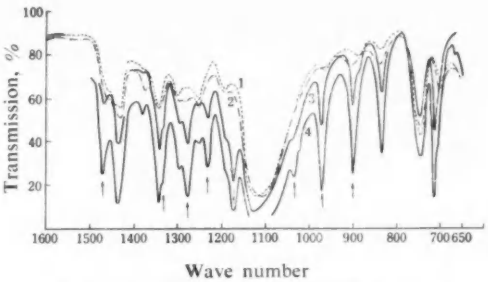

Fig. 1. Infrared spectra of the polymers of epichlorohydrin. Curve 1 ------: liquid polymer by BF_3-etherate, curve 2 -·-·-: fraction III, curve 3 ——: fraction I (KBr disk), curve 4 ——: fraction I (film). The curve of fraction II (pasty) was almost identical to that of fraction III.

Table III. Polymerization of epichlorohydrin by some organometallic compounds

No.	Catalyst	%	Time, hr.	Temp., °C	Solvent	Total conv., % wt.	Fraction %		
							I	II	III
50	$AlEt_3$-$ZnCl_2$	2	96	80	—	37.2	8.6	9.2	82.2
401	$AlEt_3$	2	20	r.t.	—	41.3	nil	100	nil
410	$AlEt_3$	2	6 days*	−78~r.t.	*n*-hexane	72.7	56.2	17.5	26.3
403	$AlEt_3$-$ZnCl_2$	2	4 days*	80	benzene	ca.100	2.2	11.1	86.7
405	$AlEt_3$-$FeCl_3$	2	4 days*	80	benzene	50.9	10.5	17.0	72.5
13	$ZnEt_2$	2	8	r.t.	—	81.8	nil	0.5	99.5
14	$ZnEt_2$-Alumina		18 days	r.t.	—	none	—	—	—
40	$ZnEt_2$-$ZnCl_2$	2	8 days*	r.t.	benzene	29.2	nil	4.6	95.6

* After solidification of reaction mixture (two days), these had been kept standing with catalytic systems.

Table IV. X-ray patterns of crystalline polymers

Propylene oxide		Epifluorohydrin		Epichlorohydrin	
Spacing (in Å)	Relative intensity	Spacing (in Å)	Relative intensity	Spacing (in Å)	Relative intensity
5.17	s	5.44	m		
		4.35	w	4.56	s
4.23	s	4.33	s		
4.05	w			3.83	m
3.63	w	3.67	m		
3.46	w	3.21	w		
3.10	w				
		2.85	m	3.09	w
2.78	w	2.69	m		
		2.49	w		
		2.35	w		
		2.20	w		
		1.87	w		
		1.81	w		
		1.75	w		

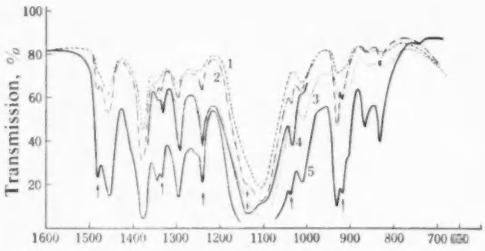

Fig. 2. Infrared spectra of the polymers of propylene oxide. Curve 1 ------: fraction III (viscous liquid), curve 2 -·-·-: fraction II (pasty), curve 3 ·····: fraction III (pasty), curve 4 ——: fraction I (KBr disk), curves ——: fraction I (film).

in the crystalline fraction (Fig. 2).

Among organometallic compounds, some, such as aluminum triethyl, zinc diethyl and aluminum isopropoxide in conjunction with zinc chloride were found to be effective catalysts in converting epichlorohydrin to its polymer. The details were given in Table III. The polymerization proceeded rapidly at room temperature with the first two catalysts and went on fairly below room temperature, while with the last catalyst it was necessary to operate at higher temperatures. But in all cases, it was found that the amount of the crystalline fraction (fraction I) of the polymer obtained by these three catalysts was less than that of the $FeCl_3$-PO catalyst.

In the case of epifluorohydrin, ferric chloride complex catalyst was used. The polymer obtained was a solid powder which was soluble in acetone, and was insoluble in methanol, carbon tetrachloride and carbon disulfide. The polymer melted at about 68°C and was highly crystalline, a feature confirmed by X-ray examination. The molten polymer could be formed into a fiber and a film.

Table IV records the data from the X-ray

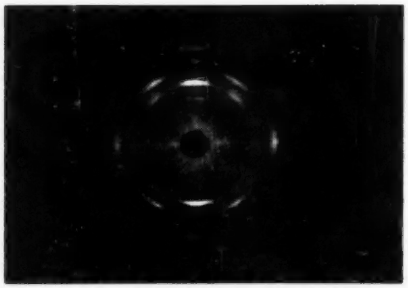

Fig. 3. X-ray pattern of a drawn fiber of polyepichlorohydrin. (fraction I).

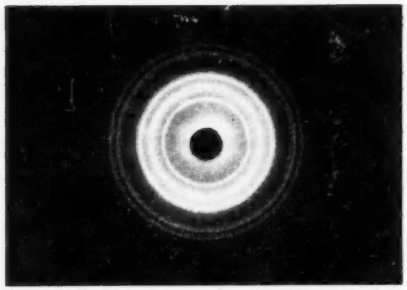

Fig. 4. X-ray pattern of polyepifluorohydrin.

patterns of the crystalline polymers of epichlorohydrin and epifluorohydrin together with that of crystalline polymer of propylene oxide for reference. X-ray diffraction patterns of the former two are shown in Figs. 3 and 4.

The author wishes to express his sincere thanks to Professor S. Murahashi for his guidance and encouragement throughout this work. Thanks are also due to Dr. S. Nozakura for his helpful discussions and to Mr. K. Katayama (Textile Research Laboratory, Asahi Chem. Ind, Co., Ltd.) for X-ray examinations.

Department of Polymer Science
Faculty of Science
Osaka University
Nakanoshima, Osaka

*Polyethers. II. Copolymerizations of Propylene Oxide with Epihalohydrins**

By Shin'ichi ISHIDA†

(Received October 22, 1959)

Although copolymerization of vinyl monomers has been extensively studied, none of the detailed information on the copolymerization of olefine oxide or polymerizable epoxy compounds has been published. The work to be reported here was undertaken for the purpose of investigating the copolymerization of epoxides using a catalyst which commonly stereospecifically catalyzes to individual monomers.

It has been reported that propylene oxide[1-3] epichlorohydrin[1] and epifluorohydrin[4] can be polymerized by ferric chloride complex catalyst to give products which are of crystalline nature.

The present paper deals with the copolymerization of propylene oxide with epichlorohydrin using the ferric chloride complex catalyst ($FeCl_3$–PO)[1] which has been shown to be the common stereospecific catalyst. An attempted copolymerization of epifluorohydrin with propylene oxide is also contained.

Experimental

Monomers and Catalyst.—Commercial epichlorohydrin and propylene oxide were dried over a molecular sieve, fractionally distilled before use. Epifluorohydrin was prepared from epichlorohydrin and anhydrous potassium fluoride by Cryszkiewicz-Trochmowski's method[5], b. p. 85~86°C. The catalyst was prepared as previously reported by Price's procedure[1,4].

Copolymerization.—All copolymerizations were carried out, as in our previous report on the stereospecific polymerization of epihalohydrins, in sealed glass tubes containing 10 g. of the varied monomer compositions and 5% by weight of catalyst. The tubes were thoroughly flushed with nitrogen before sealing and they were maintained at 85°C in an oil bath.

Purification of Polymer.—At the end of the reaction time, tubes were cooled and opened. The products were fractionated into three parts by the following procedure.

Fraction I.—To the reaction mixture was added acidified (HCl) acetone, and the insoluble material was filtered and washed with dilute HCl-acetone and methanol successively, and then reprecipitated from a hot acetone solution with methanol.

Fraction II.—The acetone solution separated from fraction I was added dropwise under stirring to a large volume of methanol. A tacky mass, or in some cases a paste, separated out from the solution.

Fraction III.—The acetone-methanol solution separated from fraction II and the methanol washing of fraction II were combined, concentrated to a small volume and poured into a large excess of water, then centrifuged to give fraction III which was a viscous liquid.

Results and Discussion

The copolymerization of epichlorohydrin with propylene oxide was studied over a wide range of monomer compositions in the presence of $FeCl_3$–PO catalyst. Results were given in Table I. The products usually were able to be fractionally separated into three fractions; an acetone-insoluble (at room temperature) fraction (I), an acetone-soluble but methanol-insoluble fraction (II), and a methanol-soluble fraction (III).

Table I. Copolymerization of epichlorohydrin (EpCl) with propylene oxide by $FeCl_3$-PO catalyst

No.	EpCl in comonomer mole %	Total conversion wt. %	Fraction %		
			I	II	III
37	100	62.5	55.0	10.7	34.3
39	85.4	35.0	27.8	15.4	56.8
30	72.2	26.3	11.2	15.9	72.9
31	48.6	26.7	0.8	14.2	85.0
32	38.6	38.9	0.1	12.4	87.5
33	29.5	—	trace	5.5	94.5
34	21.2	47.0	0.4	1.0	98.6
35	13.6	50.7	nil	nil	100
36	6.5	59.0	nil	nil	100
38	0	70.2	45.0	nil	55.0

Polymerization was carried out at 85°C in bulk for 96 hr.

The acetone-insoluble fraction (I) was a solid, the yield of which was markedly affected by the composition of epichlorohydrin in comonomer mixture. Fractions II and III were a pasty mass or a viscous liquid and their purification and

* Presented at the 8th Annual Meeting of the Society of Polymer Science, Tokyo, May, 1959.

† Present address: Textile Research Laboratory, Asahi Chem. Ind. Co., Ltd., Takatsuki, Osaka.

1) C. Price et al., *J. Am. Chem. Soc.*, **78**, 4787 (1956); *J. Polymer Sci.*, **34**, 153 (1959).
2) R. Colclough et al., ibid., **34**, 171 (1959).
3) J. Furukawa et al., ibid., **34**, 541 (1959).
4) S. Ishida, This Bulletin, **33**, 727 (1960)
5) MM. E. Cryszkiewicz-Trochimowski et al., *Rec. trav. chim.*, **66**, 413 (1947).

exact fractionation and its evaluation appeared to be difficult. Accordingly in this paper only fraction I was investigated in some details, and the other fractions left untouched because of the difficulties of handling.

The relationships between mole per cent of epichlorohydrin in comonomer and the yield of total product as well as the percentage relationships of each fraction were shown in Fig. 1.

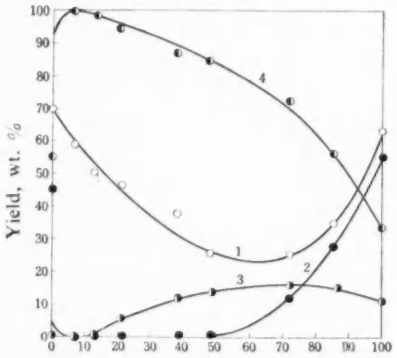

Fig. 1. The plots of yield of each fraction versus the mole % of epichlorohydrin in the comonomer.
Curve 1: total conversion, curve 2: fraction I, curve 3: fraction II, curve 4: fraction III.

Since an amorphous polypropyleneoxide is soluble in acetone and methanol, it can hardly be suspected to be contained in fraction I. Fraction I was therefore further purified by extraction with boiling ether so as to remove the crystalline homopolymer of propylene oxide. The products thus treated were white, crystalline solids. As they were believed to be true copolymers from the following evidences, they were referred as "copolymer" and were discriminated from Fraction I. Artificial mixtures of each homopolymer (crystalline polypropylene oxide : Crystalline polyepichlorohydrin =1:1 and 1:3 by weight) could be separated completely to the original components by an extraction with boiling ether.

The further evidence that the "copolymer" was not a mixture of homopolymer of epichlorohydrin and a copolymer but a genuine copolymer, was proved by the analysis of the fractions from the "copolymer"; a successive, careful fractionation of the "copolymer" from a tetrahydrofuran solution using methanol and water as precipitants gave fractions having almost the same chlorine contents. (Table II)

All "copolymers" exhibited the X-ray patterns contributed solely by the polyepichlorohydrin part, while an artificial co-precipitated mixture

TABLE II. FRACTIONATION AND ANALYSIS OF A "COPOLYMER"

Fraction	wt. %	Cl %	EpCl mole %
"copolymer"	origin	29.89	69.3
F11	2.8	32.10	76.0
F12	27.6	29.76	67.2
F2	53.7	29.86	69.2
F3	15.9	27.47	61.9

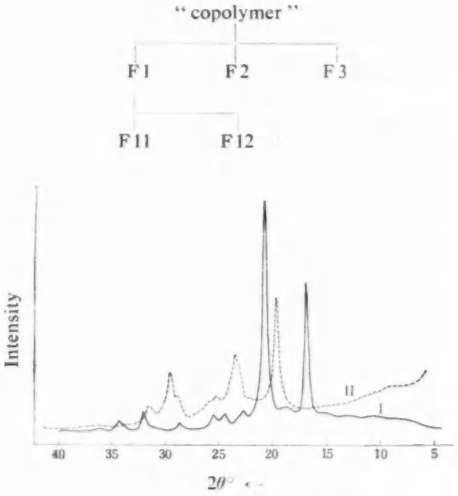

Fig. 2. X-ray diffraction spectra of the crystalline polymers.
I) Crystalline polypropylene oxide (full line).
II) Crystalline polyepichlorohydrin (dotted line).

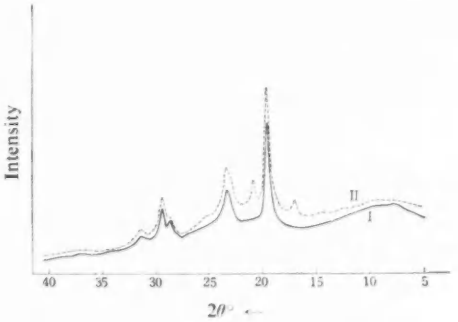

Fig. 3. X-ray diffraction spectra of the "copolymer" and "artificial mixture" of the homopolymers.
I) "Copolymer" (Found. EpCl mole % 67.2; full line).
II) "Artificial mixture" (poly-EpCl; 65 mole %, poly-PO; 35 mole %; dotted line).

of both the crystalline homopolymers which had the composition corresponding to that of the "copolymer", showed a superposed pattern of two crystalline homopolymers.

A comparison of a "copolymer" of 67.2 mole % of epichlorohydrin content with an artificial mixture of 65 mole % of crystalline polyepichlorohydrin and 35 mole % of crystalline polypropyleneoxide was shown Figs. 2 and 3, together with both crystalline homopolymers.

The experimental data were presented in Table III and the copolymer composition curve for this system together with the melting points of the "copolymers" by the capillary method were illustrated in Fig. 4.

Table III. Compositions of "copolymers" and their melting points

No.	Comonomer EpCl mole %	Cl %	"Copolymer" EpCl mole %	m. p. °C
16	17.3	29.21	67.3	87
25	33.3	30.46	71.0	88
13	36.0	31.66	75.3	88
14	56.2	32.74	79.0	91
30	72.2	34.06	83.7	—
15	78.2	34.31	85.0	95
39	85.4	35.49	92.6	102
37	100	38.32	100	117

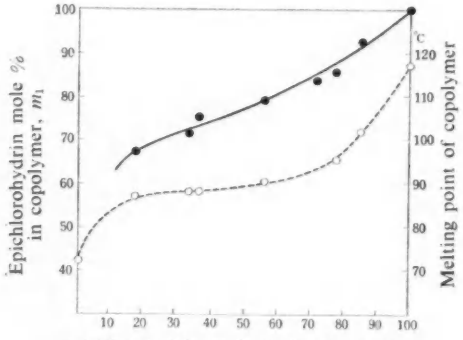

Fig. 4. Copolymer composition curve (● full line) for a system of epichlorohydrin and propylene oxide together with melting points of "copolymers" (○ dotted line).

From these data, the monomer reactivity ratios of epichlorohydrin and propylene oxide in copolymerization to crystalline "copolymer" were estimated by Mayo's method[6].

$$r_1(\text{epichlorohydrin}) = 1.8 \pm 0.3$$

$$r_2(\text{propylene oxide}) = 0.6 \pm 0.5$$

A soild non-tacky product which had been obtained by polymerization of equimolar mixture of propylene oxide and epifluorohydrin using $FeCl_3$–PO catalyst was purified by reprecipitation from an acetone solution with methanol-water. Then a fraction which was insoluble in methanol was separated from the acetone solution of the above product by adding a large excess of methanol. This fraction was a white non-tacky powder, and could not be further fractionated by reprecipitation using the same solvents and precipitants. It seemed to be possible that a crystalline polypropyleneoxide and a crystalline polyepifluorohydrin were contained in this fraction, as may be seen from the solubility data of both homopolymers in the preceding paper[1].

In fact, it was found by X-ray examination, that this fraction showed a superposed pattern of each specimen and so it might be a mixture of both the crystalline homopolymers. The attempted separation was unsuccessful because the author could not find a suitable solvent for the separation.

Attempts to copolymerize epichlorohydrin with 1, 1-dimethylethylene oxide by aluminum triethyl as catalyst did not give a copolymer but a mixture of each homopolymer.

The author wishes to express his sincere thanks to Professor S. Murahashi for his guidance and encouragement throughout this work. He is also indebted to Dr. S. Nozakura for his helpful discussions and suggestions and to Mr. K. Katayama (Textile Research Laboratory, Asahi Chem. Ind. Co., Ltd.) for X-ray examinations.

Department of Polymer Science
Faculty of Science
Osaka University
Nakanoshima, Osaka

6) F. R. Mayo and F. M. Lewis, *J. Am. Chem. Soc.*, **66**, 1594 (1944).

An Interpretation of the Elovich Equation for the Rate of Chemisorption on the Basis of Surface Heterogeneity

By Yutaka KUBOKAWA

(Received September 9, 1959)

Taylor and Thon[1] showed that a number of chemisorption rate data are represented by the Elovich equation

$$dq/dt = ae^{-bq}$$

where q is the amount of gas adsorbed and a and b are constants. In order to explain this equation, they postulated the annihilation of adsorption sites in the course of adsorption. Being stimulated by this work, various workers[2] discussed the applicability of this equation for chemisorption processes and presented various models leading to this equation. Although there is, of course, no reason to believe that only one and the same mechanism is operative in all systems to which the Elovich equation is applicable, the most probable interpretation of the equation seems to be the one based on surface heterogeneity at least for the adsorbents for which the existence and the effect of surface heterogeneity have been established.

Such an interpretation has been proposed by Porter and Tompkins[2] for a simple case where the distribution function of adsorption site is constant and the rate of desorption is negligibly small. The purpose of the present paper is to elaborate a similar interpretation for more complex cases where the distribution is variable and/or the rate of desorption can not be neglected and to discuss some available data with respect to the variation of constant b in the Elovich equation with pressure and temperature.

Adsorption Rate on a Heterogeneous Surface. —For a heterogeneous surface the adsorption sites over the whole surface may be divided into a number of sets, each of which consists of sites of the same kind; the number of sites in each set is given by a distribution function which may, in the present case, be assumed to be a function of the activation energy E for a given chemisorption. Taking account of desorption, the net rate of adsorption on any set of sites may be given by

$$v = d\theta/dt = kp(1-\theta) - k'\theta$$

where θ is the fraction of the sites covered and p the pressure in the gas phase. Since $\theta=0$ when $t=0$, this rate gives on integration at a constant pressure

$$\theta = \theta_e[1 - e^{-(kp+k')t}]$$

where θ_e is the equilibrium coverage. Differentiating with respect to time

$$v = (kp+k')\theta_e e^{-(kp+k')t} = kpe^{-(kp/\theta_e)t} \quad (1)$$

The rate for the whole surface may be obtained by integration, by assuming a continuous distribution function of sites. First, let us consider the simplest case where desorption is negligible and the distribution function N is constant. Since $\theta_e=1$ in this case, Eq. 1 becomes

$$v = Ke^{-Kt} \quad (2)$$

where $K=kp$. The rate for the whole surface under such conditions will be

$$N\int_0^\infty v(E)dE = N\int_\infty^0 [v(E)dE/dK]dK \quad (3)$$

From the expression $k = \text{const.}\, e^{-E/RT}$, it follows that

$$dE/dK = -RT/K \quad (4)$$

Introduction of Eqs. 2 and 4 into Eq. 3 gives

$$N\int_0^\infty v(E)dE = -NRT\int_\infty^0 e^{-Kt}dK = NRT/t \quad (5)$$

On the sites with a high value of E the rate will naturally be small, while on those with a low value of E it will again be small because the coverage is here close to the equilibrium value. For a particular set of sites with an intermediate magnitude of E, therefore, the rate will pass through a maximum. This condition may be written as

$$\frac{dv}{dE} = \frac{dv}{dK}\frac{dK}{dE} = e^{-Kt}(1-Kt)\left(-\frac{K}{RT}\right) = 0$$

Consequently, v shows a maximum at $Kt=1$. The maximum rate, being equal to NKe^{-1} or N/te, is proportional to the rate over the whole surface represented by Eq. 5.

When the distribution function is not constant and the rate of desorption can not be ignored, the over-all rate can not easily be integrated. However, it may be assumed as a first approximation that in this case the over-all rate is also

1) H. A. Taylor and N. Thon, *J. Am. Chem. Soc.*, **74**, 4169 (1952).

2) A. S. Porter and F. C. Tompkins, *Proc. Roy. Soc.* **A217**, 529 (1953); H. J. Engell and K. Hauffe, *Z. Elektrochem.*, **57**, 762 (1953); R. T. Landsberg, *J. Chem. Phys.*, **23**, 1079 (1955); D. D. Eley, *Trans. Faraday Soc.*, **49**, 643 (1953) etc.

proportional to the maximum rate.

As described above, the rate for any set of sites can be represented by

$$v = NKe^{-Kt/\theta}$$

where θ is written for θ_e for brevity. The condition for the maximum rate is

$$\frac{dv}{dE} = \frac{dv}{dK}\frac{dK}{dE} = \left(-\frac{K}{RT}\right)Ne^{-Kt/\theta}\left[1 + \frac{dN}{N}\frac{K}{dK} - Kt\frac{d(K/\theta)}{dK}\right] = 0$$

The dependence of K on θ is determined by the relation between the activation energy of adsorption E and the heat of adsorption Q, which is assumed to be given by

$$E - E_0 = (1/\alpha)(Q - Q_0)$$

where α is a constant and Q_0 is the heat of adsorption on the sites with the lowest activation energy E_0. Assuming the Langmuir isotherm to be applicable,

$$1/\theta = 1 + (A/P)e^{-Q/RT}$$

so that

$$\frac{d(1/\theta)}{d(-Q/RT)} = \frac{A}{p}e^{-Q/RT} = \frac{1}{\theta} - 1$$

It follows then

$$\frac{d\theta}{dK} = \frac{d\theta}{d(1/\theta)}\frac{d(1/\theta)}{d(-Q/RT)}\frac{d(-Q/RT)}{d(-E/RT)}\frac{d(-E/RT)}{dK} = \alpha\left(\frac{1}{\theta} - 1\right)\left(-\frac{\theta^2}{K}\right) \quad (6)$$

Hence

$$\frac{d(K/\theta)}{dK} = \frac{1}{\theta} - \frac{K}{\theta^2}\frac{d\theta}{dK} = \frac{1 + \alpha - \alpha\theta}{\theta}$$

By defining $\beta = (dN/N)(K/dK)$, we find that the rate v shows a maximum at

$$Kt = [(1+\beta)\theta]/(1 + \alpha - \alpha\theta) = F\theta \quad (7)$$

where $F = (1+\beta)/(1+\alpha-\alpha\theta)$. So that the maximum rate v_m is

$$v_m = NKe^{-F} \quad (8)$$

Taking the logarithm of Eq. 8 and differentiating it with respect to $\ln K$

$$\frac{d\ln v_m}{d\ln K} = 1 + \beta - \frac{dF}{d\ln K}$$

Hence, we may write,

$$\frac{d\ln v_m}{dq} = \frac{d\ln v_m}{d\ln K}\frac{d\ln K}{dE}\frac{dE}{dq} = \left(1 + \beta - \frac{dF}{d\ln K}\right)\left(-\frac{1}{RT}\right)\frac{dE}{dq} \quad (9)$$

where q is the amount adsorbed at a given time. Taking the logarithm of Eq. 7, differentiating it with respect to time,

$$\frac{d\ln K}{dE}\frac{dE}{dt} + \frac{1}{t} = \frac{1}{F}\frac{dF}{d\ln K}\frac{d\ln K}{dE}\frac{dE}{dt} + \frac{1}{\theta}\frac{d\theta}{dK}\frac{dK}{dE}\frac{dE}{dt} \quad (10)$$

Inserting Eqs. 6 and 4 in Eq. 10, and rearranging

$$\frac{dE}{dt} = \left(\frac{RT}{t}\right)\left(1 + \alpha - \alpha\theta - \frac{1}{F}\frac{dF}{d\ln K}\right)^{-1} \quad (11)$$

Using the definition of F, we can write Eq. 11 as

$$\frac{dE}{dt} = \left(\frac{RT}{t}\right)F\left(1 + \beta - \frac{dF}{d\ln K}\right)^{-1} \quad (12)$$

Eqs. 7 and 8 give

$$v_m = (N/t)F\theta e^{-F}$$

As was described above, a relationship $v_t = cv_m$ holds where v_t is the over-all rate and C a constant. Hence,

$$v_t = \frac{dq}{dt} = C(N/t)F\theta e^{-F} \quad (13)$$

comparing Eq. 12 with Eq. 13, we obtain

$$\frac{dE}{dq} = \frac{RT}{CN\theta}\left[\frac{e^F}{1 + \beta - (dF/d\ln K)}\right]$$

Inserting this expression into Eq. (9)

$$\frac{d\ln v_m}{dq} = \frac{d\ln v_t}{dq} = -\frac{1}{CN\theta}e^F \quad (14)$$

When desorption is negligible and N is constant, Eq. 13 becomes

$$dq/dt = CN/te$$

Comparing this expression with Eq. 5, we obtain $C = RTe$. Hence, Eq. 14 becomes

$$\frac{d\ln v}{dq} = -\left(\frac{1}{N\theta RTe}\right)e^F = -\left(\frac{1}{N\theta RTe}\right)e^{1+\beta+\alpha\theta} \quad (15)$$

where v is written for v_t for the sake of simplicity of representation. Eq. 15 gives the physical meaning of constant b of the Elovich equation on the basis of surface heterogeneity.

Variation of the Constant b of the Elovich Equation with Temperature and Pressure.—For the sake of simplicity, let us assume the values of α and β to remain constant on changing pressure or temperature in the rate measurements, and discuss the dependence of b on temperature and pressure for the following four different cases.

Case 1: Desorption is negligible and N is constant. In this case Eq. 15 becomes

$$\frac{d\ln v}{dq} = -\frac{1}{NRT} = \text{const}$$

Accordingly, strict applicability of the Elovich equation is expected. As described by various

workers[2], the value of b should be independent of pressure and vary in proportion to $1/T$.

Case 2: Desorption is negligible but N is not constant. In this case Eq. 15 becomes

$$\frac{\mathrm{d}\ln v}{\mathrm{d}q} = -\left(\frac{1}{NRT}\right)\mathrm{e}^{\beta}$$

The right hand side of this equation varies as adsorption proceeds. However, if the range of coverage is limited, and the change of N during adsorption is not marked, we may expect that the Elovich equation will still, though approximately, be obeyed. Variation in the value of b expected in this case may be as follows: If N increases with E, the value of N for the sites mainly responsible for adsorption may increase with pressure or temperature, since the set of sites with a higher value of E may be covered at a higher pressure or temperature. This increase of N will result in the decrease of b with increasing pressure or temperature.

Case 3: Desorption can not be neglected but N is constant. In this case, Eq. 15 becomes

$$\frac{\mathrm{d}\ln v}{\mathrm{d}q} = -\left(\frac{1}{N\theta RT\mathrm{e}}\right)\mathrm{e}^{\frac{1}{1+\alpha-\alpha\theta}}$$

As described in Case 2, the Elovich equation will approximately be obeyed in a limited range of coverage. Let us consider the pressure dependence of b for the case $1<\alpha<2$, which seems to be the most probable case for α positive. Plotting $\theta\mathrm{e}^{\frac{-1}{1+\alpha-\alpha\theta}}$ against θ for the two different values of α, $\alpha=1$ and $\alpha=2$, we obtain Fig. 1, which shows that, except in the range $\theta\simeq 1$, $\theta\mathrm{e}^{\frac{-1}{1+\alpha-\alpha\theta}}$ increases with θ. This result together with the fact that the sites with a higher value of E, i.e., with a larger value of θ come to operate at a higher pressure leads to the conclusion that the value of b decreases with increasing pressure.

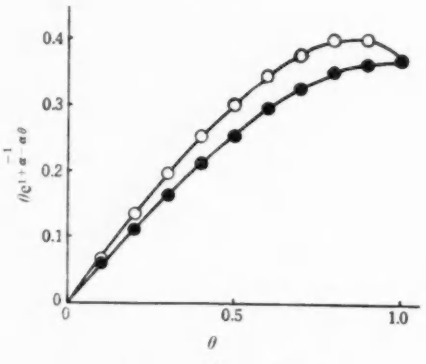

Fig. 1. Plot of $\theta\mathrm{e}^{\frac{-1}{1+\alpha-\alpha\theta}}$ against θ.
—●—, $\alpha=1$; —○—, $\alpha=2$

Case 4: Desorption can not be neglected and, in addition, N is not constant. Let us consider only the special case when both conditions, $\mathrm{d}N/\mathrm{d}E>0$ and $1<\alpha<2$, are satisfied. Remembering that $\beta<0$ in this case, the following conclusion in the pressure dependence of b may be drawn. The extent of decrease of b with increasing pressure may be greater than that in the case where either N or θ alone varies, i. e., in Case 2 or 3 described above.

So far we have tacitly assumed an undissociative adsorption. For a dissociative adsorption, the adsorption rate corrected for desorption may be given by $k\sqrt{p}\,(1-\theta)-k'\theta$, or $kp(1-\theta)^2-k'\theta^2$. It is clear that the former equation leads to the same expression for the maximum rate as in the undissociative adsorption, except for the term $\sqrt{p}$. As regards the latter equation, it may also easily be shown that, in case desorption is negligible, this gives a similar expression for the maximum rate to that for the undissociative adsorption. It may therefore be expected that qualitative conclusions concerning the pressure dependence of b described in Cases 3 and 4 will not be altered for the dissociative adsorption.

A Criterion for the Negligible Desorption.— It follows from Eq. 15 that

$$-\frac{\mathrm{d}(\ln v-\ln v_0)}{\mathrm{d}q} = \frac{\mathrm{e}^{\frac{1+\beta}{1+\alpha-\alpha\theta}}}{N\theta RT\mathrm{e}} = \frac{\mathrm{e}^{\gamma}}{N\theta RT}$$

where $\gamma=(1+\beta)/(1+\alpha-\alpha\theta)-1$ and v_0 represents the initial rate when $t=0$ or $q=0$, that is, the adsorption rate on the set of sites with the lowest value of E. Integration of this equation gives

$$q = RT\int N\theta\mathrm{e}^{-\gamma}\mathrm{d}(\ln v_0-\ln v)$$

Substituting the expression, $\ln v_0=\ln p+\ln v_0'$, where v_0' represents the pressure independent terms in v_0, we obtain

$$q = RT\int N\theta\mathrm{e}^{-\gamma}\mathrm{d}[\ln v_0'-(\ln v-\ln p)]$$

This equation leads to the conclusion that if desorption can be neglected, i. e., the conditions $\theta=1$ and $\gamma=\beta$ are satisfied, the plots of q against $\ln v-\ln p$ at different pressures should lie on the same curve, provided that the temperature is constant. On the contrary, if desorption is not negligible, such plots will give separate curves.

Discussion of Some Available Data with Respect to Variation of b with Pressure.—*1) Hydrogen on Zinc Oxide.*—Values of constant b for this system were obtained from the following integrated form of the Elovich equation

$$q=(2.3/b)\log(t+t_0)-(2.3/b)\log t_0,\quad t_0=1/ab$$

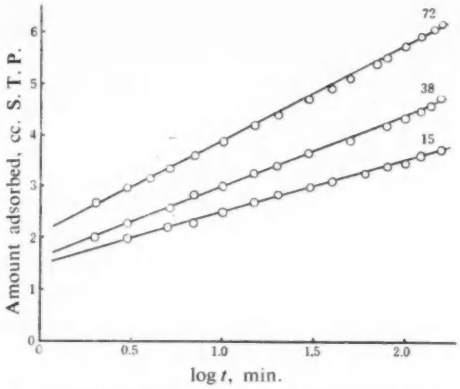

Fig. 2. Elovich plots for the hydrogen chemisorption on zinc oxide at 140°C. Figures indicate the initial pressure in mmHg.

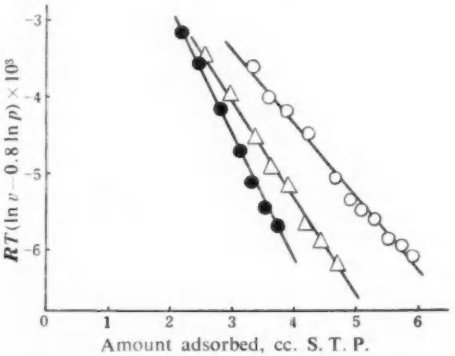

Fig. 3. Plots for the hydrogen chemisorption on zinc oxide at 140°C. —○—, 72 mmHg; —△—, 38 mmHg; —●—, 15 mmHg.

Plotting $\log(t+t_0)$ against q with t_0 adjusted to give a linear plot, the value of b was determined from the slope. The results shown in Fig. 2 indicate that the slope $2.3/b$ increases with initial pressure[2].

The same data are shown in Fig. 3 as the plots of q against $\ln v - 0.8 \ln p$. The term $\ln p$ is here multiplied by a factor of 0.8, for the rate was found to be proportional to $p^{0.8}$ as reported previously[4]. As seen in this figure, the plots at different pressures give distinctly separate curves, indicating that appreciable desorption takes place during adsorption rate measurements, which is also expected from the results described in the previous paper[4].

3) The adsorption rate was measured by pressure change, using an adsorption apparatus of constant volume. The pressure decrease due to adsorption was no more than 10~20% of the initial pressure. The latter quantity was measured one minute later than the time of admission of hydrogen into the vessel.

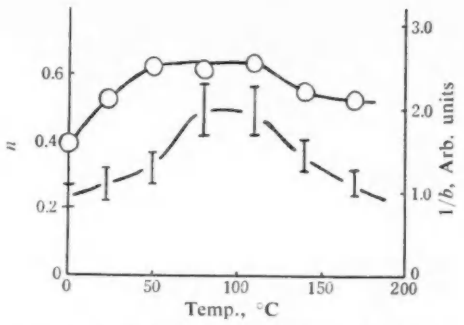

Fig. 4. Variation with temperature of the exponent n and $1/b$ at the pressure 65 mmHg. —|—, n; —○—, $1/b$

The pressure dependence of $1/b$ for this chemisorption was found to be approximately represented by $1/b \propto p^n$. As shown in Fig. 4, the exponent n varies with temperature and passes through a maximum, indicating that the pressure dependence of $1/b$ is considerably influenced by temperature. As given together in the figure, $1/b$ itself obtained at a particular pressure shows a similar dependence on temperature. It seems impossible to explain such behavior in terms of the concept that only the value of θ varies with pressure but the distribution function N is constant[5]. It may therefore be concluded that hydrogen chemisorption on zinc oxide belongs to the case where both N and θ change, i.e., to Case 4.

2) Hydrogen on Chromic Oxide Gel.—As an example for the case where the rate of desorption is negligibly small, we may mention the chemisorption of hydrogen on chromic oxide gel investigated by Burwell and Taylor[6]. Taking into account that the rate of adsorption for this system was found to be proportional to $p^{0.8}$ by these investigators, their data have been reexamined by plotting q against $\ln v - 0.8 \ln p$ with the results shown in Fig. 5. As seen in the figure, all of the plots at different pressures lie on a single curve. In addition, $-\mathrm{d} \ln v/\mathrm{d}q$ increases with decreasing value of E[7]. We

4) Y. Kubokawa, This Bulletin, 33, 550 (1960).

5) If the value of θ alone were variable, such a marked increase in n with increasing temperature from 20 to 80°C as seen in Fig. 4 would be accompanied by decrease in $1/b$ at a particular pressure, in contradiction to what was observed.

6) R. L. Burwell and H. S. Taylor, *J. Am. Chem. Soc.*, **58**, 697 (1936).

7) Strictly speaking, this conclusion is valid provided that β is unaltered with decreasing value of N. Even if β is altered, however, it seems unlikely that the decrease in e^{β} offsets the effect of the decrease in N, since in most cases $|\beta|$, i.e., $|\mathrm{d}\ln N/\mathrm{d}\ln K|$ may be less than 1, and the change of β may be small compared with that of N. It will be shown in a later paper that the inference given here is reasonable for this adsorption.

may therefore regard this chemisorption as an example for Case 2 with N increasing with E. In fact, the value of b obtained by applying the integrated form of the Elovich equation decreases with increasing pressure as shown in Table I, in accordance with the above statement.

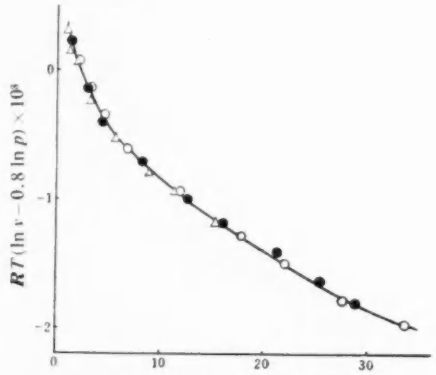

Fig. 5. Plots for the hydrogen chemisorption on chromic oxide gel at 457°K.
—○—, 1 atm.; —●—, 0.5 atm.; —△—, 0.25 atm.

TABLE I. VALUES OF b OBTAINED FROM THE INTEGRATED FORM OF THE ELOVICH EQUATION FOR THE HYDROGEN CHEMISORPTION ON CHROMIC OXIDE GEL AT 457°K

Pressure, atm.	b, 1/cc.
1	0.061
0.5	0.065
0.25	0.091

On the Constant t_0 in the Integrated Form of the Elovich Equation.—As described in a previous section, if desorption is negligible and N is constant, we may write

$$dq/dt = RTN/t$$

Hence,

$$d \ln t/dq = (d \ln t/dt)(dt/dq) = 1/RTN$$

It is clear from this equation that, in this case, the plot $q - \log t$ is linear. Consequently, the constant t_0 in the integrated form of the Elovich equation should be very small in this case. Furthermore, as described above, Case 1 is the only case to which the Elovich equation is expected to apply strictly. We may therefore conclude as follows: So far as the present interpretation of the Elovich equation is applicable, the constant t_0 of an appreciable magnitude such as is frequently employed to make the plot $q - \log(t + t_0)$ linear implies that in such cases, the equation holds only approximately, and the constant b thus determined can not be given any physical meaning such as stated above, although the equation may be useful for evaluating initial rates.

Summary

For the heterogeneous surface where the distribution function was variable and/or desorption could not be neglected, the rate of adsorption was derived and the physical meaning of constant b in the Elovich equation was given. It was shown that in complicated case the Elovich equation is expected to apply only approximately in a limited range of coverage. The variation in constant b with pressure or temperature was qualitatively explained in terms of the concept that on changing pressure or temperature, different sets of sites are covered and/or the contribution of desorption in adsorption rate measurements, is altered. The chemisorption of hydrogen on zinc oxide and on chromic oxide gel was discussed on the basis of the present interpretation of the Elovich equation. Finally, it was shown that, on the basis of surface heterogeneity, the constant b obtained from the integrated form of the Elovich equation can not be given any physical meaning when the constant t_0 of an appreciable magnitude is required.

The author wishes to express his sincere thanks to Professor O. Toyama for his guidance and encouragement throughout the course of this study.

Department of Applied Chemistry
College of Engineering
University of Osaka Prefecture
Sakai-shi, Osaka

Effect of Hydrogen and Carbon Monoxide on the Electrical Conductivity of Zinc Oxide

By Yutaka KUBOKAWA

(Received September 9, 1959)

The increase in electrical conductivity of zinc oxide caused by hydrogen was investigated in previous works[1,2] in order to get a clue to the nature of the chemisorption of hydrogen, with the results summarized as follows: On admission of hydrogen no significant change in the conductivity is observed below 100°C, while at higher temperatures a marked increase takes place; moreover, the rate and the amount of chemisorption decrease with increasing temperature up to 110°C but increase at higher temperatures. On the basis of these results, it was suggested that two types of hydrogen chemisorption exist on zinc oxide; one is predominating at higher temperatures and responsible for the increase in conductivity, and the other is observed at lower temperatures, with little effect on conductivity. Making use of the rate of increase in conductivity, the activation energy for the chemisorption of the high temperature type was estimated as 25 kcal./mol.

However, the existence of two such types of chemisorption can not yet be regarded as established, since later studies[3,4] on the rate of desorption and the adsorption isotherm in addition to those on the rate of adsorption, covering wide ranges of pressure and temperature, showed that the heterogeneity of zinc oxide surface should be taken into account. The aim in the present work has been to reinvestigate the relation between the hydrogen chemisorption and the conductivity change by more extensive experiments.

Experimental

Materials.—Zinc oxide was prepared as described previously[3]. The experiments with hydrogen were carried out with zinc oxide sintered at 800°C for 5 hr., while non-sintered zinc oxide was used for the study with carbon monoxide. Hydrogen and carbon monoxide were obtained as given in previous papers[3,5].

Apparatus and Procedure.—Conductivity measurements were made with a powdered specimen held between two electrodes, by means of a Wheatstone bridge. Details of the apparatus and procedure were described in the previous paper[2]. In the measurements of the rate of conductivity decrease, an auxiliary heater of nickel wire was mounted in the reaction vessel for the purpose of changing the temperature rapidly, taking into account the slow attainment of thermal equilibrium at low pressures.

Results and Discussion

Relationship between the Rate of Conductivity Increase and that of the Formation of Donors.—There seems to be little doubt that the observed increase in conductivity of zinc oxide brought in contact with hydrogen is related to the formation of donors of a certain type. In view of the well-known difficulties, especially in the case of a powdered sample such as used in the present work, it seems questionable to discuss the kinetics of the formation of donors, from the conductivity-time curves at a constant temperature, on the assumption of a relationship between conductivity and the number of donors. However, as shown in the previous paper[2], the activation energy of the formation of donors may be obtained in the following way. The rate of formation of donors at the time when the number of donors present is c may be written as

$$(\mathrm{d}n/\mathrm{d}t)_c = (\mathrm{d}n/\mathrm{d}\kappa)_c(\mathrm{d}\kappa/\mathrm{d}t)_c$$

where κ is the conductivity and n the number of donors. The activation energy for the formation of donors, E is therefore given by $E=E_2-E_1$, where E_1 and E_2 are the activation energies of conductivity itself and of conductivity increase, respectively, both referring to the number of donors c. Using this equation, we can obtain the value of E provided that E_1 and E_2 are known.

Temperature Coefficient of Conductivity.—E_1 decreases with increasing number of donors as described by various workers. The value for the state with a negligible number of donors was estimated from the temperature coefficient of conductivity with the specimen evacuated at about 400°C. Fig. 1 shows a typical result, which gives a value of 1.2 kcal./mol. Values

1) Y. Kubokawa and O. Toyama, *Bull. Naniwa Univ.* (at present *Bull. Univ. Osaka Prefecture*) **A2**, 103 (1954).
2) Y. Kubokawa and O. Toyama, *J. Phys. Chem.*, **60**, 833 (1956).
3) Y. Kubokawa, This Bulletin, **33**, 546 (1960).
4) Y. Kubokawa, ibid., **33**, 550 (1960).
5) Y. Kubokawa, ibid., **33**, 555 (1960).

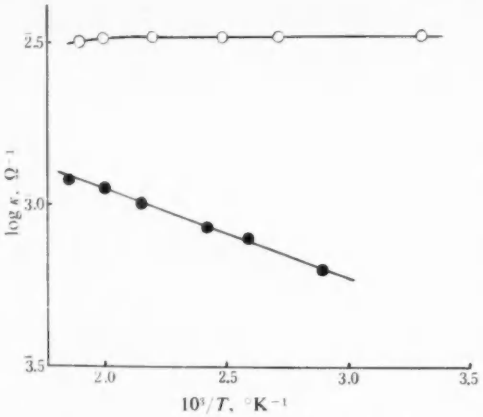

Fig. 1. Conductivity as a function of temperature.
—●—, in vacuo; —○—, in H_2.

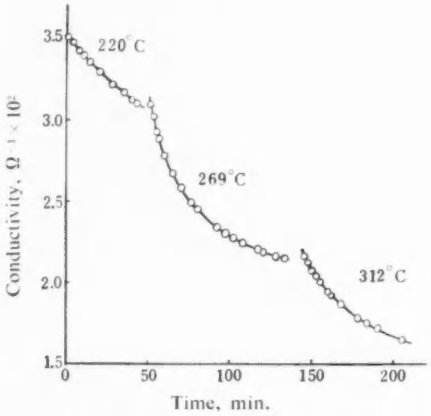

Fig. 2. Conductivity decrease by reducing pressure and the effect of a sudden temperature change.

TABLE I. VALUES OF E_1 AND THE ACTIVATION ENERGY OF CONDUCTIVITY DECREASE FOR THE DATA IN FIG. 2

Temp. range (°C)	220~269	269~312
E_1 (kcal./mol.)	0.4±0.1	0.7±0.2
Activation energy of cond. decrease (kcal./mol.)	31±2	31±2

of E_1 at an appreciable number of donors can not easily be obtained because the temperature coefficient in hydrogen such as shown in Fig. 1 does not give the true value of E_1, since in this case the change of conductivity with temperature may arise from two factors, i. e., from the temperature coefficient of conductivity itself and from the variation of the number of donors with temperature. However, approximate values of E_1 may be obtained as follows.

After hydrogen was introduced at about 400°C, the whole vessel was cooled down to a lower temperature, where the conductivity decrease by evacuation was followed for some time. Then the vessel was abruptly heated to a higher temperature, where the conductivity measurement was continued. The results are shown in Fig. 2. As described in a previous paper[4], by extrapolation of the $\kappa \sim t$ curves to the time of the abrupt change in temperature, the conductivities at different temperatures corresponding to equal numbers of donors were obtained. Values of E_1 thus determined are given in Table I. They are appreciably less than the value determined at the evacuated state.

Dependence of the Rate of Conductivity Increase on Temperature.—This was determined in two ways, i. e., by measuring the initial rates of conductivity increase at varied temperatures as described previously[2] and by observing the rate increase caused by an abrupt temperature elevation during the conductivity increase measurements. The latter method is similar in principle to that used in the adsorption rate measurements[4]. By extrapolation of the rates

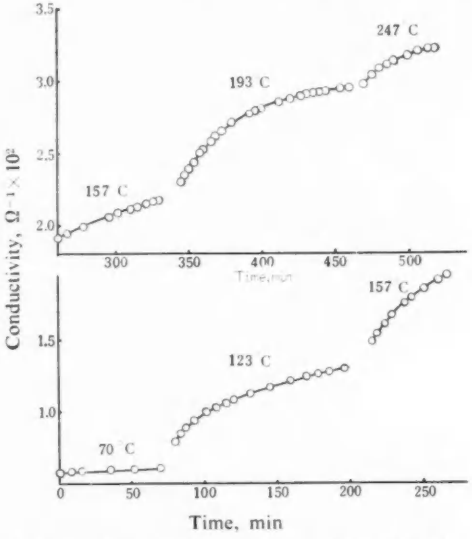

Fig. 3. Conductivity increase by hydrogen and the effect of a sudden temperature change. Pressure, 56 mmHg.

TABLE II. VALUES OF E_2 FOR THE DATA IN FIG. 3

Temp. range (°C)	70~123	123~157	157~193
E_2 (kcal./mol.)	18±1.5	21.7±1.5	20.5±1.5

to the time of the abrupt change, the rate at the two different temperatures corresponding to equal numbers of donors and consequently E_2 for that number of donors were obtained. In a typical example shown in Fig. 3, the temperature was raised in stages up to about 300°C after hydrogen was admitted at room temperature. The value of E_2 found here was about 21 kcal./mol., being roughly constant in the temperature range 120~200°C (Table II). E_2 is therefore of much greater magnitude compared with E_1 described above, indicating that the activation energy of the formation of donors is almost equal to that of conductivity increase.

The initial rate measurements, i. e., the other one of the two methods mentioned above, gave a value of 20 kcal./mol. for E_2, in agreement with that obtained by a rapid temperature elevation. The conductivity-time curves obtained were similar to those described in the previous paper[2].

Dependence of the Rate of Conductivity Increase on Pressure.—This was determined in two ways similar to those used for the temperature dependence. Fig. 4 shows the results obtained by a rapid pressure change during the measurements of conductivity increase. The pressure dependence was supposed to take the form p^n and the values of the exponent n were determined from this figure, as given in Table III. It is seen that the rate of conductivity increase is proportional to $p^{0.85}$ at increasing as well as decreasing pressure. The measurements of the initial rates of conductivity increase gave a similar pressure dependence.

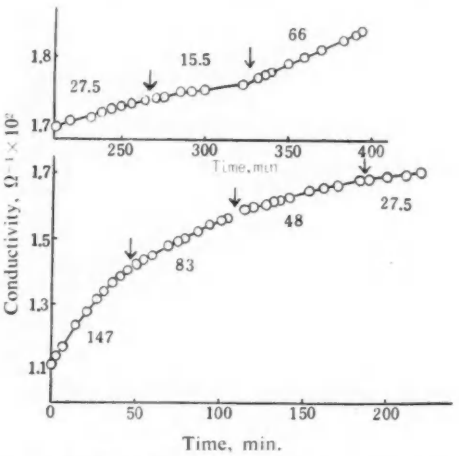

Fig. 4. Conductivity increase by hydrogen at 130°C and the effect of a sudden pressure change. Figures indicate the pressure in mmHg.

TABLE III. VALUES OF n IN THE EXPRESSION, RATE $\propto p^n$ FOR THE DATA IN FIG. 4

Pressure before and after the pressure change (mmHg)	n
147 ⟶ 83	0.82
83 ⟶ 48	0.85
48 ⟶ 27.5	0.85
27.5 ⟶ 15.5	0.88
15.5 ⟶ 66	0.93

An upper limit of the experimental error was ±10%.

Dependence of the Rate of Conductivity Decrease by Reducing Pressure on Temperature.—This may be estimated by the comparison of the rates at different temperatures corresponding to equal numbers of donors. For this purpose we may utilize the results described in Fig. 2, which were used for the determination of E_1. In the same manner as described above, the activation energy of conductivity decrease was estimated as 31 kcal./mol. (Table I).

Variation of the Conductivity with Hydrogen Pressure.—Above 300°C, the rate of conductivity increase on admitting hydrogen was found to be very great, suggesting that in this temperature range the conductivity increased to an equilibrium value may be obtained as a function of pressure in a manner similar to the adsorption equilibrium measurements. Thus hydrogen was introduced at 350°C, and the conductivity was measured at various pressures and a constant temperature by decreasing pressure successively. The results were reproducible when pressure was inversely increased as shown in Fig. 5.

Conductivity Increase by Carbon Monoxide.—Using carbon monoxide, in place of hydrogen, similar measurements were performed. Fig. 6 shows the $\kappa \sim t$ curves at varied temperatures and an approximately constant initial pressure, which gives a value of 25 kcal./mol. for the activation energy of conductivity increase. This

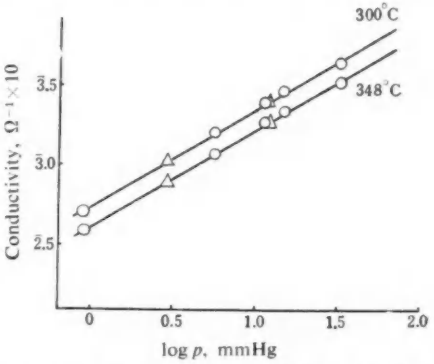

Fig. 5. Conductivity as a function of hydrogen pressure. —○—, on decreasing pressure; —△—, on increasing pressure.

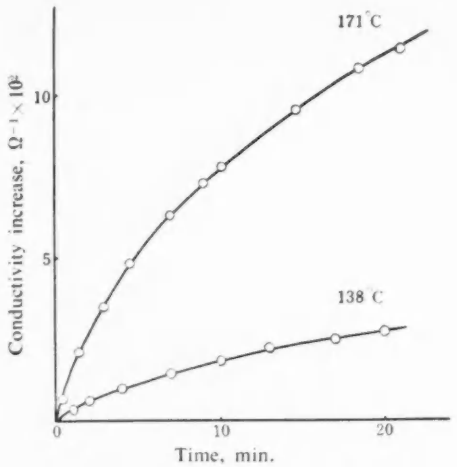

Fig. 6. Conductivity increase by carbon monoxide. Pressure, 1.4 mmHg. The activation energy was estimated as 25 kcal./mol.

may be regarded approximately as that of the formation of donors because of the negligible value of E_1. Almost the same value of activation energy was obtained in the method of a rapid temperature elevation. The conductivity increase was reversible as with hydrogen: by evacuation at 400°C the original conductivity was restored.

Relation between the Hydrogen Chemisorption and the Conductivity Increase.—As described in the previous paper[2], the conductivity enhanced by hydrogen was restored nearly to the original value by pumping out at 400°C. In addition, the conductivity increased to an equilibrium value varies reproducibly on increasing as well as decreasing pressure. These results, together with the fact that the amount of hydrogen adsorbed is almost completely desorbed as such, appear to indicate that this conductivity increase may not arise from the reduction of zinc oxide, but from the hydrogen adsorption of a certain type.

However, from the results obtained in this work, the assumption that the conductivity increase is due to a sort of chemisorption leads to the heat of chemisorption of 10 kcal./mol. and the activation energy of 21 kcal./mol. Relative magnitudes of these values are quite unusual for a chemisorption. Moreover, the activation energy of hydrogen chemisorption obtained from adsorption measurements[4] is 7~10 kcal./mol. in the comparable temperature range 100~140°C, and hence markedly less than the above value of 21 kcal./mol. These considerations suggest that the conductivity increase is not directly related to the hydrogen chemisorption of any type, and that the hydrogen uptake associated with the conductivity increase, if any, is only a negligible portion of the total uptake. It seems therefore necessary to modify the conclusion drawn from the earlier conductivity measurements[2] that two types of chemisorption exist, one of them being responsible for the conductivity increase while the other is not.

As described in the previous paper[2], the rate of adsorption and the adsorbed amount decrease with any increase in temperature up to 110°C, but increase at higher temperatures. Although such behavior, apparently, is adequately explainable in terms of the two types of chemisorption, this can not be the only explanation. Now that the heterogeneity of zinc oxide surface is undeniable through desorption measurements, the concept of single type chemisorption on a heterogeneous surface seems to present a more probable explanation. In addition, as previously described[2], the change in the activation energy of desorption is continuous, in contrast with that of carbon monoxide for which the presence of the two types of chemisorption was confirmed[5]. This again appears to favor the concept of single type chemisorption on a heterogeneous surface.

Nature of the Conductivity Increase by Hydrogen.—As regards the nature of the conductivity increase, an interpretation is that hydrogen atoms diffuse as protons into the lattice close to the surface, as suggested by various workers[6]. However, such an interpretation may not easily be reconciled with the following results obtained: The rate of conductivity increase is proportional to $p^{0.85}$; essentially the same behavior is observed with carbon monoxide on zinc oxide where there is no possibility of dissolution into crystals; in addition, this conductivity increase is an exothermic phenomenon, in contrast with hydrogen dissolution into a crystal of zinc oxide which is an endothermic phenomenon, as reported by Mollwo and others[7].

At present, the most plausible interpretation of the conductivity increase seems to be that proposed by Thomas et al.[8], who attributed it to the surface reduction of zinc oxide. This possibility was excluded previously on the basis of the fact that no water vapor was detected on desorption and that the conductivity increase was reversible. However, the amount of hydrogen uptake is a negligible portion of the total uptake as shown above. Hence such a

6) e.g., F. S. Stone, "Chemisorption", edited by W. E. Garner, Butterworths Scientific Publications, London (1957), p. 181.
7) E. Mollwo, *Z. Physik.*, **138**, 478 (1954); D. G. Thomas and J. J. Lander, *J. Chem. Phys.*, **25**, 1136 (1956).
8) D. G. Thomas and J. J. Lander, *J. Phys. Chem. Solids*, **2**, 318 (1957).

small amount of water vapor will not be detectable. Moreover, the recovery of the original conductivity by pumping out at high temperature and the reproduction of the conductivity on increasing and decreasing pressure may be explained on the assumption that zinc atoms produced by reduction evaporate rapidly at high temperature. This seems to be a plausible assumption, since the reduction is probably confined to the surface layer[9,10].

This interpretation may be applied in the temperature range above 100°C, but a slight conductivity change observed below this temperature described in the previous paper[2] probably arises from the chemisorption of hydrogen, although this behavior has not been studied in detail.

Summary

The rate of increase in conductivity of zinc oxide caused by hydrogen was found to be proportional to $p^{0.85}$ and to have an activation energy of 21 kcal./mol. For this system the activation energy of the increase of donors was shown to be almost the same as that of the conductivity increase. The activation energy of the decrease of donors by evacuation was 31 kcal./mol. A similar conductivity increase was observed with carbon monoxide. On the basis of these results together with those of adsorption measurements reported previously, it was concluded that the conductivity increase was scarcely related at all to the hydrogen chemisorption, indicating that it is untenable to postulate two such types of hydrogen chemisorption as was believed in the previous work, i. e., one responsible for the conductivity increase and the other without such effect. As for the cause of the conductivity increase, the surface reduction of zinc oxide was suggested.

The author wishes to express his sincere thanks to Professor O. Toyama for his guidance and encouragement throughout the course of this study.

Department of Applied Chemistry
College of Engineering
University of Osaka Prefecture
Sakai-shi, Osaka

9) The conductivity increase observed on the oxidized state described in a previous paper[1] may also be attributed to the surface reduction of zinc oxide.

10) According to the previous work[2], the activation energy of the conductivity increase is 25 kcal./mol., being somewhat different from the value of 21 kcal./mol. found in the present work. Considering that this activation energy is a composite quantity including the activation energy of adsorption and that of the surface reduction, this difference may be explained by different proportions of the contributions of the two processes.

Effect of Oxygen Pretreatment on Hydrogen and Carbon Monoxide Chemisorption on Zinc Oxide

By Yutaka KUBOKAWA

(Received September 9, 1959)

Since the treatment of an electron barrier layer was suggested for the chemisorption on semiconductors by Hauffe, Weisz, and others[1], the chemisorption and catalysis on oxide catalysts have been discussed on the basis of this model, and the relation between the catalytic activities of oxides and their properties as semiconductors have been emphasized by a number of workers[2,3]. As for the catalysis by zinc oxide, Parravano and others[4] found that the activity towards hydrogen-deuterium exchange reaction increases with its electrical conductivity. On the basis of these results, Hauffe[2] emphasized the fact that the properties of oxides as semiconductors play a large part in determining the activity towards this reaction.

However, for hydrogen or carbon monoxide chemisorption on zinc oxide which belongs to a "cumulative chemisorption", the barrier is so thin that it is doubtful whether this model

1) K. Hauffe and H. J. Engell, *Z. Elektrochem.*, **56**, 366 (1952); **57**, 763, 773 (1953); P. Aigrain and C. Dugas, ibid., **56**, 363 (1952); P. B. Weisz, *J. Chem. Phys.*, **21**, 1531 (1953).

2) K. Hauffe, *Angew. Chem.*, **67**, 189 (1955).

3) F. S. Stone, "Chemistry of the Solid State", edited by W. E. Garner, Butterworths Scientific Publications, London (1955), p. 367; T. Takaishi, *Z. Naturforsch.*, **11a**, 286, 297 (1956).

4) E. Molinari and G. Parravano, *J. Am. Chem. Soc.*, **75**, 5233 (1953); L. F. Heckelsberg, A. Clark and G. C. Bailey, *J. Phys. Chem.*, **60**, 559 (1956).

will be applicable to such systems. It appears more likely that covalent-bonding, similar to that in the chemisorption on metals determines the behavior of these systems, as pointed out by several workers[5].

It was aimed in the present work to obtain unambiguous information on the relation between the electronic state of zinc oxide and the chemisorption of hydrogen as well as carbon monoxide. For this purpose, the effect of high temperature oxygen treatment of zinc oxide was investigated, inasmuch as it is well established that such treatment markedly reduces the electrical conductivity of zinc oxide.

The present work was designed with another object in addition to that stated above. As regards hydrogen chemisorption on zinc oxide, Morrison[6] proposed a model, according to which the chemisorption means nothing but an interaction of hydrogen with adsorbed oxygen remaining after high temperature evacuation in the form of O^-_{ads} or O^{2-}_{ads}. This mechanism may be written as

$$O^-_{ads} + 1/2\,H_2 \rightarrow OH^-_{ads}$$

$$O^{2-}_{ads} + 1/2\,H_2 \rightarrow OH^-_{ads} + \text{electron}$$

He is of the opinion that the two types of chemisorption for this system as described by Taylor et al.[7], may be explained in terms of these two processes. According to Garner[8], however, OH_{ads} produced by the interaction of hydrogen with adsorbed oxygen is irreversible, in contradiction to Morrison's view. It may then be expected that the present study of the effect of oxygen treatment on hydrogen chemisorption would also serve to solve this problem.

Experimental

Materials.—For zinc oxide, ZnO I described in a previous paper[9] was used. Hydrogen and carbon monoxide were prepared and purified as in the previous work[9,10]. Oxygen was obtained by the electrolysis of 30% potassium hydroxide solution, and purified in the same manner as hydrogen.

Apparatus and Procedure.—The apparatus used in the present work was the same as that used in the previous work[9] except that a Pirani gauge was attached to the flask in which the gas desorbed was collected. By measuring the voltage required to balance the bridge, the composition of the desorbed gas could be calculated from the calibration curves for hydrogen and oxygen.

5) D. A. Dowden, N. Mackenzie and B. M. W. Trapnell, *Proc. Roy. Soc.* **A237**, 245 (1956); F. S. Stone, loc. cit.
6) S. R. Morrion, "Advances in Catalysis", Vol. 7, Academic Press Inc., New York (1955), p. 259.
7) H. S. Taylor and C. O. Strother, *J. Am. Chem. Soc.*, **56**, 586 (1934); H. S. Taylor and S. C. Liang, ibid., **69**, 1306 (1947).
8) W. E. Garner, *J. Chem. Soc.*, **1947**, 1239.
9) Y. Kubokawa, This Bulletin, **33**, 546, 550 (1960).
10) Y. Kubokawa, This Bulletin, **33**, 555 (1960).

Results

Effect of Oxygen Pretreatment on the Amount of Hydrogen Adsorbed.—After oxygen adsorption was allowed to proceed for 3 hr. at 450°C and at a pressure of 30 mmHg, the temperature was lowered to 260°C. The system was evacuated for 30 min. at this temperature, and then the chemisorption rate measurements were carried out at room temperature (Run A). After this run, the system was evacuated for 1 hr. at 500°C and similar measurements were taken (Run B). Run B was further followed by evacuation for 15 hr. at 500°C and thereafter the chemisorption rate measurements were repeated (Run C). The results are shown in

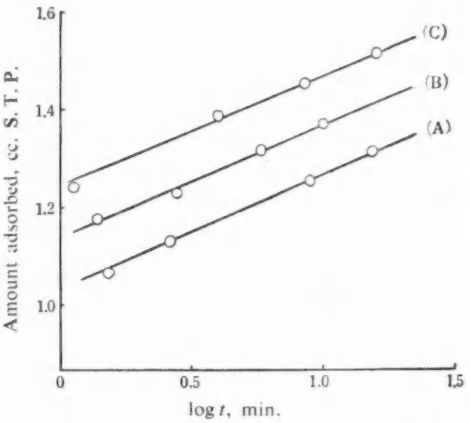

Fig. 1. Effect of oxygen pretreatment on the amount of hydrogen adsorbed at 14°C. Pressure, 20~25 mmHg.

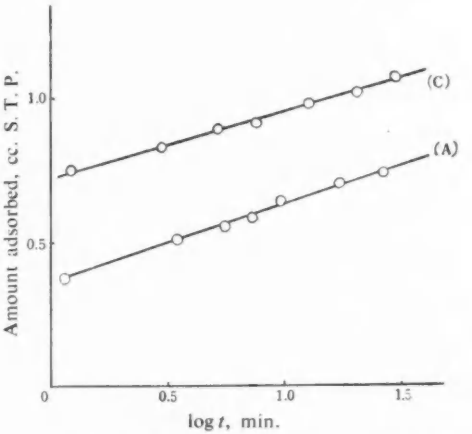

Fig. 2. Effect of oxygen pretreatment on the amount of hydrogen adsorbed at 189°C. Pressure, 20~25 mmHg.

Fig. 1. In these runs the order of the amounts of oxygen adsorbed is expected to be A>B>C. As seen in this figure, the amount adsorbed at a particular time also increases in this order. The amount adsorbed after 16 hr. was 1.95 cc. in run A and 2.21 cc. in run C, showing a slight difference. Fig. 2 represents the results obtained at a higher temperature. It follows from the figure that, in this case too, the decrease in the amount adsorbed after oxygen treatment will become unmarked in a later stage of adsorption.

Effect of Oxygen Pretreatment on the Rate of Desorption of Hydrogen.—After hydrogen was allowed to be chemisorbed at room temperature on the specimen pretreated with oxygen at 450°C followed by evacuation at 260°C, the activation energies of desorption at various coverages were determined in the manner described previously[9]. For comparison, similar measurements were carried out with the specimen before such pretreatment. Allowing for the different amounts initially adsorbed on these specimens, the activation energy of desorption was plotted in each case against the ratio of the amount desorbed to that initially adsorbed. As seen in Fig. 3, the results obtained with the two specimens were essentially indentical. Moreover, the comparison at various temperatures between the amount desorbed from the two specimens before the rates of desorption fell to a particular value shows, as seen in Table I, that there is no marked difference between the rates of desorption from these specimens. It may therefore be concluded that the rate of desorption as well as its activation energy is scarcely affected at all by oxygen treatment of the adsorbent at a temperature as high as 450°C.

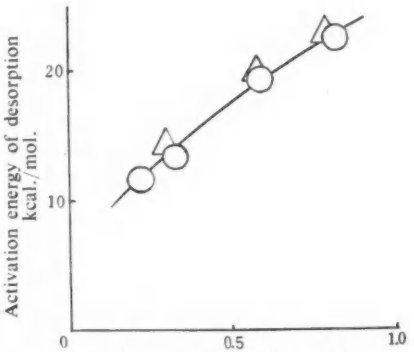

Fig. 3. Effect of oxygen pretreatment on the activation energy of desorption of hydrogen.
-○-, before oxygen pretreatment; -△-, after oxygen pretreatment. The amount of hydrogen adsorbed before desorption was 2.15 cc. before pretreatment and 1.82 cc. after pretreatment.

TABLE I. RATIO OF THE AMOUNT DESORBED BEFORE THE RATE OF DESORPTION FELL TO 3.73×10^{-3} cc. S. T. P./min. TO THE AMOUNT ADSORBED BEFORE DESORPTION

Temp. of desorption (°C)	−30	20	71
Before oxygen pretreatment	0.323	0.572	0.759
After oxygen pretreatment	0.295	0.582	0.741

Interaction of Hydrogen with Adsorbed Oxygen.—After hydrogen was allowed to be chemisorbed at room temperature, the temperature of the system was raised up to 400°C, and after several hours it was again lowered to room temperature. Then the amount of gas desorbed during the temperature elevation up to 400°C was measured and its composition was analyzed by means of the Pirani gauge. These measurements were carried out with a specimen which had been subjected to the same oxygen treatment as that used in the experiment shown in Fig. 1. The results are shown in Table II. In the Runs A and B the gas desorbed below 400°C consisted solely of hydrogen, while above 400°C a considerable amount of water was detected in the gas desorbed and its uncondensable fraction was found to be almost entirely oxygen. This indicates the occurrence of an irreversible chemisorption of hydrogen, the extent of which may be estimated from the amounts not removed by pumping out at 400°C. As seen in Table II, the amount of irreversible chemisorption increases with that of the oxygen adsorbed. On the other hand, in Run C where little or no oxygen remained adsorbed, no water vapor was detected even above 400°C, suggesting that hydrogen chemisorption was completely reversible in this case.

TABLE II

	Amount absorbed at room temp. before desorption (1)	Amount desorbed below 400°C (2)	Residual amount adsorbed (1)—(2)
Run A	3.94	3.48	0.46
Run B	3.85	3.54	0.31
Run C	4.10	3.96	0.14

Amount adsorbed is in cc. S. T. P. The order of the amounts of oxygen adsorbed is A>B>C.

Effect of Oxygen Pretreatment on Carbon Monoxide Chemisorption.—As described in the

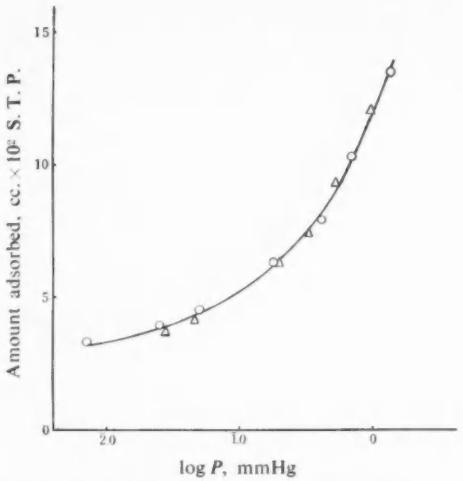

Fig. 4. Effect of oxygen pretreatment on carbon monoxide chemisorption at 15°C. -○-, before oxygen pretreatment; -△-, after oxygen pretreatment.

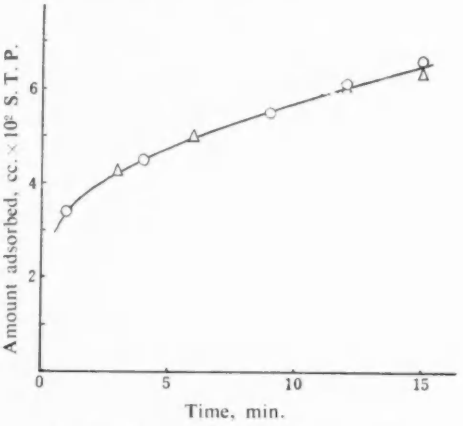

Fig. 5. Effect of oxygen pretreatment on carbon monoxide chemisorption at 90°C. -○-, before oxygen pretreatment; -△-, after oxygen pretreatment. Pressure, 0.1 ~0.2 mmHg.

previous paper[10], there are two types of chemisorption for carbon monoxide, one of them being a non-activated adsorption at low temperature, and the other an activated absorption at high temperature. The effect of oxygen treatment was therefore investigated in the following two ways. Fig. 4 shows the effect on the adsorption isotherm at room temperature obtained on a desorption branch, such as was described previously. It follows from this figure that the oxygen treatment has no effect on the chemisorption of low temperature type, in agreement with the results obtained by Garner et al.[11] For the chemisorption of high temperature type, similar results were obtained, as shown in Fig. 5. Oxygen treatment in this case was conducted at 450°C, followed by evacuation at 260°C.

Discussion

If the electronic state of zinc oxide had played a large part in determining the behavior of hydrogen chemisorption, the amount adsorbed as well as the rate of desorption of hydrogen would have been seriously affected by oxygen treatment at high temperature, in contradiction to what was found actually in this work. It may therefore be concluded that the change of the electronic state of zinc oxide has little or no effect on hydrogen chemisorption.

This conclusion in turn suggests that a slight decrease in the amount adsorbed caused by the oxygen treatment is not due to the change of the concentrations of electrons. In view of the existence of surface heterogeneity in this system as revealed in a previous work[9], this decrease may probably be ascribed to the variation of the distribution function of sites, although details of the variation are unknown at present.

According to Parravano et al.[4], the activity of zinc oxide towards hydrogen-deuterium exchange reaction decreases markedly after oxygen treatment. On the basis of the considerations given above, it seems unlikely that this decrease in the catalytic activity is attributed to the change of the concentrations of free electrons. In addition, the extent of decrease in the activity after oxygen treatment as reported by these authors appears to be markedly greater than that in the amount of hydrogen adsorbed in the present work, although there may be more or less uncertainty in such comparisons, as no measurements with the same specimen of zinc oxide were carried out. Such a marked difference, if it is real, suggests that only a negligible portion of the total amount of hydrogen adsorbed is responsible for the exchange reaction, in agreement with what may be expected from the surface heterogeneity established for this system.

Various workers[12] have emphasized the fact that hydrogen chemisorption on zinc oxide is confined to interstitial zinc atoms or F-centers which probably exist after evacuation at high temperature. The observation in this work

11) W. E. Garner and J. Maggs, *Trans. Faraday Soc.*, 32, 1744 (1936).
12) J. H. de Boer, "Advances in Catalysis", Vol. 8 (1956), p. 18; W. E. Garner, "Advances in Catalyss", Vol. 9 (1957), p. 169.

that the amount adsorbed is not seriously affected by the oxygen treatment indicates that such interpretation is unjustifiable.

The decrease in the amount of hydrogen adsorbed after oxygen treatment and the increase of the extent of irreversible adsorption with the increasing amount of oxygen adsorbed suggest that Morrison's mechanism is unjustifiable and that OH_{ads}, produced by the interaction of hydrogen with adsorbed oxygen, is irreversible and desorbed as water above 400°C, in accordance with Garner's view.

As for carbon monoxide chemisorption, the results obtained in the present work indicate again and still more clearly that this chemisorption is not affected by the electronic state of zinc oxide. Moreover, these results together with the fact that the amount adsorbed at $\theta=1$, estimated from the isotherms, amount to about a half of the amount of nitrogen adsorbed in a monolayer determined by the B. E. T. method as previously described[10] suggest that carbon monoxide chemisorption is not confined to special active sites, e. g., interstitial zinc atoms or F-centers, but the entire surface of zinc oxide participates in the chemisorption.

Finally, with respect to the change of the catalytic activity of zinc oxide caused by the addition of small amounts of Li_2O or Al_2O_3 as shown by a number of workers, the results presented here, seem to indicate that it is doubtful in some cases that this effect can be attributed to the change of the electronic state of zinc oxide caused by the addition.

Summary

The effect of oxygen treatment at about 500°C of zinc oxide upon the chemisorption of hydrogen as well as of carbon monoxide was investigated in order to clarify the relation between the electronic state of the adsorbent and the chemisorption. In the case of hydrogen chemisorption, the amount adsorbed was reduced only slightly and the rate of desorption remained practically unaltered after oxygen treatment. On carbon monoxide chemisorption the oxygen treatment gave no effect. It was concluded from these results that both the chemisorption of hydrogen and that of carbon monoxide are essentially independent of the electronic state of zinc oxide. On the basis of such a conclusion combined with other results, the inapplicability of the model of hydrogen chemisorption proposed by Morrison was pointed out.

The author wishes to express his sincere thanks to Professor O. Toyama for his guidance and encouragement throughout the course of this study.

Department of Applied Chemistry
College of Engineering
University of Osaka Prefecture
Sakai-shi, Osaka

Hydrogen Chemisorption on $ZnO \cdot Cr_2O_3$, $ZnO \cdot MoO_3$ and Cr_2O_3

By Yutaka KUBOKAWA

(Received September 9, 1959)

In previous papers[1] hydrogen chemisorption on zinc oxide was studied by measuring the rate of adsorption, adsorption equilibrium and the rate of desorption, which made it possible to obtain quantitative information on the energy relation for this system. The behavior of desorption under various experimental conditions suggested the existence of a heterogeneity of the surface, the nature of which was such that the activation energy of adsorption and the heat of adrorption varied in the same direction, in contrast with carbon monoxide chemisorption on zinc oxide where these quantities varied in the reverse direction to each other.

It seemed then desirable to ascertain whether the conclusion obtained with zinc oxide is generally applicable to hydrogen chemisorption on oxides or not. As a first step in such an investigation, the hydrogen chemisorption was measured with $ZnO \cdot Cr_2O_3$, $ZnO \cdot MoO_3$ and Cr_2O_3, in the same manner as with zinc oxide and the results obtained are reported in this paper.

Experimental

Materials. — $ZnO \cdot Cr_2O_3$ and $ZnO \cdot MoO_3$ were prepared in the same way as described in the previous work[2]. Cr_2O_3 was prepared by controlled

1) Y. Kubokawa, This Bulletin, 33, 546, 550 (1960).

2) Y. Kubokawa and O. Toyama, *J. Phys. Chem.*, 60, 833 (1956).

ignition of CrO_3 of extra pure grade in a stream of dry air at 450°C as described by Bevan et al.[3] The gases were obtained as described in the previous papers[1]. The weight of the adsorbent and surface area determined by the B. E. T. method using nitrogen adsorption were as follows: $ZnO \cdot Cr_2O_3$, 6.71 g., 28 m^2/g.; $ZnO \cdot MoO_3$, 8.83 g., 13 m^2/g.; Cr_2O_3, 14.13 g., 17 m^2/g.

Apparatus and Procedure.—Details of the apparatus and procedure were described in the previous papers[1]. Before a series of experiments, all the adsorbents were subjected to repeated pretreatments with hydrogen at 450°C followed by evacuation at this temperature.

Results and Discussion

Dependence of Chemisorption Rate on Temperature.—The problem was investigated in two ways, one comparing, as usual, the rate at varied temperatures after admission of a known amount of hydrogen to a degassed sample and the other observing the rate increase caused by an abrupt temperature elevation during an adsorption rate measurement as previously applied to hydrogen chemisorption on zinc oxide. Measurements making use of the former method were already carried out in the previous work[2] with the following results: With $ZnO \cdot Cr_2O_3$ an instantaneous chemisorption followed by a slow process occurred and apparent activation energies of adsorption in the low and high temperature ranges were 7 and 13~16 kcal./mol., respectively, while with $ZnO \cdot MoO_3$, only a slow chemisorption with an activation energy of 28 kcal./mol. was observed.

Figs. 1 and 2 represent the results obtained by the latter method: After hydrogen was allowed to be adsorbed at room temperature, the temperature was raised up in stages. As seen in Fig. 1, in the case of $ZnO \cdot MoO_3$ the amount of rapid desorption due to the abrupt temperature raise is negligibly small, and the rate of slow uptake increases steadily with temperature as in the carbon monoxide chemisorption on zinc oxide described previously[4]. Similar behavior was observed on Cr_2O_3. On the other hand, the result obtained with $ZnO \cdot Cr_2O_3$ is similar to that for hydrogen chemisorption on zinc oxide, as seen in Fig. 2. Here on increasing the temperature a rapid desorption was followed by the occurrence of a slow

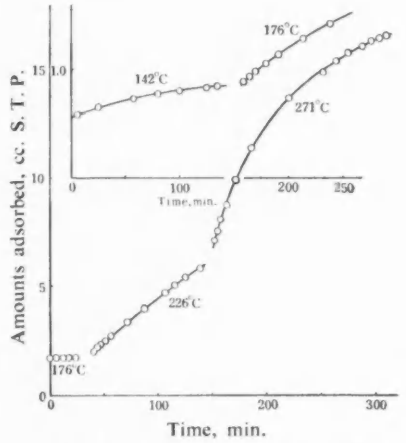

Fig. 1. Effect of temperature change during adsorption on the rate of hydrogen chemisorption on $ZnO \cdot MoO_3$. Pressure, 60~80 mmHg. Run at 176°C was interrupted by cooling the adsorbent to room temperature.

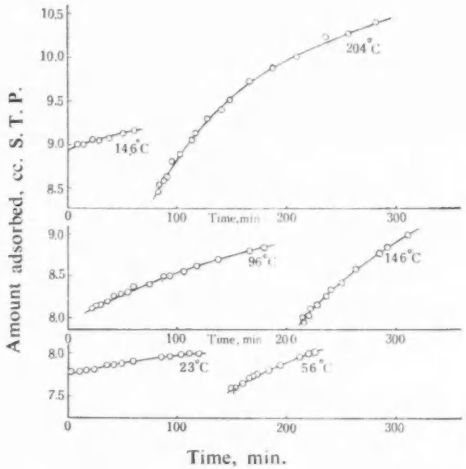

Fig. 2. Effect of temperature change during adsorption on the rate of hydrogen chemisorption on $ZnO \cdot Cr_2O_3$. Pressure, 60~80 mmHg. Both after the run at 56°C and during that at 146°C, the rate measurement was interrupted by cooling the adsorbent to room temperature.

TABLE I. ACTIVATION ENERGIES OF ADSORPTION

Adsorbent	Temp. range °C	Activation energy of adsorption kcal./mol.
$ZnO \cdot MoO_3$ (Fig. 1)	142~176	14.5±1.0
	176~226	23 ±1.5
	226~271	25 ±1.5
Cr_2O_3	160~205	13 ±1.5
$ZnO \cdot Cr_2O_3$ (Fig. 2)	23~ 56	8.0±1.0
	96~146	9.5±1.0
	146~204	12 ±1.0

3) J. M. Bevan, J. P. Shelton and J. S. Anderson, *J. Chem. Soc.*, **1948**, 1729.

4) Y. Kubokawa, This Bulletin, 33, 555 (1960).

uptake. Apparent activation energies were determined by a method similar to that described in the previous papers[1], i.e., by comparison of the rates at different temperatures, corresponding to equal amounts of the slow chemisorption. The results obtained are shown in Table I.

Although a rapid desorption on an abrupt temperature raise is observed with $ZnO \cdot Cr_2O_3$, which shows, on the whole, a normal pattern of an activated adsorption according to the previous work[2], i.e., except in the temperature range 80~110°C, the rate of adsorption increases steadily with temperature. In addition, both methods of obtaining the dependence of rate on temperature give similar values of activation energy, contrary to the results for zinc oxide. This may be attributed to a much smaller proportion of the amount desorbed rapidly on raising the temperature to the amount adsorbed before the temperature rise.

Dependence of Chemisorption Rate on Pressure.—As described in previous papers[1,4], the pressure dependence was determined by observing the rate change caused by an abrupt pressure change during adsorption. As an example, the results obtained with $ZnO \cdot MoO_3$ are shown in Fig. 3. The comparison of the rates at different pressures corresponding to equal amounts of slow uptake gives the pressure dependence, with the results listed in Table II.

With $ZnO \cdot MoO_3$, the rate was found to be proportional to $P^{0.8}$ on both increasing and decreasing pressure, indicating that desorption is negligible during adsorption. The results obtained with Cr_2O_3 were similar. In the case of $ZnO \cdot Cr_2O_3$, it is clear that desorption can not be neglected, since on decreasing pressure the exponent n in the expression Rate $\propto P^n$ is, markedly larger than the value when desorption is negligible, namely 0.8, and on increasing pressure too, a value somewhat greater than 0.8 was obtained, as seen in Table II.

Activation Energies of Desorption at Various Coverages.—The temperature of the adsorbent which had already adsorbed hydrogen at about

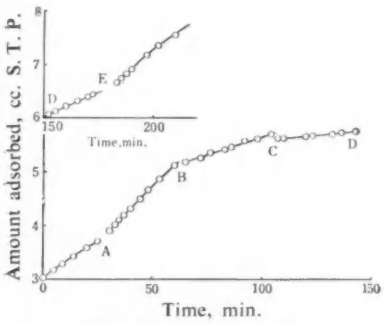

Fig. 3. Effect of pressure change during adsorption on the rate of hydrogen chemisorption on $ZnO \cdot MoO_3$. Temp., 228°C. Pressures before and after the pressure change are shown in Table II.

TABLE II. VALUES OF n IN THE EXPRESSION, RATE $\propto P^n$

Adsorbent		Pressure before and after the pressure change, mmHg	n
$ZnO \cdot MoO_3$*	(A)	27.0 →73.2	0.77
(Fig. 3)	(B)	64.8 →19.0	0.80
	(C)	15.4 → 4.6	0.81
	(D)	3.7 →27.7	0.83
	(E)	24.2 →67.5	0.79
$ZnO \cdot Cr_2O_3$		20.5 →86.5	0.95±0.1
		77.1 →49.2	2.5 ±0.5

* An upper limit of the error was ±7%.

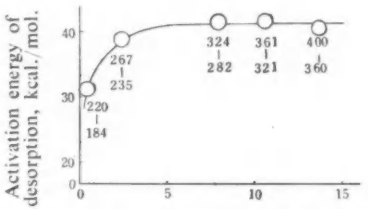

Fig. 4. Activation energies of desorption of hydrogen chemisorbed on $ZnO \cdot MoO_3$. The amount adsorbed and equilibrium pressure at room temperature before desorption were 15.42 cc. and 22.0 mmHg, respectively. Figures indicate the temperature interval where the activation energy was determined.

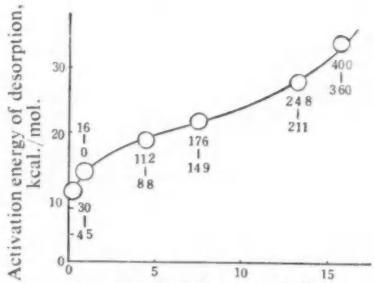

Fig. 5. Activation energies of desorption of hydrogen chemisorbed on $ZnO \cdot Cr_2O_3$. The amount adsorbed and equilibrium pressure at room temperature before desorption were 16.82 cc. and 42.3 mmHg respectively. Figures indicate the temperature interval where the activation energy was determined.

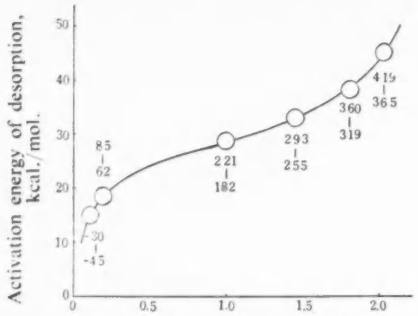

Fig. 6. Activation energies of desorption of hydrogen chemisorbed on Cr_2O_3. The amount adsorbed and equilibrium pressure at room temperature before desorption were 2.18 cc. and 36.4 mmHg respectively. Figures indicate the temperature interval where the activation energy was determined.

400°C was raised up from −72 to about 400°C in stages at each of which the activation energy of desorption was determined in the same manner as described previously[1]. The results obtained are shown in Figs. 4, 5 and 6. For all the systems studied in the present work, it was confirmed that adsorption could be neglected during desorption rate measurement as in the case of hydrogen chemisorption on zinc oxide. In the case of $ZnO \cdot MoO_3$, the amount desorbed with an activation energy less than 30 kcal./mol. is a negligible fraction of the total amount desorbed. In addition, the greater part of the chemisorbed hydrogen desorbs with an approximately constant activation energy of 41 kcal./mol. On the other hand, for the other systems, the activation energy of desorption varies considerably with the amount desorbed, i.e., for $ZnO \cdot Cr_2O_3$ from 10 to 35 kcal./mol. and for Cr_2O_3 from 15 to 45 kcal./mol. Moreover, in the former case a considerable fraction of chemisorbed hydrogen desorbs with a low activation energy of desorption (<20 kcal./mol.), while in the latter, this fraction is negligibly small.

Adsorption Isotherms. — After hydrogen was allowed to be adsorbed at a high temperature, the adsorption isotherm was determined by successive withdrawals of the gas. The isotherm thus determined on the desorption branch was, as in the case of hydrogen chemisorption on zinc oxide, reproducible at increasing as well as decreasing pressure. The results obtained with $ZnO \cdot Cr_2O_3$ and $ZnO \cdot MoO_3$ are shown in Figs. 7 and 8[5]. The

5) The isotherm for Cr_2O_3 was not determined.

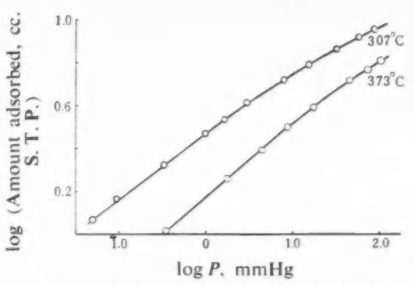

Fig. 7. Adsorption isotherms of hydrogen on $ZnO \cdot Cr_2O_3$ at 307 and 373°C.

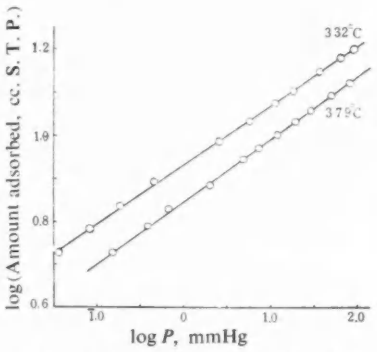

Fig. 8. Adsorption isotherms of hydrogen on $ZnO \cdot MoO_3$.

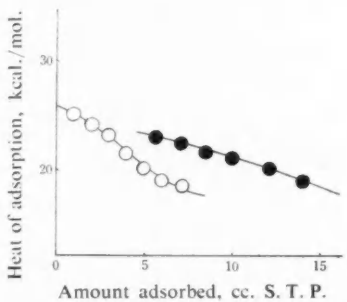

Fig. 9. Heats of adsorption of hydrogen on $ZnO \cdot Cr_2O_3$ and $ZnO \cdot MoO_3$. -○-, $ZnO \cdot Cr_2O_3$; -●-, $ZnO \cdot MoO_3$.

variations of the heat of adsorption determined from these isotherms with the amount adsorbed are represented in Fig. 9.

As seen in Fig. 5, with $ZnO \cdot Cr_2O_3$, the chemisorption with a low activation energy of desorption occurs to a considerable extent. The heat of adsorption for such chemisorption was estimated from the adsorption isotherms at 115 and 85°C, determined in desorption branch with the specimen which had chemisorbed hydrogen at about 300°C. The result

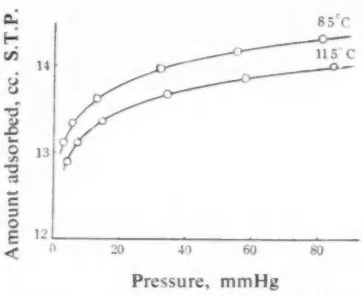

Fig. 10. Adsorption isotherms of hydrogen on $ZnO \cdot Cr_2O_3$ at 85 and 115°C.

obtained is shown in Fig. 10, from which the heat of adsorption is estimated as 7~8 kcal./mol.

Nature of Heterogeneity of the Surface.— The problem was dealt with as described in the previous papers[1,4]: At a particular temperature, hydrogen was left in contact with the adsorbent for some time; then, by pumping a known amount of gas from the system, the desorption rate was measured. The measurement was conducted with various times for each adsorbent. The results obtained with $ZnO \cdot MoO_3$, as shown in Fig. 11, are similar to those for carbon monoxide chemisorption on zinc oxide: The rate of desorption is greater on the surface with a larger amount adsorbed and there is a marked difference between the value of $d \log R_{dep}/dq$ for the runs of different times of contact with hydrogen. This suggests the existence of a heterogeneity of the surface where the heat of adsorption and the activation energy of adsorption vary inversely to each other as described in the previous paper[4].

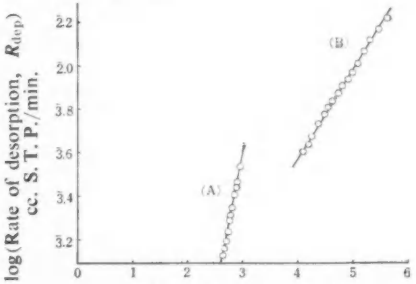

Fig. 11. Rate of desorption of hydrogen chemisorbed on $ZnO \cdot MoO_3$ as a function of the amount left adsorbed. Temp., 266°C. The weight of adsorbent used in these runs was 3.81 g. The amount adsorbed at room temperature before desorption was 3.54 cc. in Run A and 6.41 cc. in Run B. (A) After 30 min.; (B) After 3 hr.

In contrast to the case with $ZnO \cdot MoO_3$, the behavior observed on $ZnO \cdot Cr_2O_3$ was almost identical with that of hydrogen chemisorption on zinc oxide, i. e., a marked difference between the rates of desorption at equal amounts adsorbed after different contact times. Such behavior together with a rapid desorption observed on raising temperature suggests that the existence of an a priori heterogeneity of the surface where the activation energy of adsorption and the heat of adsorption vary in the same direction as was concluded in the previous work[1].

In the case of Cr_2O_3, although the result obtained at 162°C was similar to that with $ZnO \cdot MoO_3$ mentioned above (Fig. 11), at 206°C, somewhat different behavior was observed, as seen in Fig. 12 and Table III. Here in an early stage of adsorption, the proportion of the amount desorbed rapidly to the total amount adsorbed increases as adsorption proceeds, while after one hour since the admission of hydrogen, the situation is reversed, i. e., this proportion is now smaller on the surface with a larger amount adsorbed, indicating that the sites with a higher heat of adsorption are covered in a later stage. This behavior may be explained by assuming that the sites

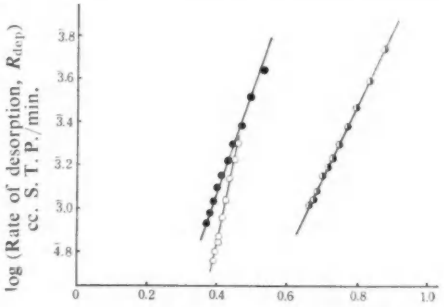

Fig. 12. Rate of desorption of hydrogen chemisorbed on Cr_2O_3 as a function of the amount left adsorbed. Temp., 206°C. Time of contact: -○-, 15 min.; -●-, 50 min.; -◑-, 15 hr.

TABLE III.

Time of contact	Amount desorbed rapidly* cc.	Amount adsorbed at room temp. before desorption cc.
15 min.	0.04	0.55
50 min.	0.27	0.77
15 hr.	0.21	1.05

* This amount was estimated by the amount desorbed before $\log R_{dep}$ fell to $\bar{3}.64$. (cc. S. T. P./min.)

with the highest heat of adsorption are not accessible to the gas phase, but can be reached by a surface or bulk diffusion process from the sites with a lower heat of adsorption. Such an explanation may be more plausible than one assuming that the relationship between the heat of adsorption and the activation energy of adsorption changes abruptly in the final stage of adsorption. Irrespective of the explanation for this phenomenon, it may be concluded that the nature of surface heterogeneity in this system is, in principle, such that the heat of adsorption varies inversely to the activation energy of adsorption, since the desorbed amount in question is only a small fraction of the total amount desorbed.

On the basis of the relationship between the heat of adsorption and the activation energy of adsorption described above, we can estimate the activation energy of adsorption indirectly from the heat of adsorption and the activation energy of desorption. In the case of $ZnO \cdot MoO_3$, from the maximum value of heat of adsorption, 26 kcal./mol., and that of the activation energy of desorption, 41 kcal./mol., the minimum value of the activation energy of adsorption can be estimated as 15 kcal./mol., in agreement with that obtained directly from adsorption measurements. Similar estimation with $ZnO \cdot Cr_2O_3$ yields 10 kcal./mol. as the maximum activation energy of adsorption, in approximate agreement with that directly determined. Considering that for the latter system the minimum activation energy of desorption is 10 kcal./mol. and the minimum heat of adsorption will be below 7 kcal./mol., it may be concluded, as in the case of hydrogen chemisorption on zinc oxide, that almost the whole process of chemisorption involves activation energy.

It may be noted that the following correlation is obtained from the results described above and in previous papers[1,4]: When desorption can not be neglected during adsorption, a rapid desorption on an abrupt temperature raise always takes place. Moreover, the presence of the fraction with a low activation energy of desorption is always associated with a rapid desorption on raising the temperature. Such correlation can be expected for the surface heterogeneity, the pattern of which is characterized by a continuous distribution function of sites with the heats of adsorption varying in the same direction with the activation energy of adsorption.

Hydrogen Chemisorption on Oxides. — From the results presented here, combined with those described in previous papers[1], the following common features for hydrogen chemisorption on oxides may be mentioned:

1) On oxides of reduced state, hydrogen chemisorption is reversible, in the sense that hydrogen is desorbed as such. For zinc oxide, this was already described in the previous work[6]. For $ZnO \cdot Cr_2O_3$, $ZnO \cdot MoO_3$ and CrO_3, essentially the same conclusion was obtained although the complete desorption requires a very long time.

2) When desorption is negligible, the rate of chemisorption is proportional to $P^{0.8}$ over a wide range of temperatures, indicating that the rate-determining step is not a sort of surface migration but an adsorption.

3) Almost the whole process of hydrogen chemisorption on oxides involves activation energy which becomes higher as the adsorption proceeds, although its magnitude varies from one oxide to another.

4) There is no evidence to support the existence of two types of hydrogen chemisorption which was believed to exist previously[2]. Although extensive conductivity measurements were not made with $ZnO \cdot Cr_2O_3$ and $ZnO \cdot MoO_3$ as in the case of zinc oxide, the concept of two types chemisorption is not required for these systems either, since all the results can be explained by the concept of single type chemisorption on a heterogeneous surface. The fact that the variation of activation energy of desorption is continuous over the whole range of the amount adsorbed appears to favour this concept.

5) The change of activation energy of adsorption with the amount adsorbed mainly arises from an a priori heterogeneity of the surface and not from the induced heterogeneity or the formation of electrical double layer owing to charge transfer between the gas adsorbed and the surface. At present the reason for the fact that the relation between the heat of adsorption and the activation energy of adsorption varies from one oxide to another is unknown. As regards the chemisorption of hydrogen on oxides other than those studied by the present author, the results obtained in this work may serve to make some prediction. In the cases of MnO and $MnO \cdot Cr_2O_3$ investigated by Taylor et al.[7], the activation energy of adsorption and the heat of adsorption will vary inversely to each other, since a rapid desorption on raising temperature is not observed. The situation with V_2O_3 studied by Tarama and Teranishi[8], may be similar, since the general features of the chemisorption are similar to those with $ZnO \cdot MoO_3$, i. e., the chemisorption measurement is possible

6) Y. Kubokawa, This Bulletin, 33, 743 (1960).
7) H. S. Taylor and A. T. Williamson, *J. Am. Chem. Soc.*, 53, 2168 (1931).
8) K. Tarama and S. Teranishi, *J. Chem. Soc. Japan, Ind. Chem. Sec.*, (*Kogyo Kagagu Zasshi*), 55, 376 (1952).

only above 200°C, and the rate increases steadily with increasing temperature. It may be concluded that the variation of the activation energy and the heat of adsorption in the reverse direction is more frequently encountered in hydrogen chemisorption on oxides.

Summary

For hydrogen chemisorption on $ZnO \cdot Cr_2O_3$, $ZnO \cdot MoO_3$ and Cr_2O_3, the rates of adsorption and desorption, and adsorption equilibrium were investigated. The activation energy of adsorption ranged from 8 to 12 kcal./mol. for $ZnO \cdot Cr_2O_3$, and from 15 to 25 kcal./mol. for $ZnO \cdot MoO_3$. The value for Cr_2O_3 was about 13 kcal./mol. In the cases of $ZnO \cdot MoO_3$ and Cr_2O_3, where desorption is negligible during adsorption, the rate of adsorption was proportional to $P^{0.8}$, while with $ZnO \cdot Cr_2O_3$ desorption was found to occur appreciably. The activation energy of desorption increased with a decreasing amount adsorbed from 10 to 35 kcal./mol. for $ZnO \cdot Cr_2O_3$, and from 15 to 45 kcal./mol. for Cr_2O_3, while an approximately constant value of 41 kcal./mol. was obtained with $ZnO \cdot MoO_3$ except in the initial stage of desorption. The maximum heat of adsorption estimated from adsorption isotherms was about 25 kcal./mol. for both $ZnO \cdot Cr_2O_3$ and $ZnO \cdot MoO_3$. For all the systems studied, desorption experiments suggested the existence of surface heterogeneity with the activation energy of adsorption and heat of adsorption varying inversely in the cases of $ZnO \cdot MoO_3$ and Cr_2O_3, while with $ZnO \cdot Cr_2O_3$ the variation in the same direction was observed. On the basis of the results hitherto obtained, the general characteristics of hydrogen chemisorption on oxides were discussed.

The author wishes to express his sincere thanks to Professor O. Toyama for his guidance and encouragement throughout the course of this study.

Department of Applied Chemistry
College of Engineering
University of Osaka Prefecture
Sakai-shi Osaka

Monolayers of Some Cyclic Peptides. Fungisporin and Gramicidin J_1

By Shoichi IKEDA and Toshizo ISEMURA

(Received September 19, 1959)

Chemical structures of many naturally occurring cyclic peptides and their modes of biological action have been investigated and elucidated in recent years. While many informations concerning the chain configuration and other properties of linear polypeptides in spread monolayer are obtained, the studies on cyclic peptides on surface are relatively deficient and stimulate our interest in several respects. Spread linear polypeptides are generally accepted to take the β-configuration[1,2] but spread cyclic peptides, unless the size of their rings is large enough, can not accomodate with this configuration. Thus it is desired to examine the configuration of cyclic peptides in the monolayer. Further, it is noticed that while ordinary linear polypeptides form monolayers of a condensed type owing to the intramolecular hydrogen bonding, the presence of prolyl residue[3] or ionized amino acid residue[4] in amino acid sequence, causes their monolayers to expand more. It is of importance to investigate whether or not this effect is exhibited in the monolayers of cyclic peptides.

Some investigations on the monolayers of cyclic peptides have been performed mainly by Few[5], but their configurations on the surface have so far been discussed only in the cases of tyrocidine A and B and gramicidin SA and SB[6].

From these points of view, the monolayers of two cyclic peptides, i.e., fungisporin and gramicidin J_1, have been studied by measuring surface pressure, potential and viscosity. Fungisporin[7],

1) C. W. N. Cumper and A. E. Alexander, *Trans. Faraday Soc.*, **46**, 235 (1950).
2) J. T. Davies, *Biochim. Biophys. Acta*, **11**, 165 (1953).
3) T. Isemura and S. Ikeda, This Bulletin, **32**, 178 (1959).
4) T. Isemura and K. Hamaguchi, ibid., **27**, 339 (1954); K. Hamaguchi and T. Isemura, ibid., **28**, 9 (1955); T. Isemura, K. Hamaguchi and S. Ikeda, *J. Polymer Sci.*, **23**, 651 (1957).
5) A. V. Few and J. H. Schulman, *Biochem. J.*, **54**, 171 (1953); A. V. Few, *Biochim. Biophys. Acta*, **16**, 137 (1955); idem., *Proc. Second Int. Cong. Surface Activity*, **2**. CZ 168 (1957), Butterworths Scientific Publications, London.
6) A. V. Few, *Trans. Faraday Soc.*, **53**, 848 (1957).
7) Y. Sumiki and K. Miyao, *J. Agr. Chem. Soc. Japan (Nippon Nogei-kagaku Kaishi)* **26**, 27 (1952); K. Miyao, *Bull. Agr. Chem. Soc. Japan*, **19**, 86 (1955).

isolated from spores of some species of *Penicillium* and *Aspergillus*, is an octapeptide, cyclo-(D-Phe-L-Phe-D-Val-L-Val)$_2$[8]. Gramicidin J_1[9] is a heptapeptide, cyclo-(D-Orn-L-Val-L-Orn-D-Phe-D-Leu-L-Phe-L-Pro)[10]. Fungisporin has given a monolayer of condensed type, whereas gramicidin J_1 that of an expanded type. The behavior of these monolayers has been discussed in the light of the configurations of these cyclic peptides.

Experimental

Fungisporin was prepared by Dr. Miyao and was offered to our disposal. It is soluble only in dichloroacetic acid. As its spreading solvent was used a dichloroacetic acid-benzene (1 : 1 v/v) mixture which was found to be the most suitable for the surface potential measurement. Gramicidin J_1 dihydrochloride was a gift of Professor Otani. It was spread from a methanol solution.

Surface pressure, Π, was measured by a balance of a hanging plate type in higher pressure region, but it was measured by a balance of a float type of a better sensitivity in lower pressure or dilute region. The surface potential, ΔV, was measured by the vibrating electrode method and surface viscosity, η, by the damped rotatory oscillation of a disk. From surface potential, the apparent surface moment, μ, was calculated by the Helmholtz equation

$$\Delta V = \frac{4\pi\mu}{A}$$

where A was the area per amino acid residue.

Results

Fungisporin.—The $\Pi-A$, $\Delta V-A$, $\mu-A$ and $\eta-A$ curves of fungisporin on 0.01 M potassium chloride are shown in Fig. 1. The monolayer was found to be of a condensed type. The condensation of the film may be ascribed mainly to the hydrogen bonding and partly to the cohesion between hydrocarbon side chains. At the region of rise of the $\Pi-A$ curve the surface pressure declined gradually with time after each compression. In Fig. 1 the values at 1 min. per interval are plotted. The delay for attaining a steady surface pressure after each compression has been noticed in some condensed films of long chain substances and of high polymers with long side chain and is, therefore, closely related to the structure of fungisporin. The surface potential was reproducible only at the areas smaller than about 40 Å^2. This is also commonly observed for condensed films of low molecular weight substances, and consequently, consistent with the fact that fungisporin is a small molecule, an octapeptide. The surface viscosity was manifest at the areas below

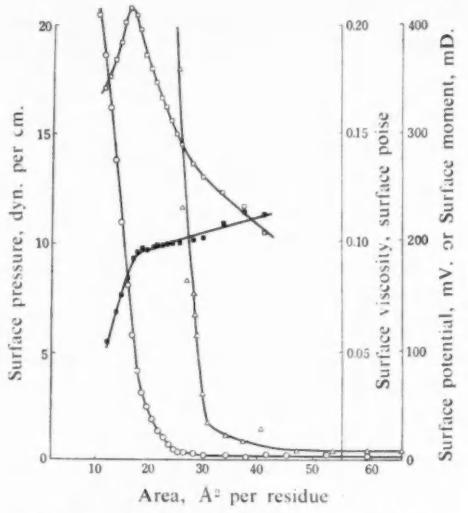

Fig. 1. Monolayer of fungisporin on 0.01 M potassium chloride (14°C). ○ surface pressure; □ surface potential; ■ surface moment; △ surface viscosity.

40 Å^2, where a surface potential was found to be reproducible.

The area, A_μ, where the slope of $\mu-A$ curve suddenly changed was found to be 17.5 Å^2 and the area, $A_{//}$, of the minimum surface compressibility was 16.0 Å^2. These areas are nearly identical with each other and will represent the area occupied by an amino acid residue. The surface moment, μ_c, at the area, A_μ, was 200 mD. Both the area and surface moment are larger than those found for linear polypeptide monolayers.

Gramicidin J_1.—Since gramicidin J_1 contains two ornithyl residues in a molecule, it forms an ionized monolayer on distilled water and an unionized monolayer on aqueous solution at pH higher than 10.5.

The unionized monolayer of gramicidin J_1 on 0.01 M potassium carbonate at pH 11.2 showed a characteristic feature, when a neutral salt such as potassium chloride was added into the aqueous subphase. The effect of the concentration of potassium chloride on the $\Pi-A$ curve is illustrated in Fig. 2. The $\Pi-A$ curve in the absence of neutral salt was smooth, but a break point appeared when potassium chloride was present. The break point was found to be independent of salt concentration and was 27 Å^2 and 5.6 dyn. per cm. In the absence of salt or on 0.001 M potassium chloride, slight time effects were observed in the region of surface pressure higher than the break point. The $\Pi-A$ curves were not altered by salt concentration between 0.01 M and 1 M. In Fig. 3 are

8) K. Miyao, ibid., **24**, 23 (1960).
9) S. Otani and Y. Saito, *Proc. Japan Acad.*, **30**, 991 (1954).
10) S. Otani, "Chemistry of Proteins" ed. by S. Akabori and S. Mizushima, Vol. 5, Kyoritsu Shuppan Co., Ltd., Tokyo (1957), p. 297.

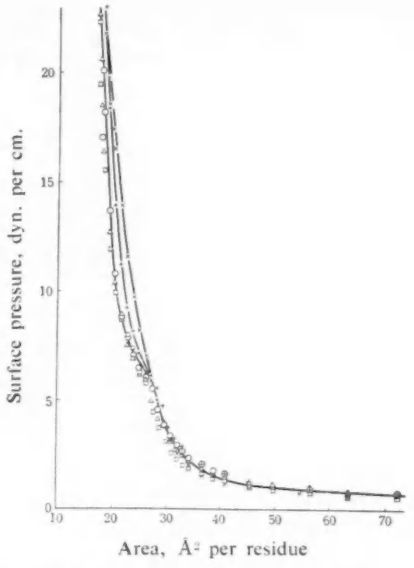

Fig. 2. Effect of potassium chloride on the surface pressure-area curve of gramicidin J_1 on 0.01 M potassium carbonate (15°C). × no salt; + 0.001 M; ○ 0.01 M; △ 0.1 M; □ 1 M.

shown the $\Pi-A$, $\Delta V-A$, $\mu-A$ and $\eta-A$ curves on 0.01 M potassium carbonate when 0.01 M potassium chloride are added. Surface potential was scarcely affected by salt concentration and the corresponding break point such as observed in the $\Pi-A$ curve was not found in both $\Delta V-A$ and $\mu-A$ curves.

It was noticed that the $\Pi-A$ curves of gramicidin SA and SB likewise exhibited the same kind of break points on 1 M potassium chloride at pH 12.5, and the break was attributed to the reorientation of side chains of ornithyl residues[6]. However, no break on the $\Delta V-A$ and $\mu-A$ curves for gramicidin J_1 suggests that the break on the $\Pi-A$ curve would not come from the reorientation of ornithyl residues but presumably from the micelle formation as proposed for fatty acid monolayers[11].

At pH 11.2 where they were unionized, the monolayers of gramicidin J_1 were of an expanded type, as shown in Fig. 2. Correspondingly, the surface viscosity was manifest first in the region of high surface pressures[1,12] as shown in Fig. 3. A constant value of the surface moment was observed over a wide area. The smallest area, A_μ, of constant surface moment was found to be 19.0 Å², the area, $A_{//}$, of minimum surface compressibility to be 20.5 Å² and the gelling area, A_η, to be 20.0 Å². All these areas were scarcely dependent on salt concentrations not less than 0.01 M and nearly identical

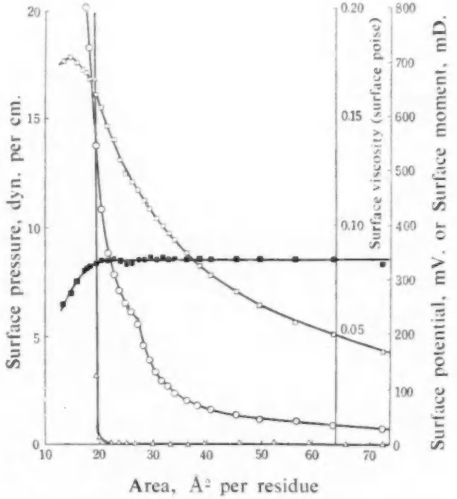
Surface pressure, dyn. per cm.
Surface viscosity (surface poise)
Surface potential, mV. or Surface moment, mD.
Area, Å² per residue

Fig. 3. Monolayer of gramicidin J_1 on 0.01 M potassium carbonate in the presence of 0.01 M potassium chloride (15°C). ○ surface pressure; □ surface potential; ■ surface moment; △ surface viscosity.

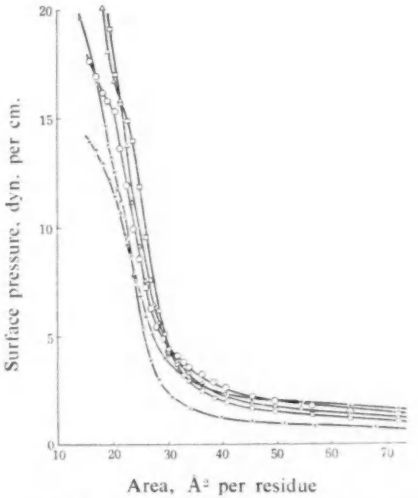

Fig. 4. Effect of potassium chloride on the surface pressure-area curve of gramicidin J_1 on distilled water (15°C). × no salt; + 0.001 M; ○ 0.01 M; △ 0.1 M; □ 1 M.

11) I. Langmuir, *J. Chem. Phys.*, **1**, 756 (1933).
12) S. Ikeda and T. Isemura, This Bulletin, **32**, 659 (1959).

with one another. Consequently, they represent the area occupied by an amino acid residue. The constant surface moment, μ_c, was about 340 mD.

On distilled water at pH 5.6 gramicidin J_1 forms an ionized monolayer. In this case, the monolayer behaves unlike the unionized monolayer but in a quite specific manner, as the salt concentration is varied. The variation of the $\Pi-A$ curves with the concentration of patassium chloride is shown in Fig. 4. In the absence of salt or on 0.001 M potassium chloride, the monolayers were somewhat unstable and had a tendency to dissolve into aqueous subphases on compression. On potassium chloride of the concentrations of 0.01 M to 1 M, however, the monolayers exhibited a typical behavior of ionized monolayer. Monolayers were more condensed at higher salt concentrations and more expanded at lower concentations. The $\Pi-A$ curves pass a reversal point[13], 30.5 Å^2 and 4.3 dyn. per cm.

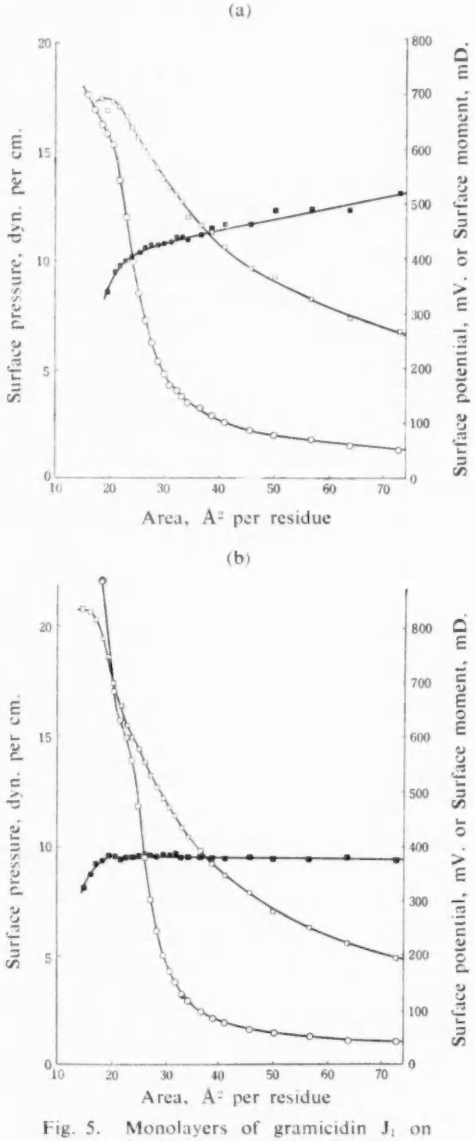
(a)
Surface pressure, dyn. per cm.
Surface potential, mV. or Surface moment, mD.
Area, Å² per residue
(b)
Surface pressure, dyn. per cm.
Surface potential, mV. or Surface moment, mD.
Area, Å² per residue

Fig. 5. Monolayers of gramicidin J_1 on distilled water in the presence of potassium chloride (15°C). a, 0.01 M; b, 1 M. ○ surface pressure; □ surface potential; ■ surface moment.

In Fig. 5 are illustrated some of the $\Delta V-A$ and $\mu-A$ curves together with the $\Pi-A$ curves. The surface moment gave no constant value on 0.01 M potassium chloride but a constant value, 380 mD, on 1 M potassium chloride. On the $\Delta V-A$ and $\mu-A$ curves no significant change was observed at the area corresponding to the reversal point on the $\Pi-A$ curve. The surface viscosity was very low and not detected even at an area as small as 10 Å^2 on 0.01 M potassium chloride.

In the presence of 0.01 M potassium chloride, the ionized monolayer of gramicidin J_1 on neutral subphase was more expanded than the unionized monolayer on 0.01 M potassium carbonate and the surface potential of the former was higher than that of the latter.

Discussion

Configurations of Cyclic Peptides in Monolayer.—The molecular configuration of cyclic peptide has so far been investigated by a polarized infrared spectra[14] and an X-ray diffraction[15] on gramicidin S crystal. The infrared study suggested, that a gramicidin S molecule consists of ten seven-membered rings, each with a hydrogen bond between the imino and carbonyl groups. Few[6] has proposed the configurations of tyrocidines and gramicidin SA in a monolayer in such a way, as the maximum number seven-membered of rings can be formed in a plane and the other peptide bonds can take the β-configuration. We can deduce the configurations of fungisporin and gramicidin J_1 in monolayer in the same way.

In accordance with the above conditions, the configurations of fungisporin in a monolayer are confined to be square-like ones. One of them is illustrated as follows:

13) J. N. Philips and E. Rideal, *Proc. Roy. Soc.*, **A232**, 159 (1955).
14) N. B. Abbott and E. J. Ambrose, ibid., **A219**, 17 (1953).
15) D. Crowfoot-Hodgkin, *Cold Spring Harbor Symp. Quant. Biol.*, **14**, 65 (1950).

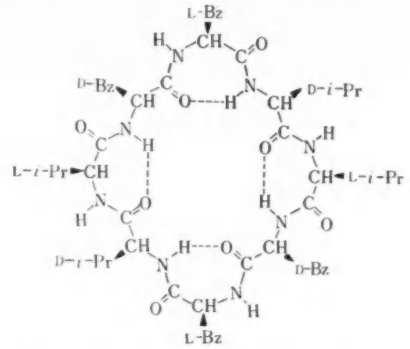

An alternative configuration is obtained by shifting each side chain one by one, in either sence, along the perimeter of this configuration, the orientation of side chains being altered. The other possibilities can be obtained by turning each of these two configurations over. It can not be distinguished which side of the molecular plane is exposed to the air or to the aqueous phase, when the molecule is put on surfaces, and consequently all of these four configurations are equally probable.

The unionized gramicidin J_1 molecule can take only one confiugration in the monolayer, subject to the foregoing requirements:

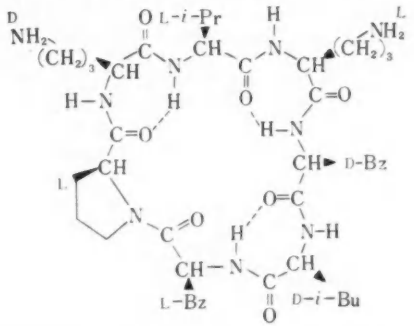

An alternative is obtained by turning of this configuration. In considering the difference of D-leucyl and L-valyl residues in hydrophilic nature, it is a little more favorable to choose the latter configuration (if the air is above the plane).

In all these cases of fungisporin and gramicidin, the areas occupied by a residue are consistent with those obtained experimentally. It is remarkable to note that the side chains of all the D-amino acid residues orientate oppositely to these of all the L-residues with respect to the plane of a molecule. Thus, if the side chain of the L-ornithyl residue in gramicidin J_1 tends towards the aqueous phase, that of the D-ornithyl residue is directed to the air.

Since the formation of a seven-membered ring will force the carbonyl groups to direct towards the aqueous phase, the surface moment is expected to be higher than that of the β-configuration. The surface moment of fungisporin is mainly composed of two different orientations of the carbonyl groups, one hydrogen bonded intramolecularly and the other not participating in hydrogen bonding. It was found to be about 200 mD, which is actually higher than that of the β-configuration, 160 mD[15]. On the other hand, the surface moment of gramicidin J_1 is a mean value of three orientations of carbonyl groups, hydrogen bonded, not hydrogen bonded and belonging to L-phenylalanyl residue, and two amino groups of D- and L-ornithyl residues. The experimental value was very high and 340 mD. It is much higher than 273 mD and 274 mD for gramicidin SA and SB[15]. If the contribution of each carbonyl group is assumed to be equally 200 mD, as in fungisporin, the two amino groups must contribute about 980 mD or, in the average, an amino group about 490 mD. This value would be compared with the surface moments of long chain amines, 300 to 400 mD[16]. However, this value is too high if the opposite directions of two ornithyl residues are taken into account. The reason for this and, accordingly, for the large values of the surface moment, as compared with those of gramicidin SA is not clear.

Condensation and Expansion of the Monolayers. — Fungisporin gave a monolayer of

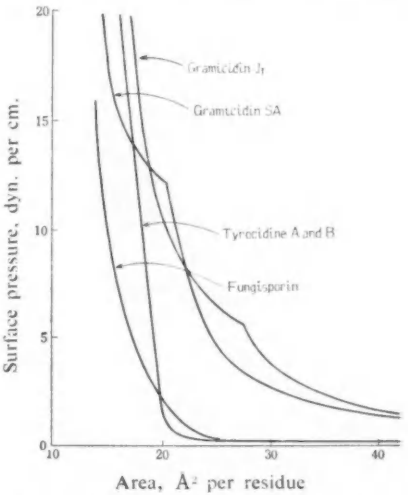

Fig. 6. Surface pressure-area curves of some cyclic peptides. Gramicidin SB gives a nearly identical curve with gramicidin SA.

16) E. F. Porter, *J. Am. Chem. Soc.*, **59**, 1883 (1937); J. Glazer and M. Z. Dogan, *Trans. Faraday Soc.*, **49**, 448 (1953).

condensed type but gramicidin J_1 gave an unionized monolayer of expanded type. It was noticed[6] that tyrocidine A and B formed condensed films on aqueous subphases at the ionic strength 1.0, irrespective of pH, but gramicidin SA and SB formed expanded films under the same condition. These results are summarized in Fig. 6. It was concluded by Few[6] that the expansion of films of cyclic peptides is closely related to the content of ornithyl residues. It is, however, known in the case of unionized linear polypeptides[4] that the L-lysyl residue, which has a longer side chain than the ornithyl residue only by one methylene group, does not influence the type of monolayers but remains to be of a condensed type. We, therefore, no longer regard his proposed explanation as adequate. We have previously observed that the monolayers of synthetic linear polypeptides are transformed gradually from a condensed type to an expanded type as the content of prolyl residue is increased[3,12] and further, this effect is virtually demonstrated in the case of protein films such as gelatin[17]. It can be seen that even for the monolayers of cyclic peptide the prolyl residue plays the same role as for linear polypeptides. In comparing the amino acid composition, fungisporin contains no prolyl residue in a heptapeptide[5], gramicidin J_1 one in an octapeptide[18], both tyrocidine A and B one in a decapeptide[18,19] and gramicidin SA two in a decapeptide[20]. The proportion of prolyl residues in gramicidins are higher than in fungisporin and tyrocidines. Thus the former peptides give more expanded monolayers than the latter. On the contrary, gramicidin SB, whose complete structure is still unknown, but whose monolayer expands to the same extent as gramicidin SA, will have two prolyl residues if it is a decapeptide.

Ionization of Dilute Gramicidin J_1 Monolayer.—Because of the expanded nature of gramicidin J_1 monolayers, it was possible to measure accurately the surface pressure and potential at the region of very large areas. Then the behavior of dilute ionized monolayers of gramicidin J_1 when spread on neutral salt solution can be treated in terms of the theory of the ionized monolayer so far presented.

In general, the surface pressure of an ionized monolayer can be divided into two parts:

$$\Pi = \Pi_0 + \Pi_i$$

where Π_0 is the surface pressure of an unionized monolayer, which is independent of salt concentration, when the other effect is ignored. In this equation the contribution of deformation due to the electric repulsion is not included. The surface pressure due to ionization, Π_i, is, according to the theory of the electric double layer[21,22], given by

$$\Pi_i = 2kT\left\{-\frac{2n}{\kappa}+\sqrt{\left(\frac{2n}{\kappa}\right)^2+\frac{1}{A_i^2}}\right\}$$

where k is the Boltzmann constant, T the absolute temperature, n the salt concentration (molecules per cm^3) and κ the Debye-Hückel parameter. Here A_i is the area per ionized group. Evidently, the surface pressure is lower, as neutral salt is more concentrated in an aqueous phase. However, values of the surface

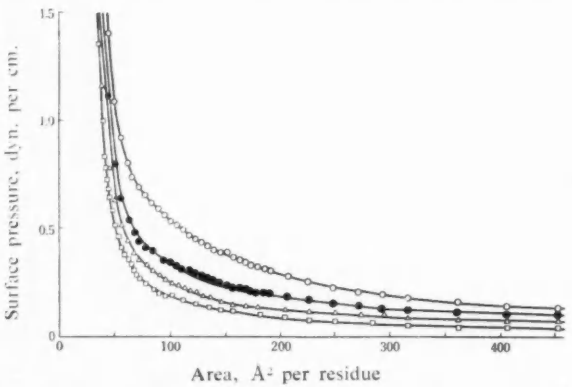

Fig. 7. Effect of potassium chloride on the surface pressure-area curve of dilute gramicidin J_1 monolayer on distilled water (15°C). ○ 0.01 M; ● 0.025 M; △ 0.1 M; □ 1 M.

17) S. Ikeda and T. Isemura, This Bulletin, 33, 137 (1960).
18) A. Paladini and L. C. Craig, *J. Am. Chem. Soc.*, 76, 688 (1954).
19) T. P. King and L. C. Craig, ibid., 77, 6627 (1955).
20) R. Consden, A. H. Gordon, A. J. P. Martin and R. L. M. Synge, *Biochem. J.*, 41, 596 (1947); A. R. Battersby and L. C. Craig, *J. Am. Chem. Soc.*, 73, 1887 (1951).
21) J. T. Davies, *Proc. Roy. Soc.*, A208, 224 (1951).
22) S. Ikeda and T. Isemura, This Bulletin, 33, 131 (1960).

Table I. Surface pressure due to ionization at 200 Å² per residue

n	Π	(A) an ionized residue Π_i	Π_0	(B) two ionized residues Π_i	Π_0
mol./l.	dyn./cm.	dyn./cm.		dyn./cm.	
0.01	0.29	0.230	0.06	0.699	−0.41
0.025	0.19	0.159	0.03	0.550	−0.35
0.1	0.12	0.087	0.03	0.326	−0.21
1	0.07	0.032	0.04	0.111	−0.04

pressure, Π_0, at a constant area, which are obtained by subtracting the calculated values of Π_i from the experimental values of Π, should be independent of salt concentration, even if the salt concentration is varied.

The $\Pi-A$ curves of dilute ionized gramicidin J_1 monolayers on potassium chloride solutions of various concentrations are shown in Fig. 7. The surface pressure is virtually lower at higher salt concentrations. In the monolayer of gramicidin J_1 in an unionized state the two amino groups of ornithyl residues, which are responsible for the ionization of the molecule, are assumed to be oppositely directed to each other. If this configration is still retained in the state of ionization, the electric double layer will be concerned with only one amino group, probably of the L-ornithyl residue. Taking account of this, we have estimated the values of Π_0 at an area, $A=200$ Å², by the foregoing procedure for both cases, that only one ionized amino group ($A_i=7A$) and two ionized groups ($A_i=(7/2)A$) are assumed to concern the electric double layer. The results are given in Table I. In the former case the obtained values of Π_0 are nearly constant and positive, unlike in the latter case. Thus it is likely, that the electric double layer is formed by the ionization of only one amino group and not related to that of the other. This might support the proposed configuration of gramicidin J_1 in monolayer.

According to Schulman and Hughes[23], the surface potential of an ionized monolayer can be expressed by

$$\Delta V=\frac{4\pi\mu_M}{A_i}+\psi_M$$

where μ_M is the surface moment of an ionized group (one or two seventh of the moment per amino acid residue according as one or two ionized ornithyl residues) and ψ_M is the potential of the monolayer. In this equation the first term assumes the ordinary Helmholtz equation and the second term is, according to the theory of electric double layer[21,22], expressed by

$$\psi_M=\frac{2kT}{e}\sinh^{-1}\frac{\kappa}{4nA_i}$$

23) J. H. Schulman and A. H. Hughes, *Proc. Roy. Soc.*, **A138**, 430 (1932).

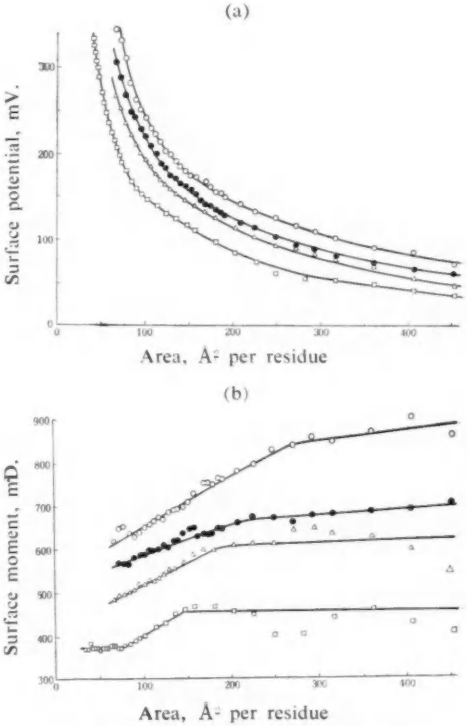

Fig. 8. Effect of potassium chloride on dilute monolayer of gramicidin J_1 (15°C). a, surface potential; b, apparent surface moment. ○ 0.01 M; ● 0.025 M; △ 0.1 M; □ 1 M.

where e is the elementary charge. These equations indicate that the surface potential is lower, as neutral salt is more concentrated in the aqueous phase. In Fig. 8a is shown the variation of the $\Delta V-A$ curves with concentration of potassium chloride in the aqueous phase, which is in accord with the above indication. We have found, however, that the same procedure as done for the surface pressure is not suitable to distinguish whether one or two ornithyl residues concern the electric double layer, since the surface potential can not be measured with sufficient accuracy so as to allow it. Instead of doing so, we have tested the above equations by another method. These

equations show that the apparent surface moment, μ, calculated from $A \cdot \Delta V/4\pi$, generally falls on compression and its value is lower at higher salt concentrations. On highly concentrated salt solutions the apparent surface moment should be constant over a wide region of areas, In Fig. 8b is shown the $\mu - A$ curves for gramicidin J_1 on potassium chloride solutions. Although a minor error in surface potential measurement causes a marked scatter of the surface moment at large areas, it can be seen that the general trend of the $\mu - A$ curves is consistent with the prediction. On such a concentrated salt solution as 1 M, however, the Helmholtz equation appears to be obeyed by the ionized monolayer at areas smaller than 90 A^2 but fails to hold at larger areas.

In addition, it was found that only at moderate areas the ionized monolayer obeys the electrochemical equation[24]

$$\left(\frac{\partial \Delta V}{\partial \ln n}\right)_A = -\frac{kT}{e}$$

as illustrated in Fig. 9.

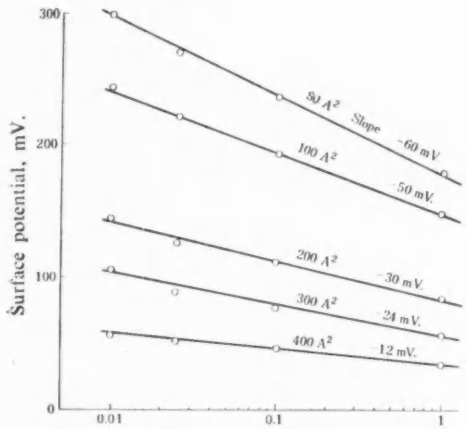

Fig. 9. Surface potential plotted against logarithm of concentration of potassium chloride. Theoretical slope at moderate areas, −57 mV. at 15°C.

Summary

Monolayers of two naturally occurring cyclic peptides, fungisporin and gramicidin J_1, were investigated by the measurements of surface pressure, potential, and viscosity. Fungisporin, an octapeptide composed of phenylalanyl and valyl residues, gave a monolayer of a condensed type. Gramicidin J_1, an electrolytic heptapeptide containing a prolyl and two ornithyl residues, gave an unionized monolayer of an expanded type on an alkaline subphase. It behaved in a somewhat specific manner when neutral salt such as potassium chloride was present.

The configurations of these cyclic peptides in monolayer were suggested in such a way as intramolecular hydrogen bonding could cause a maximum number of seven-membered rings. Then fungisporin can take four possible square-like configurations, which are equally probable, and gramicidin J_1 can take two possible configurations. When these configurations of both peptides are put on surfaces, side chains of all the D-residues always orientate oppositely to those of all the L-residues with respect to the surfaces.

In taking account of the condensation and expansion of these monolayers, together with those of tyrocidine A and B and gramicidin SA, it was concluded that cyclic peptides give more condensed monolayers as the contents of prolyl residue are higher. Thus a prolyl residue plays the same role in cyclic peptides as in linear polypeptides.

Gramicidin J_1 gave a monolayer of more expanded type on a neutral subphase, and exhibited a characteristic behavior common with ionized monolayers when neutral salt such as potassium chloride was added. At very large areas the the behavior was adequately explained by the theory of the electric double layer, when only one ionized residue was assumed to concern the double layer.

The authors are indebted to Professor S. Otani of the Medical School, Osaka City University, and to Dr. K. Miyao of the Faculty of Agriculture, the University of Tokyo, for the gifts of valuable peptides. This work was partly supported by a grant from the Ministry of Education, to which the authors' thanks are also due.

Faculty of Science and
Institute for Protein Research
Osaka University, Osaka

24) D. J. Crisp, Research, "Surface Chemistry", Butterworths Scientific Publications, London (1949), p. 65.

Spectrophotometric Determination of Tellurium(IV) by Extraction with Tributylphosphate

By Seiichiro HIKIME

(Received October 21, 1959)

Several spectrophotometric methods for tellurium determination have been reported[1-7]. However these methods have still some disadvantages, e. g. troubles in separation by precipitation.

In the study of separation of tellurium from iron[8], the authors have found that tellurium-(IV) complex with thiourea is extracted by tributylphosphate (TBP) from a dilute hydrochloric acid solution in the presence of potassium thiocyanate and the yellow color develops more deeply in the TBP phase than in the aqueous phase. When thiourea or potassium thiocyanate exists alone in the solution, tellurium complex is not extracted by TBP, whereas in case where a large excess of thiocyanate ions exists in the solution whose hydrochloric acid concentration is more than 0.1 N, even a small amount of tellurium is extracted by TBP. The coloration thus developed in TBP was applied to the spectrophotometric determination of tellurium.

Experimental

Reagents, Materials and Apparatus.—*Hydrochloric acid and nitric acid.*—A guaranteed reagent is diluted with pure water to the required concentrations.

Potassium thiocyanate solution.—The guaranteed reagent 500 g. is dissolved in pure water and diluted to 1000 ml.

Thiourea solution.—The guaranteed reagent 80 g. is dissolved in water at 70°C and diluted to 1000 ml.

Standard solutions of tellurium(IV).—Metallic tellurium (2 g.) supplied by Nippon Kogyo Co. Ltd., is dissolved in 30 ml. of aqua regia and the solution is evaporated on a water bath. Concentrated hydrochlorlc acid (10 ml.) is added to the residue and the liquid is evaporated to dryness; this procedure is repeated twice in order to expel any traces of nitric acid from the solution. The residue is again dissolved in hydrochloric acid and diluted with pure water. By this procedure two solutions of tellurium are prepared as a stock solution, i. e., 6 N hydrochloric acid solution containing tellurium in a concentration of 10 g./l. and 3 N hydrochloric acid solution containing 2 g. Te/l. Several standard series of tellurium are prepared by diluting one of these stock solutions with dilute hydrochloric acid.

n-Tributyl phosphate (TBP).—TBP is purified by the method reported by Alock et al.[9], and used without dilution after saturation with the reagent solutions under experimental conditions.

A Beckman DU spectrophotometer with 10 mm. cell was used for the measurements of absorbances. pH values were determined by Horiba H-type pH-meter with a glass electrode.

Procedure.—The same volume of TBP with that of the sample solution was used for a single extraction without any organic diluent. Although under the experimental conditions tellurium complex is extracted completely with TBP by shaking in a separatory funnel for 30 sec. The shaking was continued for 2 min. to ensure the extraction. The extraction was carried out only at room temperature.

After extraction, both TBP- and aqueous-phase became turbid to some extent, the extent depending on the initial acidity of the aqueous solution. A clean solution, however, was obtained by centrifuge; this treatment gave no remarkable volume change of the two phases.

Potassium thiocyanate solution is added to a sample solution whose pH was controlled to about 1, to which thiourea solution is added. The solution is finally fitted to a constant volume (10 or 20 ml.) and the pH value adjusted to 1 with hydrochloric acid. After 20 min., the same volume of TBP as that of the aqueous solution is added and the mixture shaken for 2 min. with a shaker. When the TBP phase is separated from the aqueous phase, the former is taken out with a centrifugal separator and the absorbance of tellurium(IV) complex in TBP is measured at 400 mμ.

Results and Discussion

Absorption Spectrum of Tellurium(IV) Complex in TBP.—Hydrochloric acid solutions containing 20, 50 and 100 γ of tellurium per ml. were prepared, and to its 10 ml. portion were added 5 ml. of potassium thiocyanate solution and 4 ml. of thiourea solution. The

1) E. A. Golubtsova, *Zavodskaya Lab.*, **16**, 623 (1950).
2) M. Inarida, *J. Chem. Soc. Japan, Pure Chem. Sec. (Nippon Kagaku Zasshi)*, **79**, 968 (1958).
3) M. W. Hanson, W. C. Dradbury and J. K. Corlton, *Anal. Chem.*, **29**, 490 (1957).
4) W. Nielsch and G. Böltz, *Z. Metallkunde*, **45**, 380 (1954).
5) H. Goto and Y. Kakita, *Japan Analyst (Bunseki Kagaku)*, **3**, 299 (1958).
6) K. Geiersberget and A. Durst, *Z. anal. Chem.*, **135**, 11 (1952).
7) E. G. Brown, *Analyst*, **79**, 50 (1954).
8) S. Hikime, H. Yoshida and Y. Uzumasa, *Japan Analyst (Bunseki Kagaku)*, **8**, 531 (1959).
9) K. Alcock, S. S. Grimley, T. V. Healy, J. Kennedy and H. A. C. McKay, *Trans. Faraday Soc.*, **52**, 39 (1956).

solution was made pH 1.0 with hydrochloric acid and made up to 20 ml. with 0.1 N hydrochloric acid. After 20 min., 20 ml. of TBP was added to the solution, and this mixture was shaken for 2 min. so that the tellurium complex could be extracted to the TBP phase thoroughly. The TBP phase was colored more deeply yellow than that obtained by the use of thiourea solution alone. This coloration was stable at least for 2.5 hr. The absorbance of the solution was measured spectrophotometrically over the range of wavelength, 330 mμ to 560 mμ. The results are shown in Fig. 1.

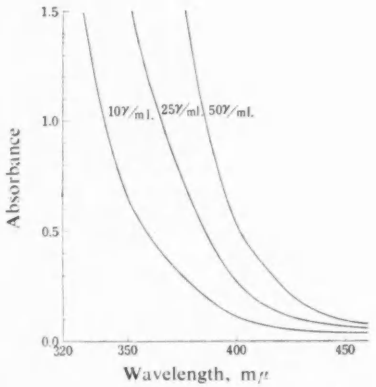

Fig. 1. Absorption curves of tellurium(IV) complex in TBP. KSCN 5 ml., $(NH_2)_2CS$ 4 ml., pH 1, total volume 20 ml., TBP 20 ml.

As shown in Fig. 1, tellurium complex in TBP has strong absorption in ultraviolet region. Although these absorption spectra are similar to those of tellurium-thiourea complex in dilute hydrochloric acid solution, absorbances of the former are several times greater than those of the latter.

Effect of Potassium Thiocyanate.—Varying amounts of potassium thiocyanate solution were added to solutions each containing 500 γ of tellurium and 4 ml. of thiourea solution. The pH of the solutions was kept about 1. The final volume of each solution was then made up to 20 ml.

Table I shows the absorbance of these solutions as a function of the amount of the reagent added. Constant absorbances were obtained adding more than 2 ml. of the reagent solution; one gram of the reagent, therefore, is sufficient for extracting thoroughly 500 γ of tellurium. To refer the effect of potassium thiocyanate on the extraction of tellurium, the amounts of tellurium remaining in the aqueous phase were determined also by thiourea method and the percentages of tellurium extracted were calculated from those values. The results agree with those obtained by the absorbance measurements.

In the absence of potassium thiocyanate, tellurium complex is not extracted with TBP under the experimental condition. However when potassium thiocyanate exists together with thiourea in the tellurium solution, percentage of the extracted tellurium increases with increasing amount of the reagent added, and the tellurium complex is extracted almost completely with TBP, when more than 1 ml. of the reagent is added.

Table I. Effect of potassium thiocyanate

KSCN solution ml.	Absorbance of TBP-phase at 400 mμ	Te		
		Taken γ	Found, aq. phase γ	Extracted %
—	0.000	500	497	0.6
0.01*	0.004	500	479	4.8
0.02*	0.013	500	450	10.0
0.05*	0.037	500	398	20.4
0.5	0.221	500	47	90.6
1.0	0.262	500	7.5	98.5
2.0	0.278	500	0.5	99.9
4.0	0.279	500	0.5	99.9
8.0	0.284	500	0.0	100

Thiourea solution 4 ml., pH 1, total volume 20 ml., TBP 20 ml.
* Added after dilution of the stock solution.

Effect of Thiourea.—Since the amount of thiourea also affects the color development of tellurium complex in dilute hydrochloric acid solution, several experiments were carried out to determine its effect. Measurements of the absorbance of the TBP phase showed that 80 mg. of thiourea is sufficient for complexing thoroughly 500 γ of tellurium and absorbances are constant beyond this concentration of thiourea.

In order to ensure the results, the amounts of tellurium remaining in the aqueous phase were determined and the percentage of tellurium extracted into TBP phase was calculated. (Table II) The results agree with those obtained by the absorbance measurements.

Table II. Effect of thiourea

Thiourea solution ml.	Absorbance of TBP-phase at 400 mμ	Te		
		Taken γ	Found, aq. phase γ	Extracted %
—	0.002	500	420	16
0.5	0.071	500	289	42
1	0.277	500	2	99.6
2	0.278	500	0	100
3	0.276	500	4	99.2
5	0.277	500	0	100
8	0.276	500	2	99.6

Potassium thiocyanate solution 2 ml., pH 1, total volume 20 ml., TBP 20 ml.

Effect of pH.—In view of possible decomposion of either potassium thiocyanate or thiourea in an acid solution, experiments were carried out in low acidity solutions. A series of solutions were prepared, containing 500 γ of tellurium, 2 ml. of potassium thiocyanate solution and 2 ml. of thiourea sulution. The pH values of these solutions were controlled around 1 with hydrochloric acid and similarly extracted with TBP. Results are shown in Table III. The absorbance at 400 mμ remains constant in the range from pH 0.6 to 1.7, indicating that tellurium complex is extracted with TBP so that it is possibe to extract and determine tellurium over this pH range.

TABLE III. EFFECT OF pH

pH values before extraction	Absorbance of TBP-phase at 400 mμ	Te	
		Found, aq. phase γ	Extracted %
0.34	0.262	2	99.6
0.6	0.275	0	100
1.0	0.278	0	100
1.3	0.277	1	99.8
1.7	0.275	2	99.6

Te 500 γ, KSCN soln. 2 ml., thiourea soln. 2 ml., total volume. 2 ml., TBP 20 ml.

Stability of Color.—The yellow color of tellurium complex extracted into TBP phase is very stable and is several times as deep as that of the complex formed with thiourea in dilute hydrochloric acid solution. Four solutions containing 5, 12.5, 25 and 50 γ of tellurium per milliliter respectively were prepared and, after extraction, the stability of the color of each solution was tested. No changes were found in the absorbance after exposure in diffused light for 150 min.

Recommended Procedure.—To 15 ml. of a sample solution (ca. 0.1 N hydrochloric acid solution containing up to 500 γ of tellurium), add 2 ml. of potassium thiocyanate solutions (500 g./l.) and 2 ml. of thiourea solution (80 g./l.). Adjust pH to 1, and make the final volume of the solution to 20 ml. with 0.1 N hydrochloric acid. After 20 min. add 20 ml. of TBP to the solution, and shake for 2 min.

When the TBP phase separates from the aqueous phase, centrifuge the former for 2 min. The absorbance of TBP phase is measured at 400 mμ with a spectrophotometer with 10 mm. cells.

Calibration Curves.—Prior to the determination of tellurium in the sample solution, calibration curves were prepared with a series of solutions containing 1 to 75 γ of tellurium per milliliter. The curves are shown in Fig. 2.

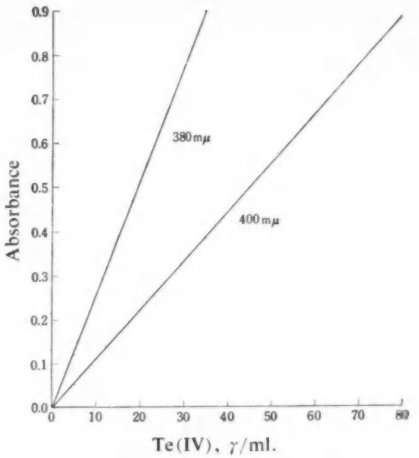

Fig. 2. Calibration curve for tellurium.

TABLE IV. ANALYSIS OF SAMPLES OF TELLURIUM

Absorbance vs. blanc	Te		Difference
	added γ	found γ	γ
0.277	250	249	− 1
0.275	〃	247	− 3
0.277	〃	249	− 1
0.279	〃	251	1
0.278	〃	250	0
0.270	〃	243	− 7
0.282	〃	254	4
0.285	〃	257	7
0.273	〃	247	− 3
0.279	〃	251	1
	mean	249.7	− 0.2
0.552	500	497	− 3
0.553	〃	498	− 2
0.570	〃	514	14
0.556	〃	501	1
0.539	〃	485	−15
0.544	〃	490	−10
0.546	〃	492	− 8
0.552	〃	497	− 3
0.564	〃	508	8
0.558	〃	503	3
0.545	〃	491	− 9
0.548	〃	494	− 6
0.554	〃	499	− 1
0.546	〃	492	− 8
0.565	〃	509	9
0.554	〃	499	− 1
0.548	〃	494	− 6
0.558	〃	503	3
0.564	〃	508	8
0.546	〃	492	− 8
	mean	498.3	− 1.7

TABLE V. INTERFERENCE STUDY OF DIVERSE IONS ON ABSORBANCE OBTAINED WITH 25 p.p.m. OF TELLURIUM

Ions present	Added as	Concentration p.p.m.	Difference of absorbance ×1000	Tolerance p.p.m.
Bi^{3+}	$Bi(NO_3)_3$	2.5	21	0
		5.0	36	
Cu^{2+}	$CuSO_4$	10	0	10
		25	7	
		100	34	
Ni^{2+}	$Ni(NO_3)_2$	50	0	50
		125	4	
		250	16	
Te^{6+}	Na_2TeO_4	75	6	75
Co^{2+}	$CoCl_2$	50	− 2	500
		500	− 3	
Fe^{3+}	$FeCl_3$	0.3	0	0.3
		0.9	20	
Cr^{3+}	$CrCl_3$	50	2	50
		250	7	
Hg^{2+}	$HgCl_2$	400	1	large excess
Zn^{2+}	$ZnCl_2$	50	0	500
		500	− 3	
Cd^{2+}	$CdCl_2$	500	0	large excess
Mn^{2+}	$MnSO_4$	250	0	〃
Al^{3+}	$AlCl_3$	500	0	〃
Mg^{2+}	$MgCl_2$	50	0	〃
		500	− 2	
PO_4^{3-}	H_3PO_4	1400	0	〃
SO_4^{2-}	H_2SO_4	1250	− 2	〃
NO_3^-	HNO_3	500	0	〃
WO_4^{2-}	Na_2WO_4	50	− 1	50
		500	−45	
VO_3^-	NH_4VO_3	10	3	10
		50	17	
CrO_4^{2-}	K_2CrO_4	50	−54	0

A linear relationship exists between the absorbance and the tellurium concentration over the range investigated. In many respect, however, measurement at 400 mμ is preferable to that at 380 mμ.

Reproducibility.—Several samples were prepared separately in the same way as unknown samples and analysed by the recommended procedure. As shown in Table IV, the reproducibility of this procedure is satisfactory.

Effect of Diverse Ions.—Separate tests were made to elucidate the interference of various cations as well as anions on the tellurium determination. The results are shown in Table V. In this table, by "tolerance" is meant the value that gives no significant interference. Under these values the difference between the absorbance of tellurium of the test solution and that of the standard containing no other ions is less than 3%.

A pre-extraction test was also made in which a previous attempt to remove Bi^{3+}, Cu^{2+}, Ni^{2+} and Fe^{3+} was made, since these ions were considered to have relatively larger interfering behavior. In this experiment, only potassium thiocyanate and no thiourea was added first to the solution of tellurium containing these ions. After a single extraction with the same volume of TBP at pH 1, the organic layer was separated off and the remaining aqueous solution was used to determine the amount of tellurium. Some more potassium thiocyanate and also a necessary amount of thiourea were added to this aqueous solution; tellurium was shaken out to the TBP layer according to the recommended procedure, and then determined spectrophotometrically. As shown in Table VI, a single pre-extraction treatment is not sufficient to give a satisfactory value for tellurium, since about 6% positive error results in the absorbance of tellurium. This means that even after the pre-extraction, there remain some fractions of these ions which are transferred to the TBP layer when the recommended procedure is applied. In the single pre-extraction, Cu^{2+} and Ni^{2+} seems to be extracted only partly although Fe^{3+} and Bi^{3+} may be extracted fairly well. It would be possible, however, to eliminate them to such an extent that they give little effect on the determination

of tellurium, if a better experimental condition were further sought.

TABLE VI. PRE-EXTRACTION TEST

Te taken p.p.m.	Ions added p.p.m.	Absorbance at 400 mμ in TBP
25	—	0.139
25	Bi^{3+} 5, Cu^{2+} 25, Ni^{2+} 50, Fe^{3+} 1.3	0.147
—	Bi^{3+} 5, Cu^{2+} 25, Ni^{2+} 50, Fe^{3+} 1.3	0.006

Summary

Spectrophotometric determination of tellurium-(IV) by means of extraction with 100% TBP was studied. Tellurium forms yellow complex, as seen in the literature, with thiourea in a dilute hydrochloric acid solution, and the complex is extracted into TBP whenever potassium thiocyanate is present in excess in the solution.

Conditions on the extraction and the determination of tellurium were examined. It was found that addition of 2 ml. of thiourea solution (80 g./l.) and 2 ml. of potassium thiocyanate solution (500 g./l.) to the sample solution is enough to extract 1 to 500 γ of tellurium per 20 ml. from the dilute hydrochloric acid solution with 20 ml. TBP. Tellurium complex was extracted thoroughly with TBP at pH 1. For the determination of tellurium, the absorbance of the TBP phase was measured spectrophotometrically at 400 mμ.

The effect of the diverse ions on the absorbance of tellurium complex was examined and also pre-extraction test on the removal of interference ions was carried out.

The author wishes to express his grateful thanks to Professor Y. Uzumasa for his kind encouragement and discussion and to Mr. H. Yoshida for technical assistance in this study.

Department of Chemistry
Faculty of Science
Hokkaido University
Sapporo

---

*A Rapid Method for Determining Fission Products Contained in Waters Using an Ion Exchanger**

By Hiroyuki TSUBOTA and Yasushi KITANO

(Received November 9, 1959)

It is essential to select a proper elutriant in order to separate many constituents in solutions by ion exchange resins. Many elutriants have been used by various researchers[1-7]; among them citrate buffer is used most extensively. However, most of these methods are time-consuming, and the preparation and preservation of elutriants are sometimes rather difficult. Moreover, it is often troublesome to treat the effluent for further chemical or radiochemical examinations. This paper deals with a procedure for rapid and easy separation of alkali, alkaline earth and rare earth elements contained in mixed fission products, by using the formate buffer solution.

A good elutriant should have the following characteristics: 1) There must be complete separation of elements; degree of separation can be expected from the complexity constants between cations in a sample and the anion of the complexing agent used as an elutriant[2,8,9]. When the complexity constants of various cations in the sample differ considerably from each other, these cations can be eluted separately

* A part of this work was done at Kobe University, Kobe.

1) R. H. Diamond, K. Street, Jr. and G. T. Seaborg, *J. Am. Chem. Soc.*, **76**, 1461 (1954).
2) E. R. Tompkins, J. X. Khym and W. E. Cohn, ibid., **69**, 2769 (1947).
3) W. E. Cohn, G. W. Parker and E. R. Tompkins, *Nucleonics*, **3**, No. 5, 22 (1948).
4) K. Kimura, E. Minami, M. Honda et al., *Japan Analyst (Bunseki Kagaku)*, **3**, 335 (1954).
5) B. H. Ketelle and G. E. Boyd, *J. Am. Chem. Soc.* **73**, 1862 (1951).
6) E. C. Freiling and L. R. Bunney, ibid., **76**, 1021 (1954).
7) R. C. Vickery, *J. Chem. Soc.*, 1952, 4357.
8) F. H. Spedding et al., *J. Am. Chem. Soc.*, **69**, 2777 (1947).
9) E. R. Tompkins and S. W. Mayer, ibid., **69**, 2859 (1947).

as the elutriant passes through a column of ion exchanger. 2) Buffer solutions having various pH values should be prepared easily and should be stable. 3) The reagent must be vaporized easily and completely because it is essential that all coexisting materials, other than a compound of the element in question, be removed before radioactive assay. 4) Besides these conditions, the reagents of high quality can be obtained at low cost. From the result of this experiment a formate buffer solution was proved to satisfy these conditions* and to be the best elutriant.

Experimental

Elutriants.—The following elutriants were used for the present experiment:

(A) Hydrochloric acid: 0.2 N.

(B) Oxalic acid: 0.5%.

(C) A buffer solution of 1 M formic acid and 1 M ammonium formate (a formate buffer solution): As shown in Fig. 1, the buffer solutions having various pH values can be prepared by mixing 1 M formic acid solution with varying quantities of 1 M ammonium formate solution.

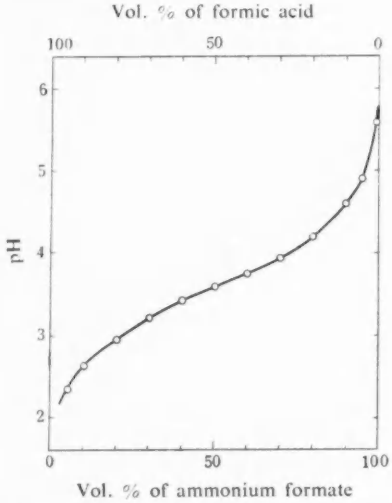

Fig. 1. pH of the buffer solution prepared by mixing 1 M formic acid and 1 M ammonium formate solution.

Columns.—Two columns were used:

No. 1, Dowex 50, X8, 100~150 mesh, 1.0×8.0 cm., H^+-saturated resin, (exchange capasity, ca. 14 meq.).

No. 2, Dowex 50, X8, 200~250mesh, 1.0×20 cm., H^+-saturated resin, (exchange capacity, ca. 35 meq.).

Flow Rate.—0.3~0.4 ml./min.

Sample Solution of Mixed Fission Products.—The fission products mixture used in this experiment had been supplied from ORNL, U. S. A., and was three years old. Nitric acid was added to the fission product solution, and was evaporated on a water bath. More nitric acid was added to the residue. And 0.1~1 ml. of the nitric acid solution (concentration, approx. 10 μc/ml.) were diluted with 5~10 ml. of 0.2 N hydrochloric acid. This hydrochloric acid solution was used as a sample solution.

Procedure.—(A) The sample solution is passed through the column No. 1.

(B) Ruthenium is eluted with about 20 ml. of 0.2 N hydrochloric acid*,[4]. The column is washed by passing 10~20 ml. of distilled water.

(C) Next, zirconium, niobium and uranium are eluted together by passing 50~70 ml. of 0.5% oxalic acid[3,4]. The column is washed with 10~20 ml. of distilled water.

(D) When the formate buffer solution of pH 3.2 (1 M formic acid: 1 M ammonium formate=7: 3, in volume) has passed through the column, cesium is eluted in the effluent of a quantity between 50 and 110 ml. Thymol blue is used as indicator because cesium begins to be eluted after the thymol blue indicator in the effluent changes to yellow.

(E) When the formate buffer solution of pH

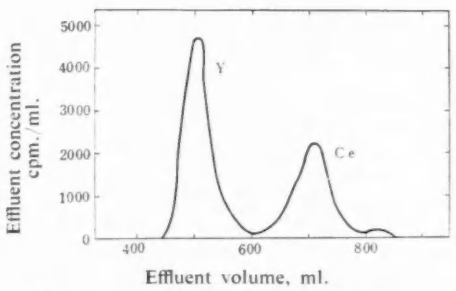

Fig. 2. Separation of rare earth elements.
Column: No. 2.
Elutriant: the buffer solution, pH 3.8.
Flow rate: 0.2~0.3 ml./min.

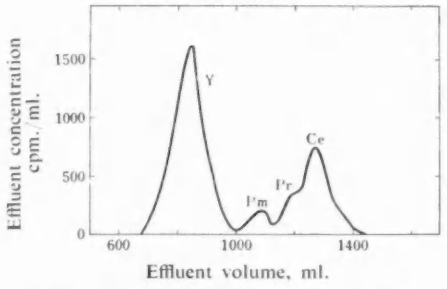

Fig. 3. Separation of rare earth elements.
Column: No. 2.
Elutriant: the buffer solution, pH 3.6.
Flow rate: 0.2~0.3 ml./min.

* They will be discussed in detail elsewhere.

* If I and Te are present, they are eluted together with Ru.

3.8 (1 M formic acid : 1 M ammonium formate=4 : 6, in volume) has passed through the column, all rare earth elements are simultaneously eluted in a fraction between 50 and 170 ml. of the effluent. After this fraction of the effluent has been vaporized, the residue containing rare earth elements is dissolved in a small amount of dilute hydrochloric acid. The resultant solution is passed through the column No. 2, and rare earth elements are adsorbed on it. When the formate buffer solution having pH 3.8 has passed, rare earth elements are separated into yttrium and cerium groups, as shown in Fig. 2. When the formate buffer solution having pH 3.6 (1 M formic acid : 1 M ammonium formate=1 : 1) is used, cerium group elements are further separated into promethium, praseodymium and cerium fractions, as shown in Fig. 3.

(F) After ruthenium, zirconium, niobium and cesium and rare earth elements have been removed, strontium is eluted by passing about 120 ml. of the formate buffer solution of pH 4.2 (1 M formic acid : 1 M ammonium formate=2 : 8) through the column No. 1.

The method is summarized in Table I, and the results are shown in Fig. 4.

Radioactibity Measurement. — The effluent is divided into 5 ml.-fractions by means of a fraction collector, and 1~2 ml. of each fraction is transferred into a counting dish. Evaporation and sublimation of the effluent is done by heating the counting dish with an infrared lamp and an electric heater. After the formate is removed completely, the radioactivity is measured by using a G. M. counter. The nuclides can be identified from the decay curves and the absorption curves.

TABLE I. METHOD FOR SEPARATION OF FISSION PRODUCTS WITH CATION EXCHANGE RESIN

Sample (in dil. HCl)

↓

Column No. 1

Elutriant	Elements eluted
0.2 N HCl 20 ml.	Ru
(washed with water)	
0.5% oxalic acid 50~70 ml.	U, Pu, Zr, Nb
the buffer solution, pH 3.2 110 ml.	Cs (found in a effluent intermediate between 50 and 110 ml.)
the buffer solution, pH 3.8 170 ml.	Rare earth elements (found in a effluent between 50 and 170 ml.)
the buffer solution, pH 4.2 100 ml.	Sr
2 M ammonium formate solution 100 ml.	Ba

Rare earths fraction
(dissolved in dilute HCl after evaporation)

↓

Column No. 2

1) Y- and Ce-groups can be separated with the buffer solution, pH 3.8.
2) When the buffer solution having pH 3.6 is used, the elements of Ce-group can be separated partially.
3) To separate exactly, use the buffer solution having pH 3.3~3.4 or use a longer column.

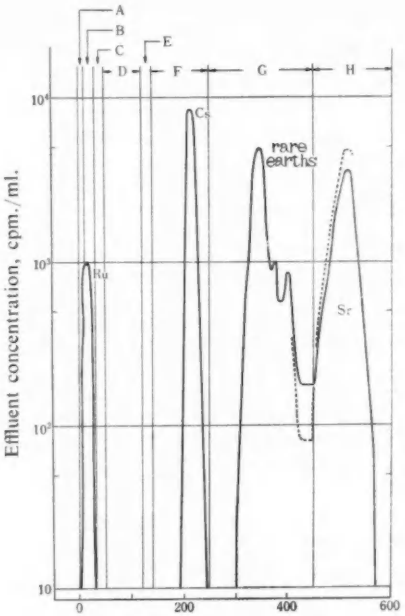

Fig. 4. Separation of fission products.
Column: No. 1.
Influents: A sample solution, B 0.2 N HCl, C H_2O, D 0.5% oxalic acid, E H_2O, F the buffer solution, pH 3.2, G the buffer solution, pH 3.8, H the buffer solution, pH 4.2.
Flow rate: 0.33 ml./min.
The curve in dotted line shows the radioactivity of each fraction 60 hours after the original measurements.

Discussion

Elution of Cesium. — Up to the present time, the elution of cesium has been conducted with hydrochloric acid or citrate buffer solution[10], but neither of these elutriants is satisfactory for the following reasons. When cesium is completely eluted with hydrochloric acid from the column, the adsorption band of strontium moves downward, and consequently, when a further separation of rare earth and alkaline earth elements is to be carried out, a part of

10) M. Honda, Y. Sasaki and H. Natsume, *Japan Analyst (Bunseki Kagaku)*, **4**, 240 (1955).

strontium is eluted together with the rare earth elements and the separation is incomplete. When a citrate buffer solution is used as the elutriant, the process is complicated because, to avoid the uncertainty of separating rare earth and alkaline earth elements, cesium and rare earth elements must be eluted together, and afterwards cesium and rare earth elements must be separated by resorption and chromatographic elution. Finally, it is very difficut to remove citrate from the effluent. When the formate buffer solution having a pH less than 3.4 is used, the adsorption bands of both rare earth and alkaline earth elements never move downward. Therefore cesium alone can be eluted completely by using the formate buffer solution having pH 3.2, as shown in Fig. 5. Ammonium formate and formic acid sublime easily and completely. Therefore, when the effluent containing cesium is evaporated, and an adequate acid is added to the residue and re-evaporated, pure and carrier-free cesium salts can be obtained.

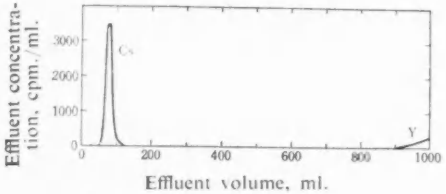

Fig. 5. Elution curve of Cs.
Column: No. 1.
Elutriant: the buffer solution, pH 3.3.
Flow rate: 0.40 ml./min.

Separation of Rare Earth and Alkaline Earth Elements.—As shown in Fig. 4, a fairly high radioactivity is found in the effluent intermediate between yttrium and strontium fraction. It is, however, possible to conclude that the radioactivity of this fraction is not due to the incomplete separation of rare earth from alkaline earth elements, but to the elution of ^{90}Y coming from ^{90}Sr adsorped on the column from the decay of this fraction.

When the formate buffer solution is used, lanthanum is to be eluted last among all rare earth elements to be eluted in the effluent. In other words, amoung rare earth elements lanthanum is the most difficult element to be separated from alkaline earth elements. The solution of fission products used in this experiment is not fresh; hence, it does not contain ^{140}La having a half-life of 40 hr. Complete separation of lanthanum from strontium is essential if the sample contains fresh fission products. For this purpose, separation of the two elements was examined by using nonradioactive strontium and lanthanum. One meq. of strontium and 1 meq. of lanthanum are passed through the column No. 1 and are adsorbed, and they are eluted by the formate buffer solution as described above. The effluent is divided into 5 ml.-fractions, and lanthanum and strontium in each fraction are determined by a semi-quantitative method, and the result is obtained as shown in Fig. 6. Fig. 6 also shows the result of 1 meq. of strontium and 1 meq. of mixed rare earth elements, viz., lanthanum, neodymium, praseodymium and cerium. From the figure, it can be seen that strontium is easily and completely separated from lanthanum and also from other rare earth elements by using column No. 1 with the buffer solution having pH 3.8. It can be concluded from this experiment that by using the formate buffer solution, rare earth elements and alkaline earth elements can be separately eluted even when fairly large amounts of carriers are present in the sample to be analysed.

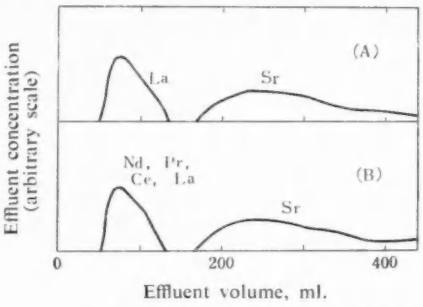

Fig. 6. (A) Separation of La-Sr, (B) Separation of rare earth elements-Sr.
Column: No. 1.
Elutriant: the buffer solution, pH 3.8.
Flow rate: (A) 0.24 ml./min., (B) 0.30 ml./min.

Separation of Rare Earth Elements. — Since fresh fission products contain various kinds of the rare earth element, the authors conducted separation of rare earth elements as follows:

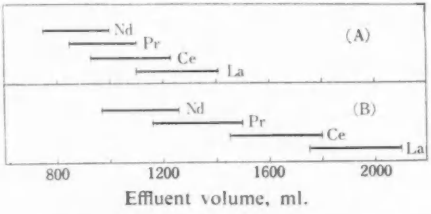

Fig. 7. Separation of rare earth elements.
Column: No. 2.
Elutriant: the buffer solution, (A) pH 3.6, (B) pH 3.4.
Flow rate: 0.25 ml./min.

a mixture of 1 meq. each of neodymium, praseodymium, cerium and lanthanum is adsorbed on column No. 2; the rare earth elements are eluted with the formate buffer solution. The effluent is divided into 10 ml.-fractions, and the elements in each fraction are determined. As shown in Fig. 7, the separation is incomplete when the formate buffer solution having pH 3.6 is used, but when the buffer solution of pH 3.4 is used the separation becomes rather complete. This procedure will be applied for the purification of rare earth elements.

Separation of Strontium and Barium.—With the same purpose as described in the preceding section, the authors carried out separation of strontium and barium by adsorbing 1 meq. of strontium and of barium on the column No. 1. As shown in Fig. 8, barium can be separated from strontium very easily and completely.

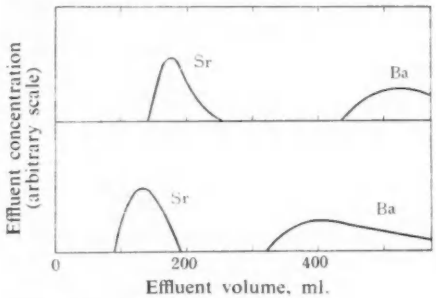

Fig. 8. Separation of Sr–Ba.
Column: No. 1.
Elutriant: the buffer solution, (A) pH 4.0, (B) pH 4.2.
Flow rate: (A) 0.40 ml./min., (B) 0.42 ml./min.

Separation of Fission Products from Iron.—To determine exactly fission products in natural waters by ion exchange resin, it is essential that the coexisting elements or carriers must be separated from fission products. Sodium, potassium, magnesium, calcium, ferric and aluminum ions are often found in natural waters, and barium and ferric ions are used as carriers. By using the formate buffer solution fission products can be separated easily from the other metals such as alkali, alkaline earth elements and iron. The separation of alkali and alkaline earth elements will be reported eleswhere[11], and the separation of iron and fission products is reported here; this is particularly important for the determination of fission products in natural waters. As shown in Fig. 9, the ferric ion is completely eluted before thymol blue indicator in the effluent changes from red to yellow. By using the buffer solution of pH 3.2, the ferric ion can be eluted long before cesium is eluted.

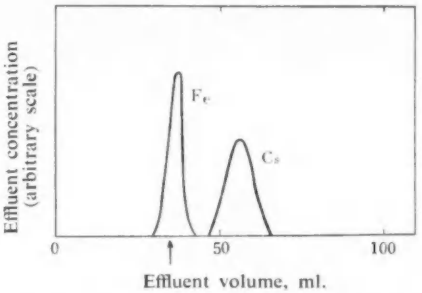

Fig. 9. Separation of Fe(3 meq.) from Cs.
Column: Dowex 50, X8, 1.1×10 cm., (100~150 mesh) H^+-saturated resin.
Elutriant: the buffer solution, pH 3.2.
Flow rate: 2.0 ml./min.
Arrow indicates the point at which thymol blue indicator changes to yellow from red.

Summary

The essential point of this method is the use of the formate buffer solution. This method would be used for the analysis of fission products in natural waters and for the preparation of pure and carrier-free radioactive elements from mixed fission products.

The authors express their sincere appreciation to Professor Yasuo Miyake of Tokyo University of Education and Mr. Masami Izawa of National Institute of Radiological Sciences for their helpful advice and encouragement throughout this work.

National Institute of Radiological Sciences
Kurosuna-machi, Chiba (H. T.)
Water Research Laboratory
Faculty of Science
Nagoya University
Chigusa-ku, Nagoya (Y. K.)

11) H. Tsubota and Y. Kitano, This Bulletin, 33, 770 (1960).

*A Rapid Method for Determining Alkali and Alkaline Earth Elements Using an Ion Exchanger**

By Hiroyuki TSUBOTA and Yasushi KITANO

(Received November 9, 1959)

The present authors previously reported[1] that fission products can be separately eluted more easily and rapidly by using a buffer solution of formic acid and ammonium formate as the elutriant than by using any other elutriants. As reported in that paper, even when fission products in a sample coexist with large amounts of other elements or carriers, they can be completely separated.

Many researchers have separated alkali metals[2-7] and alkaline earth elements[8-10] by using an ion exchanger. They have tried to analyse a mixture of alkali and alkaline earth elements containing other metal ions by using an ion exchange resin; moreover, separation of sodium, potassium, magnesium and calcium ions, which are abundant in nature, has been successful[6,11,12]. They did not, however, include in their experiments such rare elements as cesium or barium. Without including the cesium ion in their experiments, some researchers have stated that univalent ions and divalent ions can easily be separated with an ion exchanger[13,14]. However, the separation between cesium and magnesium ions would be difficult because the cesium ion is eluted last among alkali metals and the magnesium ion is eluted first among alkaline earth elements. The authors conducted systematic experiments on these elements with an ion exchanger and finally succeeded by using the buffer solution of 1 M formic acid and 1 M ammonium formate (the formate buffer solution).

Experimental and Discussion

Selection of an Elutriant.—Separation of alkali metals from alkaline earth metals has been conducted by using hydrochloric acid as an elutriant, when cesium was not included. To find out whether efficient separation can be realized when cesium is present, the following experiment was carried out. 0.1~1 meq. of potassium, cesium and magnesium ions, respectively, were mixed and passed into the column, Dowex 50, X12, 200~250 mesh, 1.1×15 cm., H^+-saturated resin, (exchange capacity, ca. 37 meq.), and eluted chromatographically with 1 N hydrochloric acid or 0.5 N hydrochloric acid at the flow rate of 1 ml./min. The effluent was divided into 10 ml. fractions. After evaporation of the fractions potassium and cesium in each fraction were determined from chloride content using silver nitrate standard solution and fluorescent indicator, and magnesium was determined by EDTA standard solution and Eriochrom Black T(EBT) indicator after the pH of the fractions had been adjusted to 10 with ammonium hydroxide.

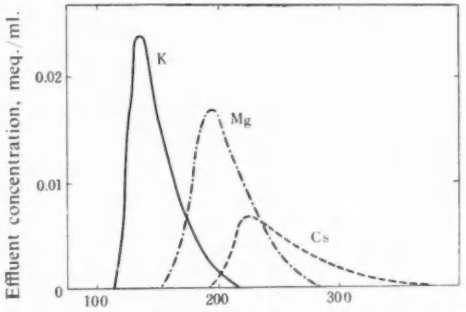

Fig. 1. Elution curves of K^+, Cs^+ and Mg^{2+} with HCl.
Column: Dowex 50, X12, 200~250 mesh, 1.1×15 cm.
H^+-saturated resin.
Elutriant: 1.0 N HCl.
Flow rate: 1.0 ml./min.

* A part of this work was done at Kobe University, Kobe.

1) H. Tsubota and Y. Kitano, This Bulletin, **33**, 765 (1960).
2) W. E. Cohn and H. W. Kohn, *J. Am. Chem. Soc.*, **70**, 1986 (1948).
3) G. Kayas, *Compt. rend.*, **228**, 1002 (1949).
4) G. Kayas, *J. Chim. Phys.*, **47**, 408 (1950).
5) H. Okuno, M. Honda and T. Ishimori, *Japan Analyst (Bunseki Kagaku)*, **2**, 228 (1953).
6) J. Beukenkamp and W. Rieman III, *Anal. Chem.*, **22**, 582 (1950).
7) W. Buser, *Helv. Chim. Acta*, **34**, 1635 (1951).
8) D. N. Campbell and C. T. Kenner, *Anal. Chem.*, **26**, 560 (1954).
9) M. Lerner and W. Rieman III, ibid., **26**, 610 (1954).
10) M. Honda, *Japan Analyst (Bunseki Kagaku)*, **3**, 132 (1954).
11) H. Kakihana, *J. Chem. Soc. Japan, Pure Chem. Soc. (Nippon Kagaku Zasshi)*, **72**, 203 (1951).
12) R. C. Sweet, W. Rieman III and J. Beukenkamp, *Anal Chem.*, **24**, 952 (1952).
13) O. Samuelson, "Ion Exchangers in Analytical Chemistry", John Wiley & Sons, Inc., N. Y. (1954), p. 35.
14) M. Honda, *J. Chem. Soc. Japan, Pure Chem. Sec. (Nippon Kagaku Zasshi)*, **71**, 118 (1950).

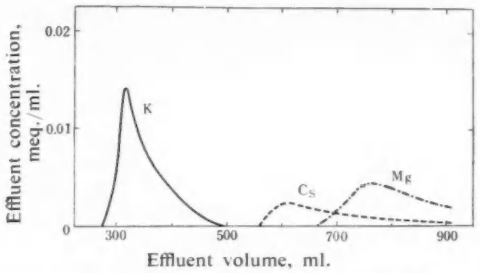

Fig. 2. Elution curves of K^+, Cs^+ and Mg^{2+} with HCl.
Column: Dowex 50, X12, 200~250 mesh, 1.1×15 cm.
H^+-saturated resin.
Elutriant: 0.5 N HCl.
Flow rate: 1.0 ml./min.

When 1 N hydrochloric acid is used, potassium and cesium can be partially separated from each other, but magnesium and cesium can not be separated at all although magnesium begins to be eluted shortly before the elution of cesium (Fig. 1). When 0.5 N hydrochloric acid is used, potassium and cesium can be separated completely, but cesium and magnesium can not be separated although cesium begins to be eluted shortly before the elution of magnesium (Fig. 2). Based on these results, it can be concluded that, when cesium and magnesium are to be separated completely, a much longer column and a larger amount of a very dilute hydrochloric acid must be used. In other words, hydrochloric acid is not a practical elutriant for separating cesium from magnesium. The effect of the concentration of hydrochloric acid on the elution of magnesium, as seen in Figs. 1 and 2, can be understood by the fact that the magnesium ion forms $MgCl^+$ complex ion with the chloride ion. Therefore, in order to separate magnesium from cesium, it is essential to use an acid or salts other than chloride. As previously reported[1], when a formate buffer solution was used as the elutriant, cesium and magnesium were completely separated. This elutriant could be prepared and preserved easily and after-treatment of the effluent was done easily because ammonium formate could be sublimed easily and completely. Thus, it was decided to use the formate buffer solution as the elutriant, and separation of elements by using the buffer solution was examined.

Examination of Methods for Analyzing Alkali and Alkaline Earth Elements. — (A) *Alkali metals.*—The following two methods were used for determination of alkali metal ions in an effluent.

i) When an effluent containing alkali metals is evaporated and the residue is heated with infrared lamp or electric heater to remove ammonium formate completely, only alkali formate remains. A small amount of hydrochloric acid is added to the alkali formate and evaporation is repeated. The chloride content of the residue is determined by silver nitrate standard solution and fluorescent indicator;

Table I. The effect of ammonium formate on the determination of alkali ions by silver nitrate titration method

Metal	Added, mg.	Method of evaporation	Found, mg.		
Na^+	3.63	Water bath	3.93	5.60	
	3.63	Infrared lamp	3.63	3.65	
	3.63	Heat after using water bath	3.63	3.62	3.63
K^+	7.53	〃	7.55	7.53	7.57

Table II. The effect of ammonium formate on the determination of alkali ions by flame photometric method

Metal	Wavelength	Added, p. p. m.	Brightness of flame in various solutions		
			H_2O	0.5 M NH_4HCOO	1 M NH_4HCOO
Li^+	671 mμ	10~100	100	100±1	99±1
Na^+	589	10~100	100	100±1	99±1
K^+	766	10~100	100	100±1	99±1
Rb^+	420	10~100	100	100±5	100±5
Cs^+	455	10~100	100	100±5	100±5

Apparatus: Shimadzu-flame photometer, Type QB-50.
Fuel: H_2 gas
The brightness of ions in distilled water are set on 100.

Table III. The effect of ammonium formate on the determination of alkaline earth ions with EDTA

Metal	Indicator	Added, meq.	Found, meq. (average) in various solutions			
			H_2O	0.1 M NH_4HCOO	1 M NH_4HCOO	2 M NH_4HCOO
Mg^{2+}	E. B. T.	0.225	0.225	0.225	0.224	
Ca^{2+}	E. B. T.	0.108	0.108	0.108	0.108	
Sr^{2+}	E. B. T.	0.165	0.165	0.165	0.164	*
	P. C.		0.164	0.165	0.165	*
Ba^{2+}	E. B. T.	0.148	0.15**	0.15*	0.15**	*
	P. C.		0.148	0.148	0.149	*

E. B. T.: Eriochrom Black T
P. C.: Phthalein Complexone
*: End point of titration can not be detected.
**: End point is not clear.

then, alkali content can be determined from the chloride content. The results are shown in Table. I.

ii) Alkali content in an effluent is determined directly by flame photometric method. The effect of a large amount of ammonium and formate ions upon the determination of alkali metals must be carefully examined. As given in Table II, however, interference of ammonium formate is not found in 0.5 M ammonium formate solution, and is found slightly in 1.0 M.

(B) *Alkaline earth elements.*—Alkaline earth elements are titrated by EDTA solution containing the magnesium ion using EBT indicator. The formate ion does not interfere, as shown in Table III. It is necessary to adjust pH over 9.5 for the titration with EDTA. As the effluent has a buffer action, the use of an indicator will be preferable, since it does not obscure the end point of the titration by EDTA and changes its color at pH 9.5. Thymol blue indicator satisfies the conditions. One drop of 0.1% water solution of thymol blue is added to an effluent to be titrated, and ammonium hydroxide is added until the color of the solution changes from yellow to blue and then the solution is titrated by EDTA with EBT indicator. As shown in Table IV, the values obtained by EDTA titration are about 1% lower than the added values, and therefore the observed value must be corrected. In some cases strontium and barium are determined by EDTA standard solution and phthalein-complexone indicator.

Table IV. The effect of pH-indicator on the determination of alkaline earth ions with EDTA

Sample solution: Mg^{2+} is contained in 50 ml. of 0.5 M ammonium formate solution.
pH-indicator: 0.1% Thymol Blue-water solution; 1 drop
Metal chelate indicator: Eriochrom Black T

Added; meq., Mg^{2+}	Found; meq., Mg^{2+}	Error, %
0.022_5	0.022_4	−0.9
0.045_0	0.044_5	−1.1
0.067_5	0.067_0	−0.7
0.090_0	0.089_0	−1.1
0.112_5	0.111_5	−0.9
0.135_0	0.133_5	−1.1
0.157_5	0.156_0	−1.0
0.180_0	0.178_0	−1.1
0.202_5	0.200_0	−1.2
0.225_0	0.223_5	−0.7

Examination of Conditions for the Separation of Alkali and Alkaline Earth Elements.—It is desirable to use a short column and a small

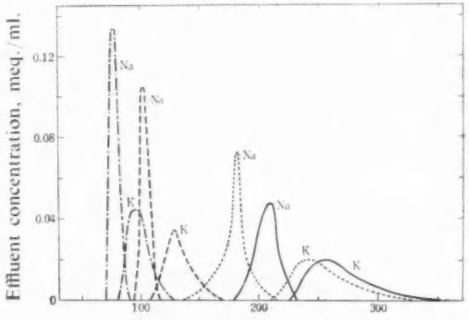

Fig. 3. Elution curves of Na^+ and K^+.
Column: Dowex 50, X8, 100~150 mesh, 1.1×8 cm.
Flow rate: 1.0~1.1 ml./min.
Resin form and elutriant:
—— H^+-saturated resin, with 0.1 M ammonium formate solution
····· NH_4^+-saturated resin, with 0.1 M ammonium formate solution
---- H^+-saturated resin, with 0.2 M ammonium formate solution
-·-·- H^+-saturated resin, with the buffer solution, pH 3.2

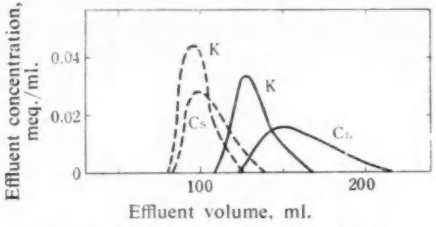

Fig. 4. Elution curves of K^+ and Cs^+.
Column: Dowex 50, X8, 100~150 mesh, 1.1×8 cm., H^+-saturated resin.
Flow rate: 1.0 ml./min.
Elutriants:
—— 0.2 M ammonium formate solution.
---- the buffer solution, pH 3.2.

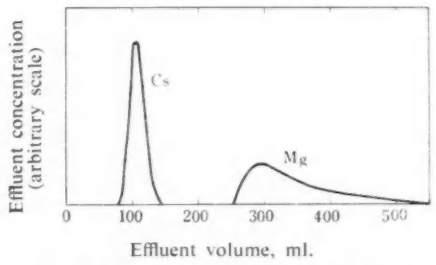

Fig. 5. Elution curves of Cs^+ and Mg^{2+}.
Column: Dowex 50, X8, 100~150 mesh, 1.1×8 cm., H^+-saturated resin.
Elutriant: the buffer solution, pH 3.2.
Flow rate: 0.50 ml./min.

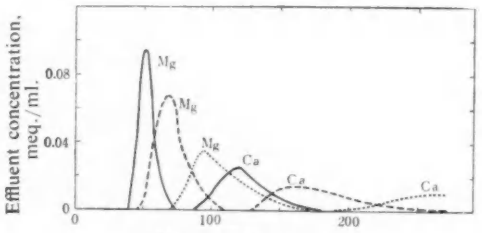

Fig. 6. Elution curves of Mg^{2+} and Ca^{2+}.
Column: Dowex 50, X8, 100~150 mesh, 1.1×8.5 cm., H^+-saturated resin.
Folw rate: 0.40~0.50 ml./min.
Elutriant: —— the buffer solution, pH 4.0
---- the buffer solution, pH 3.8
····· the buffer solution, pH 3.6

amount of elutriant for separation. To decide a suitable elutriant to be used with a column of Dowex 50, X8, 100~150 mesh, 1.1×8 cm., H^+-saturated resin, (exchange capacity, ca. 17 meq.), and at rate of 2~3 ml./min., elution curves were made as follows: An effluent was divided into fractions of 5~10 ml. and elements

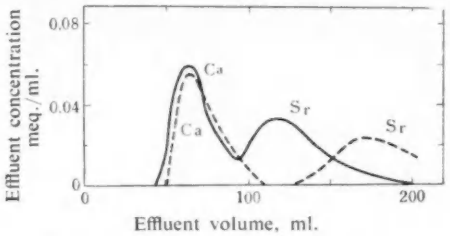

Fig. 7. Elution curves of Ca^{2+} and Sr^{2+}.
Column: Dowex 50, X8, 100~150 mesh, 1.1×8.5 cm., H^+-saturated resin.
Flow rate: 1.0 ml./min.
Elutriant: —— the buffer solution, pH 4.2
---- the buffer solution, pH 4.1

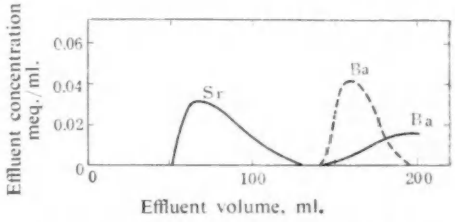

Fig. 8. Elution curves of Sr^{2+} and Ba^{2+}.
Column: Dowex 50, X8, 100~150 mesh, 1.1×8.5 cm., H^+-saturated resin.
Flow rate: 1.0 ml./min.
Elutriant:
—— the buffer solution, pH 4.5.
---- 2 M ammonium formate solution.

in each fraction were determined by the same method as shown above. The results are as follows:

(A) Separation of alkali metals.—It is known that separation factors of sodium, potassium and ammonium in cationic resin of sulphonic type are increased according to the series: sodium < ammonium < potassium. It is, therefore, expected that sodium and potassium can be easily separated when ammonium salt is used as an elutriant. Fig. 3 shows the elution curves of sodium and potassium when ammonium formate solution and the formate buffer solution are used. The separation of potassium and cesium, however, can not be conducted with this buffer solution, as shown in Fig. 4.

(B) Separation of cesium and magnesium.—As shown in Fig. 5, cesium and magnesium can be separated completely from each other by using the formate buffer solution having pH 3.2.

(C) Separation of alkaline earth elements.—The elution curves of magnesium and calcium, as shown in Fig. 6, are obtained when the formate buffer solutions of various pH are used as an elutriant. From Fig. 6, it can be seen

that magnesium and calcium can be easily separated by the buffer solutions. As shown in Fig. 7, calcium and strontium can be separately eluted by the buffer solution having pH 4.1. Finally, to separate strontium and barium, strontium is first eluted by the buffer solution of pH 4.5, and then barium is eluted by 2 M ammonium formate solution, as shown in Fig. 8.

(D) Separation of alkali and alkaline earth elements.—To separate completely alkali and alkaline earth elements, a column of 10 cm. in length may be used. This column length was determined by the plate theory[6] for two ions, sodium and potassium ions which are most difficult to separate in the above experiments.

Sodium and potassium can be separately eluted by using 0.1 M ammonium formate solution. For an early start of elution of sodium, 0.2 M ammonium formate solution may be passed through a column before 0.1 M ammonium formate solution is passed.

To separate potassium and cesium with the formate buffer solution, it is necessary to use a very long column and a large amount of the elutriant. Therefore first it was better to elute

TABLE V. DETERMINATION OF IONS IN MIXTURES

No.		Na^+	K^+	Cs^+	Mg^{2+}	Ca^{2+}	Sr^{2+}	Ba^{2+}
1	Added, meq.	0.481	0.493		0.450	0.434	0.412	0.403
	Found, meq.	0.491	0.488		0.453	0.432	0.424	0.40
	Error, %	+2.3	−1.0		+0.7	−0.5	+2.9	
2	Added, meq.	0.961	0.987	0.498	0.450	0.469	0.412	0.403
	Found, meq.	0.953	1.491		0.451	0.466	—	0.40
	Error, %	−0.8	+0.4		+0.2	−0.6		
3	Added, meq.	0.481	0.493	0.498	0.450	0.469	0.412	0.403
	Found, meq.	0.470			0.448	0.472	0.397	0.40
		(0.009)	(0.495)	(0.488)				
	Error, %	−2.3			−0.4	+0.6	−3.6	
		(−0.4)	(+0.4)	(−2.0)				
4	Added, meq.	0.961	0.987	0.498	0.450	0.469	0.412	0.403
	Found, meq.	0.965			0.451	0.469	—	0.40
		(0.000)	(0.982)	(0.495)				
	Error, %	+0.5			+0.2	−0.0		
			(−0.5)	(−0.6)				

The values in parenthesis are obtained by resorping the K^+ and Cs^+ fraction in longer column (1.1×15 cm.) and eluting with 0.5 N HCl separately (as shown in Fig. 2).

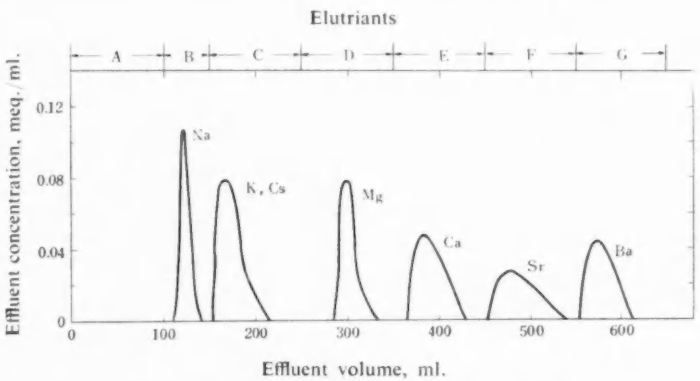

Fig. 9. Elution of alkali and alkaline earth elements.
Column: Dowex 50, X8, 1.1×10 cm., 100~150 mesh, H^+-saturated resin.
Flow rate: 2 ml./min.
Elutriants: A 0.2 M ammonium formate solution, B 0.1 M ammonium formate solution, C the buffer solution, pH 3.2, D the buffer solution, pH 4.0, E the buffer solution, pH 4.1, F the buffer solution, pH 4.4, G 2 M ammonium formate solution.

both simultaneously with the formate buffer solution of pH 3.2, and then to separate potassium and cesium by resorption and chromatographic elution with 0.5 N hydrochloric acid.

Cesium and magnesium can be separated by the formate buffer solution having pH 3.2. And the separation of magnesium, calcium, strontium and barium can be conducted by using the same buffer solution with different pH.

Using the column of Dowex 50, X8, or Amberlite IR-120, 100~150 mesh, 1.1×10 cm., and H^+-saturated resin, (exchange capacity, ca. 21 meq.), 0.5~1 meq. of sodium, potassium, cesium, magnesium, calcium, strontium and barium ions, respectively, are separated at a flow rate of 2~3 ml./min. The results are shown in Fig. 9 and Table V. Alkali and alkaline earth elements can be successfully separated from each other by the procedure shown in Fig. 9.

Summary

Alkali and alkaline earth elements, including their rare elements, can be separately eluted easily, rapidly and completely by the elutriants here described. This procedure and its modified procedures* can be applied to routine analysis of natural waters.

The authors express their sincere appreciation to Professor Yasuo Miyake of Tokyo University of Education and Mr. Masami Izawa of National Institute of Radiological Sciences for their helpful advice and encouragement throughout their work.

National Institute of Radiological Sciences
Kurosuna-machi, Chiba (H. T.)

Water Reserch Laboratory, Faculty of Science
Nagoya University, Chigusa-ku, Nagoya (Y. K.)

* The modified procedures will be reported elsewhere.

*Studies on Organic Peroxides. V. Decomposition of Benzoyl Peroxide by Iron(II)**

By Shigeo HASEGAWA and Norio NISHIMURA

(Received October 28, 1959)

It has been found that the rate of the decomposition of peroxides was greatly accelerated by ferrous ion[1]. In the presence of the latter, the decomposition is supposed to take place according to the Haber-Weiss one-electron transfer mechanism as follows[2]:

$$P + Fe^{2+} \xrightarrow{k_1} RCOO\cdot + RCOO^- + Fe^{3+} \quad (1)$$

where P and R denote benzoyl peroxide and phenyl group respectively. It is noted that this decomposition is not homolytic but semi-ionic. Therefore, it would be expected that the physical properties of solvents play an important role apart from the discussions about the induced decomposition of benzoyl peroxide. In the previous paper[3], this mechanism was postulated in order to explain the dependence of the initial rate of polymerization of vinyl acetate in the benzoyl peroxide-Fe(II)-benzoin redox system on the initial concentration of ferrous ion. In this paper, the analytical method was applied to the ferrous ion catalysed decomposition of peroxide in order to verify this mechanism.

Experimental

Reagents used were of reagent grade or prepared by the method reported previously[3]. A definite amount of ferrous chloride crystals ($FeCl_2 \cdot 4H_2O$) was dissolved in ethanol (50 ml.) in a three-necked flask provided by a condenser. The reaction was initiated by the addition of ethanolic solution (50 ml.) of benzoyl peroxide. Oxygen-free carbon dioxide gas was bubbled through the reaction mixture for the purpose of stirring the solution and preventing the ferrous ions from being oxidized by air. Reactions were carried out at temperatures between 15 and 32°C. The analytical procedures of benzoyl peroxide was a modification of the method recommended by Nozaki[4]. At specified times after

* Presented at the Annual Meeting of the Chemical Society of Japan, Tokyo, April 5, 1958.

1) M. S. Kharasch, A. Funo and W. Nudenberg, *J. Org. Chem.*, **15**, 763 (1950).

2) F. Haber and P. Weiss, *Proc. Roy. Soc. London*, **A147**, 332 (1934).

3) S. Hasegawa et al., This Bulletin, **31**, 696 (1958).

4) K. Nozaki, *Ind. Eng. Chem., Anal. Ed.*, **19**, 872 (1947).

the beginning of the reaction, aliquots of the reaction mixture were pipetted out from the flask into an Erlenmeyer flask containing 1 ml. of saturated sodium hydrogen phosphate to eliminate ferric ions, which would, otherwise, disturb the correct analysis of benzoyl peroxide. Five milliliters of acetic anhydride in which 0.3 g. of sodium iodide had been dissolved was added and then allowed to stand about half an hour at room temperature. Iodine liberated was titrated with 0.01 N sodium thiosulfate solution adding 1% starch solution towards the last. This method of analysis is favored by the fact that the atmosphere above the solution to be analysed need not be replaced by inert gas.

Ferrous ion is known to react with $\alpha\alpha'$-bipyridyl forming a very stable red complex which has the maximum absorbance at 510 mμ. Colorimetric measurement was, therefore, applied to determine the concentration of the ferrous ion in the reaction mixture. One milliliter of an aqueous solution of 1% $\alpha\alpha'$-bipyridyl was buffered at pH of 4.75 by acetic acid~sodium acetate solution. Ten milliliters of the reaction mixture was added to the solution followed by dilution with water. When it was allowed to stand at room temperature, colloidal particles of benzoyl peroxide appeared which grew up to precipitate after standing for 2~3 hr. This precipitate was filtered off and the absorbance of the solution at 470 mμ was measured by a photoelectric colorimeter. A plot of the absorbance against the ferrous ion concentration in a series of blank experiments showed a straight line relationship up to about 1.5×10^{-4} mol./l. of ferrous ion, in accordance with Beer's law.

The initial concentration of benzoyl peroxide was 5×10^{-3} mol./l. in each run.

Results and Discussion

The extent of the decomposition of benzoyl peroxide induced by ferrous ions was plotted against time as shown in Fig. 1. As is seen from the figure, this reaction takes place with considerable rate even at room temperature.

According to the reaction 1, the rate of the ferrous ion induced decomposition of benzoyl peroxide should be expressed as follows:

$$-\mathrm{d}[P]/\mathrm{d}t = k_1[P][\mathrm{Fe}^{2+}] \qquad (2)$$

or rearranging Eq. 2,

$$-\mathrm{d}\ln[P]/\mathrm{d}t = k_1[\mathrm{Fe}^{2+}] \qquad (3)$$

Instead of the extent of the decomposition, the logarithm of the corresponding volume v of sodium thiosulfate consumed in titration, was plotted against time t; this is shown in Fig. 2 for various initial ferrous ion concentrations at 25°C. Extrapolated values of each curve evidently correspond to the initial concentration of benzoyl peroxide. It is to be noted from Fig. 2 that the slope of the curves, i.e., $\mathrm{d}\log[P]/\mathrm{d}t$ has not suffered a marked change during the reaction. This means that the apparent decomposition rate of benzoyl peroxide is

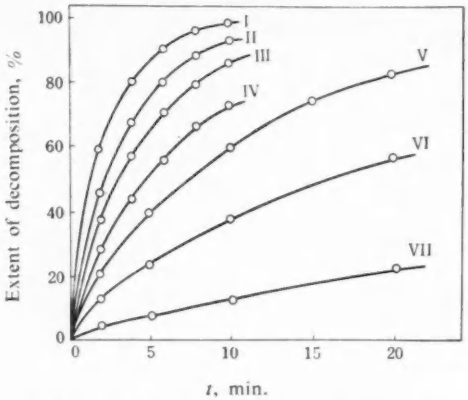

Fig. 1. Extent of decomposition of benzoyl peroxide in ethanol at 25°C. $[FeCl_2]_0\times10^4$: I, 25.1; II, 16.5; III, 13.6; IV, 10.6; 6.8; VI, 5.4; VII, 2.5 mol./l., respectively; $[BPO]_0$: 5×10^{-3} mol./l.

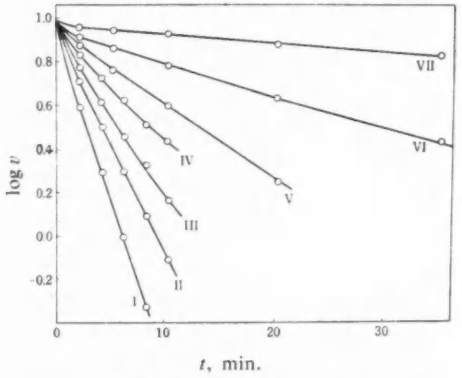

Fig. 2. Relation between $\log v$ and t. Numbers are identical with those in Fig. 1.

nearly of the first order with respect to benzoyl peroxide. Another evidence for the first order reaction lies in the fact that the slope of the curves in Fig. 3 in which $\log v$ was plotted against t, seems to be independent of the initial concentration of benzoxyl peroxide.

The slopes of the curves in Fig. 2 seem to be linearly proportional to the initial concentration of ferrous ion. Although care was taken to remove oxygen, the trace of oxygen in the solution might oxidize the ferrous ions. In addition, ferrous ions are oxidized by reaction 1. Therefore, it is necessary to determine the true concentration of ferrous ions in solution.

The ferrous ion concentration in the reaction mixture at any time was determined by the colorimetric method. The slope $-\mathrm{d}\log$

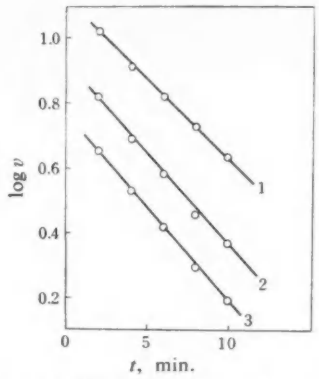

Fig. 3. Relation between $\log v$ and t at 25°C; $[BPO]_0 \times 10^3$: 1, 7.5; 2, 5.0; 3, 3.3 mol./l., respectively; $[FeCl_2]_0$: 10.1×10^{-4} mol./l.

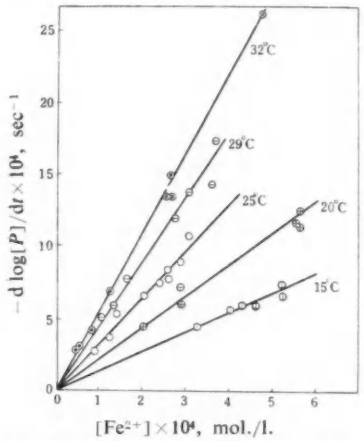

Fig. 4. Plots of $-d \log [P]/dt$ against actual ferrous ion concentration in ethanol at various temperatures.

$[P]/dt$ was plotted against the ferrous ion concentration as shown in Fig. 4. The plots gave straight lines, all of which converged to the origin of the coordinate at each temperature.

Thus it could be said that equation 2 is the complete expression for the reaction rate in accordance with the mechanism postulated above.

Table I shows the numerical values for $[Fe^{2+}]$, $-d \log [P]/dt$ and k_1 at various temperatures. Fig. 5 shows the Arrhenius plot which gives a straight line. The Arrhenius equation for the decomposition reaction was calculated to be $k_1 = 2.2 \times 10^{11} \exp(-14.21 \times 10^3/RT)$ mol^{-1} l. sec^{-1} with a standard deviation of 0.40 for $\log A$ and 0.55 kcal. mol.$^{-1}$ for E, where A and E represent the frequency factor and the activation energy, respectively.

Table I. Rate constants for benzoyl peroxide-iron(II) reaction

t °C	$[Fe^{2+}] \times 10^4$ mol. l^{-1}	$-d \log [P]/dt \times 10^4$ sec^{-1}	k_1 mol.$^{-1}$ l. sec^{-1}	k_1 av.
	4.65	29.0	14.4	
	2.65	15.0	13.0	
	2.60	16.7	14.8	
32	2.50	15.0	13.8	14.4±0.2
	1.20	7.67	14.7	
	0.80	4.67	13.4	
	0.50	3.33	15.3	
	0.43	3.00	16.1	
	3.65	19.3	12.2	
	3.55	16.0	10.4	
	3.05	15.3	11.6	
29	2.70	13.3	11.3	11.8±0.2
	1.60	8.67	12.5	
	1.30	6.67	11.8	
	1.00	5.67	13.1	
	3.00	12.0	9.21	
	2.85	10.0	8.08	
	2.55	9.33	8.43	
	2.55	8.67	7.83	
25	2.35	8.33	8.16	8.44±0.14
	2.00	7.33	8.44	
	1.35	5.67	9.67	
	1.20	4.17	8.00	
	0.85	3.00	8.13	
	5.55	14.0	5.84	
	5.55	12.7	5.27	
20	5.45	13.0	5.49	5.71±0.12
	2.85	8.00	6.46	
	2.85	6.67	5.39	
	1.98	5.00	5.82	
	5.15	8.33	3.73	
	5.15	7.33	3.28	
15	4.55	6.67	3.38	3.56±0.05
	4.20	6.67	3.66	
	3.95	6.33	3.69	
	3.20	5.00	3.60	

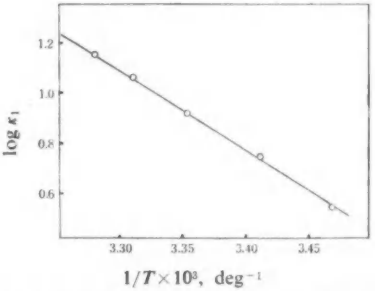

Fig. 5. Arrhenius plot of $\log k_1$ against $1/T$.

As is seen above, the reaction proceeds bimolecularly in accordance with the Haber-Weiss mechanism, and hence the reaction should be of the second order. However, as shown in Fig. 2, the apparent decomposition was approximately of the first order. In order for the reaction to be of the first order, the ferrous ion concentration in Eq. 2 must be kept constant during the reaction. Ferrous ion concentration was decreased rapidly at first, but became nearly contant within 2~3 min. It could be said therefore, that ferrous ion concentration was roughly kept constant during the stationary state.

It is well known that the thermal decomposition rate of peroxides in various solvents can be expressed as[5]

$$-\mathrm{d}[P]/\mathrm{d}t = k_d[P] + k_i[P]^x \qquad (4)$$

where k_d represents the specific rate of spontaneous cleavage, k_i the specific rate constant of induced decomposition and x the order of the induced reaction which may vary between 0.5 and 2.0. In ethanol solution, x was reported to be unity[6], and the apparent decomposition rate was of the first order. In this case, the essential reactions were considered to take place as follows:

$$\mathrm{P} \xrightarrow{k_d} 2\mathrm{RCOO}\cdot \qquad (5)$$

$$\mathrm{RCOO}\cdot + \mathrm{CH_3CH_2OH} \xrightarrow{k_2} \mathrm{RCOOH} + \mathrm{CH_3\dot{C}HOH} \qquad (6)$$

$$\mathrm{CH_3\dot{C}HOH} + \mathrm{P} \xrightarrow{k_3} \mathrm{CH_3CHO} + \mathrm{RCOO}\cdot + \mathrm{RCOOH} \qquad (7)$$

$$\mathrm{CH_3\dot{C}HOH} + \mathrm{RCOO}\cdot \xrightarrow{k_4} \mathrm{RCOOH} + \mathrm{CH_3CHO} \qquad (8)$$

and the apparent decomposition rate was given by

$$-\mathrm{d}[P]/\mathrm{d}t = k'[P] \qquad (9)$$

where k' is a constant including some specific rate constants in the equations given above. The specific rate constant for the spontaneous decomposition k_d may be negligible at room temperature. Hence, in the presence of ferrous ion, reaction 7 will take part in the decomposition of benzoyl peroxide together with reaction 1. The overall rate of the decomposition reaction may be expressed as

$$-\mathrm{d}[P]\,\mathrm{d}t = k_1[P][\mathrm{Fe}^{2+}] + k'[P] \qquad (10)$$

If the reaction 7 occurs predominantly, the mole ratio of benzoyl peroxide decomposed to ferrous ion consumed will be greater than unity. In fact as is seen from Fig. 2, the amount of the peroxide decomposed in each case was much greater than those expected from reaction 1. However, comparing Eq. 10 with Eq. 2 which was confirmed experimentally, the second term of the right hand side in Eq. 10 could be neglected. This indicates that radical-induced decomposition of benzoyl peroxide may be suppressed by the presence of ferrous ions, as in the case of the decomposition of benzoyl peroxide by dimethyl aniline[7].

In order to explain both the first order decomposition and the suppression of reaction 7, reduction of ferric to ferrous ion may be postulated. Since ethanol radical is considered as an electron donor, this reduction would take place through reaction 11:

$$\mathrm{CH_3\dot{C}HOH} + \mathrm{Fe}^{3+} \xrightarrow{k_5} \mathrm{CH_3CHO} + \mathrm{Fe}^{2+} + \mathrm{H}^+ \qquad (11)$$

Thus it may be assumed that the reactions 1, 6, 8 and 11 are predominant. If the stationary state conditions for radicals are applied, then for RCOO·,

$$k_1[P][\mathrm{Fe}^{2+}] = k_2[\mathrm{RCOO}\cdot][\mathrm{CH_3CH_2OH}] + k_4[\mathrm{RCOO}\cdot][\mathrm{CH_3\dot{C}HOH}] \qquad (12)$$

and for $\mathrm{CH_3\dot{C}HOH}$,

$$k_2[\mathrm{RCOO}\cdot][\mathrm{CH_3CH_2OH}] = k_4[\mathrm{RCOO}\cdot][\mathrm{CH_3\dot{C}HOH}] + k_5[\mathrm{CH_3\dot{C}HOH}][\mathrm{Fe}^{3+}] \qquad (13)$$

Therefore, from these equations, it follows

$$k_1[P][\mathrm{Fe}^{2+}] = k_5[\mathrm{CH_3\dot{C}HOH}][\mathrm{Fe}^{3+}] + 2k_4[\mathrm{RCOO}\cdot][\mathrm{CH_3\dot{C}HOH}] \qquad (14)$$

The left hand side in Eq. 14 represents the rate of the oxidation of ferrous ion and the first term of the right hand side is that of reduction of ferric ion. As mentioned earlier, the ferrous ion concentration did not suffer a marked change during the reaction after a stationary state was attained. Hence, the second term of the right hand side in Eq. 14 may be neglected. The main reactions in this study may, therefore, be reduced to reactions 1, 6 and 11. Among these reactions, iron may be considered to serve as electron transferer.

Swain et al.[8] believe that two benzoxy groups

5) P. D. Bartlett and K. Nozaki, *J. Am. Chem. Soc.*, **68**, 1686 (1946); ibid., **69**, 2299 (1947); W. E. Cass, ibid., **68**, 1976 (1946).

6) S. Kato and F. Mashio, *J. Chem. Soc. Japan, Ind. Chem. Sec.* (*Kogyo Kagaku Zasshi*), **59**, 380 (1956).

7) M. Imoto and C. Suckon, *Chem. High Polymers* (*Kobunshi Kagaku*) **11**, 396 (1954).

8) C. G. Swain, W. T. Stockmayer and J. T. Clarke, *J. Am. Chem. Soc.*, **72**, 5426 (1950); ibid., **68**, 1686 (1946).

in benzoyl peroxide are dipoles attached to one another in such a way as to repel each other:

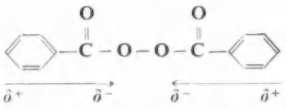

and they ascribed the driving force of the decomposition of the peroxide to the electrostatic repulsion between two benzoxy groups. Whereas, Imoto et al.[7] proposed that the driving force was due to the repulsion between oxygen atoms on carbonyl groups,

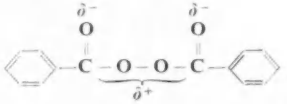

and successfully explained the effect of substituents on phenyl rings of benzoyl peroxide upon the rate of decomposition in the presence of dimethyl aniline.

In the reaction of benzoyl peroxide with ferrous ion, as is the case for the reaction between benzoyl peroxide and dimethyl aniline, the two species, when they approach, will interact with each other forming an activated complex:

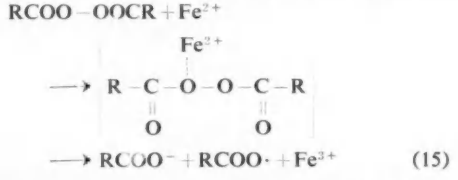

$$\longrightarrow RCOO^- + RCOO\cdot + Fe^{3+} \qquad (15)$$

An electron jump from ferrous ion to either of the oxygen atoms bonded to each other will easily take place. Orr and Williams[9] suggested the formation of the activated complex by coördination of the ferrous ion and hydroperoxide.

The spontaneous decomposition of benzoyl peroxide in various solvents has been widely studied by many authors[10] and they found that the activation energy was 28~30 kcal./mol., which is slightly lower than the O–O bond energy, 34 kcal./mol., calculated by Pitzer[11].

A short discussion of activation entropy may be relevant to the present problem. It is noted that the frequency factor of the thermal decomposition of benzoyl peroxide in various solvents is of the order of 10^{13}~10^{15} mol^{-1} l. sec^{-1}, the value for which is abnormally large owing, probably, to the chain process. But, as already stated, in the present case, the factor A was found to be 2.2×10^{11}. This will also suggest the fundamental difference in the reaction mechanisms in two cases. Rollefson[12] considers that the activation entropy is a measure of the bond strength of activated complex. The frequency factor of 2.2×10^{11} corresponds to the entropy loss of about 11.2 e.u. provided the transmission coefficient is unity. The value may be compared with $\Delta S^{\neq}$ of -10 e.u. which is accompanied by the loss of only one degree of translational freedom[9]. Accordingly, it seems that ferrous ion forms a weakly combined complex with benzoyl peroxide molecule. From the standpoint of the entropy factor, the decomposition mechanism proposed above could again be considered to be reasonable.

Summary

An investigation of the rate of decomposition of benzoyl peroxide by ferrous ion in ethanol has been made. The rate of the reaction was linearly proportional to the concentrations of benzoyl peroxide and ferrous ion, in accordance with Haber-Weiss one electron transfer mechanism. But the apparent decomposition rate was of the first order. The Arrhenius equation was $k_1=2.2\times10^{11}\exp(-14{,}210/RT)\,mol^{-1}$ l. sec^{-1}.

Department of Chemistry
Faculty of Science
Okayama University
Tsushima, Okayama

9) R. J. Orr and H. L. Williams, *J. Phys. Chem.*, **57**, 925 (1953).
10) K. Nozaki and P. D. Bartlett, *J. Am. Chem. Soc.*, **68**, 1686 (1946); P. F. Hartman, H. G. Sellers and D. Turnbull, ibid., **69**, 2416 (1947); A. T. Blomquist and A. J. Buselli, ibid., **73**, 3883 (1951).
11) K. S. Pitzer, ibid., **70**, 2140 (1948).
12) G. K. Rollefson, *J. Phys. Chem.* **56**, 976 (1952).

Molecular Complexes between Ketones and Alkali Salts

By Haruka YAMADA

(Received December 14, 1959)

Sodium or lithium perchlorate and sodium iodide have high solubilities in ketones. These salts form a sort of molecular complex with ketones. From infrared studies[1,2] it has been shown that the change of the ketone band with salt concentration differs from that in general solvation case, and the non-complexed ketone band is replaced by the shifted band of the complexed ketone; namely, one absorption maximum falls gradually in intensity to be replaced by another. Further, it has been shown that the separation between the complexed and non-complexed ketone bands is independent of anion species. Based on these facts, it has been understood that the formation of the complex is due to the bonding between the C=O group and metallic cation.

These complexes are of interest, because they will give information upon the covalent bond formation, besides the other intermolecular interactions such as ion-dipole, dipole-dipole interaction, London force etc., of alkali metallic ions with some electron donor molecules. The present studies are undertaken to elucidate the electronic states of the complexes.

In ultraviolet absorption spectra, the shifts caused by the formation of the complexes are measured for the $n\rightarrow\pi^*$ and $\pi\rightarrow\pi^*$ bands. In order to know whether or not the experimental results obtained here are interpreted based on the theory of charge transfer complex[3], the covalent characters and the stabilization energies of the complexes have been estimated by use of Pauling's "bond-length" relation[4]. By these estimated values, the $n\rightarrow\pi^*$ transition energies of the complexes have been calculated and compared with the observed data.

Experimental

Ultraviolet absorption spectra were taken with a modified* Perkin-Elmer Model 112 Infrared Spectrophotometer equipped with LiF prism. A H_2-lamp and a 1P28 photomultiplier were used as light source and detector, respectively. Wavelength calibration was made by means of the spectra of Hg-lamp and benzene vapor. Cells had quartz windows and lead Spacers. The thickness of the cell was measured by interference method. Spectral slit width ranged from $10\,cm^{-1}$ to $20\,cm^{-1}$.

Infrared spectra were taken with the spectrophotometer mentioned above, by use of CaF_2 prism.

Organic compounds were purified by fractionating after drying. Guaranteed commercial anhydrous sodium iodide was used without further purification. Anhydrous sodium perchlorate was obtained heating $NaClO_4 \cdot H_2O$ in an air bath. Lithium perchlorate was prepared by neutralizing lithium carbonate with a slight excess of 60% perchlorate acid, and digesting the mixture on a hot plate until evolution of carbon dioxide ceased, and a clear solution remained. The solution was heated to remove excess acid and the white solid remained. The salt was dehydrated by heating in vacuo to approximately 100°C over phosphorus pentoxide. The anhydrous salts were stored in the dark in a desiccator. Measurements were made for pure ketones and the ketone solutions of the salts. No diluent was added, as no suitable solvent for the complexes was found.

Experimental Results

Infrared Absorption Spectra.—The wave numbers for C=O stretching bands are tabulated in Table I. From this table, it can be seen that the wave numbers for the NaI- and the $NaClO_4$-ketone system are about the same and that the observed shifts are larger for lithium salt than for sodium salt and exhibit a similarity between the acetone- and the cyclohexanonesalt system.

TABLE I. WAVE NUMBERS FOR C=O STRETCHING BANDS

	Pure liquid	NaI-ketone complex	$NaClO_4$-ketone complex	$LiClO_4$-ketone complex
Acetone	1717	1709	1710	1702
Cyclohexanone	1714	1706	1706	1702
Acetophenone	1685	(1684)	(1680)	(1677)

Ultraviolet Absorption Spectra.—The curves obtained for the $NaClO_4$- and the $LiClO_4$-acetone systems both in 1:4 mole ratio are shown in Fig. 1. The non-complexed acetone band attributed to the $n\rightarrow\pi^*$ transition has a maximum at $36400\,cm^{-1}$. By the addition of the salt the band shifts to higher frequencies with

1) A. D. E. Pullin and J. McC. Pollock, *Trans. Faraday Soc.*, **54**, 11 (1958).
2) H. Yamada, This Bulletin, **33**, 666 (1960).
3) R. S. Mulliken, *J. Am. Chem. Soc.*, **72**, 600 (1950); ibid., **74**, 811 (1952); *J. Phys. Chem.*, **56**, 801 (1952).
4) L. Pauling, *J. Am. Chem. Soc.*, **69**, 542 (1947).

* Thanks are due to Mr. W. Suëtaka and Mr. S. Saito for their help in this modification.

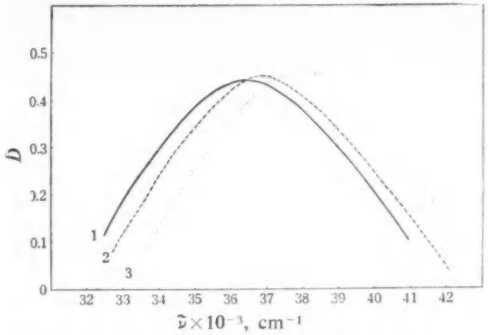

Fig. 1. $n\rightarrow\pi^*$ bands of acetone and acetone-salt solutions.
1. Pure acetone.
2. Acetone-$NaClO_4$ solution (in 4 : 1 mole ratio).
3. Acetone-$LiClO_4$ solution (in 4 : 1 mole ratio).

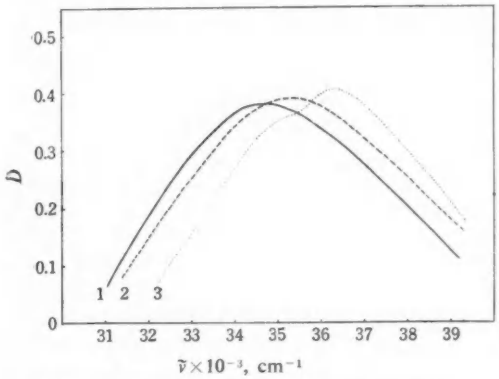

Fig. 2. $n\rightarrow\pi^*$ bands of cyclohexanone and cyclohexanone-salt solutions.
1. Pure cyclohexanone.
2. Cyclohexanone-$NaClO_4$ solution (in 4 : 1 mole ratio).
3. Cyclohexanone-$LiClO_4$ solution (in ca. 6.5 : 1 mole ratio).

the maximum at 36900 cm^{-1} for the $NaClO_4$-acetone system and at 38000 cm^{-1} for the $LiClO_4$-acetone system. The band for the $LiClO_4$-acetone system shows a contour with two peaks at a lower perchlorate concentration. In 1 : 4 mole ratio, almost all the acetone molecules are, therefore, regarded as forming the complex with the salt. For the $NaClO_4$-acetone system the separation between acetone and the complex bands is relatively small and the variation of band contour is not found for changing mole ratio.

The observed curves for the $NaClO_4$- and the $LiClO_4$-cyclohexanone system are shown in Fig. 2. The $n\rightarrow\pi^*$ band maximum of cyclohexanone at 34700 cm^{-1} shifts to 35300 cm^{-1} by the addition of $NaClO_4$ and to 36400 cm^{-1} by that of $LiClO_4$. The curves for the $LiClO_4$-cyclohexanone system measured for various concentrations are shown in Fig. 3. Each band shows the contour of two components. Since all these curves intersect at about 35600 cm^{-1} and the number of cyclohexanone molecules in unit volume, calculated from the specific gravity of the solution, is almost constant over this range of concentration, this point at about 35600 cm^{-1} is the so-called isosbestic point for the $LiClO_4$-cyclohexanone system.

The curves for the $NaClO_4$- and the $LiClO_4$-acetophenone system are shown in Fig. 4. Acetophenone shows a $\pi\rightarrow\pi^*$ band together with the $n\rightarrow\pi^*$ band in ultraviolet region. Although the solubilities of the salts in acetophenone are relatively low, the shifts are observed distinctly. By adding the salt the $n\rightarrow\pi^*$ band, having a maximum at 31250 cm^{-1}, shows the blue shift similar to the $n\rightarrow\pi^*$ bands of the other ketones. The red shift of the $\pi\rightarrow\pi^*$ band was observed, although the band maximum was difficult to determine owing to the high intensity. As shown in Fig. 4, the peak of $n\rightarrow\pi^*$ band for the $LiClO_4$-acetophenone system is hardly ever found in 1 : 10 mole ratio and can not be found in 1 : 6 mole ratio, because it is covered with the $\pi\rightarrow\pi^*$ band shifted to lower frequencies.

Although it might be expected from the results of infrared studies that the ultraviolet spectrum of the sodium iodide-ketone system is similar to that of the sodium perchlorate-ketone system, it is not actually the case.

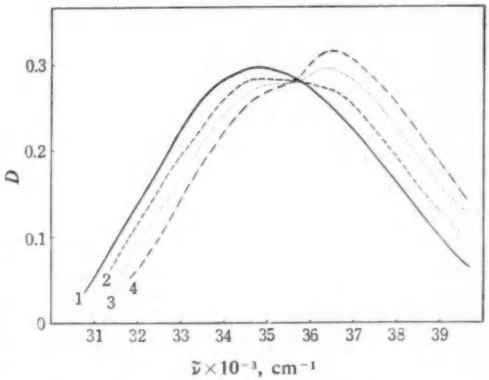

Fig. 3. Curves for cyclohexanone-$LiClO_4$ solutions in various concentrations (27.2 μ cell).
1. Pure cyclohexanone.
2. ca. 15 : 1 mole ratio.
3. 8.1 : 1 mole ratio.
4. 6.5 : 1 mole ratio (saturated).

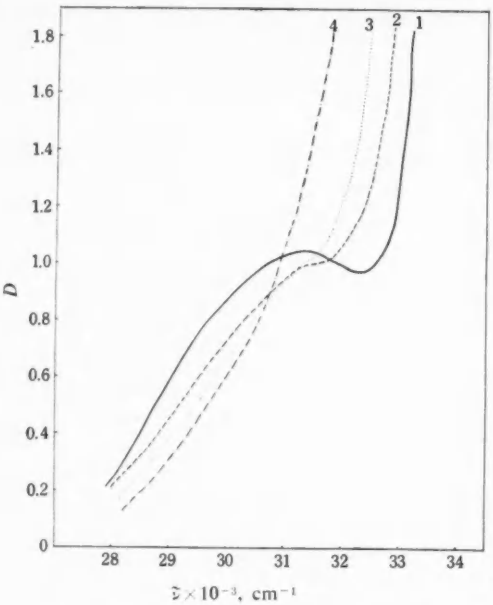

Fig. 4. Spectra of acetophenone and acetophenone-salt solutions.
1. Pure acetophenone.
2. Acetophenone-$NaClO_4$ solution (in ca. 12 : 1 mole ratio).
3. Acetophenone-$LiClO_4$ solution (in ca. 10 : 1 mole ratio).
4. Acetophenone-$LiClO_4$ solution (in ca. 6 : 1 mole ratio).

The curve measured for the sodium iodide-ketone system, however, has a strong absorption ranging from about 31000 cm^{-1} to higher frequencies, which is probably caused by the iodide ion in the solution.

The $n \rightarrow \pi^*$ blue shift and $\pi \rightarrow \pi^*$ red shift phenomena observed here are similar to but generally much larger than those usually observed as general solvent effects. The band contours can be separated into two components. These phenomena are just like those observed for the hydrogen bond formation.

Interpretations

Infrared Spectra.—Although only the C=O bands are shown in Table I, the slight changes for the other ketone bands were also found similar to the sodium iodide-acetone complex[2]. From the fact that the $NaClO_4$-ketone and NaI-ketone complexes show the same frequencies, it follows that the formation of the complexes is independent of anion species. The solubilities of the salts in acetophenone are low and the spectra of the saturated solutions are not those of the complexes but those of the complexed acetophenone overlapped with the non-complexed one. The observed shifts for the acetophenone-salt systems, therefore, are small.

Covalent Contribution to the Intermolecular Bond.—By considering a charge transfer force between C=O group and metallic ion, besides the other intermolecular interactions such as ion-dipole, dipole-dipole interaction, London force etc., the intermolecular bonding is expressed as a resonance between following two structures.

$$\text{(A)} \quad C{=}O \quad M^+$$

$$\text{(B)} \quad C{=}\overset{+}{O}{-}M$$

The structure A expresses a no-bond structure and the structure B dative one which is formed by the transfer of the lone pair electrons of oxygen atom to the cation.

To estimate the contribution of the B structure to the complex, Pauling's "bond-length" relation[4] seems to be useful for the complex[5], since this relation holds for intermetallic compounds and also for organic compounds. The relation is represented by

$$R(n) - R(1) = -C \log_{10} n$$

Here, R expresses the atomic radius, n is the number of shared electron pairs involved in the bond and is proportional to the bond order[5], and C a constant. As for the bond length L the following formula is obtained from the formula described above.

$$L(n) - L(1) = -2C \log_{10} n$$

The values of $L(n)$ are estimated to be 2.15 and 2.46 Å for O—Li^+ and O—Na^+ bonds, respectively. These values are the same as those obtained for $LiClO_4 \cdot 3H_2O$[6a] and $Na_2SbS_4 \cdot 9H_2O$[6b] or $Na \cdot Al(SO_4)_2 \cdot 12H_2O$[6c] crystals in which the Li^+ or Na^+ ion combines with the ligands of six water molecules by the coordination of the lone pair electrons of oxygen atoms. As C is usually 0.30 for intermetallic compounds and 0.35 for organic compounds, the mean value of them, 0.325, is used for these complexes. By use of the usual covalent radii for $R(1)$[7], the relation $L(1) = R_O(1) + R_M(1)$ and the values of $L(n)$, the values of n are obtained. The suffixes O and M refer to

5) Coulson and Danielson applied in to the hydrogen bonds to estimate the contribution of the B structure, and reported that the results obtained agreed satisfactorily with the results calculated by a semi-empirical method. C. A. Coulson and U. Danielson, *Arkiv För Fysik*, **24**, 239 (1954).

6) a) C. D. West, *Z. Krist.*, **88**, 198 (1934).
b) A. Grund and A. Preisnger, *Acta Cryst.*, **3**, 363 (1950).
c) H. Lipson, *Proc. Roy. Soc.* (*London*), **A151**, 347 (1935).

7) The covalent radii used are $R_O(1) = 0.66$, $R_{Li}(1) = 1.34$ and $R_{Na}(1) = 1.54$Å.

oxygen and metal, respectively. From the meaning of n, the following formula should hold for the complexes,

$$b^2 = n \times (\text{covalent character of the } L(1) \text{ bond})$$

Since the covalent character of the $L(1)$ bond can be estimated from the difference between the electronegativities of two atoms, the covalent character of $L(n)$ bond, b^2, is calculated. The results are contained in Table II.

Table II

	n	Difference of electronegativities	Covalent character of the $L(1)$ bond	b^2
O—Li^+	0.59	2.5	22%	0.13
O—Na^+	0.40	2.6	20%	0.08

The covalent character of O—Li^+ is 13% and that of O—Na^+ 8%. It can be seen that these complexes mainly consist of the no-bond structure and the covalent character of O—Li^+ is about 1.5 times that of O—Na^+.

Stabilization Energy of the Complex.—By use of the amount of contribution of the B structure obtained above, the stabilization energy of the complex per one ketone molecule was estimated. According to Mulliken[3], the ground state wave function of the complex is written by

$$\Psi_N = a\phi_A + b\phi_B$$

and the stabilization energy of the complex in ground state is given by

$$W_{AA} - W_N = (W_{BB} - W_{AA})b^2/a^2$$

where ϕ_A is the no-bond wave function and ϕ_B the dative one,

$$W_{AA} = \int \phi_A H \phi_A d\tau$$

$$W_{BB} = \int \phi_B H \phi_B d\tau = I_P - E_A + V$$

In this case, I_P is the ionization potential of the oxygen atom for lone pair electrons, E_A the electron affinity of the metallic ion and V the energy of the covalent bond between the oxygen atom and the ion. Although the exact values of I_P and E_A are not available, the following ones seem to be reliable, i.e. $I_P = 10.1$ eV., $E_A = 5.39$ eV. for Li^+ and 5.14 eV. for Na^+. The energy V may be expressed by Morse's function, i. e.

$$V = D_e(e^{-2a(L-L_e)} - 2e^{-a(L-L_e)}),\ L_e = L(1)$$

where the dissociation energy, D_e, is given by the geometric mean of the bond energies D(O—O) and D(M—M), and a is determined by Badger's rule.

$$a = (k/2D_e)^{1/2}$$

where k expresses the force constant.

Table III

	D_e (kcal./mol.)	k (dyne/cm.)	a ($Å^{-1}$)	V (eV.)
O—Li^+	30.8	0.808×10^5	1.37	−1.29
O—Na^+	25.3	0.847×10^5	1.55	−0.977

The formation energy of the complex bond, namely the stabilization energy of the lone pair electrons is determined as follows.

$$W_{AA} - W_N = (I_P - E_A + V)b^2/a^2$$
$$= 0.51 \text{ eV. } (O—Li^+)$$
$$0.34 \text{ eV. } (O—Na^+)$$

where W_{AA} is taken to be zero.

Computation of the $n \rightarrow \pi^*$ Transition Energies of the Acetone-salt Complexes.—By taking into account the stabilization energies, the $n \rightarrow \pi^*$ transition energies of the complexes can be calculated. As the energy level of lone pair electrons is approximately expressed by the coulomb integral of oxygen atom, the stabilization energy of the complex is due to the decrease of the coulomb integral of oxygen atom. The stabilized energy level may be expressed by

$$\alpha_O' = \alpha_O + (W_{AA} - W_N)/2$$

Here, α_O expresses the coulomb integral of oxygen atom. As for the other numerical values required for the computations, Nagakura's values[8] for acetone molecule are used. They are, $X_C = 2.5$, $X_O = 3.5$, $k = 4.1$, $\alpha_C = 4.35\beta$, $\alpha_O = 5.44\beta$ and $\beta_{CO} = 0.838\beta$ in his notation. The calculated results are shown in Table IV(A), in which the $n \rightarrow \pi^*$ transition energy is expressed by $E_2 - \alpha_O'$. In Table IV(B) the calculated $n \rightarrow \pi$ transition energies are shown in wave number unit, together with the observed data. Here, $\beta = 2.84$ eV. $= 23000$ cm^{-1}. It seems more reasonable to compare the calculated

Table IV

(A)

	Acetone	$NaClO_4$-acetone complex	$LiClO_4$-acetone complex
E_1	5.895β	5.94β	5.96β
E_2	3.895	3.91	3.92
α_O'	5.44	5.50	5.53
$E_2 - \alpha_O'$	−1.55	−1.59	−1.61

(B)

Cal.	35600	36600	37000
Obs.	35800 (in non-polar solvent)	36900	38000
	36400 (in liquid)		

8) S. Nagakura, This Bulletin, 25, 164 (1952).

value for acetone with the observed value in non-polar solvent than that in liquid.

Although the formation of the complexes is mainly due to the no-bond structures, the $n \rightarrow \pi^*$ blue shift phenomenon is interpreted by use of the results calculated by considering the charge transfer interaction.

The author wishes to express her sincere thanks to Professor K. Kozima for his kind guidance.

Research Laboratory of Spectroscopy
Tokyo Institute of Technology
Meguro-ku, Tokyo

Intramolecular Interaction between N–H Group and π-Electrons in N-Benzylanilines

By Michinori ŌKI and Kiyoshi MUTAI

(Received December 14, 1959)

The discovery[1] of the rotational isomers and the intramolecular interaction between the hydroxyl group and π-electrons in benzyl alcohol derivatives has prompted the authors to examine the N–H stretching absorption of the benzylamine derivatives, since the situation will be much similar in these two series of compounds. The observation of two ν_{N-H} bands for *N*-benzylaniline was reported by Ōki and Iwamura[1], while Russel and Thompson[2] had reported the presence of two ν_{N-H} bands for *N*-benzylaniline and attributed them to the rotational isomerism. Moritz[3] also noticed the existence of two ν_{N-H} bands for some derivatives of *N*-benzylaniline while the present paper was in preparation and the observation of two ν_{N-H} bands for *N*-allylaniline by Schleyer et al.[4] may also fall into this category.

The present paper deals with the rotational isomers of *N*-alkylanilines in respect of the C_{aliph}–N axis and the intramolecular interaction between the N–H group and π-electrons in N-benzylanilines. Aniline derivatives are not the indispensable choice but are convenient for handling, since they do not absorb carbon dioxide from the air owing to the low basicity.

Experimental

Measurement and Calculation.—They were performed as reported previously[5]. The concentration of the carbon tetrachloride solution ranged from 0.003 to 0.005 mol./l.

Materials.—The compounds used in the present study are known compounds unless otherwise stated, and were purified through the known method. Their physical constants agreed well with those reported.

N-(m-Methoxybenzyl)-aniline.— *m*-Methoxybenzanilide obtained by heating methyl *m*-methoxybenzoate with aniline was reduced with lithium aluminum hydride in ether and the product was purified through fractional distillation. It is a colorless oil, b. p. 200~202°C/21 mmHg, $n_D^{25.5}$ 1.6039.

Found: C, 78.97; H, 7.34. Calcd. for $C_{14}H_{15}NO$: C, 78.84; H, 7.09%.

N-(m-Dimethylaminobenzyl)-aniline.—It was prepared similarly as above, starting from *m*-dimethylaminobenzanilide, and recrystallized from ethanol. It forms colorless needles melting at 60–61°C.

Found: C, 79.65; H, 8.12. Calcd. for $C_{15}H_{18}N_2$: C, 79.60; H, 8.02%.

Results and Discussion

***N*-Alkylanilines.**—The apparent absorption curves for N–H stretching of *N*-alkylanilines are shown in Fig. 1. The curves for *N*-methylaniline is symmetric, while those for N-ethylaniline and for *N*-isopropylaniline are unsymmetric. The unsymmetric curves are divided, assuming that the curve is an overlap of two symmetric curves which can be expressed by the Lorentz function. The results are summarized in Table I.

Inspection of Table I reveals that the positions of absorption curves can be classified as three categories. Namely, band I is located at about 3444 cm^{-1}, band II at about 3421 cm^{-1} and band III, at about 3395 cm^{-1}. The origin of the splitting of the ν_{N-H} absorption cannot be attributed to hydrogen bonding among the solute molecules, because firstly, the low concentration such as 0.005 mol./l.

1) M. Ōki and H. Iwamura, This Bulletin, **32**, 955 (1959).
2) R. A. Russel and H. W. Thompson, *J. Chem. Soc.*, **1955**, 483.
3) A. G. Moritz, *Spectrochim. Acta*, **12**, 242 (1959).
4) P. von Schleyer, D. S. Trifan and R. Bacskai, *J. Am. Chem. Soc.*, **80**, 6691 (1958).
5) M. Ōki and H. Iwamura, This Bulletin, **32**, 567 (1959).

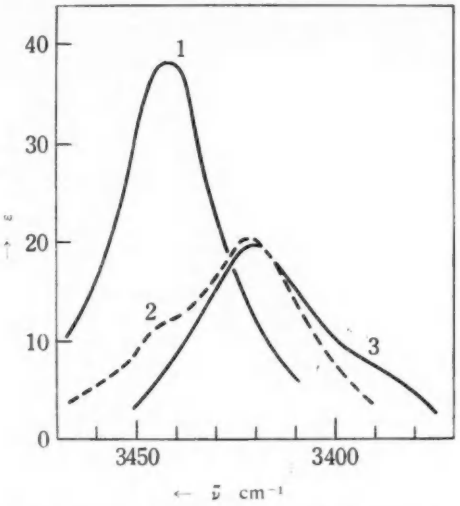

Fig. 1. ν_{N-H} absorptions of methylaniline (1), ethylaniline (2) and isopropylaniline (3).

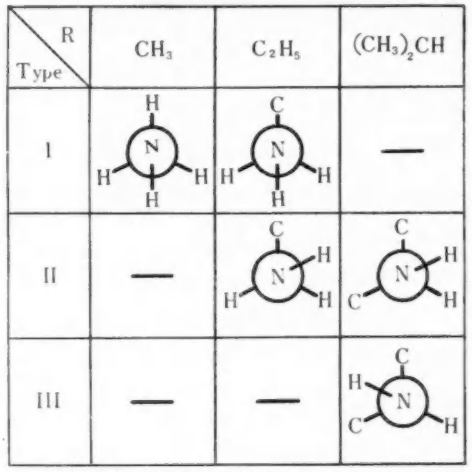

Fig. 2. Classification of rotational isomers in alkylanilines.
The phenyl group is omitted from the diagram for convenience.

TABLE I. ν_{N-H} ABSORPTION OF *N*-ALKYLANILINES ($RNHC_6H_5$)

R	Band	ν_{max} cm^{-1}	$\Delta\nu_{1/2}$ cm^{-1}	$A\times10^{-3}$ mol^{-1}·l.·cm^{-2}
CH_3	I	3442.6	29.8	4.13
C_2H_5	I	3445.2	18.2	0.28
	II	3421.4	34.2	2.44
$(CH_3)_2CH$	II	3420.5	31.2	2.19
	III	3394.5	22.0	0.30

would not permit the dimeric form to exist and secondly any kind of association of the molecules does not explain the symmetry of the absorption curve of *N*-methylaniline examined under the similar conditions as the others.

Thus the variation of the curves must be attributed to the variation of the alkyl group attached to the nitrogen atom and the concept of the rotational isomerism about the C_{aliph}–N axis will be valid for the explanation as for a similar phenomenon in the aliphatic alcohols[6].

In Fig. 2, the projection of the molecule through the C_{aliph}–N axis, the nitrogen atom being located at the upper side, is shown. A circle indicates a carbon atom as is customary in Newman projection. It is assumed that the molecule does not take an eclipsed form, thence the hydrogen atom of the N–H group in *N*-methylaniline must be in the same situation, because it always comes between the two hydrogen atoms attached to the alpha-carbon atom, no matter what rotational position is taken. On the other hand, when the alkyl group is an ethyl, there are two posibilities, that the hydrogen atom of the N–H group comes either between the two hydrogen atoms of the alpha-carbon atom or between the carbon and the hydrogen atoms combined with the alpha-carbon atom. Thus two rotational isomers are possible for *N*-ethylaniline. Similarly, *N*-isopropylaniline can take two conformations. Band I may be considered to correspond to rotational isomer I, band II to isomer II and band III to isomer III.

The probability of isomer II is 2/3 for both *N*-ethylaniline and *N*-isopropylaniline. However, the observed values widely differ from those expected and isomer II seems to be an overwhelming majority, since it is probable to assume that the light absorption of a molecule is the same irrespective of its conformation. The reason is not completely understood at the present time but it is clear that the steric effect plays an important role, because the nitrogen atom carries a large phenyl group.

N-Arylmethylanilines.—*N*-Benzylaniline derivatives have two distinct maxima for N–H stretching absorption and the separation of the two bands are much clearer than in *N*-alkylanilines (compare Fig. 3 with Fig. 1). The apparent absorption curves for *N*-(*p*-nitrobenzyl)-aniline, *N*-benzylaniline and *N*-(*p*-dimethylaminobenzyl)-aniline are shown in Fig. 3.

The electron-withdrawing group such as the nitro group enhances the band at the higher wave number and diminishes the band at the lower wave number. On the other hand, the electron-donating group such as the dimethylamino group shows just the contrary tendency

6) M. Ōki and H. Iwamura, ibid. 32, 950 (1959).

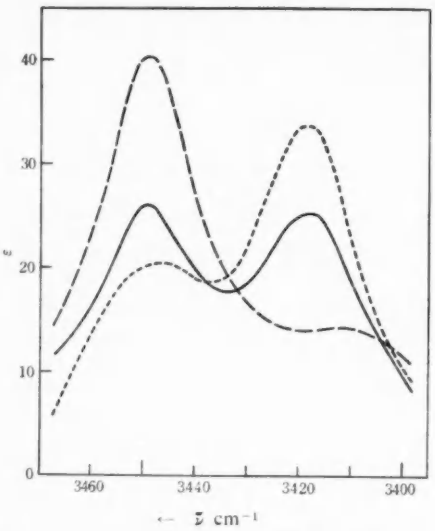

Fig. 3. ν_{N-H} absorptions of benzylaniline (——), *p*-nitrobenzylaniline (----) and *p*-dimethylaminobenzylaniline (------).

and the absorption at the lower wave number forms the main peak. It is again assumed that the curves are the overlaps of the two symmetric curves which obey the Lorentz function and the apparent curves are divided by Ramsay's first method. The results are shown in Table II.

The ratio A_i/A_f, where A_i is the integrated intensity of the absorption due to the interacting form and A_f that of the free form, varies with the electron-donating or electron-withdrawing nature of the substituent and the tendency is indicative of the interaction between the π-electron and the N-H group. The summation of the integrated intensities due to the two forms also changes when the substituent varies, but this fact may be left out, for comparison of the ratio A_i/A_f.

Hammett's σ values[7] of the substituents are taken and the relation with $\log(A_i/A_f)$ is compared. $\mathrm{Log}(A_i/A_f)$ instead of A_i/A_f is taken, because the equilibrium between the interacting and the free forms is the subject of the present discussion. As is seen from Fig. 4, the relation is linear when the σ constants representing the electron density on the carbon atom[8] (C_1), to which the anilinomethyl group is attached, are taken. However, σ values for the other carbon atoms or for the position between two carbon atoms are not proportional to $\log(A_i/A_f)$.

Since the benzylaniline derivatives are secondary amines, which belong to the *N*-ethylaniline type (Fig. 2), they should have two

TABLE II. ν_{N-H} ABSORPTION OF *N*-(ARYLMETHYL)-ANILINES (x-$RC_6H_4CH_2NHC_6H_5$)

R	*x*	Band	ν_{max} cm^{-1}	$\Delta\nu_{max}$ cm^{-1}	$\Delta\nu^{e}_{1/2}$ cm^{-1}	$A\times10^{-3}$ mol^{-1}·l.·cm^{-2}	$\log(A_i/A_f)$	σ
$(CH_3)_2N$	*p*	i[a]	3418.2	30.5	27.6	3.15	0.382	−0.83
		f[b]	3448.7		24.2	1.31		
	m	i	3419.0	31.8	29.6	2.86	0.276	−0.20 (−0.55)[d]
		f	3450.8		25.6	1.51		
CH_3O	*p*[c]	i	3418.0	32.1	27.8	2.63	0.182	−0.27
		f	3450.1		23.7	1.73		
	m	i	3417.0	32.4	28.4	2.22	0.017	0.12
		f	3449.4		26.8	2.14		
H[c]		i	3417.4	32.8	28.6	2.24	0.025	0.00
		f	3450.2		25.6	2.11		
Cl	*p*	i	3415.3	34.6	37.6	2.76	−0.034	0.23
		f	3449.9		29.2	2.60		
	m	i	3411.9	38.0	27.2	2.23	−0.066	0.37
		f	3449.9		38.4	2.60		
NO_2	*m*	i	3406.6	42.1	45.2	2.03	−0.248	0.71
		f	3448.7		29.4	3.58		
	p	i	3407.9	42.2	51.6	1.94	−0.244	0.78
		f	3450.1		25.2	3.41		

a) i denotes interacting form of the N-H group.
b) f denotes free form of the N-H group.
c) The values are taken from Ref. 1.
d) See the discussion below.

7) L. P. Hammett, "Physical Organic Chemistry", McGraw-Hill Book Co., Inc., New York, (1940); H. H. Jaffé, *Chem. Revs.*, **53**, 191 (1953); D. M. McDaniel and H. C. Brown, *J. Org. Chem.*, **23**, 420 (1958).

8) H. H. Jaffé, *J. Chem. Phys.*, **20**, 279, 778 (1952); *J. Am. Chem. Soc.*, **76**, 5843 (1954).

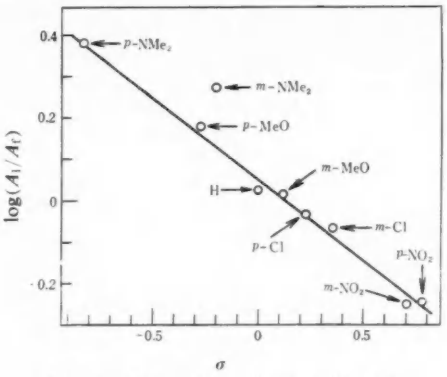

Fig. 4. Comparison of $\log(A_i/A_f)$ of *N*-(arylmethyl)-anilines with σ-values.

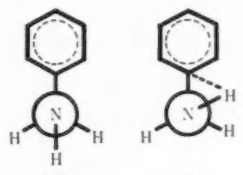

IV V

Fig. 5. Possible rotational isomers of benzylaniline (ring B is abbreviated).

rotational isomers. The absorption due to the free form is closely related to type I of *N*-ethylaniline, because it lies at about 3450 cm^{-1}, while type I of *N*-ethylaniline absorbs at 3445 cm^{-1}. Thus, the free form of *N*-benzylaniline corresponds to the rotational isomer IV and the interacting form to structure V in Fig. 5. The interaction takes place between the π-electron on C_1 atom and the N-H group, as judged from the relation between σ constants and $\log(A_i/A_f)$. Therefore, the structural formula for the interacting form can be represented by structure V.

One problem remains in the above assignment. That is, the number of molecules of the free form of the *N*-benzylaniline derivatives seem to increase in spite of the expectation that the formation of the internal interaction will lessen the free molecules when compared with the number of molecules belonging to type I in *N*-ethylaniline. In the earlier paper[1], it was pointed out that the internal interaction between the hydroxyl group and π-electrons decreases the number of free molecules. This contradiction may be attributed to the steric effect, since the nitrogen atom carries a large phenyl group. And/or it may be attributed to the difference of the nature of the interactions with the N-H group and with the O-H group series.

The far deviation of the point for *N*(*m*-dimethylaminobenzyl)-aniline might be interpreted in the following way. Jaffé[7] gave σ value of -0.20 for the *m*-dimethylamino group and this value is taken in Fig. 4. On the other hand, σ value of the *p*-dimethylamino group has been given by Jaffé as -0.60, while the recent paper by McDaniel and Brown[7] gives -0.83. From an analogous consideration, σ_m given by Jaffé may be smaller than the true and ambiguous, because of lack of examples. The authors obtain -0.55 ± 0.05 for the σ_m of the dimethylamino group from Fig. 4.

Fluctuation of the position for the interacting ν_{N-H} will be discussed in "the nature of the interaction".

***N*-Benzylarylamines.** — The substituent is introduced into the benzene ring which carries the N-H group to understand the electronic effect. It is expected, that the substituent will vary the nature of the N-H bond. The results are given in Table III.

The effect of the substituent on A_i/A_f is not found in Table III. Thus the electron density at the site of hydrogen approach seems

TABLE III. ν_{N-H} ABSORPTION OF *N*-ARYLBENZYLAMINE ($C_6H_5CH_2NHC_6H_4R$-*p*)

R	Band	ν_{max} cm^{-1}	$\Delta\nu_{max}$ cm^{-1}	$\Delta\nu^a_{1/2}$ cm^{-1}	$A\times10^{-3}$ $mol^{-1}\cdot l.\cdot cm^{-2}$	A_i/A_f	σ
CH_3O	i	3405.6	37.1	35.8	1.93	1.11	−0.27
	f	3442.7		30.5	1.74		
CH_3	i	3413.5	34.8	34.6	2.34	1.30	−0.17
	f	3448.3		28.0	1.79		
H[a]	i	3417.4	32.8	28.6	2.24	1.06	0.00
	f	3450.2		25.6	2.11		
Cl	i	3420.7	31.1	26.6	2.55	1.10	0.23
	f	3451.8		23.0	2.32		
Br	i	3421.5	30.0	27.4	2.75	1.08	0.23
	f	3451.5		23.6	2.54		
NO_2	i	3431.8	23.2	17.6	5.45	1.34	0.78
	f	3455.0		17.4	4.05		

a) The values are taken from reference 1.

to determine the number of internally interacting molecules.

The things which vary with the varying substituent are the individual absorption peak of the free and the interacting molecules, and the difference of positions of peaks ($\Delta\nu_{max}$) corresponding to each species of the molecule. The absorption maxima of both free and interacting forms move to higher frequencies as the substituent becomes more electronegative, although the relation between the σ constants and the frequencies of absorption is not perfectly linear. This result roughly agrees with the data obtained by others[9] who have revealed the relationship in aniline derivatives.

One thing noticeable is that $\Delta\nu_{max}$ between the free and the interacting forms relates linearly with the σ value of the substituent (Fig. 6), although the rate of increase or decrease of the frequencies of the free and the interacting forms is not the same and the straight lines, which show the relation between σ value and ν_{max}, are not parallel to each other. The phenomenon will be discussed in "the nature of the interaction".

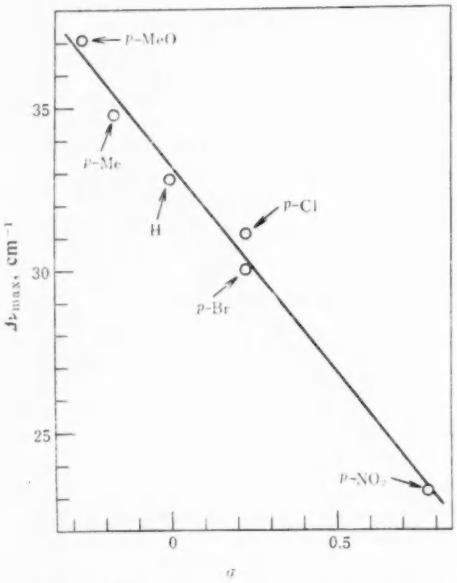

Fig. 6. Comparison of $\Delta\nu_{max}$ of *N*-arylbenzylamines with σ-values.

Nature of the Interaction.—It is now known from Table II that the ν_{N-H} absorption due to the interacting form does not always appear at the constant wave number, when the substituent is introduced into the benzene ring (ring A) which is included in the benzyl group. This is the striking difference when the situation of the benzyl alcohol derivatives is considered, of which interacting hydroxyl groups

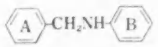

absorb at a reasonably constant frequency. As was already pointed out, the free form absorbs at the constant wave number, ca. 3450 cm^{-1}, irrespective of the substituent, indicating the effect of the substituent through the methylene group is negligible.

The relation between $\Delta\nu_{max}$ and σ values for the compounds carrying a substituent in ring A, is shown in Fig. 7, which reveals, that the slope of the straight line is not constant but shows a crease at some point. When the electron density on ring A is decreased, σ constants and $\Delta\nu_{max}$ are in linear relation, the slope being positive. On the other hand, when σ value is below 0.00~0.10, the slope of the straight line is almost zero, i. e., $\Delta\nu_{max}$ seems to have no connection with the substituent.

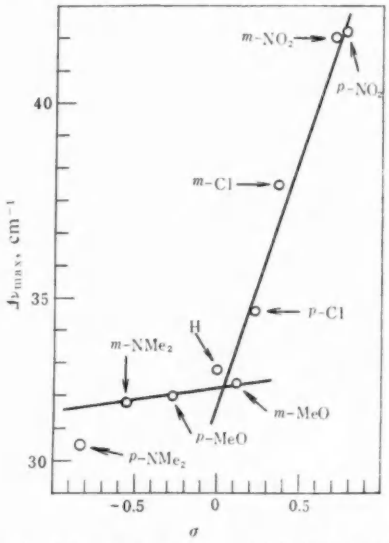

Fig. 7. Comparison of $\Delta\nu_{max}$ of *N*-(arylmethyl)-anilines with σ-values.

Yet, splitting of the ν_{N-H} band into two distinct maxima must be attributed to the intramolecular interaction between the N–H group and the π-electron, no matter which ring carries the substituent. The mechanism of the interaction must also be common in both series of compounds and will satisfy the following conditions. 1) The larger the σ constant, the

9) M. St. C. Flett, *Trans. Faraday Soc.*, **40**, 767 (1944); S. Califano and R. Mocca, *Gazz. chim. ital.*, **86**, 1014 (1956); P. J. Krueger and H. W. Thompson, *Proc. Roy. Soc.*, **A243**, 143 (1957).

smaller is the $\Delta\nu_{max}$, when the benzene ring (ring B), which carries the N–H group, bears the substituent. In the case of the substituent involved in ring A, $\Delta\nu_{max}$, increases as the σ value increases, as far as the σ value is larger than 0.1. 2) When a substituent of which the σ-constant is less than 0.1 is introduced into ring A, $\Delta\nu_{max}$ changes to a negligible extent, regardless of the substituent.

It must be noticed that condition 1 is just the contrary to the case mentioned in ω-aryl-alkanols[10], In the case of ω-arylalkanols, the hydrogen atom of the hydroxyl group possesses at least a proton-like character and the increasing electron density in the benzene nucleus favors the interaction. The above considerations lead to an idea that is quite different from that developed for the interaction between the hydroxyl group and π-electrons.

That is, one of the possibilities which will explain the results is the idea of "flow-in" of the electron from the N–H group to ring A. If this idea were taken into consideration, above conditions 1 and 2 would be explained in the following way. The greater the electron-density gap between ring A and the N–H group, the easier the flow of the electron of the latter into the former, as far as the electron density of the N–H group is higher, Thus the force constant of the N–H group is lessened to result in appearance of the N–H band at a lower wave number and also in more $\Delta\nu_{max}$. If the difference of electron densities between ring A and the N–H group approaches zero or the electron density of ring A is higher than that of the latter, the electron of the N–H group does not "flow-out". Then, it will be the field effect that plays the most important role, and $\Delta\nu_{max}$ may appear at the constant wave number, irrespective of the substituent.

Furthermore, if the above assumption is made, it is easier to understand the phenomenon found in *N*-benzylarylamines. When an electron-withdrawing substituent is introduced into ring B, the electron of ring B is attracted to the substituent, hence the electron of the N–H group flows into ring B. The lack of the electron in the N–H group results in a smaller electron-density difference between ring A and the N–H group. This permits the flow of the electron from the N–H group to ring A to a very limited extent, the interaction between π-electron and N–H group becoming weaker. Thus the strength of the interaction or $\Delta\nu_{max}$ may be proportional to σ constant of the substituent, when the substituent is introduced into ring B.

In the above hypothesis, it is assumed, that the interaction takes place as a mere probability. The interaction must be caused by an overlap of the orbitals belonging to the electrons of the N–H group and the π-electrons of ring A. And the overlap of orbitals will occur more easily, when the electron density of ring A is heightened by the presence of an electron-repelling group. Accordingly, the molecular species which has the internal interaction increases when the electron density of ring A is higher, although the electron flows out of the N–H group into ring A.

A support to the above hypothesis is being sought.

The authors are thankful to Professor Y. Urushibara and Professor T. Shimanouchi for their valuable advice and encouragement and to Mr. H. Iwamura for his technical assistance. The authors are also indebted to the Ministry of Education for the Grant in Aid for the Fundamental Scientific Research.

Department of Chemistry
Faculty of Science
The University of Tokyo
Hongo, Tokyo

10) M. Ōki and H. Iwamura, This Bulletin, 32, 1135 (1959).

Hydrogen Reduction of a Single Crystal of Nickel Oxide

By Yoshio IIDA and Kenzo SHIMADA

(Received November 24, 1959)

In an earlier paper[1] it was shown that the reduction of nickel oxide was strongly affected by a small amount of additive incorporated in the nickel oxide lattice. Little attention has been paid to the mechanism of hydrogen reduction of metal oxide, while the mechanism of oxidation of metal has been studied successfully since Wagner's theory[2]. Recently Baba[3] explained the mechanism of hydrogen reduction of germanium dioxide by assuming that the reduction is governed by an autocatalytic behavior. Murata[4] reported that a diffusion process of cation or anion is a rate-determining process in the hydrogen reduction of iron oxide. In their experiments oxide powder was used as a specimen. As powder exhibits complicate properties resulting from particle size and shape, powder is thought to be unfavorable to the study of the mechanism of the hydrogen reduction. From these points it is desirable to study the hydrogen reduction of a single crystal. In the present study the hydrogen reduction of a single crystal of nickel oxide has been carried out to explain the mechanism of the reduction.

Experimental Procedure

A single crystal of nickel oxide was prepared by Tochigi-Kagaku Co. in a way similar to Verneuil's method[5]. Rectangle specimens of $6\times4\times3$ mm. were cut out from the raw material. The specimens were not subjected to further treatment.

Nickel nitrate recrystallized four times was heated at 800°C for 10 hr. to obtain nickel oxide powder. The average particle size of the nickel oxide was about 0.5 μ according to an electron micrograph.

The weight loss during the reduction process was measured by the thermobalance with a sensitivity of 0.5 mg. The apparatus could be used in hydrogen or in vacuo. After the specimen was heated in vacuo at a desired temperature, it was reduced with hydrogen. Hydrogen was used from a commercially available tank after purifying it with concentrated sulfuric acid, hot platinum asbestos, potassium hydroxide and phosphorus pentoxide.

Results and Discussion

Time-dependent Study.—A comparison of a reduction-temperature curve of a single crystal of nickel oxide with that of nickel oxide powder when heated at a velocity of 100°C/hr. is shown in Fig. 1. It is seen that a rate of reduction of the single crystal is much lower than that of the powder. It should be noted that there is the stage at about 500°C in the case of the single crystal where the reduction slows down. In order to elucidate the mechanism of the hydrogen reduction of nickel oxide, the isothermal reduction of the single crystal was studied in the range of 300°C to 800°C. The results are shown in Fig. 2. To see whether

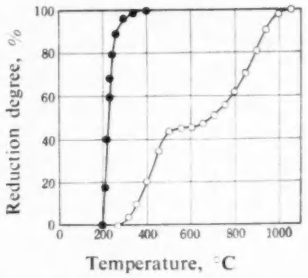

Fig. 1. Reduction-temperature curves of a single crystal of nickel oxide (○) and nickel oxide powder (●).

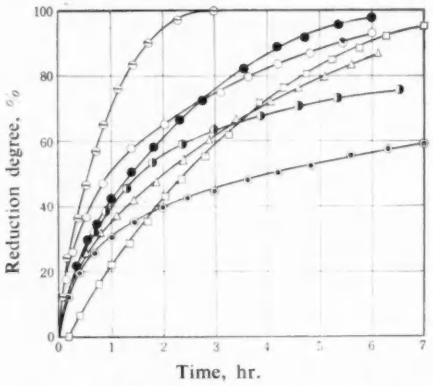

Fig. 2. Isothermal reduction of a single crystal of nickel oxide. □, 300°C: ●, 350°C: △, 400°C: ⊙, 500°C: ◑, 600°C: ○, 700°C: ⊖, 800°C

1) Y. Iida and K. Shimada, This Bulletin, to be published.
2) C. Wagner, *Z. physik. Chem.*, **49**, 735 (1936).
3) H. Baba, This Bulletin, **29**, 789 (1956).
4) Y. Murata and N. Kasaoka, *J. Chem. Soc. Japan, Ind. Chem. Sec.* (*Kogyo Kagaku Zasshi*), **61**, 1440 (1958).
5) J. Nakazumi, ibid., **59**, 1304 (1956).

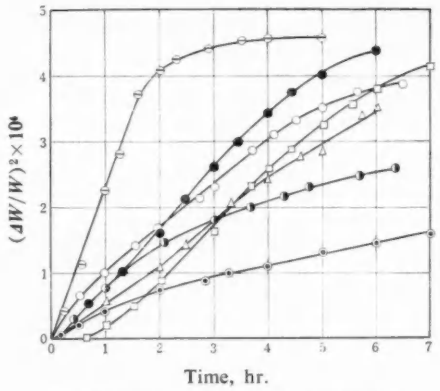

Fig. 3. Parabolic plot of isothermal reduction of a single crystal of nickel oxide. □, 300°C: ●, 350°C: △, 400°C: ⊙, 500°C: ◑, 600°C: ○, 700°C: ⓘ, 800°C.

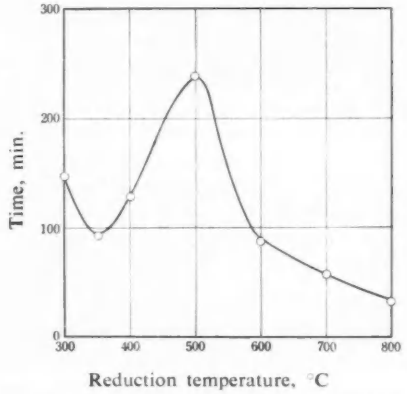

Fig. 4. Time required to obtain 50% reduction at various temperatures.

the isotherms can be expressed by the parabolic law, a square of the reduction loss per gram is plotted against the reduction time. Fig. 3 shows that the reduction of the single crystal does not obey the parabolic law. A rate of reduction of the single crystal does not always increase with an increase in the reduction temperature. In Fig. 4, the time required to obtain 50% reduction is plotted against the reduction temperature. It is seen that the time at 350°C is shorter than that at 300°C whereas the time increases with an increase in the reduction temperature in the range of 350°C to 500°C. Since the time is reversely proportional to the rate of the reduction, the rate is lowest at 500°C and then increases with an increasing temperature as do ordinary chemical reactions. The stage at which the reduction does not proceed in the reduction-temperature curve of the single crystal at 500°C is attributed to the lowest rate of the reduction at 500°C. In the reduction of nickel oxide powder or other metal oxide such as ferric oxide and tungsten oxide powder, these phenomena were not observed.

Microscopical Examination. — Reduction of the single crystal oxide proceeds layer by layer as shown in Fig. 5. The specific gravity of

Fig. 5. A section of a single crystal of nickel oxide reduced partially. A white part is a reduced nickel phase and a brack part is an unreduced nickel oxide phase. (×20)

the single crystal of nickel oxide is 6.8 and that of nickel is 8.90. As a volume ratio of nickel oxide is 6.8/8.9=0.76, the specific volume of nickel is lower than that of nickel oxide. Accordingly, the nickel layer formed on the nickel oxide by the hydrogen reduction should be very porous. The reduction mechanism is considered schematically as follows. Hydrogen passes through the porous nickel layer, and reacts with nickel oxide at the boundary of nickel and nikel oxide. The water formed as a result of the reduction is released from the boundary. The penetration of hydrogen through the porous nickel layer is very easy because of its small molecular size. However, the desorption of water through the nickel layer is thought to be very difficult because of its large molecular size. By this reduction schema, the desorption of water formed is considered to be a rate-determining step in the hydrogen reduction process. Nickel formed on the surface of nickel oxide by the reduction is composed of very fine particles, and the particles start to sinter with an increase in the reduction temperature[6,7]. It is expected that the number and size of the pores decrease at higher temperatures by sintering, and the desorption of water through the pores is retarded. It may be attributed to

6) R. Ueda, *J. Japan Inst. Metals (Nippon Kinzoku Gakkai-Shi)*, **23**, 292 (1959).
7) P. H. Emmett, "Catalysis" Vol. I The Waverly Press, Inc., New York (1954), p. 371.

the change of the pores by sintering that the rate of reduction decreases in the range of 350 to 500°C.

While the sintering is enhanced above 500°C, a pressure of water vapor increases and thus the water vapor passes through the nickel layer forming large pores at higher temperatures. Water vapor can easily be released through the large pore and then the reduction process is promoted above 500°C as shown in Fig. 4.

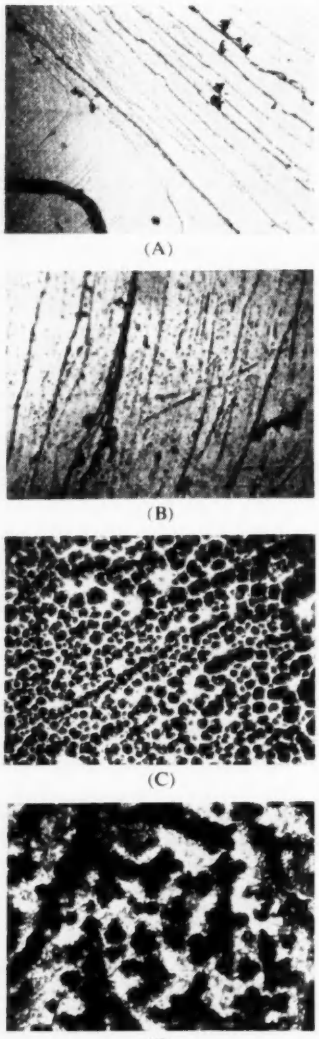

(A)

(B)

(C)

(D)

Fig. 6. Microphotographs of the surface of a single crystal of nickel oxide reduced at various temperatures. (A) is for the unreduced crystal; (B), for the crystal reduced at 400°C: (C), for the crystal reduced at 800°C: and (D), for the crystal reduced at 1000°C. (×400)

A microscopical examination shows that these explanations are correct. Fig. 6a is a microphotograph of the free surface of the unreduced single crystal. Fig. 6b shows that there are many small pores on the surface of the single crystal reduced at 400°C. It is seen in Figs. 6c and 6d that the pores become larger when the single crystal was reduced at 800 and 1000°C. From these facts it is concluded that the release of water from the boundary of the metal and the oxide is a rate-determining step in the hydrogen reduction of the single crystal of nickel oxide.

Study on the Reduction of Nickel Oxide Powder.—It is of interest to see whether the reduction of nickel oxide powder can be explained by the above mechanism. Nickel oxide powders of which praticle size was about 1 μ were compressed to a tablet of 10 $\phi \times 5$ mm. at a pressure of 1000 kg./cm^2. The bulk density of the tablet was 3.2 g./cc. and its porosity was 52%, which was thought to be sufficient for the penetration of hydrogen or the release of water. It is expected that each nickel oxide powder can be reduced homogeneously all over the tablet, and the reduction of each powder is governed by the above mechanism. The tablet was reduced at 180 and 250°C. Fig. 7 shows the section of the tablet reduced incompletely. It is seen that the reduction proceeds layer by lager in spite of the porous tablet. At 250°C at which there is no induction period, the reduction starts at the exterior of the tablet. At a reduction temperature of 180°C at which there is an induction period of reduction, the reduction starts at the interior of the tablet. It is generally accepted that a rate of oxidation of nickel is negligibly small below 300°C[8]. The outer oxide layer observed in the reduction of 180°C can not be attributed to the re-oxidation with oxygen contained in hydrogen or with water formed. These facts can not be explained completely by the mechanism reported in the previous literatures[2,3]. At present there is no

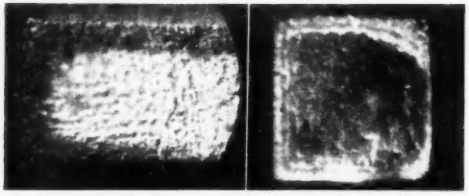

(A) (B)

Fig. 7. A section of a compact of nickel oxide powder reduced at 250°C (A) and 180°C (B). (×10)

8) A. E. Gulbransen and K. F. Andrew, *J. Electrochem. Soc.*, **101**, 128 (1954).

alternative but to say that the reduction of nickel oxide powder proceeds topochemically.

Crystal Growth of Nickel Reduced.—It is reported[9] that oxide film formed on the metal surface by oxidation has a preferential orientation related to the crystal orientation of the metal. No attention has been paid to the crystal growth of the reduced metal on the metal oxide by the hydrogen reduction from the viewpoint of the crystal orientation of the reduced metal and the metal oxide.

The plane of cleavage of the single crystal of nickel oxide is known to be (100) plane[5]. The nickel layer reduced on the (100) plane of the single crystal of nickel oxide at 1000°C was etched and examined microscopically. The result is shown in Fig. 8, where a square etch pit is seen. It is concluded that nickel formed on (100) plane of nickel oxide by the reduction has (100) plane as perferential orientation.

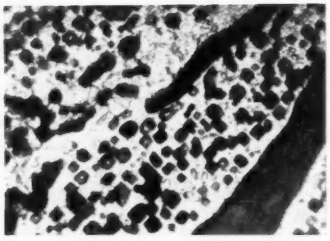

Fig. 8. Etch pit of reduced nickel. The etching reagent is concentrated nitric acid. (×400)

Summary

In the hydrogen reduction of a single crystal of nickel oxide, the rate of reduction does not always increase with an increase in the reduction temperature. In the range of 350 to 500°C the rate decreases with the temperature, and the rate is the lowest at 500°C. These facts are explained reasonably by the microscopical examination of the surface of the reduced nickel. It is concluded that the desorption of the water formed through the pores is a rate-determining step in the reduction of the single crystal of nickel oxide. The nickel formed on (100) plane of nickel oxide by the reduction has (100) plane as a preferential orientation.

The single crystal of nickel oxide was kindly presented to us by Tochigi Kagaku Kogyo Co.

Government Industrial Research Institute
Kita-ku, Nagoya

9) I. S. Kerr, *J. Inst. Metals*, **85**, 379 (1956).

Partial Molal Volumes of Butyl Alcohols and of Related Compounds in Aqueous Solution

By Koichiro NAKANISHI

(Received December 4, 1959)

The excess function of any thermodynamic quantities for liquid mixtures is symmetric in form with regards to the mole fraction of component, if the components are the "normal liquids" which consist of the spherical molecule with no specific interaction. However, this symmetry fails when the size and form of one component are different from those of another, or when a specific interaction plays an important role in intermolecular force. In the "associated solution", this specific interaction which is attributed to the formation of hydrogen bonding is predominant, and the anomaly in the behavior of the excess function is often observed for a number of such systems[1].

The same is true for the excess volume (the volume change on mixing). For binary mixtures of the normal liquids the excess volume is generally small and nearly symmetric in form, and the interrelationships with other thermodynamic properties and parameters of the intermolecular force have been also investigated, both experimentally and theoretically, by many authors[2]. On the other hand, large negative excess volume is observed generally for the liquid mixtures containing water, alcohols or other associated liquids as one or both

1) J. A. Barker, *J. Chem. Phys.*, **20**, 794, 1526 (1952); J. A. Barker and F. Smith, ibid., **22**, 375 (1954).

2) G. Scatchard, *Trans. Faraday Soc.*, **33**, 160 (1937); J. H. Hildebrand and R. L. Scott, "Solubility of Non-Electrolytes", 3rd. ed., Reinhold Publ. Corp., New York (1950), p. 138; I. Prigognie, "The Molecular Theory of Solution", North-Holland Publ. Co., Amsterdam (1957), p. 176.

TABLE I. DENSITIES OF AQUEOUS SOLUTION OF BUTYL ALCOHOLS AT 20°C

Normal		Iso		Secondary		Tertiary	
Wt. %	Density	Wt. %	Density	Wt. %	Density	Wt. %	Density
1.2684	0.99623	1.3042	0.99610	1.2149	0.99621	1.3139	0.99593
1.9816	0.99514	2.0761	0.99495	1.8892	0.99522	2.3476	0.99425
2.7038	0.99405	2.7871	0.99395	2.7195	0.99400	3.7557	0.99199
3.2835	0.99321	3.2493	0.99319	3.4639	0.99299	4.7743	0.99052
4.0939	0.99211	3.4096	0.99308	4.3960	0.99173	6.2671	0.98843
4.8138	0.99114	4.1259	0.99206	4.9808	0.99102	7.4321	0.98689
5.5200	0.99016	4.4318	0.99154	5.7904	0.99005	8.3009	0.98578
5.6470	0.98993	4.9319	0.99091	7.0477	0.98848	9.4236	0.98432
6.0442	0.98950	5.2515	0.99050	8.3458	0.98678	10.132	0.98346
6.1640	0.98924	5.6818	0.98982	8.8445	0.98620	12.143	0.98098
6.5653	0.98878	5.9351	0.98946	9.6519	0.98517	13.662	0.97907
6.6262	0.98862	6.5070	0.98875	10.637	0.98396	14.612	0.97780
6.7731	0.98842	6.7836	0.98831	11.842	0.98239	15.529	0.97671
7.2231	0.98780	7.1135	0.98798	12.753	0.98119	16.159	0.97593
7.6415	0.98722	8.0334	0.98669	13.471	0.98019	17.943	0.97331
7.7671	0.98699	8.2184	0.98639	14.066	0.97932	19.425	0.97100
78.914	0.84872	83.448	0.83552	14.824	0.97802	21.328	0.96754
90.586	0.82837	85.353	0.83193	15.742	0.97668	24.536	0.96115
100.000	0.80973	88.757	0.82521	16.886	0.97467	30.483	0.94841
		90.703	0.82140	18.612	0.97211	39.115	0.92824
		94.613	0.81375	67.968	0.87176	49.449	0.90386
		95.391	0.81194	74.591	0.85869	58.386	0.88322
		100.000	0.80185	82.684	0.84231	69.937	0.85709
				88.435	0.83043	79.027	0.83481
				93.948	0.81901		
				100.000	0.80634		

components. The partial volumes of both components show complicated behavior with the variation in the composition of the component. The case of water-ethanol system, which has often been cited in many text-books of chemical thermodynamics, is a well-known example. At present, we have no clear understanding of this phenomenon, although a qualitative explanation[3] accounts for it as the disintegration of structure in water by the solute molecule which is capable of forming the hydrogen bonding with water.

It seems to be natural to expect an anomaly similar to the above for the case of aqueous solutions of alcohols other than ethanol and of other compounds having the hydroxyl group. In the present study, we obtained the dependence of partial molal volumes in water upon the composition for four isomers of butyl alcohol from the density measurement and compared them with that of other alcohols. For comparison's sake, the partial molal volume of ethylene glycol was also evaluated. In each case concerned, the general feature of partial volume vs. composition curve was the same as that for the case of ethanol in water.

3) For example, A. G. Mitchell and W. F. K. Wynne-Jones, *Discussion Faraday Soc.*, No. 15, 161 (1953).

Experimental

Purification of Materials.—*Normal*, *iso*-, *sec*.- and *tert*.-butyl alcohols and ethylene glycol were prepared as follows. The best grade available was dried over dehydrating agents and then fractionally distilled.

n-Butyl alcohol was at first treated with dilute sulphuric acid and sodium bisulphate solution for the removal of ketones and aldehydes, and then heated under reflux with a small amount of sodium hydroxide solution for the removal of esters. After the removal of alkali, the material was dried over calcium hydroxide, refluxed with calcium oxide, and then fractionally distilled a few times.

Isobutyl alcohol and *sec*.-butyl alcohol were boiled under reflux over calcium oxide for a few hours, and then fractionally distilled.

tert.-Butyl alcohol was dried over anhydrous potassium carbonate at 46°C for a long time, and then fractionally distilled.

Ethylene glycol was distilled under reduced pressure, and the middle fraction was dried over anhydrous sodium sulphate for a long time. The material was then redistilled.

Water was obtained by the repeated distillations of conductivity water.

All the sample liquid were stored in sealed glass containers and redistilled immediately before use. The densities of the sample liquids at 20°C were within 0.00005 g./cc. of the values given in literature.

Pycnometers.—The pycnometers used were of ordinary bicapillary type. Type A held slightly more than 25 cc. of liquid, while type B slightly less than 10 cc. The main body of the pycnometer was the usual flat-bottom type. The capillaries were calibrated with a travelling microscope by the conventional method of moving a small mercury column. In the middle of each capillary, a horizontal razor mark was applied and the volume of pycnometer with meniscus on this mark was obtained by the measurement with water.

Density Measurement.—The component liquids were mixed in a glass-stoppered weigh-bottle having a narrow mouthpiece. The mole fraction of the sample solution was determined from the weight of each component.

After being kept over night, the sample solution was transfused into the pycnometer by injection with a medical syringe until each of the two meniscus was near the horizontal mark on the capillary. The pycnometer was then placed into the thermostat at 20 ± 0.005°C, and when complete thermal equilibrium was attained, the height difference between the meniscus and the mark was determined by means of a travelling microscope reading to ±0.01 mm.

Immediately after the volume determination, the apparent weights of the pycnometer and the sample solution were determined with an analytical balance. The values were converted into true weights by the cnventional procedure in which the buoyancy corrections were applied.

Thus, the densities of sample solutions were obtained with a precision of $\pm2\times10^{-5}$.

Results and Discussion

Densities.—The density data of butyl alcohol-water and ethylene glycol-water systems are summarized in two tables. Table I shows the densities of aqueous solution of four isomers of butyl alcohol, and Table II shows the densities of ethylene glycol-water system at 20°C. In all cases concerned, the densities of the solution can not be expressed by the conventional power series relation.

Table II. Densities of aqueous solution of ethylene glycol at 20°C

Wt. %	Density	Wt. %	Density
1.5193	1.00013	30.440	1.03894
3.2341	1.00231	31.957	1.04095
5.7310	1.00554	36.540	1.04717
8.7395	1.00949	40.674	1.05276
9.3383	1.01019	41.410	1.05347
10.807	1.01215	51.737	1.06704
11.243	1.01277	58.341	1.07474
14.348	1.01693	71.378	1.08876
15.768	1.01879	80.617	1.09830
17.972	1.02182	87.942	1.10459
21.213	1.02621	94.169	1.10924
23.957	1.03001	100.000	1.11313
28.545	1.03628		

Volume of Mixing (Excess Volume).—Since the specific volumes of both components are known (except for *tert.*-butyl alcohol which has the melting point above 20°C), the volume of the mixing ΔV is easily calculated from the present data. It is a common characteristic that ΔV has large negative value in the whole range of composition and that there is an inflection point below the alcohol mole fraction of 0.1. Fig. 1. shows the general feature schematically.

Partial Volumes.—Partial specific (molal) volumes of alcohols V_2 are calculated from the density data directly by Eq. 1, or from the concentration dependence of apparent specific volume ϕ_2 by Eq. 2,

$$V_2=(1/d_{12})+(1-w_2)\frac{\partial(1/d_{12})}{\partial w_2} \tag{1}$$

$$V_2=\phi_2+w_2(1-w_2)\frac{\partial\phi_2}{\partial w_2} \tag{2}$$

where the apparent specific volume is defined as follows,

$$\phi_2=(1/d_1)-(d_{12}-d_1)/(d_{12}d_1w_2) \tag{3}$$

and d_{12} is the density of solution, d_1 is the density of water and w_2 is the weight fraction of alcohols.

As in the well-known example of ethanol-water system, characteristic behaviors of partial molal volume vs. composition curves are obtained with all systems investigated. Partial molal volume of alcohol decreases with increasing its mole fraction, reaches a minimum value and then increases gradualy to the molal volume. In the whole range of composition, it is always smaller than the molal volume V_2^0. Partial molal volume of water, on the other hand, increases slightly with increasing the alcohol mole fraction, reaches an indistinct maximum and then decreases gradually.

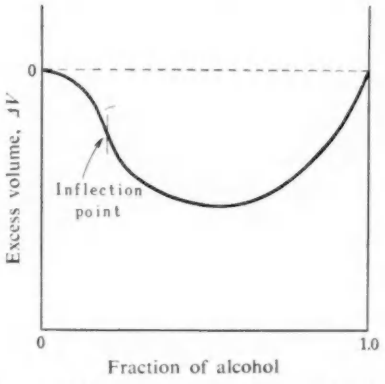

Fig. 1. Schematic diagram of excess function in alcohol-water systems.

The general feature just described above can well be understood by the case of ethylene glycol-water system given in Fig. 2.

For the partial volumes of four isomers of butyl alcohol in water, the diagram is incomplete owing to the phase separation or high melting point. Fig. 3 shows the isomeric variation in the partial volumes of butyl alcohols in their low concentration region where the characteristic behavior is clearly observed.

For comparison's sake, the partial molal volumes of methanol, ethanol, propyl alcohols and glycerol in water are calculated and plotted in Fig. 4 together with the present data. The calculation is made with the ICT data[4]. In addition, an interesting temperature dependence, which is found in ethanol, is shown in Fig. 5.

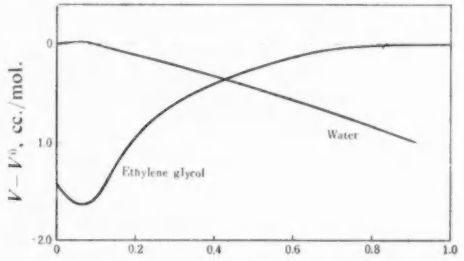

Fig. 2. Partial molal volumes of ethylene glycol-water system at 20°C.

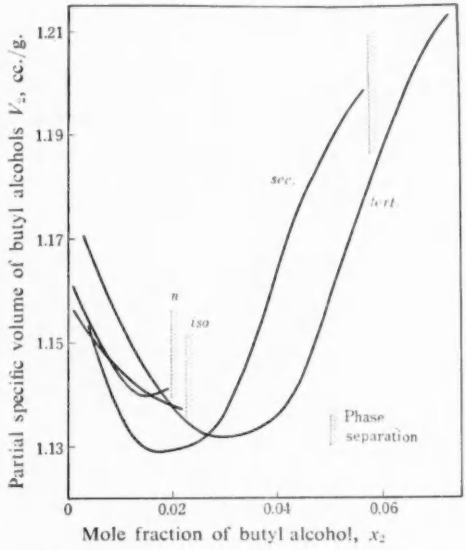

Fig. 3. Partial specific volume of butyl alcohols in water at their low concentration at 20°C.

4) International Critical Table, Vol. III, p. 115~122.

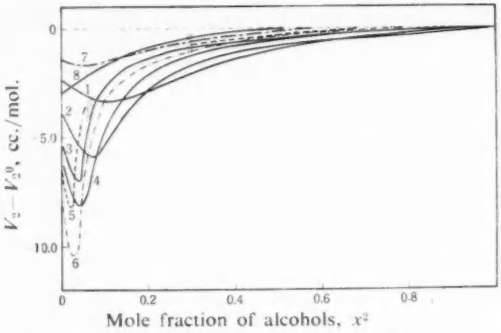

Fig. 4. Partial molal volume of alcohols in water.

1 Methanol (15°C)
2 Ethanol (20°C)
3 *n*-Propyl alcohol (15°C)
4 Isopropyl alcohol (15°C)
5 *sec.*-Butyl alcohol (20°C)
6 *tert.*-Butyl alcohol (20°C)
7 Ethylene glycol (20°C)
8 Glycerol (15°C)

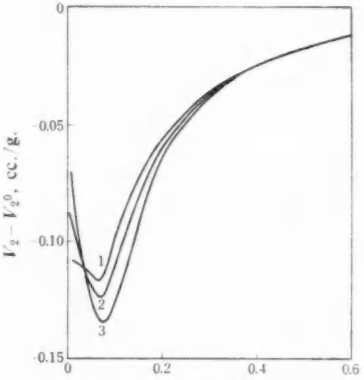

Fig. 5. Partial specific volume of ethanol in water at different temperatures.
1, 40°C; 2, 25°C; 3, 10°C;

Summary of Experimental Observations.— Partial volume behavior presented above may be summarized as in the following.

1) Partial volumes of alcohols take a minimum value at a definite point. The position of this minimum shifts systematically to the lower concentration of alcohol in the order of BuOH, PrOH, EtOH and MeOH, as is shown in Table III.

2) Depth of the minimum in $V_2-V_2^0$ depends on the kind of alcohol in a more

Table III. Minimum point in the value of $V_2-V_2^0$

Compound		Minimum point at mole %	wt. %
Monohydric alcohol	CH_3OH	10.5	17.
	C_2H_5OH	7.0	16.
	n-C_3H_7OH	4.5	14.
	iso-C_3H_7OH	5.0	15.
	n-C_4H_9OH	1.5	6.
	iso-C_4H_9OH	>2.1	>8.
	sec.-C_4H_9OH	1.8	7.
	tert.-C_4H_9OH	3.0	11.
Dihydric alcohol	CH_2OH | CH_2OH	6.0	16.
Trihydric alcohol	CH_2OH | $CHOH$ | CH_2OH	—	—

complicated manner than the above. The largest volume contraction is observed with *tert.*-butyl alcohol.

3) Volume contraction of polyhydric alcohols in water is generally smaller than that of monohydric alcohols. Moreover, it is of interest that the partial volume of ethylene glycol has a minimum value near the glycol mole fraction of 0.06, while that of glycerol has no minimum (Fig. 4).

4) Partial volume V_2 of ethanol at high dilution (below the alcohol mole fraction of 0.04) has a small temperature coefficient nearly half the value of ethanol itself. Thus, with the raise in temperature, a) the increase in the depth of $V_2-V_2^0$ at high dilution is observed, although b) the value at the minimum point decreases gradually.

Discussion.—Examination of all the experimental data available leads us to the conclusion that the partial volume behavior of mono- and dihydric alcohol-water system has a common characteristic. Qualitatively, the abrupt fold in the partial volume vs. composition curve would be interpreted[5] as the disintegration of the hydrogen-bonded structure in water by the increased strain due to the invading alcohol molecule with increasing fraction of the alcohol. It may be that there are two kinds of configuration of alcohol molecule in aqueous solution, one has a specific volume of alcohol itself, while the other has a small effective volume, and the fraction of the two may change with composition in a complicated manner in an alcohol-water system.

In this connection, it is of interest to examine the other properties of aqueous solution of alcohols. For example, ultrasonic absorption in aqueous solution of alcohol has a marked maximum in some definite composition[5]. But, this maximum in absorption does not always correspond to the minimum in partial volume, and moreover the former is found in aqueous solution of acetone which has smoothed partial volume vs. composition curve[6].

Another interesting result to be noted here is the partial volume behavior in dioxane-water system[7] in which a similar anomaly is observed. In this case, however, partial volume of water has a minimum point instead of a maximum as in alcoholic solutions, and the partial volume of dioxan has a maximum. It is an interesting fact that the role of the OH- group in alcohol molecules contrasts remarkably with that of ether bond -O- in the formation of intermolecular hydrogen bonding in aqueous solution.

In conclusion, all the available data seem to comprise only indirect evidences and it is obvious that more direct information about the inner structure of solutions is desirable for the elucidation of this phenomenon.

Summary

Partial molal volumes of four isomers of butyl alcohol and ethylene glycol in water are evaluated from the density measurement. They are compared with those of other monohydric alcohols and all the available data which have a common characteristic in the dependence upon the alcohol fraction are summarized.

The author wishes to express his sincere gratitude to Professor Mikio Tamura and to Assistant Professor Michio Kurata for their guidance and criticism

Department of Industrial Chemistry
Faculty of Engineering
Shinshu University
Wakazato 500, *Nagano*

5) O. Nomoto, *J. Phys. Soc. Japan*, **11**, 827 (1956); ibid., **12**, 300 (1957).
6) V. S. Griffith, *J. Chem. Soc.*, **1953**, 860.
7) G. N. Malcolm and J. S. Rowlinson, *Trans. Faraday Soc.*, **53**, 921 (1957).

On the Hydrolysis Products of Abietic Acid-Maleic Anhydride Adduct

By Masahiro ABO

(Received November 26, 1959)

In 1932 Ruzicka and his coworkers[1] found that the saponification product of methyl abietate-maleic anhydride adduct could not be isolated as tricarboxylic acid but identified with the anhydride adduct directly obtained from the reaction between colophony and maleic anhydride, and they stated that the tricarboxylic acid, which was produced at the beginning of the saponification, had a tendency to convert easily into the anhydride acid in the course of acidification or recrystallization.

It was also reported that *cis*-9, 10-dihydroanthracene-9, 10-endo-α, β-succinic acid[2] and alkyl-1, 4-dihydronaphthalene-1, 4-endo-α, β-succinic acid[3] had similar tendencies. These dibasic acids could not be successfully purified by recrystallization, even from the low-boiling solvents, because of their partial or complete conversion to the corresponding anhydrides. It may be seen that these tendencies are common characteristics of these structural homologues.

In the present work an attempt has been made to isolate the hypothetical tricarboxylic acid which might be directly produced by means of the hydrolysis of the abietic acid-maleic anhydride adduct. Some properties of those hydrolysis products which were obtained in a few ways were compared with those of maleic anhydride- or fumaric acid- adducts with abietic acid and discussion was offered as to their chemical structures.

Experimental

Maleic Anhydride Adduct with Abietic Acid.—60 g. of abietic acid (so-called Steele's acid which was produced by refluxing Chinese gum rosin with acetic acid) and 20 g. of maleic anhydride were heated at 170~180°C with stirring under a slow stream of carbon dioxide for two hours. The reaction mixture was dissolved in 100 ml. of glacial acetic acid, and this was poured into a large amount of water with stirring. The separated yellowish resinous product was refluxed with a small amount of carbon tetrachloride to remove the unreacted abietic acid, and recrystallized from glacial acetic acid. Further recrystallization was carried out from benzene-carbon tetrachloride according to the procedure of Ruzicka and his coworkers[1]. Thirty-two grams of fibrous white needles melting at 226~228°C were obtained.

Found: C, 71.63; H, 7.82. Calcd. for $C_{24}H_{32}O_5$: C, 71.96; H, 8.06%. $[\alpha]_D^{15}$ −31.0° (10% in chloroform).

Besides the above, the most refined sample could be obtained by purification with the aid of sublimation of the above crystal under reduced pressure of 1 mmHg at 190~210°C. Its analytical data are shown in Table I with other properties.

Fumaric Acid Adduct with Abietic Acid.—50 g. of abietic acid and 20 g. of fumaric acid were heated at 195~200°C with the same procedure as the above for two hours. The reaction mixture was dissolved in 150 ml. of glacial acetic acid, and this was poured into a large amount of hot water with stirring and filtered through a hot funnel. This procedure was repeated twice. The unreacted abietic acid was removed from the yellowish powder by refluxing in benzene, filtered and the filtrate was recrystallized from glacial acetic acid. An analytical sample was obtained by repeated recrystallization from dioxane. Its properties and analytical results are shown in Table I with others. Purification by the vacuum sublimation method was unsuccessful owing to its thermal decomposition.

Hydrolysis of Maleic Anhydride Adduct.—It was carried out in two ways. (1) 30 g. of purified maleic anhydride adduct was dissolved in 100 ml. of acetone and added 30 ml. of water. The flask was immersed in a water bath kept at 60~70°C, and boiled gently under a reflux condenser for two hours. On cooling at room temperature, white crystals began to precipitate. After the crystallizations from acetone-water were repeated, they were filtered and ground into fine powder and then dried at room temperature under reduced pressure (2~5 mmHg). They reached the constant weight after about two hours. The analytical data are shown in Table I with others. (2) Ten grams of purified maleic anhydride adduct was dissolved in excess of 10%, aqueous sodium hydroxide solution and precipitated by acidification with 2 N hydrochloric acid. The precipitate was collected, washed with water repeatedly and recrystallized from acetone. All the procedures after hydrolysis were carried out at room temperature, in order to prevent the reversion to the original anhydride. Drying was carried out under the same condition as above. The analytical data are shown in Table I with others.

Measurement of Acid Number[4].—*Total Number.* —0.2~0.3 g. of the sample in about 50 ml. of the

1) L. Ruzicka, P. J. Ankersmit and B. Frank, *Helv. Chim. Acta*, **15**, 1289 (1932).

2) W. E. Bachmann and L. B. Scott, *J. Am. Chem. Soc.*, **60**, 481 (1938); **70**, 1458 (1948).

3) M. C. Kloetzel and H. L. Herzog, ibid., 72, 1991 (1950).

4) E. F. Siegel and M. K. Moran, ibid., **69**, 1457 (1947); W. Klausch, *Farbe u. Lack*, **63**, 119 (1957).

TABLE I. PROPERTIES AND ANALYSES OF TWO KINDS OF ABIETIC ACID ADDUCT AND HYDROLYSIS PRODUCTS OF MALEIC ANHYDRIDE ADDUCT

		Adduct of fumaric acid	Adduct of maleic anhydride	Hydrolysis products of maleic anhydride adduct (1)[a]	(2)[b]
Melt. pt., °C		249~252	226~228	226~228	(187~210[c])
Analyses, %:					
Calcd.,	C	68.87	71.97	68.87[d]	
	H	8.19	8.05	8.19[d]	
Found,	C	68.96	71.69	68.70	68.73
	H	8.10	7.89	8.01	8.05
Acid number:					
Calcd.,	Apparent	393	280	393[d]	
	Total	393	420	393[d]	
Found,	Apparent	387	280	270	273
	Total	395	417	395	397
$[\alpha]_D^{13}$		+34.0°	−25.2°	−24.0°	−23.6°
(g./100 ml. ethanol)		(2.0)	(5.0)	(2.0)	(2.0)
Solubility at room temp.:					
Chloroform		insol.	sol.	insol.	
Benzene		insol.	sol.	insol.	

a) Refluxed the acetone containing water solution of maleic anhydride adduct for two hours and recrystallized from its solution. b) Precipitated by acidification of the alkali solution of maleic anhydride adduct. c) Measured in a sealed capillary tube. d) Calculated for hypothetical tricarboxylic acid $C_{24}H_{34}O_6$ which may be produced on the hydrolysis process.

mixture of 1 : 3 *tert.*-butyl alcohol and acetone was dissolved, and about 10 ml. of water were added to prevent the turbidity which happened often in titration, and titrated with 0.1 N aqueous sodium hydroxide solution by means of potentiometric titration method. — *Apparent Number.* — 0.2~0.3 g. of the sample was dissolved in about 50 ml. of ethanol and titrated with 0.1 N alcoholic sodium hydroxide.

Thermal Degradation Curves.—An apparatus of Honda's thermal balance[5] was used. About 0.5 g. of fine powdered sample was heated at constant rate of 10°C/5 min. and loss of weight of sample was measured.

Discussion

As was shown in Table I, the elementary analytical data of both hydrolysis products, which were obtained in two ways as mentioned above, were in good agreement with that expected for the aimed tricarboxylic acid $C_{24}H_{34}O_6$ respectively. They were insoluble in benzene or chloroform, similarly to fumaric acid adduct, at room temperature, but soluble at elevated temperature. Their specific rotation was negative like that of the maleic anhydride adduct, and the decrease of the rotation nearly corresponded with the decrease of the concentration of the asymmetric carbons attendant upon the increase of their molecular weights. The melting points which were measured by the ordinary method agreed with that of the maleic anhydride adduct. However, when they were measured in a sealed capillary tube they showed a remarkable depression and were distinct from anhydride.

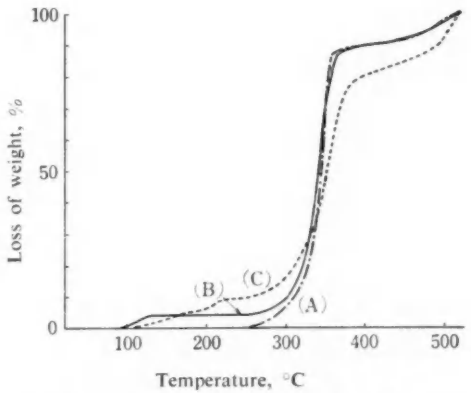

Fig. 1. Thermal degradation curves of (A) abietic acid-maleic anhydride adduct, (B) hydrolysis product of A, and (C) abietic acid-fumaric acid adduct.

Another distinguished difference was observed in the thermal degradation curves of the three kinds of adducts (Fig. 1). The hydrolysis product showed suddenly 4.1 to 4.4% weight loss at about 100 to 120°C (Curve B, Fig. 1), which corresponded approximately to the loss of

5) K. Honda, *Sci. Rep. Tohoku Univ.*, **4**, 97 (1915).

one molecule of water from one molecule of the hypothetical tricarboxylic acid. After it was heated at that temperature the weight was kept constant till it began once more to lose the weight nearly along the curve A of anhydride adduct at about 250°C. In the other run, when the heating was stopped at 150°C, it was confirmed that the remaining product was the same one as anhydride adduct by its mixed melting point and infrared spectrum.

Now, if the above mentioned hydrolysis products had the same structure as the hypothetical tricarboxylic acid (I) which corresponded with the abietic acid-maleic acid adduct, it should be expected that there would be no difference in titer between titrations in a primary alcoholic and a tertiary alcoholic medium. Contrary to our expectation, it was found that they titrated only about two thirds of the expected titration in ethanol (Table I).

Incited by this fact, we were led to find more interesting facts: (a) When the titration of above hydrolysis product was carried out in the mixed solution of acetone—*tert.*-butyl alcohol—water, with alcoholic (ethyl) alkali solution as titer, we also obtained only about the apparent acid number, two thirds of the expected one for the tricarboxylic acid I. (b) Even if it was titrated after the solution was kept at its refluxing temperature for two hours, we also found the same result. Under the same condition, ordinary anhydrides, e.g. maleic anhydride and phthalic anhydride etc., were titrated to their own total acid number respectively. (c) Furthermore, it was also confirmed that the maleic anhydride adduct itself showed only an apparent acid number under the same condition as (a) or (b).

From these facts it seems that they have not the expected tricarboxylic acid structure but an anhydride one in spite of their elementary analyses and other evidences mentioned above. And then, it seems that the anhydride adduct cannot be hydrolyzed in a hydrous medium, even at its refluxing temperature, but proceeds readily to monoesterification with primary alcohol included in titer.

On the other hand, the infrared spectra of them, compared with those of maleic anhydride- and fumaric acid- adducts (Fig. 2), supported an existence of five membered ring anhydride structure. And also, it was first revealed by these spectra that there were two forms of products according to their hydrolysis method, (1) or (2). In either case, two characteristic bands due to the carbonyls in five membered anhydride ring appeared near 1770 and 1830 cm^{-1} similar to that found in the anhydride adduct. These results make it possible to explain their anomality in acid number consistently.

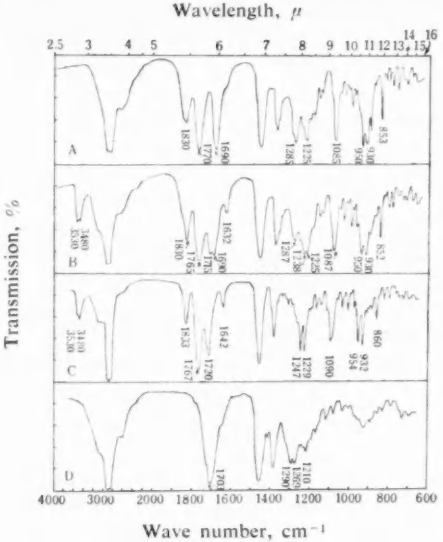

Fig. 2. Infrared spectra in Nujol of (A) abietic acid-maleic anhydride adduct, (B) hydrolysis product (α-form), recrystallized from acetone-water solution of A, (C) hydrolysis product (β-form), precipitated by acidification of the alkali solution of A, (D) abietic acid-fumaric acid adduct.

But if it is so, it becomes difficult to make compatible their elementary analytical data or their thermal degradation curves etc. with an existence of anhydride structure. The only reasonable explanation for this would be that the anhydride adduct had a tendency to form a monohydrate II without opening the anhydride ring in hydrate solution for some reason, e.g. it may be due to the stereochemically unusual approach in positions between the two carbonyl groups belonging to the succinic acid structure added to 6-, 14-carbons of abietic acid.

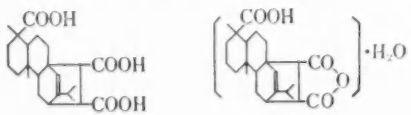

It was considered that the bands at 3530, 3480 and 1642 cm^{-1} suggested the existence of a hydrated water. Two forms of the hydrolysis products perhaps appeared from the difference in the mode of hydrogen bonding. It is considered that the carbonyl band at 1720 cm^{-1} in β-form is assigned to that of the tertiary carboxyl group under the influence of hydrogen bond caused by the hydrated water. In α-form, it divided in two bands, at 1715 and 1690 cm^{-1}.

It seems that one is under the influence of hydrogen bond and the other is not.

It seems to be almost sure that the hydrated water is stoichiometric component in the hydrolysis products, because those products which were dried to the constant weight at room temperature under reduced pressure always showed the reproducible stepwise loss of weight at the range of about 120 to 250°C in the thermal degradation curves, while abietic acid or its fumaric acid adduct which was recrystallized from acetone-water and dried under the same condition showed neither such a stepwise loss of weight in that curve nor the water bands in its infrared spectrum. It seems probable that the hydrated water is the same sort as the zeolitic water by reason of the fact that the collapse of crystals which should happen near their dehydrating temperature can not be observed in an open capillary. It could be also analyzed by Karl Fischer's method. The water content measured by this method was compared with the loss of weight at 150°C in the thermal degradation curve about the samples which were dried under various conditions in Table II.

TABLE II. DRYING TIME AND WATER CONTENT OF HYDROLYSIS PRODUCTS OF MALEIC ANHYDRIDE ADDUCT

Drying time, hr. (at 2 mmHg/28°C)	Loss of weight at 150°C, %	Water content by means of Karl Fischer's method %
1	4.43	4.20
2	4.32	—
4	4.31	4.10
6	4.15	4.42
11	4.30	3.98

Samples: Hydrolysis products precipitated from acetone containing water solution.

Summary

Hydrolysis of abietic acid-maleic anhydride adduct was carried out in two ways. The elementary analytical data of both resulting products were in good agreement with that calculated for the hypothetical tricarboxylic acid $C_{24}H_{34}O_6$, and at about 100 to 120°C these products lost the weight, which corresponded to the loss of one molecule of water from one molecule of the acid, to revert to the original anhydride adduct. But, they showed only an apparent acid number when the titrations were carried out in ethyl alcohol, similarly to the case of the anhydride adduct. Their infrared spectra suggested an existence of five-membered ring anhydride structure and a hydrated water. On the basis of these facts, we offered an anhydride adduct monohydrate structure II for the above hydrolysis products.

The author wishes to thank Dr. Shiro Tsuruta, Dr. Wataru Koga and Dr. Kiyoshi Sakashita for many stimulating discussions and helpful suggestions.

Hitachi Insulating Material Works
Hitachi Ltd., Hitachi
Ibaragi Prefecture

Pyrolysis of Organic Compounds. I. Kinetic Study of the Pyrolysis of Toluene

By Makoto TAKAHASI

(Received October 16, 1959)

In 1948 Szwarc[1] measured the reaction velocities of the pyrolysis of toluene by the flow technique in the temperature range 738~864°C. He assumed that the reaction is homogeneous, and proposed the following reaction scheme:

$$C_6H_5CH_3 \longrightarrow C_6H_5CH_2\cdot + H\cdot \quad (1)$$
initiation

$$H\cdot + C_6H_5CH_3 \longrightarrow H_2 + C_6H_5CH_2\cdot \quad (2)$$
abstraction by H atom

$$H\cdot + C_6H_5CH_3 \longrightarrow C_6H_6 + CH_3\cdot \quad (3)$$
metathesis

$$CH_3\cdot + C_6H_5CH_3 \longrightarrow CH_4 + C_6H_5CH_2\cdot \quad (4)$$
abstraction by CH_3 radical

$$2C_6H_5CH_2\cdot \longrightarrow C_6H_5CH_2CH_2C_6H_5 \quad (5)$$
termination by recombination

He considered that the rate determining step

1) H. Szwarc, *J. Chem. Phys.*, **16**, 128 (1948).

is the unimolecular reaction 1, and assumed that the velocity constant k observed by the flow method corresponds to that of the reaction 1. The activation energy and the temperature independent factor of the reaction 1 obtained by plotting $\log k$ versus $1/T$ are 77.5 kcal./mol. and 2×10^{13} respectively, and he assumed that the activation energy corresponds to the bond dissociation energy, $D(C_6H_5CH_2-H)$. H. R. Anderson Jr., H. A. Scheraga, and E. R. Van Artsdalen[2] studied the thermal bromination of toluene, and they derived 89.5 kcal./mol. for the upper limit of the bond dissociation energy of toluene. H. Blades, A. T. Blades and E. W. R. Steacie[3] repeated the study of the pyrolysis of toluene in a flow system, and they carried out a more elaborate analysis of the reaction products. Styrene, dimethylbiphenyls and anthracene were obtained in addition to bibenzyl which was reported by Szwarc to be the sole nonvolatile product in the reaction. Steacie and Blades ascribed the origin of the dimethylbiphenyls to the secondary decomposition of bibenzyl. They observed that the first order rate constant increases, as the contact time is increased, and that the rate of the reaction depends upon the condition of the surface of the reaction vessel. They calculated the apparent activation energy to be 90 kcal./mol., keeping the contact time constant at 0.068 sec., although they did not assert that the value corresponds to the true bond dissociation energy of toluene $D(C_6H_5CH_2-H)$.

Most recently, S. W. Benson and J. H. Buss[4] reviewed various attempts to determine the bond dissociation energy of toluene, and they attempted a measurement of the equilibrium constant for the reaction:

$$C_6H_5CH_3(g) + Br_2(g) \rightleftarrows C_6H_5CH_2Br(g) + HBr(g)$$

at 150°C, and they estimated the bond dissociation energy of toluene to be 84 kcal./mol., together with the known thermal data.

The bond dissociation energy was also obtained by electron impact measurement by D. O. Schissler and D. P. Stevenson[5] as 77.3 kcal./mol., and J. B. Farmer, I. H. S. Henderson, C. A. McDowell and F. P. Lossing[6] criticized the value, and they presumed that the bond dissociation energy is possibly higher by about 20 kcal./mol.

From the theoretical point of view, the present author considers that Szwarc's value of the bond dissociation energy of toluene is somewhat too low, for the difference:

$$D(CH_3-H) - D(C_6H_5CH_2-H) = 103 - 77.5 = 22.5 \text{ kcal./mol.}$$

is too large compared with the extra resonance energy of the benzyl radical which was calculated as about 14 kcal./mol.[7] If such an abnormal weakening of toluene bond were assured by experiments, the fact might be an interesting theoretical problem, but at present it seems to be premature to discuss this point, for there remain many points which should be made clear in the experiments.

It is to be noted that the value obtained by Steacie and his collaborators for the activation energy of the pyrolysis of toluene is different from that by Szwarc, although the method was the same. A. F. Trotman-Dickenson[8] pointed out that Steacie and his collaborators measured the rate constant, keeping the contact time far less than in the experiments by Szwarc.

However, the present author considers that it is very unfortunate that the two groups made experiments in the different ranges of the reaction temperatures; that is, Szwarc in the range between 738~864°C, and Steacie and his collaborators between 860~940°C. Therefore, the present experiment was carried out to cover the whole temperature range 737~953°C, and efforts were made to elucidate the cause of the discrepancy of the bond dissociation energies of toluene obtained by the two groups.

Experimental Procedure

Materials.—Both Szwarc's and Steacies groups used toluene prepyrolyzed to remove interfering impurities which would give extra hydrogen and light hydrocarbons by pyrolysis. The present author attempted to obtain toluene of higher purity which is usable without prepyrolysis. Toluene from two sources were examined, the one of which was obtained by the usual purification process combined with azeotropic distillation with acetonitrile to remove interfering impurities which were presumed to be cycloalkanes. This toluene was conceived to be of very high purity, but nevertheless it gave some amount of ethylene and propylene in addition to hydrogen and methane by pyrolysis, if it was subjected to prepyrolysis.

In order to obtain toluene of higher purity which contains no alkanes nor cycloalkanes, the author prepared toluene from toluidine by applying the method described in Organic Syntheses[9]. A cold diazonium solution was prepared from 105 g. of toluidine, 190 ml. of concentrated hydrochloric acid,

2) H. R. Anderson Jr., H. A. Scheraga and E. R. Van Artsdalen, ibid., **21**, 1258 (1953).
3) H. Blades, A. T. Blades and E. W. R. Steacie, *Can. J. Chem.*, **32**, 1142 (1954).
4) S. W. Benson and J. H. Buss, *J. Phys. & Colloid Chem.*, **61**, 104 (1957).
5) D. O. Schissler and D. P. Stevenson, *J. Chem. Phys.*, **22**, 151 (1954).
6) J. B. Farmer, I. H. S. Henderson, C. A. McDowell and F. P. Lossing, ibid., **22**, 1948 (1954).
7) M. Takahasi, This Bulletin, **29**, 625 (1956).
8) A. F. Trotman-Dickenson, "Gas Kinetics", Butterworths Scientific Publications, London (1955), p. 108.

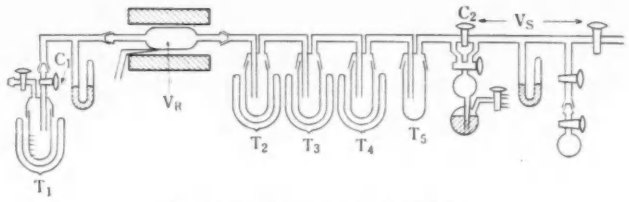

Fig. 1. Apparatus for Pyrolysis.

TABLE I. VELOCITY CONSTANTS IN THE CASE OF THE REACTION VESSEL I

Exp. No.	Vap. pressure mmHg	Reaction temp., °C	$-\log k$	Mole ratio of H_2 to CH_4	Contact time, sec.
95	7.24	763.5	3.24		
94	8.38	787.2	2.95		
93	9.60	819.0	2.52		
40	4.98	856.5	1.81		0.26
41	4.94	863.9	1.71		
42	5.24	866.3	1.65		
90	8.00	879.8	1.54		
89	7.54	880.6	1.58		
91	7.00	894.0	1.34		
47	5.04	912.0	1.11	2.0	
48	5.15	933.1	0.78		
49	5.98	936.9	0.72		
50	5.34	939.3	0.69		

and 69 g. of sodium nitrite in 200 ml. of water, and it was poured into a flask containing 520 g. of sodium hypophosphorite, $NaH_2PO_2 \cdot H_2O$, 256 g. of concentrated hydrochloric acid and 40 g. of water. Evolution of nitrogen was controlled, keeping the solution at 5°C. The flask was placed in a refrigerator overnight, and the reaction product was transfered to a separating funnel, and the upper oil was separated from the aqueous phase. Ether extraction should be avoided, for it causes the contamination of toluene with ether. A fraction boiling at 110°C. was gathered by simple distillation which weighed about 55 g., and then it was distilled through a spinning band fractionating column of 150 cm. in length. This toluene did not give any appreciable amount of ethylene and higher hydrocarbons in the pyrolysis, even if prepyrolysis was not carried out, and therefore the latter toluene was used in the present kinetic study.

Apparatus and Procedure—The general arrangement of apparatus for pyrolysis shown in Fig. 1 is similar to that used by Szwarc but with a small modification to improve experimental accuracy. Toluene which had been refluxed with sodium for about one hour was distilled under reduced pressure into the storage vessel T_1. This vessel was weighed before and after each run of experiment, to measure the amount of toluene passed in each run, if it was necessary to calculate accurate contact time. In the usual runs, the amount of toluene was determined by volume in the storage flask. During runs, the vessel was kept in a Dewar vessel contaning water maintained at a temperature constant to 0.1°C. Toluene was evaporated from T_1 through cock C_1 to maintain its vapor pressure 4~10 mmHg, and led into a silica reaction vessel heated by an electric furnace. Contact time was controlled by replacing silica reaction vessels which were designated as I, II, and III. (Table V). The electrical furnace was about 70 cm. long, and the variation of temperature along the reaction vessel was ±2°C. The temperature of the reaction vessel was measured by a calibrated Pt-Rh thermocouple with a potentiometer. It was checked to discover whether temperature difference inside and outside the reaction vessel might be caused by passing toluene, but the difference did not exceed 2°C.

The reaction system was evacuated to 10^{-4} mmHg before the experiment, and pressure increase in the reaction system in the course of about 20 min. was checked without passing toluene. The increase of pressure was caused mainly by evaporation of toluene previously dissolved in grease of cocks but not by leakage of air, being suppressed to about 10^{-3} mmHg in the course of about 20 minutes, a time comparable to that of one usual run of pyrolysis.

The vapor leaving the reaction vessel passed through traps T_2 and T_3 which were cooled with a mixture of ether and solid carbon dioxide. Toluene and the less volatile products such as bibenzyl and dimethylbiphenyls were almost completely condensed in trap T_2. The noncondensable gas passed through trap T_4 which was cooled by liquid nitrogen or oxygen. Trap T_5 was reserved for distillation, and

9) "Organic Syntheses", Collective Vol. II. John & Willey Sons, Inc., New York, p. 1039.

TABLE II. VELOCITY CONSTANTS IN THE CASE OF THE REACTION VESSEL II

Exp. No.	Vap. pressure mmHg	Reaction temp., °C	$-\log k$	Mole ratio of H_2 to CH_4	Contact time, sec.
13	5.02	737.8	3.43		
80	8.39	741.1	3.11		
81	9.62	749.0	3.34		
88	8.14	755.2	3.24		
87	8.47	763.6	3.13		
82	9.22	770.8	3.05		
12	5.76	779.0	2.91		
86	8.64	791.3	2.71		
18	6.64	801.9	2.57		
19	5.88	801.9	2.54	2.1	
20	5.66	803.5	2.50	2.3	
85	9.20	814.1	2.38		
83	8.64	814.9	2.31		
11	7.14	821.4	2.32		
84	9.06	828.7	2.15		
77	9.26	837.5	1.98		
78	9.10	837.5	1.90		
10	7.04	839.1	2.06		
76	9.66	848.7	1.78		
79	9.10	850.3	1.92		
75	9.58	851.1	1.78		
21	6.12	855.1	1.79	2.1	
8	6.34	859.1	1.67		0.11
35	6.40	860.7	1.67		
74	9.76	860.7	1.65		
9	6.28	863.9	1.62		0.10
5	5.68	863.9	1.70		0.09
72	9.00	875.0	1.48		
73	10.02	875.8	1.42		
10	9.64	880.6	1.34		0.24
71	9.49	890.1	1.22		
17	6.50	897.9	1.14	2.3	0.11*
69	9.35	902.6	1.07		
6	5.40	908.1	0.94		0.14
68	10.14	908.9	0.93		
64	9.28	916.7	0.85		
27	6.58	918.3	0.89	2.2	
38	5.80	928.4	0.72	1.8	
65	9.94	932.3	0.60		0.14
16	6.50	937.0	0.52		
14	6.24	938.6	0.52	2.3	0.13
15	7.19	940.1	0.60		0.15
66	9.70	944.0	0.40		
67	10.60	953.3	0.26		
24	4.34	953.7	0.25	1.9	
7	6.49	955.6	0.23		0.16

* Condensable gas at liquid nitrogen temperature amounted to 2% of total gas product.

kept at room temperature. Noncondensable gas in trap T_4 was composed of hydrogen and methane, and it was pumped out by a Toepler pump and collected in a storage vessel of about 100 ml. The quantity of hydrogen and methane produced was given by reading the pressure in the storage vessel with a McLeod gauge or a U tube manometer according to the pressure. The reaction time extended from 3 to 30 minutes, according to the quantity of gas produced. After the flow of toluene vapor was stopped, the trap T_2 was warmed to room temperature to distil toluene from trap T_2 to T_3. All the produced gas, remaining in the reaction system and dissolved in toluene of trap T_2, was pumped out by a Toepler pump to the storage vessel. Hydrogen and methane expelled from trap T_2 amounted to about 10% of the total gas produced. Operation of Toepler pump was continued for 15 min. after flow of toluene was stopped. After the pressure of a mixture of hydrogen and methane was read, trap T_4 was warmed to -70°C by changing the cooling material to a mixture of ether and carbon dioxide. The amount of gas condensable in trap T_4 at liquid nitrogen temperature was at most a few per cent of that of condensable gas, if toluene which was synthesized from toluidine as described above was pyrolyzed.

As the experimental conditions were so chosen that the decomposition ranged from 0.001 percent to 0.6 percent of total toluene, the reaction rate constant for the unimolecular reaction was calculated by the equation,

$$k = \frac{P_s \times V_s \times T_R}{P_t \times t \times T_r \times V_R} \tag{6}$$

where P_t is vapor pressure of toluene (mmHg), T_R is reaction temperature (°K), V_R is volume of reaction vessel (l.), t is time of flow (sec.), and P_s is pressure of product gas (H_2+CH_4) (mmHg) at T_r °K in a storage vessel of V_s. The contact time was calculated according to Eq. 7,

$$\tau = V_R/v = \frac{V_R \times P_t \times t}{m \times 0.082 \times T_R \times 760} \tag{7}$$

$$k = \text{fractional decomposition}/\tau \tag{8}$$

where m is moles of toluene passed, and v (l.) is volume of toluene which passed through the reaction vessel per second at T °K. Contact time was calculated in several runs, but not in all runs, because it depends mainly on the value of reaction vessel and vapor pressure of toluene, the latter being varied over a small range.

TABLE III. VELOCITY CONSTANTS IN THE CASE OF THE REACTION VESSEL III

Exp. No.	Vap. pressure mmHg	Reaction temp., °C	$-\log k$	Contact time, sec.
101	9.88	811.7	2.34	
100	10.78	836.7	2.01	
99	10.80	868.8	1.58	
98	10.95	888.8	1.30	
97	10.60	908.1	0.99	
54	7.28	925.3	0.66	0.03
55	6.48	925.3	0.67	
56	6.36	939.3	0.61	
96	11.10	948.7	0.44	
57	6.51	958.7	0.38	
61	7.22	960.3	0.33	

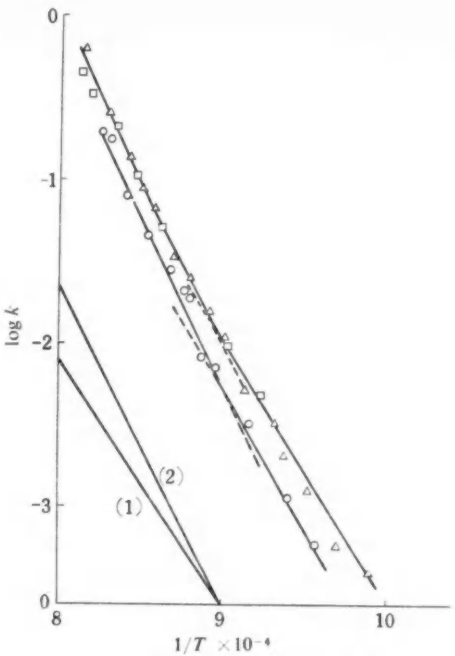

Fig. 2. Relation of $\log k$ versus $1/T$
△ Reaction Vessel I
○ 〃 II
□ 〃 III
(1) gradient corresponding to the activation energy of 70 kcal./mol.
(2) 〃 of 90 kcal./mol.

Experimental Results

The results are shown in Tables I, II and III, and the relation of $\log k$ versus $1/T$ is shown in Fig. 2. From the figure it may be apparently concluded that the relation was linear, but the more precise analysis makes clear the curve is slightly concave. Therefore, the temperature range was rather arbitrarily divided into three parts, that is, higher, medium, and lower temperature ranges, and a linear relation of $\log k$ versus $1/T$ was assumed in each range, and experimental activation energies and temperature independent factors were calculated by the least square method. The results are summarized in Table IV. Different gradients were obtained in each temperature range, corresponding to different activation energies and different frequency factors. The probable cause of deviation of the relation of

Table IV. Experimental activation energies and log A of pyrolysis of toluene under various conditions

Temp. range °C	Number of experiments	Volume of reaction vessel, ml.	Contact time, sec.	E kcal./mol.	log A
764～843	4	53.7	0.3	81.3	13.7
857～894	6	〃	〃	69.2	11.5
912～933	4	〃	〃	104.9	18.1
738～849	19	31.0	0.1～0.2	73.7	12.4
850～898	13	〃	〃	93.3	16.2
903～956	14	〃	〃	103.5	18.0
812～889	4	6.4	0.02～0.04	78.0	13.3
908～960	7	〃	〃	76.2	13.1
Szwarc[1]					
738～850	27	not described	0.2～0.9	77.5	13.1
Steacie and his collaborators[3]					
850～940	9	not described	0.068	90	not described

log K versus $1/T$ from linearity is discussed below.

Identification and Analysis of Products.—The mole ratio of hydrogen to methane was determined by a mass spectrometer of CEC 21-103A type by using peaks of m/e 2 and 16, although quantitative analysis of hydrogen by the mass spectrometer did not give sufficient accuracy. Complete analysis of solid and oily matters which were obtained in trap T_2 was not carried out, but the ultraviolet absorption spectrum (Fig. 3) showed that the main products were composed of bibenzyl and dimethylbiphenyls, and this result agrees with that of Steacie and his collaborators.

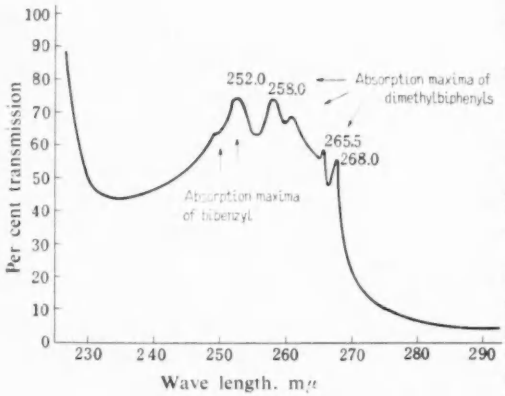

Fig. 3. Absorption spectrum of the nonvolatile reaction products of pyrolysis of toluene in ethanol.

Discussions

As described above, the present experimental results show that the relation of log k versus $1/T$ in the temperature range 737～953°C is not strictly linear and that high activation energies and high frequency factors are obtained in the higher temperature range in the series of the experiments which were carried out at contact time of 0.1～0.3 sec. In the case of shorter contact time, 0.02～0.04 sec., (Table IV), the activation energy is obtained only in the higher temperature range 812～960°C, because the experiment in the lower temperature range should give a smaller amount of gas product and involve larger experimental error, compared with the experiments of longer contact time. It is to be noted that the lower activation energy is obtained even in the higher temperature range, compared with the experiment of longer contact time in the same temperature range.

Now the author will discuss the probable cause of systematic deviation of the relation of log k versus $1/T$ from linearity.

1) Experimental errors: It may be possible that k at lower temperatures involves relatively large error, because the amount of the product gas at lower reaction temperature is very small, even if the reaction time is lengthened. As was described in the experimental part, the pressure increase in the storage vessel in the blank test amounted to about 10^{-3} mmHg in the course of about 15 min. Total pressure of product gas which was given by pyrolysis of toluene for ten minutes at the lowest reaction temperature, 738°C, amounted to about 0.06 mmHg (cf. Exp. No. 13). This may mean that the observed velocity constants at lower reaction temperatures should be reduced by some percentage, but such correction seems not to increase so much the activation energy obtained at the lower temperature range.

Alkanes and cycloalkanes which may supposedly exist in commercial toluene may be decomposed more rapidly than toluene, and

such toluene may increase the apparent k at lower reaction temperatures, but the toluene which was synthesized from toluidine may be free from such impurities.

2) Correction by using the more elaborate Arrhenius equation: As was pointed out by many authors[10], under some conditions the frequency factor is a function of the temperature and a more accurate equation 10 than the usual Arrhenius equation 9 should be used.

$$k = A\exp(-E_a/RT) \tag{9}$$

$$k = AT^n\exp(-E/RT) \tag{10}$$

or $$\ln k = -E/RT + n\ln T + \ln A$$

and the difference of the two activation energies is

$$E = E_a - nRT. \tag{11}$$

In the present case, n is not known, but if n is assumed to be 1/2 as in the usual collision theory, $n(\ln T_1 - \ln T_2)$ amounts to 0.042, when T_1 and T_2 are assumed 953°C and 737°C respectively. This may reduce activation energies in the higher temperature range to some extent, but the correction seems not to contribute so much to reducing the concave nature of the relation of $\log k$ versus $1/T$.

3) Complications due to competitive reactions: H. Blades, A. T. Blades and E. W. R. Steacie[3] pointed out that the first order rate constants for the pyrolysis of toluene depends on the condition of the surface of the reactor, and the contact time, and on the pressure. A. Frost and R. G. Pearson[10] pointed out that a plot of $\log k$ versus $1/T$ shows a curvature if there are two competing reactions with different activation energies.

One case is that where the same reaction occurs both homogeneously and heterogeneously. The homogeneous reaction usually has a higher activation energy, and it is favored at high temperatures whereas the heterogeneous reaction predominates at lower temperatures. In the present experiment, it is shown that k at the same temperature varies slightly as shown in Fig. 2, when the reaction vessel is replaced (I, II, and III). Contact time, volume and surface area of reaction vessel are varied as shown in Table V by replacing the reaction vessel, but it is not yet elucidated how these conditions affect the velocity constant and activation energy of pyrolysis of toluene. The present author presumed that any unfavorable secondary reaction may be suppressed, if the experiment is carried out under a smaller contact time, but such a presumption could not be confirmed in the present experiment.

10) A. A. Frost and R. G. Pearson, "Kinetics and Mechanism", John Wiley Sons, Inc., New York (1953), p. 24.

Table V

Reaction vessel	Volume ml.	Contact time, sec.	Surface area, cm²
I	53.7	0.3	113
II	31.0	0.2—0.1	94
III	6.4	0.03	44

Thus, the author's efforts to obtain a value as much smaller than k as possible especially in the lower temperature range appeared not to modify the concave nature of $\log k$ versus $1/T$, and another source of complications of the present reaction is now considered in the following. At the higher temperature range between 900~950°C, it may be possible that the observed k becomes rather increased, as the reaction temperature is increased, because some competitive side reaction takes place, giving hydrogen and methane. Already both Szwarc[11] and Steacie[3] considered the following reaction,

$$C_6H_5CH_3 \longrightarrow C_6H_5\cdot + CH_3\cdot$$

as one of possible side reactions, but they considered that such a reaction is less probable, because the ratio of hydrogen to methane does not vary over the whole temperature range. The present experimental results of the ratio of hydrogen to methane appear to support their conclusion. Another possible reaction is one involving the participation of ring-hydrogen in initiation and/or propagation reaction as follows:

$$C_6H_5CH_3 \longrightarrow \cdot C_6H_4CH_3 + H\cdot \quad \text{initiation}$$

$$C_6H_5CH_3 + H\cdot \longrightarrow \cdot C_6H_4CH_3 + H_2$$
abstraction by hydrogen atom

$$C_6H_5CH_3 + CH_3\cdot \longrightarrow \cdot C_6H_4CH_3 + CH_4$$
abstraction by methyl radical

Blades and Steacie[11] pointed out such a possibility in the experiment of pyrolysis of *n*-propylbenzene in the presence of toluene-α-d_3 at 722°C. They found that the amount of methane in the reaction product is unexpectedly large compared with the amount of methane-*d*. Recently S. H. Wilen and E. L. Eliel[12] assumed abstraction of ring-hydrogen by methyl radicals in the reaction of acetyl peroxide with ring-deuterated toluene at 131~147°C. which gave rise to some methane-*d*. The present author's experiment of toluene-3-*d* and toluene-4-*d* which confirms the involvement of ring-hydrogen in the pyrolytic reaction of toluene itself will be reported in the succeeding paper, although it remains unsolved whether the involvement of ring-hydrogen modifies the overall activation energy or not.

11) A. T. Blades and E. W. R. Steacie, *Can. J. Chem.*, 32, 1142 (1954).

12) S. H. Wilen and E. L. Eliel, *J. Am. Chem. Soc.*, 80, 3309 (1958).

Summary

Pyrolysis of toluene by the flow technique was carried out under various conditions, and the velocity was measured over the wide temperature range 737~953°C at contact time 0.02~0.3 sec. The relation of $\log k$ versus $1/T$ appears to be linear, but the more precise analysis shows a slight concave nature, and therefore activation energy tends to increase, as the reaction temperature is raised. Detailed investigation on its cause was made, and it is presumed that such an increase of activation energy with rise of temperature is mainly brought about by some competitive reaction, but not by experimental conditions. The present author considers that the involvement of ring-hydrogen reaction may compete with the reaction of fission of C H bond of the methyl group, and such competitive reaction may modify the activation energy of the fission of the methyl bond of toluene, if the experiment is carried out over the wide reaction temperature range.

The author wishes to express his hearty thanks to Professor Y. Urushibara and Professor O. Simamura for their kind guidance and encouragement of the present work. The author is grateful to Dr. M. Kobayashi for experimental help and for stimulating discussions, and to Dr. T. Tamura and Mr. H. Saito for fractional distillation of toluene.

Department of Chemistry
College of General Education
The University of Tokyo
Meguro-ku, Tokyo

Pyrolysis of Organic Compounds. II. Pyrolysis of Toluene-3-d and Toluene-4-d

By Makoto TAKAHASI

(Received October 16, 1959)

In recent years the bond dissociation energy of toluene, $D(C_6H_5CH_2{-}H)$, has become a topic of considerable dispute, and various attempts to determine the bond dissociation energy were reviewed by Benson & Buss[1] and by the present author[2]. Szwarc[3] estimated the activation energy of the pyrolytic reaction of toluene by the flow method to be 77.5 kcal./mol., and the frequency factor to be 2×10^{13} in the reaction temperature range 738~864°C. H. Blades, A. Blades and Steacie[4] repeated the study of the pyrolysis of toluene by the same method, and they observed that the first order rate constant increases, as the contact time is increased. They calculated the apparent activation energy of the pyrolytic reaction to be 90 kcal./mol., keeping the contact time constant at 0.068 sec. in the reaction temperature range 860~940°C, but they concluded that it is premature to assign any definite value to the bond dissociation energy of toluene. At first, in order to explain the higher activation energy and the occurrence of methane, they suggested reaction 2, which proceeds concurrently with the main reaction 1.

$$C_6H_5CH_3 \rightarrow C_6H_5CH_2\cdot + H\cdot \qquad (1)$$

$$C_6H_5CH_3 \rightarrow C_6H_5\cdot + CH_3\cdot \qquad (2)$$

Later, however, they[5] approved of Szwarc's view that the contribution of reaction 2 to the apparent activation energy of pyrolysis of toluene is of a minor degree, for they considered the facts that the ratio of hydrogen to methane in the reaction product of pyrolysis of toluene is constant over the reaction temperature range, and that the ratio does not vary even in the decomposition of *n*-propylbenzene in the presence of excessive toluene[6].

The present author[2] carried out the pyrolysis of toluene in both of the temperature ranges, 738~864 and 860~940°C, to elucidate the cause of the discrepancy of the bond dissociation energies of toluene obtained by the two groups, and it was found that the apparent activation energy for the first order rate expression of pyrolysis of toluene increases, as the reaction

1) S. W. Benson and J. H. Buss, *J. Phys. & Colloid Chem.*, **61**, 104 (1957).
2) M. Takahasi, This Bulletin, **33**, 801 (1960).
3) M. Szwarc, *J. Chem. Phys.*, **16**, 128 (1948).
4) H. Blades, A. T. Blades and E. W. R. Steacie, *Can. J. Chem.*, **32**, 298 (1954).
5) A. Blades and E. W. R. Steacie, ibid., **32**, 1142 (1954).
6) C. H. Leigh and M. Szwarc, *J. Chem. Phys.*, **20**, 403 (1952).

temperature was extended to a higher range. The author discussed the possible causes of the nonlinearity of the relation of $\log k$ versus $1/T$, and suggested complication by the involvement of some competitive reaction. Blades and Steacie[5] suggested the same possibility in the reaction, and carried out the pyrolysis of *n*-propylbenzene in an excess of deuterated toluenes (mixture of toluene-α-d_3: 66%, toluene-α-d_2: 29%, and toluene-α-d: 5%) at 722°C at contact time 0.45 sec. They found the products were composed of hydrogen, methane, ethane, ethylene, benzene and bibenzyl, and the ratios of the gaseous products were:

$$H_2 : HD : D_2 = 1 : 1 : 0$$

and

$$CD_4 : CD_3H : CD_2H_2 = 1 : 1.5 : 1$$

respectively.

The large ratio of H_2 to HD suggested that hydrogen atoms may be abstracted from the ring as well as from the side chain. In addition, they concluded that concerning two mechanisms 3 and 4 suggested by Szwarc,

$$H\cdot + C_6H_5CD_3 \text{ (or } C_6H_5CD_2H) \rightarrow C_6H_5\cdot + CD_3H \text{ (or } CD_2H_2) \quad (3)$$

$$C_6H_5\cdot + C_6H_5CD_3 \rightarrow C_6H_5D + C_6H_5CD_2\cdot$$

$$H\cdot + C_6H_5CD_3 \text{ (or } C_6H_5CD_2H) \rightarrow CD_3\cdot \text{ (or } CD_2H\cdot) + C_6H_6$$

$$CD_3\cdot \text{(or } CD_2H\cdot) + C_6H_5CD_3 \text{(or } C_6H_5CD_2H) \rightarrow CD_4 + C_6H_5CD_2\cdot \text{(or } CD_3H,\ CD_2H_2) \quad (4)$$

mechanism 3 would give CD_3H and CD_2H_2, while mechanism 4 would give CD_4, CD_3H and CD_2H_2. They considered that the production of CD_4 in their experiment is a good evidence for mechanism 4, and that mechanism 3 contributes to a minor degree. As the pyrolysis of toluene itself was not carried out in their experiment, it was not clear whether the initiations reaction of pyrolysis of toluene involves the ring-hydrogen or not. The present author attempted to study the pyrolysis of toluene-3-*d* and toluene-4-*d* in the temperature range 830~955°C, and investigated the reactivities of the meta and para positions of toluene.

Experimental

Materials.—Toluene-3-*d* and -4-*d* were prepared by the reaction of *m*- and *p*-tolylmagnesium bromide with deuterium hydroxide according to Gold[7] with some modifications. The Grignard reagent was prepared from 50 g. of *m*- or *p*-bromotoluene, 7 g. of magnesium and 120 ml. of ethyl ether; and 6 ml. of deuterium hydroxide (99.78 g. D_2O/100 g.) was added to the reaction mixture. In adding deuterium hydroxide, care should be taken to continue vigorous stirring to secure the contact of deuterium hydroxide with the Grignard reagent. The reaction mixture was refluxed for about ten minutes, and left to stand overnight. In order to decompose the remaining Grignard reagent, dry carbon dioxide was passed through for some time, and then 7 g. of ammonium chloride solution in 25 ml. of water was added, a solid material being formed. Then 20 ml. of concentrated hydrochloric acid was added to dissolve the solid. Ether layer was separated, and the aqueous layer was extracted with 100 ml. of ether. The combined ether solution was washed with a dilute sodium hydroxide solution and with distilled water successively, and dried with calcium chloride. Ether was removed by distillation with Vigreux's columm, and toluene fraction boiling at 111~112°C was collected, weighing about 15 g. The toluene fraction was then shaken with about 15% hydrochloric acid to remove a trace of ether which interferes with pyrolysis of toluene, and distilled through a spinning band column of 150 cm. in length. Although the deuterated toluenes thus obtained contained about 22% of undeuterated toluene (see the next section), some improvements of isotopic purity may be obtained by the more elaborated method proposed by Weldon[8].

Determination of Isotopic Purity of Deuterated Toluenes.—For the determination of the isotopic purity of the deuterated organic compounds, mass spectrometry under reduced ionization voltage[9] is recommended, but the available mass spectrometer of CEC 103 A type operated at ionizing voltage 70 V. was unsuitable for the present purpose. So the present author was obliged to apply the infrared spectra for the determination of the isotopic purity of synthesized deuterated toluenes, in spite of less accuracy of the method. Infrared spectra of toluene, toluene-3-*d* and toluene-4-*d* were already given by Tiers[10] in the region of 693~835 cm^{-1}. Comparison of their spectral data of toluene with those of the present author gave good agreement in the wave numbers of the absorption maxima, but not in the intensity, their absorption coefficients at characteristic absorption maxima being larger by about twice than the present author's. While standard toluene-3-*d* and -4-*d* of isotopic purity of more than 99% were not available to us, Tier's data were not proper to be applied to the present analysis, so that the present author adopted the method to determine the content of undeuterated toluene in the synthesized mixture. The infrared spectral data obtained by a Perkin Elmer 112 infrared spectrometer are shown in Table I. The absorption band of toluene at 730 cm^{-1} is too strong to determine the absorption coefficient in liquid state. Therefore, the absorption band at 695 cm^{-1} was used in the analysis of the mixture of toluene and toluene-4-*d*, the latter of which has no characteristic absorption at the wave number. The extinction coefficient of standard

7) V. Gold and D. P. N. Satchell, *J. Chem. Soc.*, **1951**, 2743.

8) L. H. P. Weldon and C. L. Wilson, *J. Chem. Soc.*, **1946**, 235.

9) The Institute of Petroleum, "Applied Mass Spectrometry", London, (1954), p. 91.

10) G. V. D. Tiers and J. H. Tiers, *J. Chem. Phys.*, **20**, 761 (1953).

TABLE I. EXTINCTION COEFFICIENTS OF STANDARD TOLUENE, AND OF MIXTURES OF TOLUENE-3-*d* OR -4-*d* AND TOLUENE

Wave numbers, cm^{-1}	3030	835	798	730	710	695
Standard toluene	430	0	0	1470	0	840
Sample I (toluene+toluene-3-*d*)	260	0	540	480	0	800
Sample II (toluene+toluene-4-*d*)	260	640	0	490	200	190

Extinction coefficient $K_\nu = \log (I_0/I)/d$.
Cell thickness $d = 0.00087$ cm.

TABLE II. COMPARISON OF MASS SPECTRA OF STANDARD TOLUENE, SAMPLES I AND II, WITH API DATA

m/e	Standard toluene	Sample I	Sample II	Toluene*	Toluene-3-*d**	Toluene-4-*d**
95	—	0.21	0.26	—	—	—
94	0.16	5.38	5.49	0.16	—	—
93	6.00	69.09	70.39	5.60	72.5	71.6
92	78.37	100	100	78.5	100	100
91	100	35.15	37.07	100	8.51	8.53
90	7.70	4.50	4.57	9.08	2.53	3.66
89	3.72	2.14	2.09	4.13	1.00	0.93
88	0.27	0.45	0.42	0.36	0.32	0.33
87	0.58	0.80	0.75	0.60	0.61	0.61
86	0.99	0.98	0.99	0.94	0.69	0.67
85	0.78	0.71	0.73	0.66	0.48	0.48
84	0.33	0.35	0.35	0.22	0.23	0.21

Ionization voltage: 70 V.
Ionizing current : 10.5 μA.
* From API Spectral Data, Serial No. 418, 687 and 688.
Components containing ^{13}C have been removed in the API Data.

toluene at 695 cm^{-1} being 840, the content of toluene in Sample II (mixture of toluene and toluene-4-*d*) was ascertained as 22%. In the analysis of Sample I (mixture of toluene and toluene-3-*d*) the band at 695 cm^{-1} is unsuitable, for toluene-3-*d* has the absorption band of nearly the same strength as toluene at the position. However, as the extinction coefficient of Sample I at 730 cm^{-1} is accidentally almost the same as that of Sample II, the content of toluene in Sample I was presumed to be nearly the same as that of Sample II, that is, 22%. Mass spectrometric data which are shown in Table II may support the above conclusion, although they are not sufficient for determining the precise isotopic purity.

Apparatus and Procedure of Pyrolysis. — They were previously described in Part I. Experiments in the temperature range lower than 830°C and at a contact time less than 0.1 sec. were not carried out, for a sufficient amount of gas for the mass spectrometric analysis was not produced under these conditions.

Analysis of Gaseous Products and Experimental Results

The gas products of pyrolysis of the mixture of toluene and toluene-3-*d* or -4-*d* consisted of H_2, HD, a trace of D_2, CH_4 and CH_3D. No complete method of determination of the ratio of HD to H_2 appeared to be established until most recently[11], in the case where the relative abundance of HD to H_2 is more than 10% and the total amount of hydrogen is small. Recent development of gas chromatography has made it possible to separate HD from H_2, using a very small amount of a sample[12], and this method may be applied to the analysis. In the present experiment, the author was satisfied with determining the ratio approximately. As pure HD for a standard was not available, its mass spectrometric sensitivity at *m/e* 3, was assumed to be equal to that of H_2 at *m/e* 2. It has been pointed out that the peak at *m/e* 3 contains the component of H_3^+, in addition to that of HD^+, but its contribution was not appreciable in the present case, using ionizing current of 10.5 μA. The contribution of D^+ to *m/e* 2 is not known, but it may be neglected,

TABLE III

m/e	18	17	16	15	14	13
			CH_4^+	CH_3^+	CH_2^+	CH^+
		$^{13}CH_4^+$	$^{13}CH_3^+$	$^{13}CH_2^+$	$^{13}CH^+$	$^{13}C^+$
		CH_3D^+	CH_2D^+	CHD^+	CD^+	CH^+
	$^{13}CH_3D^+$	$^{13}CH_2D^+$	$^{13}CHD^+$	$^{13}CD^+$	$^{13}CH^+$	$^{13}C^+$
	P_{18}	P_{17}	P_{16}	P_{15}	P_{14}	P_{13}

11) The Institute of Petroleum, "Applied Mass Spectrometry", London (1954) p. 81.
12) S. Ohkoshi, Y. Fujita and T. Kwan, This Bulletin, 31, 771 (1958).

considering that the relative abundance of H^+ produced from H_2 is 2.1% to that of H_2^+ [13].

The ratio CH_3D/CH_4 was determined according to the following procedure. As each peak of the mixture of CH_4 and CH_3D at m/e 18~13 is composed of the following several components as shown in Table III, Eqs. 5 and 6

$$P_{17}=\frac{1}{100}\{S_{CH_4}(a_{^{13}CH_4^+}\times 0.0101)X + S_{CH_3D}(b_{CH_3D^+}\times 0.9896+b_{^{13}CH_2D^+}\times 0.0101)Y\} \quad (5)$$

$$P_{16}=\frac{1}{100}[S_{CH_4}(a_{CH_4^+}\times 0.9896+a_{^{13}CH_3^+}\times 0.0101)X + S_{CH_3D}\{b_{CH_2D^+}\times 0.9896+(b_{^{13}CHD^+}+b_{^{13}CH_3^+})\times 0.0101\}Y] \quad (6)$$

are derived, where P_{17} and P_{16} are observed peak heights at m/e 17 and 16, S_{CH_4} and S_{CH_3D} are sensitivities of CH_4 and CH_3D at their parent peaks, a_{R^+} and b_{R^+} are relative abundances of ions produced from CH_4 and CH_3D, and X and Y are pressures of $(CH_4+^{13}CH_4)$ and $(CH_3D+^{13}CH_3D)$, respectively.

Table VI. Mass spectra of CH_4 and CH_3D

m/e	CH_4 (*a*)	CH_3D (*b*)	CH_4 (*a'*)
17		100	
16	100	79.8	100
15	89.3	23.7	88.1
14	19.4	10.5	19.8
	Mohler's data. $^{13}CH_4$ component has been removed.	this work	

For the measurement of standard CH_4 by the present author gave nearly the same cracking pattern *a'* as *a* of Mohler[14] (Table IV), the author applied his data *a* and *b* to the present analysis. From Eqs. 5 and 6, Eq. 7 is derived assuming $S_{CH_4}=S_{CH_3D}$, and using Mohler's data,

$$Y/X=99.052\frac{(1.00808\,P_{17}-0.0101\,P_{16})}{(98.96\,P_{16}-79.207\,P_{17})} \quad (7)$$

The data of mole ratios HD/H_2 and CH_3D/CH_4 obtained in the pyrolysis of Samples I and II under various conditions are shown in Table V, where Eq. 7 was applied to the determination of CH_3D/CH_4. The determination of the mole ratio $(H_2+HD)/(CH_4+CH_3D)$ was not performed, for sufficient accuracy was not expected for the determination by the mass spectrometric analysis, and from the previous data it may be presumed that the ratio is about 2[2].

Analyses of liquid products were carried out by both infrared and mass spectrometric methods. Toluene recovered from the reaction products of Samples I and II gave nearly the same infrared spectra as the original ones. Therefore, it may be concluded that any transfer of deuterium from the initial position did not occur in the pyrolysis. Mass spectra of the recovered toluene were also nearly the same in the mass range of C_7 groups, but some differences were observed in the range of C_6 groups as shown in Table VI.

Table VI shows that the peak at m/e 78 includes $C_6H_6^+$, $C_6H_4D^+$ and $C_5{}^{13}CH_5^+$, and the peak at m/e 79 does $C_6H_5D^+$, $C_6H_3D_2^+$ and $C_5{}^{13}CH_6^+$, but it was not carried out to determine the ratio $C_6H_6:C_6H_5D:C_6H_4D_2$ from these data. It is to be noted that the increase of benzene content due to the rise of the reaction temperature is rather small compared

Table V. Mole ratios HD/H_2, D_2/H_2 and CH_3D/CH_4 in the pyrolysis of Samples I and II

Expt. No.	Reaction temp., °C	Vapor pressure, mmHg	k, sec^{-1}	HD/H_2	D_2/H_2	CH_3D/CH_4
Sample I (mixture of 22% toluene and 78% toluene-3-*d*)						
I-4	830.3	8.92	(1.0×10^{-2})	—	—	0.060*
I-3	832.0	7.36	1.0×10^{-2}	0.11	0.000	0.052
I-1	876.6	8.80	4.2×10^{-2}	0.14	0.004	0.077
I-5	902.6	8.46	1.2×10^{-1}	—	—	0.091*
I-2	908.1	8.82	1.3×10^{-1}	0.13	0.004	0.075
Sample I' (toluene recovered from the reaction mixture of Sample I after pyrolysis)						
I'-1	850.3	3.66	—	0.17	0.006	0.058
I'-2	852.0	10.62	2.8×10^{-2}	0.19	0.007	0.082
I'-3	919.0	8.96	2.9×10^{-1}	0.18	0.007	0.085
Sample II (mixture of 22% of toluene and 78% of toluene-4-*d*)						
II-3	834.3	7.86	1.2×10^{-2}	—	—	0.053*
II-1	876.5	5.42	7.8×10^{-2}	0.15	0.005	0.074
II-4	907.3	5.60	1.9×10^{-1}	—	—	0.098*
II-2	955.6	3.90	1.1	0.19	0.004	0.079

* In these cases, sensitivity of mass spectrometer was low and unstable particularly for hydrogen.

13) API Mass Spectral Data. No. 452.

14) F. L. Mohler, V. H. Dibeler and E. Quinn, *J. Research Natl. Bur. Standards*, 61, 171 (1958).

TABLE VI. MASS SPECTRA OF UNPYROLYZED AND PYROLYZED TOLUENES

Sample No.	Reaction temp. °C	m/e 72	78	Δ 78*	79	Δ 79*	80	84	93	94
Sample I	(before pyrolysis)	0.09	1.30	—	0.16	—	0.00	0.35	69.1	100
I-4	830.0	0.08	1.42	0.12	0.21	0.05	0.00	0.35	68.2	〃
I-3	832.0	0.10	1.39	0.09	0.25	0.09	0.00	0.35	70.2	〃
I-1	876.6	0.09	1.43	0.17	0.33	0.17	0.05	0.31	71.6	〃
I-5	902.6	0.08	1.66	0.36	0.72	0.56	0.11	0.31	69.3	〃
I-2	908.1	0.09	1.48	0.18	0.56	0.40	0.08	0.34	71.1	〃
Sample II	(before pyrolysis)	0.09	11.30	—	0.17	—	0.00	0.35	70.4	〃
II-3	834.3	0.09	1.47	0.17	0.25	0.08	0.00	0.35	69.4	〃
II-4	907.3	0.09	1.52	0.22	0.93	0.76	0.16	0.36	68.8	〃

* Δ means increment of relative abundance by pyrolysis.

with the increase of velocity constant in the same reaction temperature range (cf. Table V).

These experimental results are summarized as follows:

1) Toluene-3-*d* and -4-*d* (isotopic purity: 78%) gave H_2, HD, a trace of D_2, CH_4 and CH_3D by pyrolysis, and their mole ratios were determined by mass spectrometric analysis.

2) There was not any distinct difference in the mole ratios of HD/H_2 and CH_3D/CH_4 in the reaction of either toluene-3-*d* or -4-*d*, and it may be concluded that the reactivities of *m*- and *p*-hydrogen of toluene are of the same order.

3) As the pyrolyzed toluene gave a nearly similar infrared spectra as those of unpyrolyzed one, exchange reaction of hydrogen between toluenes did not occur to an appreciable extent in the temperature range 830~900°C.

The following reaction mechanism may be presented to explain the formation of HD and CH_3D.

In the above schemes, statistical weight shows numbers of reacting hydrogens in each set of elementary processes. The production of HD may be explained by one or more of reactions 5'—7, and that of CH_3D by 10 and/or 13. If it is assumed that eight hydrogens of toluene

			Statistical weight on the assumption of equal reactivity		
	(toluene-3-*d* or -4-*d* containing 22% toluene)				
$C_6H_4D\text{-}CH_3$	⟶	$C_6H_4D\text{-}CH_2\cdot + H\cdot$ ·····	(1)	3	Initiation
〃 〃	⟶	$\cdot C_6H_3D\text{-}CH_3 + H\cdot$ ·····	(2)	4	
〃 〃	⟶	$\cdot C_6H_4\text{-}CH_3 + H\cdot$ ·····	(2')	1	
〃 〃	⟶	$\cdot C_6H_4D + CH_3\cdot$ ·····	(3)		
$H\cdot + C_6H_4D\text{-}CH_3$	⟶	$C_6H_4D\text{-}CH_2\cdot + H_2$ ·····	(4)	3	Abstraction by H atom
〃 〃	⟶	$\cdot C_6H_3D\text{-}CH_3 + H_2$ ·····	(5)	4	
〃 〃	⟶	$\cdot C_6H_4\text{-}CH_3 + HD$ ·····	(5')	1	
$D\cdot + C_6H_4D\text{-}CH_3$	⟶	$C_6H_4D\text{-}CH_2\cdot + HD$ ·····	(6)	3	Abstraction by D atom
〃 〃	⟶	$\cdot C_6H_3D\text{-}CH_3 + HD$ ·····	(7)	4	
〃 〃	⟶	$\cdot C_6H_4\text{-}CH_3 + D_2$ ·····	(7')	1	
$H\cdot + C_6H_4D\text{-}CH_3$	⟶	$\cdot C_6H_4D + CH_4$ ·····	(8)		Metathesis by H atom
〃 〃	⟶	$C_6H_5D + CH_3\cdot$ ·····	(9)		
$D\cdot + C_6H_4D\text{-}CH_3$	⟶	$\cdot C_6H_4D + CH_3D$ ·····	(10)		Metathesis by D atom
〃 〃	⟶	$C_6H_4D_2 + CH_3\cdot$ ·····	(11)		
$CH_3\cdot + C_6H_4D\text{-}CH_3$	⟶	$C_6H_4D\text{-}CH_2\cdot + CH_4$ ·····	(12)	3	Abstraction by CH_3 radical
〃 〃	⟶	$\cdot C_6H_3D\text{-}CH_3 + CH_4$ ·····	(13)	4	
〃 〃	⟶	$\cdot C_6H_4\text{-}CH_3 + CH_3D$ ·····	(13')	1	
$2\cdot C_6H_3D\text{-}CH_3$ (or $\cdot C_6H_4\text{-}CH_3$)	⟶	Deuterated and undeuterated dimethylbiphenyls ·····	(14)		Termination
$C_6H_4D\text{-}CH_2\cdot$ (or $C_6H_5\text{-}CH_2\cdot$)	⟶	Deuterated and undeuterated bibenzyls ·····	(15)		

(The reactions of undeuterated toluene omitted.)

had the reactivities of the same order both in the initiations and propagations, (that is, here both isotope effect and structure effect are neglected), the expected ratio $H_2:HD:D_2$ in the pyrolysis of toluene-*d* of 100% of isotopic purity might be $7/8\times7/8+7/8\times1/8:1/8\times7/8:1/8\times1/8=1:0.29:0.02$. On the other hand, if it is assumed that HD was produced only by the abstraction of D atom from benzene ring by hydrogen atom (reaction 5′), not by reactions 6 and 7, the ratio $H_2:HD:D_2$ might be $7/8:1/8:0=1:0.14:0$ (natural abundance 0.02% of D is neglected). As the experimental results (Table V) show the ratio, $1:0.10\sim0.19:0.000\sim0.007$, it is indicated that the ratio is in the middle of the two assumed ratios, and it may be expected that HD/H_2 is augmented, if 22% of undeuterated toluene is removed from Samples I and II. Although these results do not suffice to establish the initiation reactions 2 and 2′, they may not be a negative evidence for such processes. A more direct evidence supporting the existence of process 2′ may be obtained by pyrolyzing $C_6D_5CH_3$, for $C_6D_5CH_3$ would give D_2 by the successive reactions 2′, 6 and 7 in a high yield.

The ratio $CH_3D:CH_4$ is relatively low compared with that of $HD:H_2$ in the whole reaction temperature range. The possible processes to produce CH_3D may be 10 and/or 13′, and if it is assumed that processes 2 and 2′ gave H and D atoms in the ratio 7:1, and that processes 12—13′ proceeded with statistical weights (3:4:1), the ratio of CH_3D to CH_4 obtained by reactions 8 and 10 might be 1/7, and the ratio of CH_3D to CH_4 obtained by reactions 12—13′ might be also 1/7. On the other hand, if it is assumed that D atom was not produced by the initiation reaction 2′, CH_3D might be produced only by reaction 13. In this case, the ratio $CH_3D:CH_4$ depends on the relative velocity rate of reactions 8 and 9. If it is assumed that the relative rate ratio is $\alpha:1$, the ratio CH_3D/CH_4 should be $1/(7+8\alpha)$, and less than 1/7.

These experimental results are rather unexpected, considering the generally accepted fact that $D(C_6H_5\text{–}H)$ is larger than $D(C_6H_5CH_2\text{–}H)$. Dr. Kobayashi[15] suggested that the benzyl radical would rearrange to cycloheptatrienyl radical, considering the mass spectrometric evidence of the rearrangement of benzyl cation to cycloheptatrienium cation[16]. If such a rearrangement took place, transfer of deuterium atom in the aromatic ring would be observed. Unfortunately the amount of aromatic products produced by pyrolysis was not sufficient to be analyzed. On the other hand, it has been known that CH_3 radical abstracts hydrogen from the benzene ring[17,18], and this fact may explain the production of CH_3D. As may be described in the succeeding paper, pyrolysis of benzene proceeds in the relatively low temperature range, and its apparent activation energy is unexpectedly low. Although the reaction mechanism of pyrolysis of benzene is not yet completely established, it may be compatible with the present results.

15) M. Kobayashi, private communication.

Summary

In order to elucidate the mechanism of the pyrolysis of toluene, pyrolysis of toluene-3-*d* and -4-*d* was carried out by the flow method in the temperature range 830～955°C, and the mole ratios $D_2:HD:H_2$ and $CH_3D:CH_4$ were determined by mass spectrometry. The involvement of the reaction of ring-hydrogen in the pyrolysis has been confirmed from the formation of HD and CH_3D. As there was not any distinct difference in the mole ratios between the reactions of toluene-3-*d* nor -4-*d*, it is concluded that the reactivities of *m*- and *p*-hydrogens of toluene are of the same order. Considering these results, the possible elementary processes involving ring-hydrogen are discussed.

The author wishes to express his hearty thanks to Professor Y. Urushibara and Professor O. Simamura for their kind guidance and encouragement for the present work. The author is grateful to Professor S. Araki for kind advice in mass spectrometry, to Dr. M. Kawano for measurements of infrared spectra, to Dr. M. Kobayashi for stimulating discussions and also to Mr. A. Suzuki for experimental help.

Department pf Chemistry
College of General Education
The University of Tokyo
Meguro-ku, Tokyo

16) P. N. Rylander, S. Meyerson and H. M. Grubb, *J. Am. Chem. Soc.*, **79**, 842 (1957).
17) A. F. Trotman-Dickenson and E. W. R. Steacie, *J. Chem. Phys.*, **19**, 329 (1951).
18) S. H. Wilen and E. L. Eliel, *J. Am. Chem. Soc.*, **80**, 3309 (1958).

Studies on Dehydroalanine Derivatives. II. Synthesis of Polydehydroalanine

By Shumpei SAKAKIBARA

(Received November 30, 1959)

In the preceding paper of this series[1] the synthesis and properties of *N*-carboxy dehydroalanine anhydride (I) were described. The present investigation was designed to synthesize polydehydroalanine using the anhydride I as starting material, and to obtain some information concerning the structure of the polypeptide.

Synthesis of Polydehydroalanine. — It was previously observed, that the carbamic acid II, which formed from the *N*-carboxy anhydride I, after hydrolysis or aminolysis was unusually stable as compared with those derived from ordinary amino acids[1]. Therefore, it was expected that the rate of polymerization of the *N*-carboxy anhydride I would be much slower than that of usual *N*-carboxy anhydrides at ordinary temperature. In order to ascertain this expectation, the rate of polymerization of *N*-carboxy dehydroalanine anhydride (I) was compared with that of *N*-carboxy DL-alanine anhydride at 30°C using cyclohexylamine as initiator. As can be seen from Fig. 1, the time-conversion curve of the polymerization of the *N*-carboxy anhydride I reached the 25% line only after 5 hours, and then very slowly approached the 35% line, while the *N*-carboxy DL-alanine anhydride polymerized very quickly, and the curve arrived at the 90% line within half an hour. It was concluded from these findings that the polymerization reaction of the *N*-carboxy anhydride I should be carried out at sufficiently high temperatures to permit a more rapid rate of the decarboxylation reaction, and that tertiary amines should be used as initiators. The tertiary amine used, would overcome the inclination for low conversion of the polymerization reaction which may be induced by the formation of ureide III as the termination reaction. A rapid rate of the polymerization reaction also seemed to be desirable in order to suppress a vinyl-type polymerization.

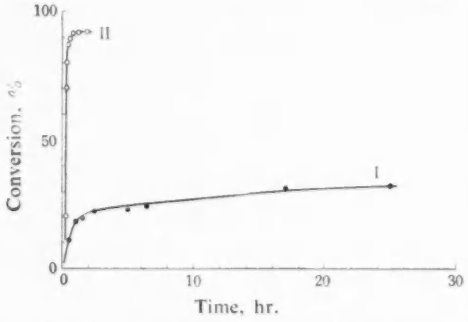

Fig. 1. Polymerization rates of *N*-carboxy anhydrides at 30±0.1°C in dioxane containing cyclohexylamine (10 mol. % against the *N*-carboxy anhydrides): I. *N*-Carboxy dehydroalanine anhydride; II. *N*-Carboxy DL-alanine anhydride.

In the present experiment, polydehydroalanine was prepared by heating a dry pyridine solution of the substance I, at 100°C, or by adding a small amount of triethylamine into a boiling dry toluene solution of the substance I. In the case of the former, the reacting solution gradually became dark-brown as the polymerization reaction proceeded and brown precipitates (IVa) formed. Evolution of carbon dioxide almost ceased after about 2 hr. In the case of the latter, the starting, slight-yellow, clear solutidn suddenly turned into brown, when a small amount of triethylamine was added into

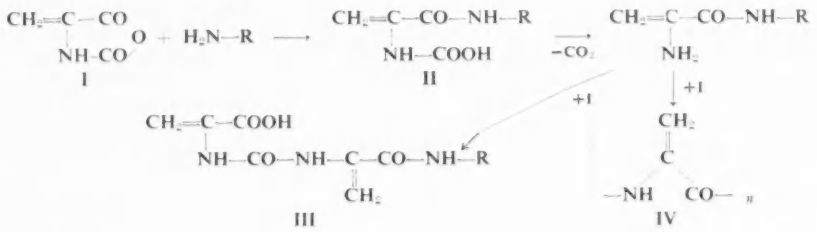

1) S. Sakakibara, This Bulletin, 32, 13 (1959).

the solution. At the same time a vigorous evolution of carbon dioxide was observed and brown precipitates gradually formed. This precipitates were partially insoluble in water, and the water soluble part was collected as polydehydroalanine (IVb).

Properties of the Polydehydroalanine. — The freshly formed brown product IV (IVa or IVb) was completely soluble in water, formic acid and dichloroacetic acid, slowly dissolved in dimethylformamide and *m*-cresol, but after complete drying it became partially insoluble in these solvents. Furthermore, about 80% of the substance IV was converted into a water-insoluble form, when preserved under ordinary conditions for about six months. Such a solubility behavior of the substance IV was similar to that of poly-DL-alanine[2,3]. It was, however, found that 34% of the aged substance IV, was completely insoluble even in formic acid, in which the aged poly-DL-alanine is readily soluble[3]. This fact seems to indicate that the substance undergoes not only α-β-configuration change of the polypeptide-bonds, but also the intermolecular cross-linkage formation due to its double bonds. After reprecipitation from water-ethanol, the polypeptide IV was still brown in color, and its ultraviolet absorption spectrum (Fig. 2) suggested the presence of some kinds of conjugated double bonds. When the polypeptide was hydrogenated as described in a later part of this paper, this absorption bands at 230~350 mμ corresponding to the conjugated double bonds vanished and the brown color extremely reduced at the same time.

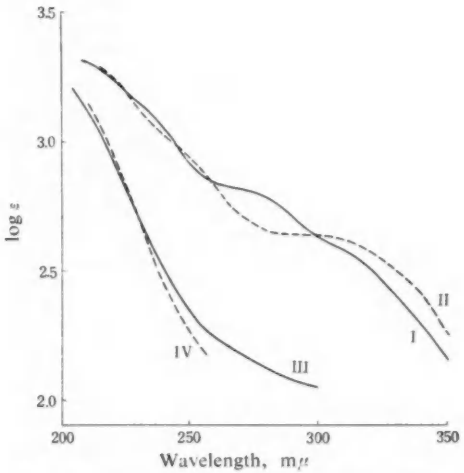

Fig. 2. Ultraviolet absorption spectra recorded on a Beckman DK-2 spectrophotometer: I. Polydehydroalanine (PDA) dissolved in distilled water; II. PDA dissolved in aq. 1 N NaOH solution; III. Hydrogenated PDA dissolved in water; IV. Poly-DL-alanine dissolved in water.

The determination of the molecular weight of the polymer was very difficult. The end-amino group of the polypeptide should not be expected to be present in this material, because of the instability of the *N*-terminal dehydroalanyl group[1]. Therefore, amino-nitrogen determination for calculating the mean molecular weight of the polymer is not significant. When this polymer was titrated with sodium methoxide for determining the end-carboxylic acid, equivalent weights of 330 and 435 were obtained, which corresponded to about 4.7 and 6.2 monomer residues, and these values were much smaller than those calculated hereafter from the expected molecular weight of the polymer. This fact suggested the following two possibilities: (1) Enolization of peptide bonds, which has been mentioned previously by Bergmann, et al. in the cases of dehydroalanyl peptides or diketopiperazines[4]. (2) Partial hydrolysis of pyrolidone rings (VI) which may be formed spontaneously from the dehydroalanyl residues as described in a later part of this paper. The delicate difference between the ultraviolet absorption spectrum of the polymer in 1 N sodium hydroxide solution and that in distilled water would also suggest the fact of enolization. Viscosities of 0.5% dichloroacetic acid solutions of these polymers, IVa and IVb, were determined at 25±0.01°C, and $\eta_{sp}/C = 1.8$ and 0.9 (C expressed in base mol./l.) were obtained, respectively. If an assumption is permitted, that this polymer behaves quite similarly to poly-DL-alanine in dichloroacetic acid, the molecular weight of the polymer may be determined by comparison of the viscosity number with that of known poly-DL-alanine under the same conditions[5]. From the above consideration, about 7000~5000 and 4000~2000 were calculated for their molecular weights, respectively.

Hydrogenation and Hydrolysis of Polydehydroalanine for Elucidation of the Actual Structure. —Elucidation of the structure of the polymer was very difficult because double bonds involved in the molecule are expected to be reactive and they may interact with one another within the molecule. If the structure of the polymer is exactly identical with the structural formula

2) C. H. Bamford, A. Elliott and W. E. Hanby, "Synthetic Polypeptide", Academic Press, New York (1956), p. 312.
3) A. Elliott, *Nature*, **170**, 1066 (1952).
4) M. Bergmann and A. Miekeley, *Ann.*, **458**, 40 (1927).
5) C. H. Bamford, A. Elliott and W. E. Hanby, "Synthetic Polypeptide", Academic Press, New York (1956), pp. 299, 314.

IV, poly-DL-alanine should be derived as a result of hydrogenation of the polymer. An attempt of catalytic hydrogenation of the polymer IV under the presence of palladium-charcoal was unsuccessful, since the polymer was adsorbed on the catalyst and separation of the catalyst from the product was very difficult. Recently, Izumi[6] has published an excellent catalyst, which was prepared by reduction of palladium chloride co-ordinated with silk-fibroin. When this catalyst was used, the hydrogenation reaction of the polymer IV, proceeded successfully, and the starting brown solution of the polymer IV turned into a slight-yellow one, after the reaction was finished. Since the palladium atoms have previously adsorbed between peptide layers of silk-protein, no more polypeptide was adsorbed on the catalyst during the reaction. From the hydrochloric acid hydrolyzate of the product V, alanine was detected in a yield of about 5% of the theoretical by the Dowex 50 column chromatography under the condtions of Moore and Stein[7] (Fig. 3).

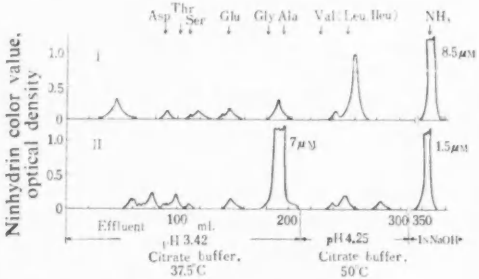

Fig. 3. Chromatographic analysis of ninhydrin-positive materials of the HCl-hydrolyzates: I. Polydehydroalanine (10 mg.); II. Catalytic hydrogenated polydehydroalanine (10 mg.). Arrows indicate the position of the peaks of standard amino acids.

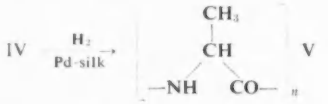

The ultraviolet absorption spectrum of the hydrogenated product V (Fig. 2) was similar to that of the poly-DL-alanine and the absorption bands corresponding to the conjugated double bonds at 250~350 mμ disappeared after hydrogenation as described previously. The infrared spectrum of the hydrogenated product V (Fig. 4), however, was neither quite different from that of the starting polymer, nor similar to that of poly-DL-alanine. This infrared spectrum resembled rather that of poly-α-amino acrylic acid[8]. Since the actual structure of the poly-α-amino acrylic acid is considered to be polypyrolidone[9], a greater part of the polymer would be composed of such a polypyrolidone-type structure VI, which might form spontaneously from the polydehydroalanine by interaction of the neighboring double bonds. The infrared absorption bands at 1700~1760 cm^{-1} (Fig. 4) supported also the presence of five membered cyclic amide. If the structure of the polydehydroalanine corresponds to the formula IV exactly, its hydrochloric acid hydrolyzate must all be pyruvic acid and ammonia. However,

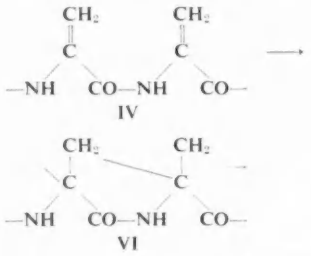

many kinds of ninhydrin-positive materials, the total yield of which was about 10% of the ideal formula IV, were detected by ion-exchanger column chromatography from the hydrochloric acid hydrolyzate (Fig. 3). Ammonia, which formed in this case was also directly ascertained[10] and amounted to 9.5% of the theoretical. These facts all supported the formation of the non-hydrolyzable material which was considered to be such a polypyrolidone. Actually, the hydrochloric acid hydrolyzate of the polymer IV became dark brown, and this fact indicated a formation of huminic material during the course of the reaction. From the result of the experiments and the above considerations, it may be appropriate to consider that the obtained polymer IV, consists of about 90% of polypyrolidone-type polypeptide and about 10% of dehydroalanyl residues. In other words, the synthesis of polydehydroalanine, which was exactly expressed as the structural formula IV, was unsuccessful in the present experiment. If the preparation of co-polymer of dehydroalanine and another stable amino acid is possible, the interaction of the neighboring double bonds would decrease more

6) Y. Izumi, This Bulletin, **32**, 932 926, 942 (1959).

7) S. Moore and W. H. Stein, *J. Biol. Chem.*, **192**, 663 (1951).

8) This material was prepared from a vinyl-type polymer of the substance I or from that of α-phthalimido acrylc acid as will be described in a later communication of the series.

9) cf. M. Vrancken and G. Smets, *J. Polymer Sci.*, **14**, 521 (1954).

10) J. E. Varner, et al., *Anal. Chem.*, **25**, 1528 (1953).

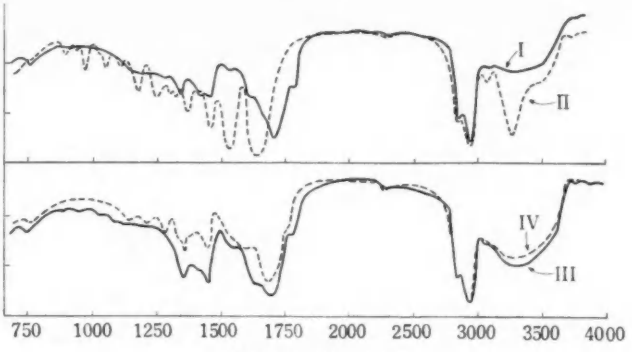

Fig. 4. Infrared absorption spectra recorded on an Adam-Hilger H-80 infrared spectrophotometer: I. Polydehydroalanine; II. Poly-DL-alanine; III. Hydrogenated polydehydroalanine; IV. Poly-α-amino acrylic acid. Nujol suspension.

distinctly. A communication on the reactivity of the dehydroalanyl groups involved in the present polymer will be published in the near future.

Experimental

Materials.—*N*-Carboxy dehydroalanine anhydride (I) and *N*-carboxy DL-alanine anhydride were prepared according to the description in the previous paper[1].

Determination of the Polymerization Rate of I.—The substance I (350 mg.) was dissolved in freshly distilled dry dioxane (15.00 ml.) containing cyclohexylamine (30.4 mg.). The solution was divided into 14 test tubes so that each tube contains 1.00 ml. of the solution, and the tubes were sealed. Then, they were allowed to react in a bath at 30±0.1°C, simultaneously. Each of the portions was opened successively at times and dry nitrogen was introduced for about one min. into the solution, which was then titrated with a methanol-benzene solution of sodium methoxide, using thymol blue as an indicator according to the description of Berger, et al.[11] (Fig. 1). The sodium methoxide solution (ca. 0.3 N) was standardized every 5 hr. with purified benzoic acid. *N*-Carboxy DL-alanine anhydride was subjected to the reaction under the same condition described above (Fig. 1).

Polymerization of I in Pyridine (Preparation of Polydehydroalanine IVa).—A solution of I (5 g.) in purified dry pyridine (15 ml.) was heated in a boiling water bath for about 2 hr. After cooling to room temperature, the reddish brown reaction mixture was poured into ethyl acetate (100 ml.). The precipitated brown material was centrifuged, washed thoroughly with ethyl acetate and ether, and dried. The brown powder obtained (3.05 g.) was reprecipitated from water-ethanol and dried under reduced pressure at room temperature. The yield was 2.4 g. (64%).

Found: C, 43.8; H, 5.76; N, 15.5; volatile part at 135°C, 17.9. Calcd. for $(C_3H_3ON+14/18\cdot H_2O+1/20\cdot C_2H_6O$ (ethanol)$)_n$: C, 43.7; H, 5.71; N, 16.5; volatile part, 18.8%.

Found*: C, 49.50; H, 4.24; N, 18.86; ash, 1.2%; Na-equiv. wt.[12], 330. Calcd. for $(C_3H_3ON)_n$: C, 52.17; H, 4.35; N, 20.3%.

This material was hard to burn up for analysis.

Polymerization of I in Toluene (IVb).—Few drops of triethylamine were added into a boiling toluene solution of I (1 g./20 ml.). The starting clear solution, which was light-yellow, suddenly turned into brown as the reaction occurred and reddish brown precipitates formed immediately under the vigorous evolution of carbon dioxide. After about 30 min., the reaction mixture was cooled and the formed precipitates were filtered off, washed three times with ethyl acetate and dried. The yield was 0.62 g. This material was extracted with sufficient amount of water. The water extract was concentrated to about 5 ml. and brown powder (0.19 g.) (IVb) was reprecipitated with ethanol. The water insoluble part of the material was about 0.18 g. Na-equiv. wt. of the material IVb was 435.

Hydrogenation of IVa.—The substance IVa (300 mg.) was dissolved in water (50 ml.) and hydrogenated in an autoclave under 100 atm. of hydrogen at 50~60°C for about 8 hr. using palladium-silk catalyst (200 mg.). After the reaction was complete, the catalyst was filtered off and the filtrate was concentrated to about 10 ml. Ethanol (100 ml.) was added into the concentrate and about 160 mg. of light-yellow powder was precipitated. This material was reprecipitated from water-ethanol and dried under reduced pressure at 118°C.

Found: C, 47.67; H, 5.13; N, 16.68. Calcd. for $(9/10\cdot C_3H_3ON+1/10\cdot C_3H_5ON+2/5\cdot H_2O)_n$: C, 47.1; H, 5.36; N, 18.3%.

11) A. Berger, M. Sela and E. Katchalski, *Anal. Chem.*, 25, 1554 (1953).

12) M. Sela and A. Berger, *J. Am. Chem. Soc.*, 77, 1893 (1955).

*) This material was dried over phosphorus pentoxide under reduced pressure at 135°C, in which procedure a certain extent of decomposition might occur, such as liberation of formaldehyde or ammonia.

The hydrogenated material (10 mg.) was hydrolyzed with 6 N hydrochloric acid for about 20 hr. and the hydrolyzate was concentrated to dryness. The residue was then subjected to column chromatography under the Stein-Moore's condition (Fig. 3). The fraction corresponding to alanine was collected, treated with 2,4-dinitrofluorobenzene and purified by celite column chromatography using ether-phosphate buffer (0.25 M, pH 6.5) as a developer. Infrared spectrum of the purified main fraction was agreed with that of authentic DNP-alanine.

Summary

The polymerization rate of *N*-carboxy dehydroalanine anhydride (I) was compared with that of *N*-carboxy DL-alanine anhydride, and it was found, that the former was much slower than the latter at 30°C. Polydehydroalanine (IV) was obtained by heating the substance I in dry pyridine at 100°C, or by adding a small amount of triethylamine into the boiling toluene solution of I. The substance IV was water-soluble brown powder, the actual structure of which was supposed to be a pyrolidone-type polypeptide VI containing about 10% of dehydroalanyl residues.

The author wishes to express his thanks to Professor Shiro Akabori and Professor Shunsuke Murahashi for their guidance and encouragement throughout the course of this study.

Institute for Protein Research
Osaka University
Nishi-ku, Osaka

Systematic Separation of Fission Products by Solvent Extraction Method

By Toshiyasu KIBA, Shigeru OHASHI and Toyoo MAEDA

(Received October 27, 1959)

Solvent extraction methods have often been employed for the separation of individual fission products. The purpose of the present investigation was to establish a new scheme of systematic separation of fission products having relatively long half-lives by combining and modifying the solvent extraction methods developed previously. The fission products considered in this investigation were limited to the nuclides, the radioactivities of which are higher than one per cent after all the fission products have been aged for one year. The nuclides which fall in this category are zirconium-niobium-95, cerium-praseodymium-144, promethium-147, strontium-yttrium-90, ruthenium-rhodium-106, cesium-137-barium-137^m, strontium-89, and yttrium-91. Since the chemical behaviors of strontium-89 and yttrium-91 are just the same as those of strontium-90 and yttrium-90, respectively, these were excluded from the scope of the present investigation. All of the other nuclides except promethium-147 are composed of the pairs of parent and daughter. Among these pairs, praseodymium-144, rhodium-106, and barium-137^m are relatively short-lived daughters. Therefore, the nuclides considered finally for this study were zirconium-niobium-95, cerium-144, promethium-147, strontium-yttrium-90, ruthenium-106, and cesium-137.

Marinsky, Hume and Ballow[1] reported that zirconium-95 and niobium-95 can be extracted from a hydrochloric acid solution into chloroform with cupferron. Kiba and Kanetani[2] found that rare earth nuclides, cerium-144, promethium-147, and yttrium-90 can be separated from an acetate solution of pH 4 to 5 into chloroform with cupferron. Kiba and Mizukami[3] investigated the separation of strontium-90 and yttrium-90 and found that strontium-90 can be extracted from an acetate solution of pH 8 with TTA dissolved in hexone. Kiba and Hirono[4] reported that ruthenium-106 can be extracted from hydrochloric acid solution into a mixture of TBP and kerosene with diphenyl thiourea. Combining and modifying the methods mentioned above the present authors have presented a new systematic method for the separation of fission products by the liquid-liquid extraction processes.

Experimental

All of the radioactive nuclides were purchased from the Oak Ridge National Laboratory of the

1) J. A. Marinsky, D. N. Hume and N. E. Ballow, "Radiochemical Studies; The Fission Products", National Nuclear Energy Series IV-9, (1951), p. 1514.
2) T. Kiba and M. Kanetani, This Bulletin, 31, 1013 (1958).
3) T. Kiba and S. Mizukami, ibid., 31, 1007 (1958).
4) T. Kiba and H. Hirono, presented at the 11th Annual Meeting of the Chemical Society of Japan, Tokyo, April 5, 1958.

United States of America. Stock solutions of these unclides were made as follows. The original solution of zirconium-niobium-95 in 0.03 M oxalic acid was diluted with 0.33 M oxalic acid. The original solution of cerium-144 as cerous nitrate in nitric acid, that of promethium-147 in hydrochloric acid, that of strontium-yttrium-90 in nitric acid, that of ruthenium-106 as nitrosyl ruthenium trinitrate in 8 M nitric acid, and that of cesium-137 in 1 M nitric acid were diluted with 3.75 M hydrochloric acid, respectively. About 0.05 to 0.1 μc of the carrier-free nuclides was used for each experiment.

TBP was purified by distillation. All other chemicals of the guaranteed or the first grade of Japan Industrial Standards were used without further purification. An electric shaker was used for shaking of separatory funnels. Whole or aliquots of both aqueous and organic phases were taken into small porcelain dishes after five to ten minute shaking for each extraction. The content of each dish was evaporated or ignited, and the beta activity was measured with an end-window type GM counter.

Results and Discussion

The whole scheme of the systematic separation is demonstrated in Table I. The method is composed of four-step extractions. The first

TABLE I. SCHEME OF SYSTEMATIC SEPARATION

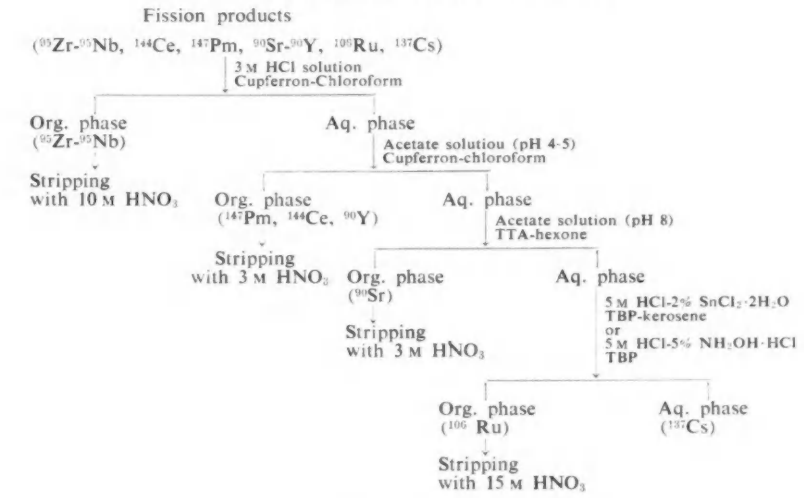

TABLE II. DETAILS OF EXTRACTION CONDITIONS

Extraction step	Composition of aqueous phase		Organic phase	
1	Sample solution	0.5 ml.		
	3.75 M HCl—0.043 M $H_2C_2O_4$	3.5 ml.	Chloroform	5 ml.
	20% NH_2OH·HCl	0.5 ml.		
	5% Cupferron	0.5 ml.		
2	Aqueous solution after the first step extraction	5 ml.		
	9 M NH_3	1.6 ml.	Chloroform	5 ml.
	0.9 M NH_4AcO	10.4 ml.		
	5% Cupferron	3 ml.		
	5% Cupferron	3 ml.	Chloroform	5 ml.
	5% Cupferron	3 ml.	Chloroform	5 ml.
3	Aqueous solution after the second step extraction	27 ml.	0.05 M TTA in hexone	10 ml.
	5.4 M NH_3	1 ml.		
4A	Aqueous solution after the third step extraction	27 ml.	TBP-kerosene (1 : 2)	10 ml.
	11 M HCl—4.4% $SnCl_2·2H_2O$	23 ml.		
4B	Aqueous solution after the third step extraction	27 ml.	TBP	50 ml.
	11 M HCl—11% NH_2OH·HCl	23 ml.		

TABLE III. EXTRACTION OF FISSION PRODUCTS

Step	Phase	^{95}Zr—^{95}Nb	^{144}Ce	^{147}Pm	^{90}Sr—^{90}Y	^{106}Ru	^{137}Cs
1	Org. phase	98.9	0.3	0.0	0.0	0.0	0.4
	Aq. phase	0.3	99.3	98.2	99.5	99.8	98.1
2	Org. phase	84.2[a]	99.4	99.6	53.2(^{90}Y)	0.5	0.6
	Aq. phase	2.0[a]	0.5	0.5	46.2(^{90}Sr)	99.6	101.6
3	Org. phase	60.7	100.0	99.6	99.4	1.2	0.4
	Aq. phase	37.8	0.0	0.6	0.5	99.6	99.6
4A	Org. phase	9.3[b]	1.0[b]	14.8[b]	0.8[b]	98.5[b]	0.0[b]
	Aq. phase	90.7	99.0	85.2	99.2	1.5	100.0
4B	Org. phase	27.6[b]	8.8[b]	13.3[b]	0.0[b]	93.9[b]	0.6[c]
	Aq. phase	72.4	91.2	86.7	100.0	6.1	82.2

a. Some of ^{95}Zr and/or ^{95}Nb was lost probably by the adsorption.
b. These values were calculated from the total activities and the activities in the aqueous phase.
c. This value was obtained by the stripping of ^{137}Cs from the organic phase with 15 M nitric acid. The loss of ^{137}Cs in the 4B step was unaccountable.

step is the extraction of zirconium-95 and niobium-95 from a 3 M hydrochloric acid solution into chloroform with cupferron. The second step is the extraction of rare earth nuclides, i. e. cerium-144, promethium-147, and yttrium-90 from an acetate buffer solution of pH 4 to 5 into chloroform with cupferron. The third step is the extraction of strontium-90 from an acetate buffer solution of pH 8 into hexone with TTA. The fourth step is the extraction of ruthenium-106 from a 5 M hydrochloric acid solution into a mixture of TBP and kerosene (1 : 2) in the presence of stannous chloride. Another method for the fourth step is the extraction of ruthenium-106 from a 5 M hydrochloric acid solution into TBP in the presence of hydroxylamine. Thus cesium-137 remains is the last aqueous solution. The detailes of the extraction procedures are tabulated in Table II. The distribution of each radioactive nuclide in the aqueous and organic phases in each extraction step was determined. The results are summarized in Table III, in which the data shown under the step-like line in each column were obtained only for reference. Recovery on the stripping of the radioactive nuclides from the organic phase is shown in Table IV. The data given in Tables III and IV are mean values obtained from three or four experiments.

TABLE IV. RECOVERY OF NUCLIDES FROM ORGANIC PHASE BY STRIPPING

Nuclide	Stripping agent	Number of stripping	Recovery %
^{95}Zr—^{95}Nb	10 M HNO_3	2	83.9
^{144}Ce	3 M HNO_3	1	98.4
^{147}Pm	3 M HNO_3	1	88.8
^{90}Y	3 M HNO_3	1	98.8
^{90}Sr	3 M HNO_3	1	98.4
^{106}Ru	15 M HNO_3	3	99.8

In the first step oxalic acid is added to the solution to prevent the adsorption of zirconium-95 and niobium-95 onto a glass vessel by forming complexes with these nuclides. Hydroxylamine protects cupferron from oxidation with air and a trace amount of nitric acid. The data disclose that by the first step extraction only zirconium-95 and niobium-95 are extracted as cupferrates into the organic phase and all other nuclides are left in the aqueous phase. The zirconium-95 and niobium-95 extracted in the organic phase can be stripped with 10 M nitric acid as shown in Table IV.

In the second step aqueous ammonia is added to the aqueous phase remaining after the first step extraction to neutralize hydrochloric acid, and then ammonium acetate solution is added to adjust the pH of the aqueous phase to 4～5. In order to complete the separation of rare earth nuclides the concentration of cupferron should be considerably high and the extraction should be repeated three times. Before each extraction with chloroform 3 ml. of a 5% cupferron solution is added to the aqueous phase. By this step cerium-144 and promethium-147 are extracted into the chloroform phase.

Strontium-90 and yttrium-90 in their radioactive equilibrium are separated from each other, the former being in the aqueous phase and the latter in the organic phase, as shown in the sixth column of Table III. The decay or the growth curve and the Harley plot of the activity in each phase indicates that the separation of the nuclides can be carried out completely. The rare earth and yttrium nuclides extracted in the organic phase can easily be stripped with 3 M nitric acid.

After the second step extraction, a small amount of aqueous ammonia is added to the resulting aqueous phase to raise the pH of the

solution up to 8[3]. Then the third step extraction is carried out with a 0.05 M TTA-hexone solution. Two extractions complete the separation of strontium-90. The data in the sixth column of Table III shows that yttrium-90, if it could be present, by the later decay of strontium-90 is also extracted into the organic phase. The strontium-90 extracted in the organic phase can be stripped with 3 M nitric acid.

The fourth step extraction is that of ruthenium-106. It was found in the previous investigation[4] that ruthenium-106 can be extracted from 6 M hydrochloric acid solution with diphenyl thiourea dissolved in a mixed solvent of TBP and kerosene (1 : 2) in the presence of stannous chloride. However, it is difficult to strip the ruthenium-106 extracted in the mixed solvent into an aqueous phase. The present authors reexamined the extraction condition for ruthenium-106 and found that ruthenium-106 can be almost completely extracted, in the presence of stannous chloride from 6M hydrochloric acid solution with the mixed solvent of TBP and kerosene containing no chelating agent such as diphenylthiourea. Almost all of the ruthenium-106 extracted in the organic phase can be stripped with concentrated nitric acid, but a part of stannous chloride which is extracted from into the organic phase is also stripped with concentrated nitric acid. It is difficult to remove the stannous chloride from the nitric acid solution as well as to obtain the salt-free aqueous solution of ruthenium-106. So this method would not be suitable for preparing carrier-free ruthenium-106, but the procedure might be used as an analytical method for ruthenium-106 in the fission products.

Another method for the extraction of ruthenium-106 is as follows: ruthenium-106 can be extracted from 5 M hydrochloric acid solution in the presence of hydroxylamine with TBP which is not diluted with kerosene but is saturated with a 5 M hydrochloric acid solution. By this method about 94 per cent of ruthenium-106 is extracted and almost all of it is stripped with concentrated nitric acid from the organic phase. Some amount of hydroxylamine is also extracted with TBP and then also with concentrated nitric acid. But it is possible to decompose the hydroxylamine stripped together with ruthenium-106 by heating after neutralizing the nitric acid with aqueous ammonia. Then we can get the salt-free aqueous solution of ruthenium-106. Although the yield of ruthenium-106 is less than that obtained by the former method, this method is superior to the former one from the point of view of the preparation of carrier-free ruthenium-106.

Summary

A new scheme for separating fission products, zirconium-niobium-95, cerium-144, promethium-147, yttrium-90, strontium-90, ruthenium-106 and cesium-137, by the four-step liquid-liquid extractions was presented. First, zirconium-95 and niobium-95 were extracted from a 5 M hydrochloric acid solution into chloroform with cupferron. Second, rare-earth nuclides, cerium-144, promethium-147 and yttrium-90 were extracted from an acetate buffered solution of pH 4 to 5 into chloroform with cupferron. Third, strontium-90 was extracted from an acetate buffered solution of pH 8 into hexone (methyl isobutyl ketone) with TTA (2-thenoyltrifluoroacetone). Fourth, ruthenium-106 was extracted from 5 M hydrochloric acid solution with TBP (tri-*n*-butyl phosphate)-kerosene in the presence of stannous chloride or extracted with TBP in the presence of hydroxylamine. then cesium-137 was left in the last aqueous solution. Strippings of nuclides extracted in the organic phases could be attained by shaking each organic phase with nitric acid.

This study was done as a part of the cooperative research on fission products and fissile materials which was superintended by Prof. N. Saito, the University of Tokyo. The authors wish to express many thanks to him and the Ministry of Education for financial help of this study.

Department of Chemistry
Faculty of Science
Kanazawa University
Kanazawa

Dielectric Properties of Polypeptide Solutions. Measurement of the Dielectric Properties of the α-Helix by the Low Frequency Bridge Method

By Akiyoshi WADA

(Received November 6, 1959)

The exhaustive research on the polypeptide solution by Doty, Blout and their co-workers[1] revealed the important fact that the α-helix can exist not only in the solid state but even in solution. One significant implication of their work is that the α-helix, one of the stable configurations of polypeptide molecules described by Pauling, Corey and Branson[2], can be studied in solution where each α-helix exists as a free molecule, that is, almost free from solute-interaction. These results then suggest the possibility and necessity of another type of research, the measurement of the electric dipole moment and the critical frequency of such a molecule with a highly ordered arrangement of residues.

The measurement of the electric dipole moment of the molecule has been considered a useful method of finding the charge distribution and the orientation of the polar groups in a molecule. The method has often been used to determine the molecular structure of a simple molecule in the field of physical chemistry. However, in the usual chain polymer molecule, because of the flexibility of the chain the observed electric dipole moment becomes a complicated function of the internal coordinates and the internal energy of the molecule, and this method does not appear to be as useful as in the case of the simple molecule. For the α-helix, however, if the Pauling-Corey model is given as the proper configuration and if the molecule is rigid as Doty et al. concluded[1], the resultant molecular dipole moment would be proportional to the degree of polymerization, unlike the usual chain polymer, and would have a tremendous value in a highly polymerized molecule.

As the measurement of the dipole moment, which is a vectoral value, is essentially different from investigations on non-directional values such as molecular dimension, the observation will approach the α-helix and related problems from an entirely different angle.

Description of the Low-Frequency Bridge Circuit

Though the heterodyne beat method or the resonance method has often been used for the measurement of the dielectric constant of solution, they could yield reliable data only in the high-frequency range and would not be adequate for the purpose of the present investigation. Because the solute, the α-helix, is a rigid and highly assymmetric rod-shaped molecule and the relaxation time of over-all molecular rotation in the solvent must be fairly great, the apparatus must be designed to cover the low-frequency range where sufficient time can be allowed for very slow orientation polarization. The bridge method seems to be appropriate for the present purpose and the apparatus by which the dielectric constant and loss factor can be measured from 30 cycle to 20 kilocycle was constructed as described below.

1) Low-Frequency Bridge.—The bridge method has been known as the best device for the measurement of the dielectric constant in the low-frequency range.[4] For instance, Cole and Gross[4] developed a transformer bridge, and Hippel et al. employed the Schering bridge method in their comprehensive research on dielectric materials.[5]

The Cole and Gross bridge was designed to fit the guard without the use of the Wagner ground. The measurement of capacitance was obtained by balancing the bridge by changing the capacity of the precision condenser which was set in the conjugated arm of the unknown capacitance. The conductance measurement is performed by a device called the conductance shifter.

The latter, designed by Hippel and his co-workers, has a sample holder in the arm of the precision condenser, and is generally known as a substitution method. In such an apparatus the cell constant used is calibrated by the standard substance. The conductance is given, in this apparatus, by the reading of the dissipation balancing condenser.

For the present purpose the apparatus was designed to combine the substitution method and the conductance shifter. The block diagram of the bridge circuit is shown in Fig. 1.

The low frequency oscillator which continuously

1) P. Doty, A. M. Holtzer, J. H. Bradbury and E. R. Blout, *J. Am. Chem. Soc.*, **76**, 4493 (1954); P. Doty, J. H. Bradbury and A. M. Holtzer, ibid., **78**, 947 (1956).
2) L. Pauling, R. B. Corey and H. R. Branson, *Proc. Natl. Acad. Sci.* **37**, 205 (1951).
3) C. P. Smyth "Dielectric Behavior and Structure", McGraw-Hill Book Co., Inc., New York, N. Y. (1955).
4) R. H. Cole and P. M. Gross, Jr., *Rev. Sci. Instr.* **20**, 252 (1949).
5) *Progress Rept. No. 1, Lab. Insulation Res.*, M. I. T., p. 7 (1947).

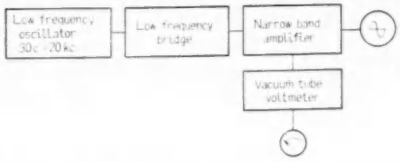

Fig. 1. Block diagram of low frequency bridge.

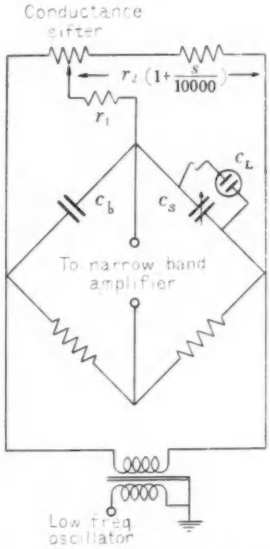

Fig. 2. Low frequency bridge circuit.

generates sine waves in the range of 30 to 20,000 cycles and output voltage from 0 to 20 volts has the same circuit as the Heathkit Model AO-1.

The circuit of the bridge section is shown in Fig. 2. C_s is the liquid cell whose capacitance is compared with that of a portion of the calibrated precision condenser. The precision condenser (Yokogawa Elect. Co. CDS-500 Variable Air Condenser), in which the use of the worm drive makes possible a scale which can be read to one part in 50,000 of full scale, has a maximum capacitance of 500 $\mu\mu$F. By using low resistance for the balancing arm the undesirable effects of stray capacitance and induction from the external field can be suppressed at the sacrifice of sensitivity. In the reading of the conductance shifter, the conductance, G, can be given as a three-digit number, s, by the following equation

$$G=\frac{(s/10000)/r_1}{1+(r_2/2r_1)\{1-(s/10000)^2\}} \tag{1}$$

when $s \ll 10000$

$$G\fallingdotseq\frac{(s/10000)/r_1}{1+r_2/2r_1} \tag{2}$$

where r_1 and r_2 are the resistances which are shown in Fig. 2. The present apparatus was designed so that r_1 can be set at four different values by the use of a rotary switch, which made the measurement of the conductance from 10^{-5} to 10^{-9} mho possible. The null detector consists of a narrow-band amplifier and vacuum tube voltmeter. The narrow-band amplifier, in which the Wien bridge and the negative feedback system are combined, has a sharp frequency response, an example of which is shown in Fig. 3, and amplifies only the given frequency, cutting out the hamper noise and harmonic frequency. The wave pattern was checked by the cathode-ray oscillograph. The null point can be obtained from the minimum reading of the vacuum tube voltmeter. The relation between the reading of the precision condenser and the vacuum tube voltmeter is plotted for different

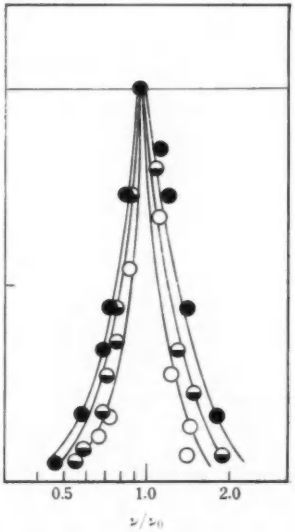

Fig. 3. Frequency response of the narrow band amplifier. Filled circle 90 cycle, half filled circle 1000 cycle, open circle 10000 cycle.

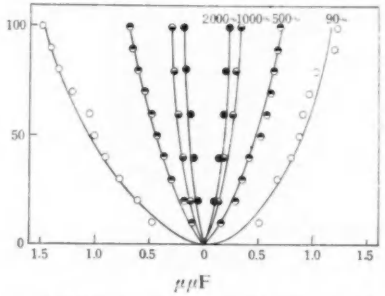

Fig. 4. Reading of vacuum tube voltmeter near null point.

TABLE I. ACCURACY IN CAPACITANCE MEASUREMENT BY BRIDGE METHOD

Frequency	100	500	1000	2000
Accuracy	±0.5	±0.2	±0.1	±0.1 $\mu\mu$F

frequencies in Fig. 4, and the accuracy of the measurement is given below.*

2) Liquid Cell.—The liquid cell consists of a concentric double cylinder of glass as shown in Fig. 5; the inside of the outer cylinder and the outside of the inner cylinder are silver gilt or spattered with gold. The latter was found to be more satisfactory in chemical and mechanical durability.

3) Calibration.—Because the substitution method was used here, the cell constant had to be determined by a pure liquid of known dielectric constant. Benzene, the dielectric constant of which has been given as 2.274 at 25°C with a probable accuracy of 0.1%, was used as a standard substance for the calibration.[6]

The dielectric constant of ethylene dichloride and dioxane measured by the calibrated liquid cell are plotted against frequency in Fig. 6. The apparent increase in the dielectric constant at low-frequency range may be due to the polarization capacitance

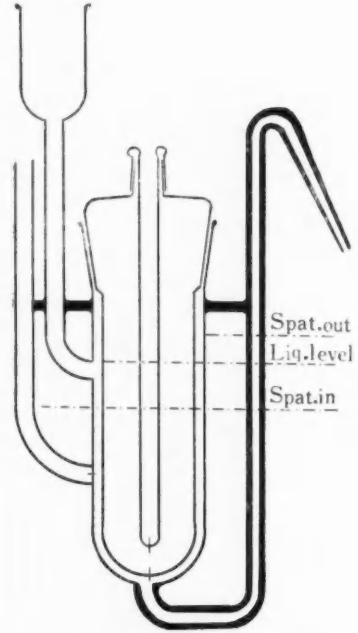

Fig. 5. Liquid cell for the measurement of dielectric constant of solution.

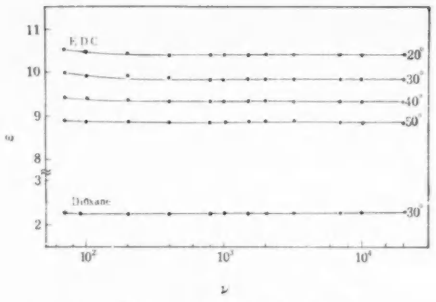

Fig. 6. Dielectric constant of ethylene dichloride and dioxane at various temperatures and frequencies.

on the electrode surface. The polarization effect increases and must be corrected for a liquid of high conductivity but it was negligible for one of small conductivity. The dielectric constants of liquids mentioned above at 1000 cycles where the polarization effect satisfactorily diminished are listed in Table II and were consistent with the values observed by other workers.

TABLE II. DIELECTRIC CONSTANT OF ETHYLENE DICHLORIDE AND DIOXANE

Ethylene dichloride

Temp., °C	ε (Wada)	ε (Smyth*)
20	10.42	10.42**
30	9.85	9.87
40	9.35	9.36**
50	8.87	8.87

Dioxane

Temp., °C	ε (Wada)	ε (Smyth***)
30	2.295	2.306**
50	2.245	2.251

* C. P. Smyth et al., *J. Am. Chem. Soc.*, **53**, 4242 (1931).
** Interpolated in Smyth's data.
*** C. P. Smyth et al., *J. Am. Chem. Soc.*, **53**, 2115 (1931).

Characterization of Poly-γ-benzyl-L-glutamate (PBLG)

1) Polymerization.—The sample used here was prepared by the Blout-Karlson method[7]. The procedure adopted consisted of polymerizing γ-benzyl-N-carboxy-L-glutamate anhydride, usually 3—5% in dioxane solution, by a sodium methoxide initiater at room temperature. After polymerization was completed the reaction mixture was poured into cold ethanol with vigorous stirring. The precipitate was redissolved in dioxane and precipitated by cold ethanol again. No difference in intrinsic viscosity was found between the reprecipitated

* The bridge was found to be stable enough that the reading of the vacuum-tube voltmeter did not fluctuate more than 3/100 full scale after a 20-min. warm-up of the apparatus.

6) A. A. Maryott and E. A. Smith, "Table of Dielectric Constant of Pure Liquids", *Natl. Bur. Standard* (*Circ.* **514** 1951); A. S. Brown et al., *J. Chem. Phys.* **19**, 1226 (1951).

7) E. R. Blout and R. H. Karlson, *J. Am. Chem. Soc.*, **78**, 941 (1956).

PBLG and that liopholyzed from the first dioxane solution.

2) Solvent. — Dimethyl formamide (DMF) was used as the solvent for the light scattering measurement because the PBLG was found to exist as a non-associated molecule in this solvent. DMF was dried by dry sodium bicarbonate and fractionally distilled at 47°C (14 mmHg). For the dielectric constant and light scattering measurement dioxane was purified according to the method of Fieser[8] and fractionally distilled after 24 hr. refluxing with sodium. For the polymerization reaction, dioxane was purified by refluxing with sodium for 24 hr. and fractionally distilled just before use. The ethylene dichloride (EDC) for the measurement of the dielectric constant was dried by P_2O_5 and fractionally distilled at 84°C.

3) Light Scattering. — The Brice Phoenix type light scattering photometer made by the Shimadzu Co. was used to obtain the molecular weight of PBLG. The apparatus was calibrated according to the Rayleigh ratio of pure benzene ($R_{90}=48.4\times10^{-6}$ at 436 mμ.[9]). The spectrophotometric calibration was independently done by Ludox solution and the result was quite consistent with the calibration by benzene. Scattering from DMF solution of PBLG was measured by the Erlenmeyer cell and the circular uniformity of which was checked with clean fluorescein by measuring the angular envelope. The cell used had good circular uniformity as the light intensity from the unit volume of the solution was constant to $\pm1\%$ from $\theta=30°$ to 135°. The angle made by the side of the Erlenmeyer cell was sufficient to exclude the effects of back reflection, so that no correction for the data was necessary. Centrifuge by a Hitachi Preparative Ultracentrifuge using a polyethylene tube with a specially constructed tefron cap, at about 60,000 *g* for 1 hr. and filtration by ultra-fine sintered glass filter were performed to make a dust-free solution and solvent respectively. Measurements were made on the solutions obtained by adding a weighed amount of 1% PBLG dust-free solution to a known volume of clean solvent in an Erlenmeyer cell, on which the scattering was already measured. The concentration after each addition was determined gravimetrically relative to the stock solution.*

The refractive index increment dn/dc for the evaluation $K=2\pi^2n_0^2(dn/dc)^2/N\lambda^4$ where n_0 is the refractive index of the solvent, λ is the wave length of the incident light in vacuo, N is the Avogadro number, was determined by the Debye-type defferential refractometer made by Shimadzu Co. The instrument was usually calibrated before each measurement with a standard KCl solution, $c=\frac{10.8691\,\text{g.}}{H_2O\,(\text{kg.})}$, for which the increment was taken as 0.0015204 on the basis of an extrapolation of data by Kruis.[10]

According to the well known equation established by Zimm,[11]

$$Kc/R_\theta=\{M_wP(\theta)\}^{-1}+2A_2c \qquad (3)$$

the weight average molecular weight M_w can

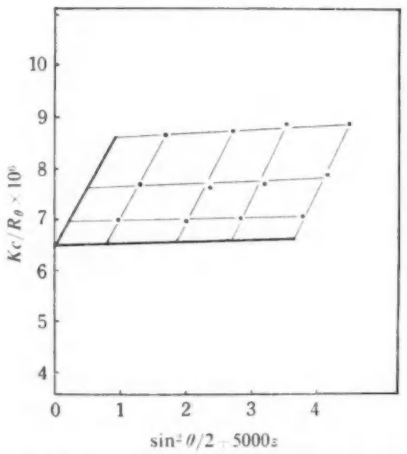

Fig. 7a. Light scattering data for PBLG sample No. 105 in DMF at 23°C.

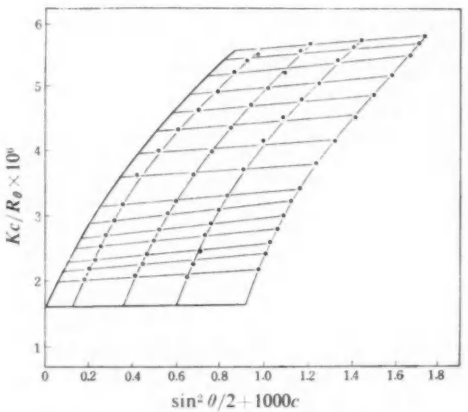

Fig. 7b. Reciprocal angular envelope of solutions PBLG No. 105 in dioxane at 23°C.

8) L. F. Fieser, "Experiments in Organic Chemistry" 2nd ed., D. H. Heath & Co., Boston, Mass., (1941).

9) B. A. Brice and M. Halwer, *J. Opt. Soc. Am.*, **40**, 765 (1950).

* The light scattering measurement was performed following a process established by Professor P. Doty and his coworkers at Harvard University.

10) A. Kruis, *Z. physik. Chem.*, **34B**, 13 (1936).

11) B. H. Zimm, *J. Chem. Phys.*, **16**, 1093, 1099 (1948).

TABLE III. MOLECULAR WEIGHT, MOLECULAR LENGTH, SPECIFIC POLARIZATION, DIPOLE MOMENT AND CRITICAL FREQUENCY OF PBLG IN EDC

PBLG	M_w	$L_{z,z+1}$	P_2^{00}(cc)	μ(D)	μ_0(D)	ν_0
202	180,000	1350	963	2910	3.54	3000
105	154,000	1100	805	2450	3.48	7000
102	102,000	750	494	1570	3.36	16000
201	86,000	690	470	1404	3.58	20000
103	70,000	600	314	1040	3.25	40000

be obtained after extrapolating to $c=0$ and $\theta=0$, where the particle scattering factor $P(\theta)$ is known to be unity. A typical double plot, that is, the so-called Zimm plot, for one of the PBLG samples in DMF is shown in Fig. 7a. Measurements were also conducted for the dioxane solution as one of the Zimm plot and are shown in Fig. 7b. The molecular length, assuming a rigid rod-shaped molecule at present, can be calculated from the initial slope of the angular envelope in the Zimm plot;

$$L_{z,z+1}=\frac{9\lambda'^2}{8\pi^2}\frac{(\text{slope})_{c=0,\,\theta=0}}{(\text{intercept})_{c=0,\,\theta=0}} \tag{4}$$

where λ' refers to the wave length in solution.

The final results of the measurement of molecular weight and molecular length are listed with the polymerization condition in Table III. The remarkable increase in molecular weight and molecular length in dioxane solution might result from molecular association which will be discussed in detail later.

Dielectric Properties of PBLG in Ethylene Dichloride and Dioxane

For a long, rigid rod-shaped molecule, the cavity field in the direction of the rod axis can be assumed to be the same as the external field, and in the α-helix having point dipoles parallel with the rod axis, only the field of this direction has to be taken into consideration. So the relation between the static dielectric constant of the solution ε_{12}^0 and the specific polarization of the solute P_2 is given in terms of the weight fraction of the solute w_2, the specific polarization of the solvent P_1, and the density of the solution d_{12} as follows[12]

$$P_2^0=[(\varepsilon_{12}-1)/3d_{12}-P_1]/w_2+P_1 \tag{5}$$

The specific polarization extrapolated to zero concentration P_2^{00} and the dipole moment of the α-helix in the solvent are related

$$\mu^*=(9k/4\pi N)^{1/2}(P_2^{00}\bar{M}_wT)^{1/2}$$
$$=0.0128(P_2^{00}\bar{M}_wT)^{1/2} \tag{6}$$

In the dipole moment μ^*, the moment induced in the polarizability α by the reaction field $\mu^*R(\varepsilon)$ is taken into consideration and it is given by the moment in vacuo μ.[13]

$$\mu^*=\frac{\mu}{1-\alpha R(\varepsilon)} \tag{7}$$

To obtain the static dielectric constant ε^0_{12} or specific polarization, those values measured by the bridge method at various frequencies must be extrapolated to zero frequency. In this procedure the following problems must be considered:

1) The relation between ε_{12} and ν is not linear.

2) The dispersion curve does not agree, in general, with Debye's theoretical one in which a single relaxation time is assumed.

3) In the low-frequency range, the polarization effect on the electrode surface of the liquid cell can not be negligible. To cope with these problems, three methods for extrapolation are proposed as follows.

I) Assuming an empirical functional relation which gives a linear relation especially at the low-frequency range, we extrapolate it to zero frequency.

II) Extrapolation is made to zero frequency on the Cole-Cole's arc plot.[12] This method, however, does not seem appropriate because of the increase in experimental error of the loss factor at low-frequency.

III) Extrapolation of the flat part at the low-frequency range in $\varepsilon_{12}\sim\nu^{-1}$ plotting to $\nu^{-1}\to 0$.[14] This extrapolation will be useful to exclude electrode polarization because it becomes zero at infinite frequency. An underestimate of the dielectric constant will result when the polydispersity in the α-helix is present.[13]

1) Ethylene Dichloride Solution. — The dispersion curve of each PBLG sample in EDC is shown in Fig. 8. It can be seen that the critical frequency becomes lower as the specific polarization and the molecular weight become larger.

In Figs. 9a, 9b and 9c three plottings of these samples are shown and the extrapolated values of P_2 are compared in Table IV. For

12) A. Wada, *J. Chem. Phys.*, **29**, 674 (1958).

13) A. Wada, ibid., **31**, 495 (1959).

14) J. L. Oncley, *Chem. Revs.*, **30**, 433 (1942).

TABLE IV. SPECIFIC POLARIZATION OF PBLG IN EDC EXTRAPOLATED TO ZERO FREQUENCY

PBLG	Method of extrapolation I		II		III
	P_2^{00}(cc)	ν_0	P_2^{00}(cc)	ν_0	P_2^{00}(cc)
202	950	3000	920	3000	900
105	800	6300	770	7000	780
103	330	33000	314	40000	320

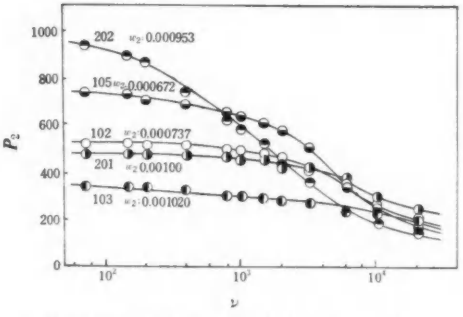

Fig. 8. Dependence of dielectric constant of the EDC solutions of PBLG samples upon frequency at 25°C.

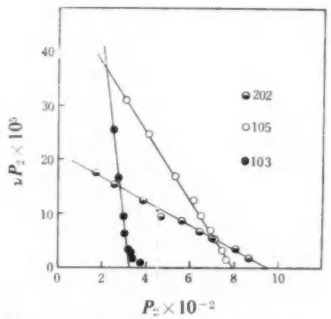

Fig. 9a. Plotting of νP_2 as a function of P_2.

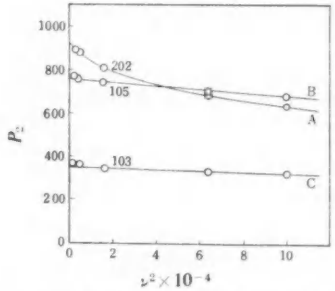

Fig. 9b. Specific polarization of PBLG as a function of ν^2.
A M_w: 180,000, B M_w: 154,000,
C M_w: 70,000.

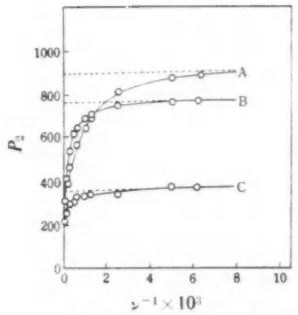

Fig. 9c. Specific polarization of PBLG as a function of ν^{-1}.
A M_w: 180,000, B M_w: 154,000,
C M_w: 70,000.

the first extrapolation method it was incidentally given a linear relation in $P_2\nu \sim P_2$ plot. This means that the relation $P_2 = P_2^0\left(1+\frac{\nu}{\nu_0}\right)^{-1}$ can be maintained in this system and P_2^0 and the critical frequency ν_0 are given from the intercept and the slope of this plot respectively. The deviation from the linearity at the low-frequency range may be due to electrode polarization. Though the extrapolated values by these three methods differ slightly, they do not seriously affect the result, as can be seen in Table IV.

For the calculation of the molecular dipole moment, the P_2^0 measured in several concentrations were extrapolated to zero concentration. A typical plot is shown in Fig. 10 and

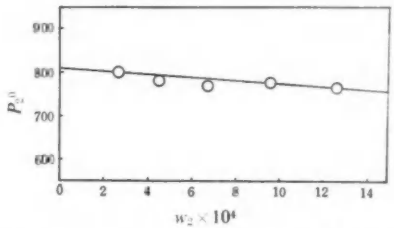

Fig. 10. Concentration dependence of specific polarization[4] of PBLG sample No. 105 in EDC at 25°C.

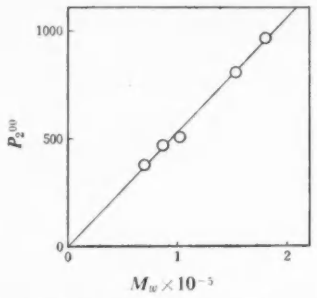

Fig. 11. Dependence of specific polarization of PBLG samples in EDC upon molecular weight.

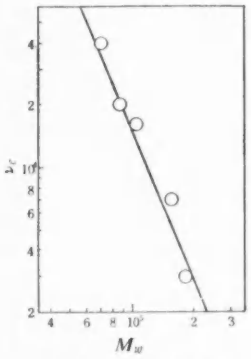

Fig. 12. Double logarithmic plot of critical frequency of PBLG samples in EDC against molecular weight.

the final results are listed with the dipole moment calculated in Table III.

The measured P_2 and dipole moments increase proportionately to the molecular weight as shown in Fig. 11. The dipole moment of the amino acid residue in the α-helix then can be calculated as 3.5 D. This value is quite consistent with the parallel orientation of the dipole moment of polar groups $\overset{H}{\diagdown}\!\!>N-C\!\!<\!\!\overset{}{\diagup}_{O}$ in the α-helix. Further, the critical frequency, on the other hand, is known to have a linear relation in double logarithmic plot as shown Fig. 12. This behavior is well explained using Perrin's equation with the hydrodynamically equivalent ellipsoid of revolution which has the same volume and length as the α-helix. That is

$$\tau_0 = (2\pi\tau)^{-1}$$

$$\tau = \frac{2\tau_0}{3} \frac{1}{2\rho^2 \ln(2/\rho) - \rho^2} \qquad (8)$$

$$\rho = b/a, \quad \tau_0 = 4\pi\eta ab^2/kT$$

The solid line in Fig. 13 is the theoretical plot corresponding to 18.3 Å of the minor axis, that is 15 Å for the diameter of the α-helix. All of the above results are consistent with and tend to support the belief that in this solvent the PBLG exists as a rigid rod-shaped molecule, the α-helix given by Pauling and Corey.

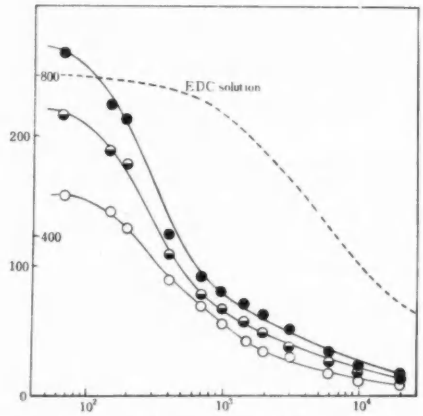

Fig. 13. Dependence of specific polarization of PBLG samples in dioxane solution upon frequency at 30°C.
Filled circle No. 105 $w_2=0.000824$. Half filled circle No. 103 $w_2=0.001282$. Open circle No. 102 $w_2=0.001112$.

2) Dioxane Solution. — In dioxane the α-helix of PBLG may be in an associated state as Doty et al. concluded.[1] They emphasized that the association is of the end-to-end type but that the rod-like form is not preserved. The increase in the molecular weight and molecular length of PBLG in this solvent, which has been given by the light scattering measurement as shown in Table III, seems to endorse this idea. Moreover, the non-linear relation between the molecular weight and the molecular length suggests that the associated molecule is no longer linear and/or rigid.

For further study on the mechanism of molecular association the information from the electric dipole moment, as a vectoral quantity along the direction of the helical axis, will be useful. Leaving quantitative considerations of this interesting problem to another report[15], we may conclude, however, that the α-helix still has a large electric dipole moment in dioxane which is the only non-polar solvent in which PBLG can dissolve.

Examining the dispersion curve of this system in Fig. 13 the critical frequency reveals

15) A. Wada, *J. Polymer Sci.*, (1960), in press.

a remarkable shift to lower frequencies compared with that of the same sample in EDC for which the dispersion curve is plotted in the same figure in a dotted line. Therefore, the third extrapolation method could not be used because the left part of the dispersion curve goes out of the range of measurement. Only the second method, the extrapolation in Cole-Cole's arc plot, is effective, as shown in Fig. 14. A linear relation in the plot which was given in the case of EDC solution no longer holds in dioxane. This discrepancy between dioxane and EDC suggests that the molecular association will change the molecular weight distribution. The molecular weight distribution seems to be more polydisperse than that of the most probable distribution as in the case of EDC solution. The broader distribution may also be suggested from the flat shape of Cole-Cole's arc in this solvent (Fig. 14). This fact means that the molecules preferably aggregate in certain ranges of molecular weight more than in others as Doty et al. mentioned.[1]

The P_2^0 depends strongly upon the concentration in dioxane as shown in Fig. 15. This strong dependence may originate from the molecular association and/or dipole-dipole interaction which becomes stronger in a nonpolar solvent such as dioxane than in a polar one such as EDC. The absence of concentration dependence in light scattering measurement will support the latter possibility. It is empirically found that the $P_2^{0-1}\sim c$ plot gives a straight line as shown in Fig. 16. From these extrapolated values the electric dipole moment is computed. In Table V the electric dipole moment, calculated from the original molecular weight and from that of the associated molecule, are listed. Though the result is no longer proportional to the molecular weight, the dipole moment 1~3 D per amino acid residue still suggests that the molecule has an ordered form which has a partial α-helical configuration.

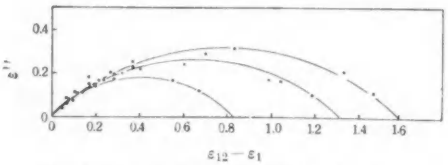

Fig. 14. Cole-Cole's arc plot for the dioxane solution of PBLG No. 105. w_2=0.003058, 0.001794, 0.000824.

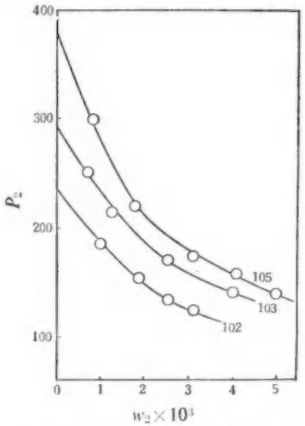

Fig. 15. Concentration dependence of specific polarization of PBLG samples in dioxane at 30°C.

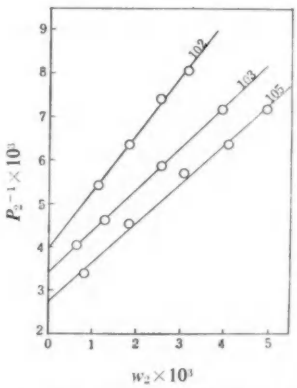

Fig. 16. Reciprocal plot of specific polarization of PBLG samples in dioxane against concentration.

TABLE V. MOLECULAR WEIGHT, SPECIFIC POLARIZATION, CRITICAL FREQUENCY AND DIPOLE MOMENT OF PBLG IN DIOXANE

PBLG	$\bar{M}_w$	P_2^{00} (cc.)	ν_0	Dipole moment calcd. from Original M_w		Associated M_w	
				μ(D)	μ_0(D)	μ(D)	μ_0(D)
105	660,000	360	400	1650	2.35	3407	1.13
102	1610,000	250	600	1115	2.39	4435	0.60
103	—	300	1100	1010	3.16	—	—

Summary

The work described above has produced the following conclusions.

(1) A large electric dipole moment corrospoinding to the α-helix described by Pauling, Corey and Branson is found in EDC and dioxane.

(2) A linear relation between the electric dipole moment and the molecular weight in EDC suggests that the molecule is linear and not flexible.

(3) The critical frequency of the orientation polarization was elucidated by using an equivalent ellipsoid model and the equation for the rotatory diffusion constant derived from Perrin's equation. This fact will support the conclusion of Doty, Bradbury and Holtzer that the α-helix is fairly rigid in the solution.

(4) In dioxane the α-helix can be found to be associated and to have a different distribution in molecular weight.

Department of Chemistry
Ochanomizu University
Bunkyo-ku, Tokyo

Spectrophotometric Determination of Traces of Boron in Uranium

By Hiroshi ONISHI, Nasumi ISHIWATARI and Hitoshi NAGAI

(Received January 7, 1960)

Various methods for determining traces of boron in uranium and its compounds were investigated because of the effect of neutron absorption. Table I summarizes most of the previous literature on the photometric determination of boron in uranium. Spectrographic

TABLE I. SUMMARY OF LITERATURE ON THE PHOTOMETRIC DETERMINATION OF BORON IN URANIUM

Samples	Reagent	Separation	Range	Reference
U_3O_8	Carmine	—*	0.05—50 μg. B	1
U_3O_8	Carmine	—	1 p.p.m. B detd. (1 g. sample)	2
$UO_2(NO_3)_2$	Carmine	Distillation	0.1—0.5 p.p.m. (4 g. sample)	3
Al-U	Carminic acid	—	10—70 μg. (0.5—2 g. sample)	4
U_3O_8	1,1'-Dianthrimide	Ion exchange	0.2—2 p.p.m.	5
UF_6	Curcumin	Distillation		6
U_3O_8	Turmeric	Distn. from H_3PO_4 soln.	0.1—1.5 μg.	7
U, U compds.	Curcumin	Distillation	0.5—5 μg.	8
U	Curcumin	Solvent extn.	>0.1 p.p.m.	9
U-Zr, U-Zircaloy	Curcumin	EtOH extn.	0.015% detd.	10
U, UO_2Cl_2	Crucumin	—	3—50 p.p.m. (0.1 g. sample)	11
U	Curcumin	Distn. from HCl soln.	0.01—0.3 p.p.m (10 g. sample)	12
Al-U	Curcumin	Distn. from HCl soln.	>30 p.p.m.	13
U	Curcumin	Ion exchange		14

* — denotes that separation is not required.

1) R. Cypres and P. Leherte, *Bull. soc. chim. Belges*, **63**, 101 (1954).
2) R. F. Cellini and L. G. Sánchez, *Proc. Intern. Conf. Peaceful Uses Atomic Energy*, **8**, 364 (1956).
3) T. Nowicka-Jankowska and H. Szyszko, *Chemia Analityczna*, **1**, 285 (1956).
4) K. W. Puphal, J. A. Merril, G. L. Booman and J. E. Rein, *Anal. Chem.*, **30**, 1612 (1958).
5) A. R. Eberle, M. W. Lerner and H. Kramer, **NBL-143**, 5 (1958).
6) E. Staple, E. D. Marshall, F. Nelson and W. Simon, **AECD-4212** (1946. Decl. 1955).
7) C. J. Rodden, *Proc. Intern. Conf. Peaceful Uses Atomic Energy*, **8**, 197 (1956).
8) J. F. Possidoni de Albinati and R. H. Rodrguez Pasqués, ibid., **8**, 339 (1956).
9) J. Coursier, J. Huré and R. Platzer, ibid., **8**, 487 (1956).
10) J. Rynasiewicz and V. Consalvo, **KAPL-M-JR-8** (1956).
11) L. Silverman and K. Trego, *Anal. Chim. Acta*, **15**, 439 (1956).
12) Chemical Services Dept., **IGO-AM/S-124** (1958).
13) I. H. Crocker, **CRDC-811** (1958).
14) T. Takeuchi, T. Yoshimori and S. Shibayama, the 12th Annual Meeting of the Chem. Soc. of Japan, April, 1959.

methods are not included in the table. Curcumin methods are generally more sensitive than carmine methods. However, the curcumin methods which have been reported up to the present consist of varied procedures according to different authors. Moreover, the reasons for using each procedure are not always evident. Consequently, in order to obtain optimum conditions, the available methods have been critically studied.

As shown in Table I, a phosphoric acid or a hydrochloric acid medium appears to be widely used for the separation of boron as methyl borate from uranium. In the case of the phosphoric acid medium, that methanol vapor must be passed through a hot sample solution[7] is considered to be disadvantageous, since connection of two distilling flasks is necessary; Otherwise phosphoric acid solutions of uranium form gels. When the hydrochloric acid medium is employed, the removal of excess of water is not easily effected[15].

In the determination of boron in uranyl sulfate, the authors found that a sulfuric acid medium was very suitable for the separation of boron as methyl borate, and that the abovementioned disadvantage and difficulty could be avoided. Further investigation has shown that satisfactory results of analyses of U_3O_8 and uranium metal (after conversion into U_3O_8) can be obtained by using the same medium for the dissolution of the sample and distillation of methyl borate. These results are reported in the present paper.

Experimental

Apparatus.—The distilling apparatus (quartz) is shown in Fig. 1. The volume of the flask is about 300 ml. Absorbance measurements were made with a Hitachi Model EPU-2A spectrophotometer, using 1-cm. cells.

Reagents. — In purification and preparation of reagents, as well as in analysis, redistilled water was used. For purification by distillation described below, a quartz distilling apparatus was used. All the solutions (except hydrogen peroxide) were kept in polyethylene bottles.

Water, redistilled.—Small amounts of mannitol (dissolved in distilled water) are added to the flask for redistillation.

Sulfuric acid, 1 : 3.—In a quartz beaker 5 ml. of 48% hydrofluoric acid is added to 100 ml. of concentrated sulfuric acid and heated to strong fumes. After cooling water is added.

Hydrogen peroxide, 30%.—Purification was effected by modification of Luke's procedure[16]. A 2.5 g. portion of Amberlite IR-120 (H^+ form) and 7.5 g. of Amberlite IRA-400 (OH^- form) are transferred to a 100 ml. polyethylene beaker. While cooling, 60 ml. of cold 30% hydrogen peroxide is added and stirred for 10 min. The product is filtered through a paper (washed with water and dried) to a brown glass bottle and kept in a refrigerator.

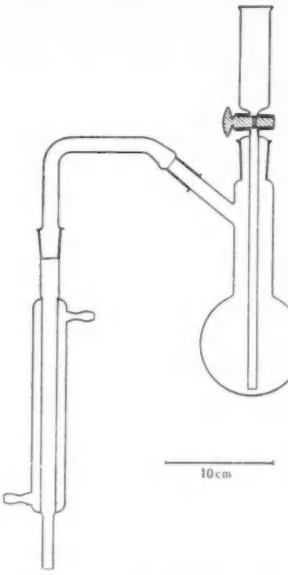

Fig. 1. Distilling apparatus.

Methanol, redistilled from sodium hydroxide.

Calcium hydroxide suspension, 0.1 N. — Distilled calcium is washed with water and the oxide scraped. One gram of calcium is dropped into a 500 ml. quartz flask and enough water is added cautiously. After cooling the contents are transferred to a bottle and diluted to 500 ml. with water.

Curcumin-oxalic acid solution[17,18].—A 0.40 g. portion of finely ground curcumin and 50 g. of oxalic acid are dissolved separately in ethanol. Both solutions are mixed and diluted with ethanol to 1 l.

Ethanol, redistilled from sodium hydroxide.

Standard boron solution.—A 0.5716 g. portion of boric acid is dissolved in 100 ml. of water (1.00 mg. B/ml.). From this stock solution 1 and 0.2 p.p.m. B solutions are prepared.

Procedure. — *Uranium metal.* — Ignite cautiously 1.00 g. of the sample in a platinum crucible at a low temperature. Then heat the crucible in an electric oven at about 800°C for one hour. Cool, and transfer the oxide formed to the distilling flask. Then continue as described below.

U_3O_8.—Transfer 1.00 g. of sample to the distilling flask and assemble the distilling apparatus. Place a 100 ml. platinum dish containing 10 ml. of water under the condenser. To the flask add 5 ml. of 1 : 3 sulfuric acid and 1 ml. of 30% hydrogen peroxide. Heat gently with a small flame until the sample is in solution. Replace the burner by an infrared lamp (300~500 W.) and distil excess of

15) H. Onishi, N. Ishiwatari and H. Nagai, the 12th Annual Meeting of the Chem. Soc. of Japan, Kyoto, April, 1959.
16) C. L. Luke, *Anal. Chem.*, **27**, 1150 (1955).
17) W. T. Dible, E. Truog and K. C. Berger, *Anal. Chem.*, **26**, 418 (1954).
18) I. Muraki and K. Hiiro, *J. Chem. Soc. Japan, Pure Chem. Sec.* (*Nippon Kagaku Zasshi*), **78**, 845, 850 (1957).

water. Heat several times the side arm of the flask to remove water droplets. Stop heating when fumes begin to appear. Cool.

Immerse the flask in a 1 l. beaker containing water (this serves as a water bath). Add 5.0 ml. of 0.1 N calcium hydroxide suspension to the platinum dish and raise the dish so that the tip of the condenser is in the solution. (The dish is protected from the heat of the burner by an appropriate shield.) From the tap funnel add 30 ml. of methanol. Raise the temperature of the bath slowly to approximately 95°C, giving a slow but steady distillation of methyl borate and methanol*. Continue heating until no more liquid comes over. Remove the burner and replace the hot water by cold water. Add 2.0 ml. of 0.1 N calcium hydroxide suspension to the solution in the dish. Add 20 ml. of methanol through the tap funnel and distil again. Lower the dish and wash down the stem of the condenser. Mix the distillate and washings with a quartz stirring rod (confirm that the solution is alkaline), and evaporate gently to dryness on a water bath.

To the residue add 2 ml. of water and 4.0 ml. of curcumin-oxalic acid solution and mix with a quartz stirring rod. Wash the rod with a small amount of water. Evaporate the solution on a water bath at 55±3°C, and allow to remain for 30 min. after the contents are dry. Cool the dish to room temperature (in a desiccator). Extract the colored products with 9 : 1 ethanol by stirring with a quartz rod. Transfer the colored solution to a 25 ml. volumetric flask and make up to volume with 9 : 1 ethanol. Mix, transfer the contents to a centrifuge tube, cover the tube with parchment paper, fasten the paper with a rubber band, and centrifuge at about 3000 r.p.m. for 10 min. Transfer the clear solution to a 1 cm. cell, and measure the absorbance at 550 mμ, using 9 : 1 ethanol as the reference.

Establish the standard curve by taking, for example, 0, 0.2, 0.5, and 1 μg. of boron, adding 7 ml. of 0.1 N calcium hydroxide suspension, and proceeding as described above. Run a blank, preferably in duplicate, throughout the entire procedure. As the recoveries of boron are low, a correction of +15% is advisable. When the standard curve is established by including the separation, this correction is naturally unnecessary.

Results and Discussion

Spectrophotometric Determination of Boron.—In general, it may be summarized that the variable factors in the curcumin methods are use of alkalis (sodium hydroxide[8,12,13,19] and calcium hydroxide[7,18]), addition of hydrochloric acid, amounts of curcumin and oxalic acid, and extractants (ethanol[7,18], methanol[8], acetone[8,11]) of the colored products. Spicer and Strickland[19] used a glycerol-sodium hydroxide reagent, of composition of 1% sodium hydroxride, 0.1% sodium chloride, and 3% glycerol, to collect methyl borate. In this case hydrochloric acid must be added before adding curcumin. Muraki and Hiiro[18] used calcium hydroxide, and did not add hydrochloric acid, while other workers (e. g., Ref. 7) added the acid.

The preparation of curcumin-oxalic acid solution, described by Muraki and Hiiro[18], appears most satisfactory, because the preparation is simple, and the solution is stable. When the solution has been allowed to stand for 2 days after preparation, the absorbance becomes practically constant (Fig. 2). The workers mentioned[18] allowed the solution to stand for 7~10 days before use. The solution can be kept for one month at room temperature in the dark.

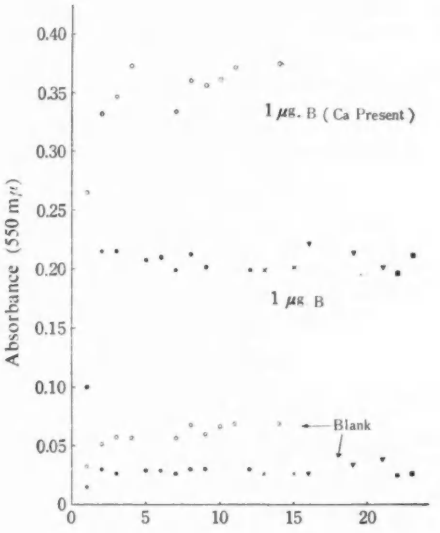

Fig. 2. Aging of curcumin-oxalic acid reagent
○ With Wako-Eastman curcumin and other points with Koso curcumin (cf. Table VII).
●: 97%(v./v.) EtOH, ○ and ×: 87% (v./v.) EtOH, ▼: MeOH, ■: acetone.

Table II shows the effects of alkalis and extractants on the determination of boron. In each case 4 ml.[18] of curcumin-oxalic acid solution was used. It is seen that the presence of calcium hydroxide increases the absorbance of colored solution*, while that of sodium chloride decreases the absorbance. Addition of hydrochloric acid to calcium hydroxide is not

* This distillation requires about 15 min., and the second distillation about 10 min.

19) G. S. Spicer and J. D. H. Strickland, *Anal. Chim. Acta*, **18**, 523 (1958).

* Data obtained by Muraki and Hiiro[18] also indicate this phenomenon.

Table II. Effects of alkalis and extractants on the determination of boron

	97% (v./v.) EtOH	87% (v./v.) EtOH	MeOH	Acetone
Blank				
Mean absorbance	0.029	0.028	0.034	0.026
No. of expts.	16	4	6	4
Std. deviation, %	9.0	8.6	9.4	8.7
1 μg. B				
Mean absorbance	0.208	0.200	0.214	0.204
No. of expts.	16	4	6	4
Std. deviation, %	3.7	1.8	5.6	4.7
5 ml. of 0.1 N $Ca(OH)_2$ was added				
Blank				
Mean absorbance	0.038	0.039	0.053	0.039
No. of expts.	6	4	4	4
Std. deviation, %	10	4.4	4.0	3.6
1 μg. B				
Mean absorbance	0.249	0.245	0.265	0.269
No. of expts.	6	4	4	4
Std. deviation, %	1.3	1.0	2.3	4.4
2 ml. of glycerol-NaOH reagent was added. 2 ml. of 1 N HCl was added after removal of glycerol				
Blank				
Mean absorbance	0.028	0.026	0.029	0.024
No. of expts.	4	4	4	4
Std. deviation, %	18	6.9	11	10
1 μg. B				
Mean absorbance	0.148	0.152	0.151	0.139
No. of expts.	4	4	4	4
Std. deviation, %	4.3	3.1	3.3	4.1

Table III. Comparison of several curcumin products

	Vol. of 0.1 N $Ca(OH)_2$ soln., ml.	Absorbance*		
		Blank	1 μg. B	Difference
Koso Chemical Co., Ltd.	5	0.038	0.249	0.211
Tokyo Kasei Kogyo Co., Ltd.	5	0.072	0.380	0.308
Tokyo Kasei Kogyo Co., Ltd.	7	0.075	0.371	0.296
Kanto Chemical Co., Inc.	7	0.069	0.367	0.298
Wako Pure Chemical Industries, Ltd.-Eastman Kodak Co.	7	0.062	0.357	0.295

* Average of 6—12 determinations.

Table IV. Effect of foreign substances on the determination of boron

Addition	Absorbance		
	Blank	1 μg. B	Difference
—	0.072	0.380	0.308
1 ml. 0.1 N HCl	0.053	0.373	0.320
2 ml. 1 N HCl	0.031	0.285	0.254
1 ml. 0.2 N H_2SO_4	0.073	0.397	0.324
2.0 ml. 0.2 N H_2SO_4	0.046	0.292	0.246
2.5 ml. 0.2 N H_2SO_4	0.083	0.303	0.220
1 ml. 0.2 N HCOOH	0.224	0.502	0.278
20 ml. H_2O, 50 ml. MeOH	0.082	0.374	0.292
1 mg. U (as UO_2SO_4)	0.080	0.394	0.314

TABLE V. DISTILLATION OF BORON AS METHYL BORATE

Acid solution	B taken, μg.	B found,* μg.	Av. recovery, %
5 ml. 1 : 3 H_2SO_4	1.00	0.82, 0.79, 0.84, 0.86, 0.89, 0.82	84
5 ml. 1 : 3 H_2SO_4, 1 ml. 30% H_2O_2	0.50	0.41, 0.45	86
5 ml. 1 : 3 H_2SO_4, 1 ml. 30% H_2O_2	1.00	0.91, 0.83	87
5 ml. 1 : 3 H_2SO_4, 1 ml. 30% H_2O_2, 1 ml. 0.1 N HCl	0.20	0.20, 0.16	90
5 ml. 1 : 3 H_2SO_4, 1 ml. 30% H_2O_2, 1 ml. 0.1 N HCl	0.50	0.38, 0.44	82
5 ml. 1 : 3 H_2SO_4, 1 ml. 30% H_2O_2 1 ml. 0.1 N HCl	1.00	0.89, 0.81, 0.86, 0.89, 0.89, 0.80	86

* Based on the standard absorbance obtained by omitting methanol distillation (direct color development).

recommended (cf. Table IV). When the glycerol-sodium hydroxide reagent is used, addition of 2 ml. of 1 N hydrochloric acid gives the maximum absorbance. From the data in Table II, it may be concluded that, on the basis of sensitivity and simplicity in manipulation, calcium hydroxide is superior to glycerol-sodium hydroxide (and sodium hydroxide) and that 87% ethanol (=9 : 1) gives most reproducible results. The method of Silverman and Trego[11] is not sensitive enough to be used for the present purpose.

The absorbances of the colored solutions (ethanol and acetone) remain practically constant for 2 hours after the beginning of extraction of colored products. After that there is a gradual decrease in absorbance. The absorbance of a methanolic solution tends to decrease more rapidly than that of other solutions.

For the purpose of studying the influence of curcumin of different origins, several products were examined (Table III).

The effects of some foreign substances on the determination of boron were investigated (Table IV). Five ml. of 0.1 N calcium hydroxide suspension and the foreign substance, with or without 1 μg. of boron, was evaporated to dryness and then subjected to color development. The addition of 2 milliequivalent of hydrochloric acid to 0.5 milliequivalent of calcium hydroxide resulted in about a 20% decrease in absorbance (1 μg. B). If the same quantity of the acid is added to 0.7 milliequivalent of calcium hydroxide, the absorbance is low by as much as 40%. The effect of formic acid was investigated because of the possible formation formic acid during methanol distillation[20]. During evaporation of the methanolic solution about 5% of boron is lost. A loss of 4% was reported by Spicer and Strickland[19] during evaporation of methanolic solution in the presence of glycerol-sodium hydroxide reagent.

Separation of Boron from Uranium. — Table V summarizes the results of methanol distillation from sulfuric acid solution. Excess of water was removed by heating and methanol distillation was carried out as described in the procedure. Larsen[21] states that the addition of chloride in catalytic amounts to a mixture of sulfuric acid and hydrogen peroxide increases the rate of solution of uranium very markedly. This is the reason that 0.1 milliequivalent of hydrochloric acid was added in some cases. The effect of this solution method will be discussed later.

On the basis of the standard absorbance obtained by omitting the methanol distillation (i.e., direct color development), the average recovery of 1 μg. of boron from sulfuric acid solution is 84% (standard deviation 4.2%). Addition of hydrogen peroxide to sulfuric acid does not affect the recovery of boron (average 87%). The weighted average of recovery from the sulfuric acid-hydrogen peroxide-hydrochloric acid mixture is 85% (standard deviation 4.9% for 1 μg. B). The loss may be due to incomplete distillation of methyl borate, volatilization of boron during the evaporation of distillate, and slight difference in the composion between the sample solution and the standard solution. Most of the previous papers (cited in Table I) lack the information

TABLE VI. DETERMINATION OF BORON IN URANYL SULFATE

1.0 g. of U (as UO_2SO_4) in 5 ml. of 1 : 3 H_2SO_4 was taken in each determination

B added, μg.	B found, μg.	B recovered, μg.
0	0.10, 0.10	
0.20	0.26, 0.35	0.16, 0.25
0.50	0.48, 0.54	0.38, 0.44
1.00	0.99, 0.94	0.89, 0.84

20) M. Codell and G. Norwitz, *Anal. Chem.*, **25**, 1446 (1953).

21) R. P. Larsen, *Anal. Chem.*, **31**, 545 (1959).

TABLE VII. DETERMINATION OF BORON IN U_3O_8 AND URANIUM METAL

Sample	B present, p. p. m.	B found, p. p. m.***		
		1	2	3
U_3O_8*	0.5	0.59, 0.57	0.62, 0.60	0.59, 0.57
U metal**	0.23		0.22, 0.22, 0.23	

* New Brunswik Laboratory, NBL-65-3. Certified values of other constituents (in p. p. m.): 0.2 Cd, 12 Cr, 12 Cu, 28 Fe, 6 Mn, 1.0 Mo, 22 Ni, 50 P, 25 Si, 0.6 Ag, 20 V.

** New Brunswick Laboratory analyzed sample No. 16. Other certified values (in p. p. m.): 10 Al, 410 C, 2 Cu, 45 Fe, 1 Pb, 2 Mg, 6 Mn, 45 Ni, 40 N, <1 K, 50 Si, <0.1 Ag, 2 Na, 0.3 Th.

*** Three methods of standardization were studied:

1. Based on the standard curve involving MeOH distillation.
2. Seven ml. of 0.1 N $Ca(OH)_2$ solution evaporated to dryness. Color development followed. +15% correction.
3. Twenty ml. of water and 50 ml. of MeOH evaporated to dryness in the presence of $Ca(OH)_2$. Color development followed. +10% correction.

on the recoveries of boron, and the calibration curves were constructed by including the distillation step. A calculation from the data reported by Muraki and Hiiro[18] gives an apparent recovery of 80% for 0.2~2.0 μg. of boron. Also, a recovery of 75% is calculated from Luke's results[22] that were obtained by the distillation of 0.2~0.6 μg. of boron from chloride solutions.

Known amounts of boron were added to uranyl sulfate (1 g. U) solution and the boron was separated by distillation after removing excess of water (Table VI). A recovery (weighted average) of 87% is obtained with 0.2~1 μg. boron. When a correction factor of +15% (100/87=1.15) is applied, the error is not likely to exceed ±0.1 p. p. m. for this concentration range.

The results of analyses of standard samples of U_3O_8 and uranium metal, obtained in applying the proposed method, are shown in Table VII. The reagent blank (against the blank of direct color development) was about 0.1 μg. of boron. The U_3O_8 sample dissolved in the mixture of sulfuric acid and hydrogen peroxide readily. Three methods of standardization give essentially the same results.

The mixture of sulfuric acid-hydrogen peroxide-hydrochloric acid, described by Larsen[21], does not dissolve uranium readily unless the sample is very fine or thin. Anodic dissolution of uranium appears promising*. Since the solution of U_3O_8 in sulfuric acid and hydrogen peroxide is easily effected, uranium metal was converted in to the oxide by ignition. From the table it is seen that boron is not lost by the heat-treatment. Because the state of this element in uranium is not well known, and other standard metal samples were not available, further experiments were not made.

Summary

Procedure is described for the spectrophotometric determination of 0.1~1 p. p. m. of boron in uranium (metal, U_3O_8, and uranyl sulfate). Uranium metal was first converted to U_3O_8, and the oxide was dissolved in sulfuric acid and hydrogen peroxide. Boron was separated by distillation as methyl borate from sulfuric acid solution, and finally determined by the curcumin method.

Japan Atomic Energy Research Institute
Tokai, Ibaraki-ken

* Larsen[21], and preliminary work of the present authors.

22) C. L. Luke and S. S. Flaschen, *Anal. Chem.*, 30, 1405 (1958).

Polarographic Studies on the Rare Earths. III. Yttrium.

By Seizo MISUMI and Yasushi IDE

(Received October 8, 1959)

Polarographic studies on the reduction of the tripositive yttrium ion had been reported and discussed by Noddack and Brukl[1], Kolthoff and Lingane[2], and Purushottam and Raghava Rao[3], but the electrode reaction in the reduction process was not completely solved, because of the special properties of the aquo yttrium complex ion and of the anomalies of the reduction wave. Noddack and Brukl obtained a double wave for 0.01 M solution of yttrium sulfate, without any supporting electrolyte, having the half-wave potentials of -1.76 V. and -1.84 V. vs. S. C. E., respectively and concluded the reduction process to be $Y^{3+} \rightarrow Y^{2+} \rightarrow Y^{0}$. However, it is very doubtful. Kolthoff and Lingane suggested that it was more probable that the first wave resulted from the reduction of hydrogen ion produced by the hydrolysis of the aquo yttrium complex ion and the second wave corresponded to the three electron reduction to metal. Purushottam and Raghava Rao also obtained the double wave with yttrium chloride using lithium chloride as supporting electrolyte. From the reciprocal slope of the logarithmic plots of both waves, they concluded that the electrode reaction of the first wave was of one-electron change, and that of the second wave, of two-electron change, that is, $Y^{3+} \rightarrow Y^{2+} \rightarrow Y^{0}$ the same as before. However, all these results were incomplete because the effects of pH and concentration of yttrium ions on the diffusion current, the half-wave potential and further on the electrode reaction in reduction process were not discussed in detail. The present authors, for the purpose of solving the electrode reaction in the reduction process, studied the reduction wave of the aquo tripositive yttrium complex ion in an unbuffered solution under various conditions and obtained a different result from other reports. By the addition of a small amount of dilute acid to prevent the hydrolysis of the aquo yttrium complex ion, the hydrogen wave was completely separated from the reduction wave of the aquo yttrium complex ion, which was generally a single wave in a perchlorate solution and often a double wave in a halide solution. The electrode reaction of the single wave was irreversible and of a three-electron reduction. This wave was due to the reduction of the hydrogen ion which was produced from the dissociation of the aquo yttrium complex ion as the yttrium acid. In the case of the double wave, the first wave was irreversible or quasi-reversible and its electrode reaction was also of a three-electron reduction. The second wave was irreversible and anomalous. The two-stepped wave in the solution of the halide ions, added as supporting electrolyte, was considered to be attributed probably to the reduction of the aquo halo complex ion.

1) W. Noddack and A. Brukl, *Z. Angew. Chem.*, **50**, 362 (1937).
2) I. M. Kolthoff and J. J. Lingane, "Polarography", Vol. II. Interscience Publishers Inc., New York (1952), p. 436.
3) A. Purushottam and Bh. S. V. Raghava Rao, *Anal. Chim. Acta*, **12**, 589 (1955).

Experimental

All current-voltage curves were recorded by a Yanagimoto photographic polarograph PEL-Model 3. All cathode potentials were referred to a saturated calomel electrode. The capillary used had an m value of 0.706 mg./sec. and drop times of 3.25 sec. at -1.8 V. and 2.98 sec. at -1.9 V. vs. S. C. E., when measured in an air-free 0.1 M lithium perchlorate solution at 57.6 cm. of effective height of mercury. The measurement of pH was done with the Hitachi glass electrode pH meter Model EHM-1 for a micro amount scale. All experiments were carried out in a thermostat of 25.0 ± 0.1°C.

An yttrium stock solution was prepared by dissolving pure yttrium perchlorate or sulfate. (As yttrium oxide, the purity was higher than 99.99%.). The concentration of the stock solution was 0.01 M. The lithium perchlorate and tetramethyl ammonium iodide which were used as the supporting electrolytes were guaranteed grade reagents and recrystallized before use. The concentration of these stock solutions were 1 and 0.2 M., respectively. The gelatine solution used as the maximum suppressor was prepared afresh in every experiment. Perchloric acid and sulfuric acid solutions of 0.01 N in concentration were prepared from the analytical pure reagents and used for the adjustment of pH.

To the sample solution of yttrium, appropriate quantities of the supporting electrolyte and gelatine were added to give the final concentrations, 0.1 M and 0.01% respectively. Then a micro amount of 0.01 N acid was added to prevent the hydrolysis of the aquo yttrium complex ion and to adjust the pH at the same time. The total volume of the solution was made up to 5 ml. with distilled water. The concentration of the yttrium ion was in the range from 0.5 to 2.0 millimol./l. and the pH of the solution

was varied from 4.00 to 2.60. Dissolved oxygen was removed by passing purified nitrogen gas through the solution at least for 20 min. The polarograms were recorded at 25.0±0.1°C.

The diffusion coefficient of the yttrium ion was calculated from Nernst's equation, using the value of equivalent conductance at infinite dilution[4]).

D: 5.721×10^{-6} cm. sec^{-1} (for $Y(ClO_4)_3$)

D: 5.764×10^{-6} cm. sec^{-1} (for $Y_2(SO_4)_3$)

Results and Discussion

The reduction wave of aquo tripositive yttrium complex ion.—The reduction wave of the aquo yttrium complex ion (Fig. 1) at pH about 4.5 differed from the true reduction wave owing to the precedence of the hydrogen wave produced by the hydrolysis of the aquo yttrium complex ion. The typical reduction wave was obtained by adding a micro amount of acid to prevent the hydrolysis when the hydrogen wave was completely separated from the reduction wave of the aquo yttrium complex ion under a certain condition. The reduction wave was generally a single wave in a perchlorate medium and often a double wave in a halide (chloride or iodide) medium.

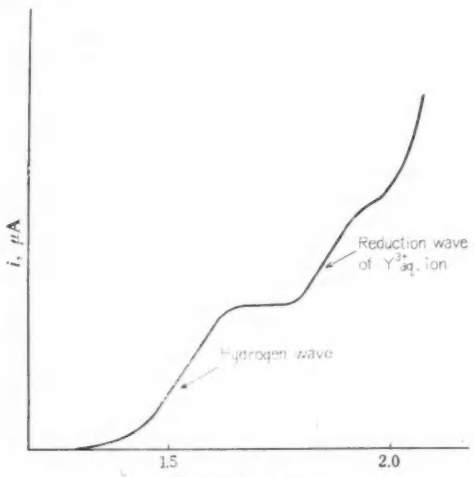

Fig. 1. Reduction wave of the aquo yttrium complex ion. (1) In perchlorate medium
Y^{3+} ion: 1.25 mM in 0.1 M $LiClO_4$ and 0.01% gelatine medium
pH: 2.95 S: 1/200 25.0°±0.1°C

From the results obtained by the variation in pH and the concentration of the yttrium ion, the following common characters of the reduction wave were derived: 1) At a pH higher than 3.4, only a single wave was obtained in both perchlorate and halide medium. 2) At a pH less than 2.7, only a single wave was observed, but as the height of the hydrogen wave became large, the wave was ambiguous. 3) At a pH between 2.7 and 3.4, in a perchlorate solution, only a single wave was obtained clearly and as the pH decreased, there was a tendency for a small maximum wave to appeare ofteh after the reduction wave. In a halide solution, when the two-stepped wave was obtained, the second wave decreased gradually as the pH decreased or the concentration of yttrium ions increased until it finally disappeared.

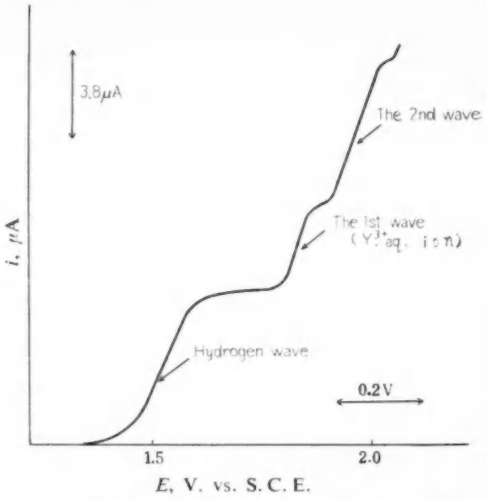

Fig. 1. Reduction wave of the aquo yttrium complex ion. (2) In iodide medium
Y^{3+} ion: 1.03 mM in 0.1 M $(CH_3)_4NI$ and 0.01% gelatine medium
pH: 3.09 S: 1/181 25.0°±0.1°C

Dependence of the limiting current on the pressure upon the dropping mercury electrode and the influence of temperature on the limiting current and the half-wave potential.—A relationship between the limiting current and the height of mercury column is shown in Table I. As the limiting current is proportional to the square root of the height of mercury column, the limiting current was diffusion-controlled.

The temperature coefficient of the half-wave potential and that of the diffusion current in the range from 25° to 35°C were 0.7 mV./deg. and 1.86%/deg., respectively, which were nearly in agreement with the values that would be expected in the case of the diffusion-controlled process.

The plots of E vs. log{$i/(i_d-i)$}.—The reduction waves of the aquo tripositive yttrium complex ion were analyzed by the logarithmic

4) F. H. Spedding and S. Jaffe, *J. Am. Chem. Soc.*, 76, 882 (1954); ibid., 76, 884 (1954).

Table I. Dependence of limiting currents of the reduction wave on the heights of mercury column

h cm.	h(corr.) cm.	i_l μA	$i_l/\sqrt{h}$	h cm.	h(corr.) cm.	i_l μA	$i_l/\sqrt{h}$
50	47.6	3.07	0.446	50	47.5	2.96	0.431
60	57.7	3.39	0.448	60	57.5	3.32	0.448
70	67.6	3.66	0.446	70	67.6	3.61	0.439

Y^{3+} ion: 0.992 mM in 0.1 M $(CH_3)_4NI$ and 0.01% gelatine medium. pH: 3.0.

Y^{3+} ion: 1.257 mM in 0.1 M $LiClO_4$ and 0.01% gelatine medium. pH: 2.9.

Table II. The reciprocal slope of E vs. $\log\{i/(i_d-i)\}$

pH	Reciprocal slope, V.		pH	Reciprocal slope, V. 1st wave.	2nd wave.
3.50	0.059		3.70	0.043	
3.35	0.037		3.35	0.020	
3.00	0.027		3.05	0.019	anomalous
2.80	0.027	max.	2.85	0.020	
2.65	0.022	〃	2.60	0.020	

Y^{3+} ion: 0.611 mM in 0.1 M $LiClO_4$ and 0.01% gelatine medium.

Y^{3+} ion: 1.00 mM in 0.1 M $(CH_3)_4NI$ and 0.01% gelatine medium.

Table III. The effects of pH on half-wave potential, diffusion current and diffusion current constant

pH	Half-wave potential, $E_{1/2}$ V. vs. S.C.E.	Diffusion current, i_d μA	Diffusion current constant, I_d
3.75	−1.725	2.47	4.48
3.50	−1.727	2.43	4.36
3.35	−1.824	2.45	4.45
3.10	−1.870	2.45	4.45
3.00	−1.865	2.45	4.45
2.95	−1.865	2.47	4.50
2.80	−1.943	2.43	4.39
2.65	−1.945	2.47	4.53

(Y^{3+} ion: 0.611 mM in 0.1 M $LiClO_4$ and 0.01% gelatine medium.)

pH	Half-wave potential V. vs. S.C.E.		Diffusion current μA		Diffusion current constant, I_d
	$(E_1)_{1/2}$	$(E_2)_{1/2}$	i_{α_1}	i_{α_2}	
3.70	−1.737		3.42		3.40
3.55	−1.773		3.46		3.51
3.35	−1.801	−1.941	3.48	3.61	3.51
3.10	−1.826	−1.970	3.49	4.70	3.55
3.05	−1.834	−1.976	3.44	4.92	3.52
2.85	−1.852	−2.000	3.52	4.85	3.58
2.75	−1.864	−2.006	3.30	4.50	3.46
2.70	−1.878	−2.012	3.34	3.84	3.40

(Y^{3+} ion: 1.043 mM in 0.1 M $(CH_3)_4NI$ and 0.01% gelatine medium.)

plot. The results are shown in Table II. With decreasing pH, the value of the reciprocal slope of the reduction wave decreased. In a perchlorate solution, the electrode reaction was irreversible and at a pH less than 3.00, it indicated a tendency to approach to a three-electron reduction, provided that the reduction of the aquo yttrium complex ion is followed by amalgamation at electrode. This tendency was evidently observed in a halide midium. In a halide solution, at a pH less than 3.4, the electrode reaction of the first wave was irreversible, but it approached from irreversible to quasi-reversible and corresponded to three-electron change. The electrode reaction of the second wave was also irreversible and very anomalous.

The effects of pH on the reduction waves.—

The reduction waves were recorded at various pH from 4.00 to 2.60 under a certain condition. The results are shown in Table III.

Half-wave potentials of all reduction waves shifted to more negative potentials as pH decreased. It is considered that this was probably due to the increasing stability of hydroxo yttrium complex ion, which was formed by the hydrolysis of the aquo yttrium complex ion owing to the weak basicity of yttrium. This shift was always dependent only on the concentration of the free hydrogen ion. It was observed that at the same pH the half-wave potential was more negative in a perchlorate medium than in a halide medium under a given condition. The diffusion current of the reduction wave, i_d, was independent of pH from 3.4 to 2.6 and almost constant in a perchlorate medium. However it was observed that at a pH higher than 3.4, the diffusion current tended to decrease slightly. In the halide medium, at a pH higher than 3.6, there was the same tendency. The diffusion current of the second wave, in a halide medium, increased slightly with the decrease of the pH down to 3.1 and had a small maximum, but with the further decrease of the pH, i_d decreased gradually and anomalously. The diffusion current constant of the reduction wave, I_d, was constant at a pH from 3.4 to 2.6 in the perchlorate medium and that of the first wave in the halide medium, I_{d_1}, was also constant at a pH less than 3.6. The value of the diffusion current constant of the second wave, I_{d_2}, was irregular, and anomalous.

The effects of concentration of the yttrium ion on the reduction wave and the value of n, calculated from diffusion current constant.—The reduction waves were recorded in the range of concentration of yttrium ion 0.5 to 2.0 millimol./l. at a constant pH. The results are shown in Table IV.

The half-wave potential of the reduction wave shifted to more negative potentials slightly, with the increasing concentration at a constant pH. The diffusion current, i_d, was apparently proportional to the concentration of Y^{3+} ion in the perchlorate medium. The first diffusion current in the halide medium gave a similar result, but the second diffusion current was anomalous. The diffusion current constant of the reduction wave was constant, independent of the concentration of the yttrium ion and its average value was about 4.46 in 0.1 M $LiClO_4$ and about 3.51 in 0.1 M $(CH_3)_4NI$, while the theoretical value of the diffusion current constant is 4.34, which was calculated by assuming that the number of the electrons associated with the electrode reaction of the reduction wave, n, was three and the value of the diffusion coefficient of the yttrium ion D, 5.721×10^{-6} cm. sec^{-1} ($Y(ClO_4)_3$). It is considered that the average value observed in 0.1 M lithium perchlorate was almost equal to the theoretical one. The diffusion coefficient of the yttrium ion ($Y_2(SO_4)_3$) is 5.764×10^{-6} cm. sec^{-1} and the diffusion current constant was calculated to be 4.35. Although the average value of the diffusion current constant in the halide medium was smaller than the calculated one, it is also considered that the former was closer to the latter than the value which would be expected in the case of $n=2$. From these experimental values of the diffusion current constants, the number of the electrons involved in the electrode reaction, n, was calculated. The calculated value of n was 3.06 in the case of 0.1 M lithium perchlorate, where the perchlorate ion has no tendency to complex with cation. Therefore, the electrode reaction was of three-electron change. The calculated value of n for the first wave in the case of 0.1 M tetramethylammonium iodide, where iodide ion forms generally an aquo iodo

Table IV. The effects of concentration of yttrium ion on the half-wave potential, the diffusion current, and the diffusion current constant

Y^{3+} ion mM	Half-wave potential, $E_{1/2}$ V. vs. S.C.E.	Diffusion current, i_d μA	Diffusion current constant, I_d
0.332	−1.815	1.39	4.54
0.428	−1.819	1.69	4.41
0.917	−1.881	3.70	4.49
1.529	−1.900	5.89	4.40

(pH=3.00, $Y(ClO_4)_3$, in 0.1 M $LiClO_4$ and 0.01% gelatine medium.)

Y^{3+} ion mM	Half-wave potential V. vs. S.C.E.		Diffusion current μA		Diffusion current constant
	$(E_1)_{1/2}$	$(E_2)_{1/2}$	i_{d_1}	i_{d_2}	
0.723	−1.850	−1.990	2.40	3.97	3.47
1.043	−1.852	−2.000	3.52	4.85	3.58
1.984	−1.857	−2.005	6.65	5.34	3.50

(pH=2.90, $Y_2(SO_5)_3$, in 0.1 M $(CH_3)_4NI$ and 0.01% gelatine medium.)

complex ion, was about 2.60, which seemed apparently smaller than three, owing to the probable formation of the aquo iodo complex ion. The value of the diffusion current constant of the second wave was irregular because of the anomaly of the reduction wave.

Polarographic depolarizing action of the hydrolyzable aquo yttrium complex ion.—The aquo tripositive yttrium complex ion, $Y(H_2O)_x^{3+}$ ion, behaves as a weak acid, "yttrium acid," in aqueous solution, owing to its weak basicity. Generally, the half-wave potential of the reduction wave which is due to the deposition of hydrogen from a weak acid, HA, has the following well known equation in excess of an indifferent electrolyte,

$$E_{1/2} = -3RT/2F \cdot \ln i_d/2 + k = -0.089 \log i_d/2 + k$$

where k is a constant. Accordingly, it follows that the half-wave potential of a weak acid should shift to more negative potentials with the increasing acid concentration and $dE_{1/2}/d\log(HA) = -0.089$ V. In fact, as shown in Table IV, the half-wave potential of the reduction wave shifted slightly to more negative potentials with the increasing concentration at a certain pH. The value of $dE_{1/2}/d\log(Y(H_2O)_x^{3+})$ for the reduction wave calculated by extrapolation and given as follows: $dE_{1/2}/d\log(Y(H_2O)_x^{3+})$ equals -0.090 V. in perchlorate medium and -0.088 V. in an iodide medium. These values are considered to be equal to the theoretical value of -0.089 V. This fact indicates that the reduction wave of the aquo yttrium complex ion was the same as the reduction wave of the hydrogen ion from the yttrium acid, that is, the reduction wave was not due to the reduction of the yttrium ion, (Y^{3+} ion), itself, but was attributed to the deposition of hydrogen from the yttrium acid. It is also in accordance with the results of irreversibility and of a three-electron change in electrode reaction. Of course, the hydrogen ion from "the yttrium acid" was at first combined and not free. Since the hydrogen ion was produced by hydrolysis of the aquo yttrium complex ion as the yttrium acid, the following equation would be given:

$$Y(H_2O)_x^{3+} + yH_2O = Y(H_2O)_{x-y}(OH)_y^{(3-y)+} + yH_3O^+$$

where x is the coordination number of the tripositive yttrium ion (usually 6 in the case of a mononuclear yttrium ion), and y is the number of the hydrogen ion produced from the yttrium acid by hydrolysis at a certain pH. The yttrium acid $Y(H_2O)_x^{3+}$ has three hydrogen ions per one molecule to be released and reduced at electrode. Therefore the quantities of electricity to be exchanged by the hydrogen ions at dropping mercury electrode are just the same as those which tervalent yttrium ions require when reduced to metal. Actually, the reduction of the hydrogen ion from the aquo yttrium complex ion at dropping mercury electrode requires a large overpotential, but still the hydrogen ion seems to take an electron more easily than the aquo yttrium complex ion or the hydroxo yttrium complex ion does. Thus the electrode reaction was irreversible (or quasi-reversible in the halide medium) and three-electron change as described above. It is considered that the reduction proceeds for example as follows:

$$Y(H_2O)_x^{3+} + 3e^- \rightarrow 3/2H_2 + Y(H_2O)_3(OH)_3$$

The second wave in the halide medium, if it existed, was supposed also to be the hydrogen wave which is due to the reduction of the hydrogen ion from dissociation of water in the aquo halo complex. This wave was also irreversible. Consequently, it was concluded that the polarographic depolarising action of the aquo yttrium complex ion was indicated by the reduction of the hydrogen ion from the yttrium acid and not by the reduction of the yttrium ion itself to metal.

Conclusion

The logarithmic plot for the reduction wave of yttrium(III) indicated a straight line, independent of concentration of yttrium(III) at a pH less than 3.4. The value of its reciprocal slope approached the theoretical value for three-electron reduction with decreasing pH. The average value of the diffusion current constant was about 4.46 in 0.1 M lithium perchlorate and 3.60 in 0.1 M tetramethylammonium iodide from which the value of n was calculated to be 3, it being assumed that in the reduction of the aquo yttrium complex ion at dropping mercury electrode, amalgamation would follow. In short, the reduction wave was irreversible and three-electron reduction. However, it was found that the aquo yttrium complex ion behaved as a weak acid, "the yttrium acid", and that the reduction wave was due to the deposition of hydrogen from the hydrolyzable aquo yttrium complex ion as the weak acid. It is also supposed that the second reduction wave, if it appeared in the halide medium, was due to the deposition of hydrogen from dissociation of water in aquo halo yttrium complex formed during the first reduction step. This second reduction wave was irreversible and anomalous.

At pH 3.00, the half-wave potential of the reduction wave was -1.881 V. vs. S.C.E. for the concentration of Y^{3+} ion of 0.917 mM in 0.1 M lithium perchlorate and 0.01% gelatine medium.

The authors wish to thank Mr. Y. Masuda for his assistance in this experiment. Their thanks are also due to the Ministry of Education for its financial support of this research.

Department of Chemistry
Faculty of Science
Kyushu University
Hakozaki, Fukuoka

*Thermodynamic Studies on Cobalt Complexes. V. On the Solubility and the Thermal Dissociation of Aquopentamminecobalt(III) Nitrate and Bromide, and on the Thermodynamic Stability of Monoacidopentamminecobalt(III) Complexes**

By Motoshichi MORI and Ryokichi TSUCHIYA

(Received December 2, 1959)

In the preceding paper[1] the authors determined the standard free energies of formation of aquopentamminecobalt(III) chloride in the solid state and in aqueous solution. In the present study the standard free energies of formation of aquopentamminecobalt(III) nitrate and bromide in the solid state were determind by measuring their solubilities, and those of nitratopentamminecobalt(III) nitrate and bromopentamminecobalt(III) bromide in the solid state were determined by measuring their dissociation pressures.

On the basis of these data the thermodynamic stability of aquopentamminecobalt(III) chloride, nitrate and bromide, that of monoacidopentamminecobalt(III) complexes and that of their ions in aqueous solution were compared and discussed.

Experimental

Aquopentamminecobalt(III) nitrate was precipitated with nitric acid from an aqueous solution of its chloride. The bromide was prepared by the double decomposition of its chloride with ammoium bromide in aqueous solution.

Solubilities of these aquopentamminecobalt(III) complexes were obtained by analyzing the cobalt content in their saturated solutions by iodometry in the same manner as described in the second paper[2] of this series. The dissociation pressures of the complexes were measured with the same apparatus as described in the third paper[3].

Results and Calculation

Solubility of Aquopentamminecobalt(III) Nitrate.—The results obtained for aquopentamminecobalt(III) nitrate are listed in Table I.

As the activity coefficient of the compound was not known, it was assumed that it was approximately equal to that of hexamminecobalt(III) chloride[4] in relatively lower concentrations. When aquopentamminecobalt(III) nitrate is dissolved in water, the change is expressed by

$$[Co(NH_3)_5OH_2](NO_3)_2\ (s) = [Co(NH_3)_5OH_2]^{3+}(aq.\ a) + 3NO_3^-(aq.\ a)$$

If the solubility of the salt in molality and its mean activity coefficient are expressed by m and $\gamma_\pm$ respectively, the equilibrium constant

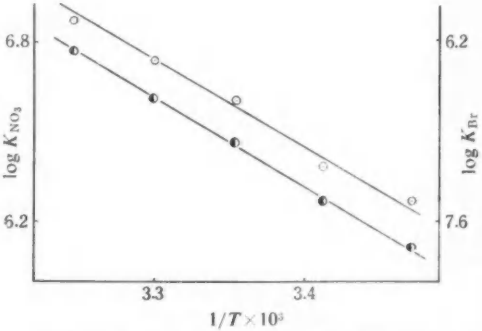

Fig. 1. The relationship between the equilibrium constant of the solution and the temperature.
-⊙-; aquopentamminecobalt(III) nitrate
-◑-; aquopentamminecobalt(III) bromide

* Read at the Symposium on Coordination Compounds of the Chemical Society of Japan, Fukuoka, Oct., 1959.

1) M. Mori, R. Tsuchiya and Y. Okano, This Bulletin, **32**, 1029 (1959).

2) M. Mori, R. Tsuchiya and Y. Okano, ibid., **32**, 462 (1959).

3) M. Mori and R. Tsuchiya, ibid., **32**, 467 (1959).

4) M. Mori and R. Tsuchiya, *J. Chem. Soc. Japan, Pure Chem. Sec.* (*Nippon Kagaku Zasshi*), **79**, 1164 (1958).

Table I. Equilibrium of solution for aquopentamminecobalt(III) nitrate

Temp. °C	Solubility in Molality m	$1/T\times10^3$	Mean activity coefficient $\gamma_\pm$	$K_{NO_3}\times10^6$	$\log K_{NO_3}$
15	0.07443	3.471	0.217	1.837	6.2642
20	0.08516	3.417	0.203	2.412	6.3823
25	0.1084	3.355	0.181	4.001	6.6022
30	0.1284	3.299	0.166	5.539	6.7434
35	0.1472	3.246	0.155	7.317	6.8643

of the solution, K_{NO_3}, is given by

$$K_{NO_3}=27m^4\gamma_\pm^4$$

The plots of its logarithm against the reciprocal of the absolute temperature are shown in Fig. 1, giving an almost straight line. Its equation computed by the method of least squares is

$$\log K_{NO_3}=3.884-2774/T$$

From this equation the heat of solution is obtained as $\Delta H=12.7$ kcal.

The standard free energy change of the solution, ΔG^0, is calculated by the following formula,

$$\Delta G^0=-RT\ln K_{NO_3}=12690-17.76T \qquad (1)$$

from which the values of the standard free energy change of the solution at 25°C, $\Delta G^0_{298}=7396$ cal. and its entropy change at 25°C, $\Delta S^0_{298}=17.76$ entropy unit are obtained.

On the other hand, the standard free energy of formation of the aquopentamminecobalt(III) ion in unit activity was calculated in the preceding paper[1] as

$$\Delta G_f{}^0=-192900+296.6T \qquad (2)$$

and that of the nitrate ion, NO_3^-, was obtained in the second paper[2] of this series as

$$\Delta G_f{}^0=-49370+77.03T \qquad (3)$$

From formulae 1, 2 and 3, the standard free energy of formation of aquopentamminecobalt-(III) nitrate in the solid state is calculated as

$$\Delta G_f{}^0=-353700+545.4T \qquad (4)$$

The value at 25°C is $\Delta G^0_{298}=-191100$ cal. and the heat of formation is $\Delta H=353.7$ kcal.

Dissociation Pressure of Aquopentamminecobalt(III) Nitrate.—The weight loss of aquopentamminecobalt(III) nitrate upon heating was followed by a thermobalance. The relationship between the weight loss and the temperature is plotted in Fig. 2, together with those of aquopentamminecobalt(III) bromide, chloride and perchlorate. It is found in this figure

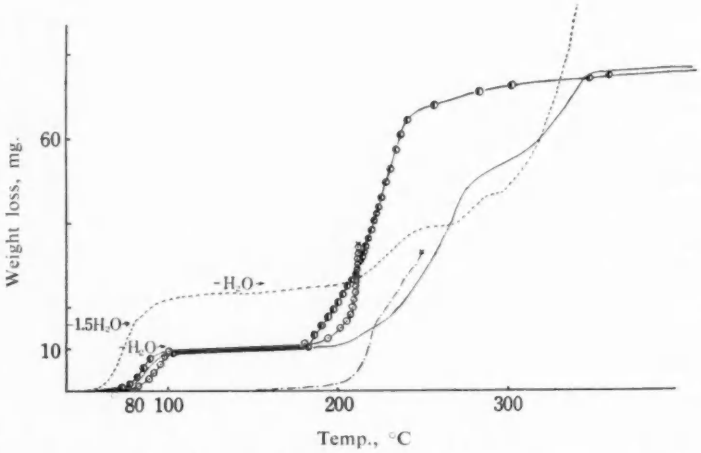

Fig. 2. The relationship between the weight loss and the temperature upon heating for several aquopentamminecobalt(III) complexes by a thermobalance.
-⊙-; aquopentamminecobalt(III) nitrate
-◐-; aquopentamminecobalt(III) bromide
——; aquopentamminecobalt(III) chloride
– – –; aquopentamminecobalt(III) sulfate hydrate
-·-·-; aquopentamminecobalt(III) perchlorate

that the nitrate decomposes upon heating at 80~100°C to nitratopentamminecobalt(III) nitrate according to the following equation;

$$[Co(NH_3)_5OH_2](NO_3)_3(s) = [Co(NH_3)_5NO_3](NO_3)_2(s) + H_2O(g)$$

The vapor pressure of water produced by this docomposition at 30~68°C, that is, the dissociation pressure of aquopentamminecobalt(III) nitrate measured is shown in Table II.

Table II. Dissociation pressure of aquopentamminecobalt(III) nitrate

Temp. °C	$1/T\times10^3$	Dissociation pressure mmHg	$\log p_{mm}$
30	3.299	1.35	0.1303
33	3.267	1.70	0.2305
39	3.204	2.19	0.3404
45	3.144	3.19	0.5038
52	3.076	4.09	0.6117
56	3.039	4.59	0.6618
62	2.984	6.34	0.8021
68	2.932	8.48	0.9284

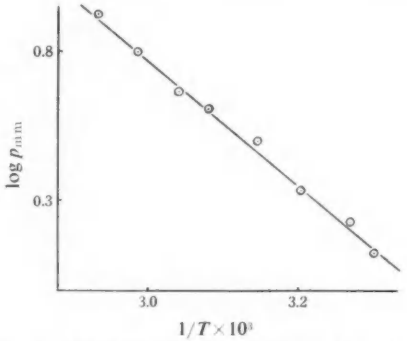

Fig. 3. The relationship between the dissociation pressure and the temperature for aquopentamminecobalt(III) nitrate.

The logarithm of the dissociation pressure, p_{mm}, is plotted against the reciprocal of the absolute temperature in Fig. 3, which shows an almost straight line. By the method of least squares the equation of this line is computed as follows:

$$\log p_{mm} = 7.045 - 2091/T$$

From this equation the heat of dissociation is obtained as $\Delta H = 9562$ cal. The standard free energy change of dissociation, ΔG^0, is given by the following formula,

$$\Delta G^0 = -RT \ln p_{atm} = 9562 - 19.05\,T \qquad (5)$$

from which the values of the free energy change of dissociation at 25°C, $\Delta G^0_{298} = 3885$ cal. and the entropy change of the solution at 25°C, $\Delta S^0_{298} = 19.05$ entropy unit are obtained.

The standard free energy of formation of aquopentamminecobalt(III) nitrate in the solid state was already calculated above as formula 4, and that of $H_2O(g)$ was obtained in the preceding paper[1] as

$$\Delta G_f^0 = -57800 + 10.61T \qquad (6)$$

By subtracting formula 6 from the sum of formulae 4 and 5, the standard free energy of formation of nitratopentamminecobalt(III) nitrate in the solid state is calculated as

$$\Delta G_f^0 = -286400 + 515.8T$$

The value at 25°C is

$$\Delta G^0_{f_{298}} = -132600 \text{ cal.} \qquad (7)$$

and the heat of formation is

$$\Delta H_{298} = -286.4 \text{ kcal.}$$

By using the solubility[5] and the heat of solution[6] of nitratopentamminecobalt(III) nitrate and by assuming that its activity coefficient is equal to that of bromopentamminecobalt(III) bromide[7], the free energy change of the solution of the former at 25°C is obtained as

$$G^0_{298} = 7347 \text{ cal.} \qquad (8)$$

Subtracting twice the standard free energy of formation of NO_3^-, -26.41 kcal.[8], from the sum of the formulae 7 and 8, the free energy of formation of nitratopentamminecobalt(III) ion in unit activity in aqueous solution is obtained as follows:

$$\Delta G^0_{f_{298}} = 72440 \text{ cal.}$$

If $\Delta H = -168.8$ kcal.[9] is used as the heat of formation of its ion, the relationship between the free energy of formation and temperature is expressed by

$$\Delta G_f^0 = -168800 + 323.3T$$

Solubility of Aquopentamminecobalt(III) Bromide.—The results obtained for aquopentamminecobalt(III) bromide are listed in Table III.

When the aquopentamminecobalt(III) bromide is dissolved in water, the change is expressed by

$$[Co(NH_3)_5OH_2]Br_3(s) = [Co(NH_3)_5OH_2]^{3+}(aq.\ a) + 3Br^-(aq.\ a)$$

5) J. N. Brönsted and A. Petersen, *J. Am. Chem. Soc.*, **43**, 2265 (1921).
6) A. Lamb and J. Simmons, ibid., **43**, 2188 (1921).
7) B. Adell, *Z. anorg. allgem. Chem.*, **246**, 303 (1941).
8) F. D. Rossini et al., "Selected Values of Chemical Thermodynamic Properties", United States Government Printing Office, Washington (1952), p. 53.
9) K. B. Yatsimirskii and L. L. Pankowa, *Zhur. Obshchei Khim.*, **18**, 2051 (1948); K. B. Yatsimirskii, "Thermochemie von Komplexverbindungen", Akademie-Verlag, Berlin (1956), p. 179.

Table III. Equilibrium of solution for aquopentamminecobalt(III) bromide

Temp. °C	Solubility in molality m	$1/T\times10^3$	Mean activity coefficient $\gamma\pm$	$K_{Br}\times10^7$	$\log K_{Br}$
15	0.03304	3.471	0.317	3.250	7.5119
20	0.03899	3.412	0.294	4.663	7.6686
25	0.04771	3.355	0.268	7.218	7.8584
30	0.05556	3.299	0.251	10.21	6.0091
35	0.06722	3.246	0.228	14.89	6.1730

The plots of the logarithm of the equilibrium constant, K_{Br}, against the reciprocal of the absolute temperature are shown in Fig. 1, giving a straight line. Its equation is calculated as follows

$$\log K_{Br} = 3.756 - 2953/T$$

The heat of solution is obtained as $\Delta H = 13.5$ kcal.

The free energy change of solution is given by the following formula,

$$\Delta G^0 = -RT\ln K_{Br} = 13510 - 17.18T \qquad (9)$$

and the value at 25°C is $\Delta G^0_{298} = 8385$ cal. and the entropy change at 25°C is $\Delta S^0_{298} = 17.18$ entropy unit.

As the standard free energy of formation of bromide ion, Br^-, was obtained in the second paper[2] of this series as

$$\Delta G_f{}^0 = -28900 + 14.51T \qquad (10)$$

that of aquopentamminecobalt(III) bromide in the solid state is obtained from formulae 2, 9 and 10 as:

$$\Delta G_f{}^0 = -293100 + 357.3T \qquad (11)$$

Its value at 25°C is $\Delta G^0_{f298} = -186600$ cal. and the heat of formation is $\Delta H = -293.1$ kcal.

Dissociation Pressure of Aquopentamminecobalt(III) Bromide. — Aquopentamminecobalt(III) bromide changes to bromopentamminecobalt(III) bromide upon heating at 75~95°C as

$$[Co(NH_3)_5OH_2]Br_3(s) = [Co(NH_3)_5Br]Br_2(s) + H_2O(g)$$

The vapor pressure of water produced by the above reaction at 18~32°C, that is, the dissociation pressure of aquopentamminecobalt(III) bromide is listed in Table IV.

Table IV. Dissociation pressure of aquopentamminecobalt(III) bromide

Temp. °C	$1/T\times10^3$	Dissociation pressure mmHg	$\log p_{mm}$
18	3.435	3.84	0.5843
20.5	3.406	5.23	0.7185
24	3.366	8.40	0.9243
26	3.343	9.35	0.9708
27	3.332	12.04	1.0806
29	3.310	14.75	1.1688
32	3.278	17.89	1.2526

The logarithm of the dissociation pressure, p_{mm}, is plotted against the reciprocal of the absolute temperature in Fig. 4, which shows an almost straight line. By the method of least squares the equation of this line is computed as:

$$\log p_{mm} = 15.65 - 4382/T$$

From this equation the heat of dissociation is obtained as $\Delta H = 9562$ cal.

The standard free energy change of dissociation is given by the formula,

$$\Delta G^0 = -RT\ln p_{atm} = 20040 - 58.41T \qquad (12)$$

from which the value at 25°C, $\Delta G^0_{298} = 2633$ cal. and the entropy change of solution at 25°C, $\Delta S^0_{298} = 58.41$ eutropy unit are obtained.

As the standard free energy of formation of aquopentamminecobalt(III) bromide in the solid state was already calculated above according to formula 11, that of bromopentamminecobalt(III) bromide in the solid state is calculated from formulae 6, 11 and 12 as

$$\Delta G^0 = -215300 + 288.2T$$

The value at 25°C is

$$\Delta G^0_{f298} = -129300 \text{ cal.} \qquad (13)$$

and the heat of formation is $\Delta H = -215.3$ kcal.

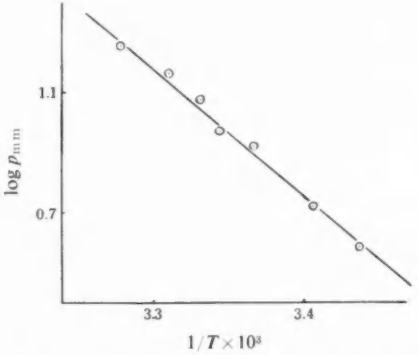

Fig. 4. The relationship between the dissociation pressure and the temperature for aquopentamminecobalt(III) bromide.

By using the solubility[5], the heat of solution[6] and the activity coefficient[7] of bromopentamminecobalt(III) bromide, the free energy change of solution of it at 25°C is obtained as

$$\Delta G^0_{298} = 8855 \text{ cal.} \quad (14)$$

Subtracting twice the free energy of formation of Br^-, $\Delta G^0_{298} = -24.57$ kcal.[10], from the sum of formulae 13 and 14, the free energy of formation of bromopentamminecobalt(III) ion in unit activity in aqueous solution is calculated as:

$$\Delta G^0_{f298} = -71340 \text{ cal.}$$

If $\Delta H = -146.8$ kcal.[11] is used as the heat of formation of its ion, the relationship between the free energy of formation and temperature is expressed by

$$\Delta G_f^0 = -146800 + 253.2T$$

Discussion

Thermodynamic Stability of Aquopentamminecobalt(III) Complexes. — The standard free energy of formation of aquopentamminecobalt-(III) nitrate and bromide in the solid state, the free energy of the solution and the heat of solution of them calculated above together with those of its chloride obtained in the preceding paper[1] and the radii of each anions are again shown in Table V.

According to these values, it will be seen that the thermodynamic stability of these three aquopentamminecobalt(III) complexes in the solid state and aqueous solution decreases in the following order,

$$[Co(NH_3)_5OH_2]Cl_3 > [Co(NH_3)_5OH_2](NO_3)_3 > [Co(NH_3)_5OH_2]Br_3$$

This order is in good agreement with the decreasing order of the thermodynamic stability of hexamminecobalt(III) complexes,

$$[Co(NH_3)_6]Cl_3 > [Co(NH_3)_6](NO_3)_3 > [Co(NH_3)_6]Br_3$$

reported as in the second paper[2] of this series.

The heat of solution of these aquopentamminecobalt(III) complexes increases in the order, chloride < nitrate < bromide, and increases with the radius of anion as shown in Table V. It is generally known[12] that for simple salts of which the radius of the cation is 2.4 Å, the heat of solution increases with the radius of the anion. It is concluded that this relationship is also valid for these aquopentamminecobalt(III) complexes, the radius of the cation, $[Co(NH_3)_5OH_2]^{3+}$, being 2.4 Å.

The solubility of these complexes decreases in the order, chloride > nitrate > bromide. This may be due to the fact that the radius of anions becomes larger and consequently the ionic character of the bond between the complex cation and anion of the salts diminishes in the order, chloride > nitrate > bromide.

Thermodynamic Stability of Monoacidopentamminecobalt(III) Complexes. — The standard free energy of formation of nitratopentamminecobalt(III) nitrate and bromopentamminecobalt-(III) bromide in the solid state obtained above, that of chloropentamminecobalt(III) chloride obtained in the third paper[3] of this series and that of chloropentamminecobalt(III) nitrate and bromide, nitratopentamminecobalt(III) chloride and bromopentamminecobalt(III) chloride and nitrate calculated from the solubility[5] and the heat of solution[9] in the literature are summarized in Table VI.

Table V. Standard free energy of formation, free energy of solution and heat of solution of aquopentamminecobalt(III) chloride, nitrate and bromide, and the radii of each anions

Complexes	Free energy of formation kcal.	Free energy of solution cal.	Heat of solution kcal.	Radius of anion, Å
$[Co(NH_3)_5OH_2]Cl_3$	−203.0	4488	8.75	1.81
$[Co(NH_3)_5OH_2](NO_3)_3$	−191.1	7396	12.7	1.89
$[Co(NH_3)_5OH_2]Br_3$	−186.6	8385	13.5	1.96

Table VI. Standard free energy of formation of monoacidopentamminecobalt(III) complexes

Complexes	ΔG^0_{298}, kcal.	Complexes	ΔG^0_{298}, kcal.
$[Co(NH_3)_5Cl]Cl_2$	−144.9	$[Co(NH_3)_5NO_3]Cl_2$	−141.4
$[Co(NH_3)_5Cl](NO_3)_2$	−133.7	$[Co(NH_3)_5NO_3](NO_3)_2$	−132.6
$[Co(NH_3)_5Cl]Br_2$	−131.7		
		$[Co(NH_3)_5Br]Cl_2$	−142.1
		$[Co(NH_3)_5Br](NO_3)_2$	−131.8
		$[Co(NH_3)_5Br]Br_2$	−129.3

10) G. Jones and S. Bäckström, *J. Am. Chem. Soc.*, **56**, 1524 (1934).
11) K. B. Yatsimirskii, "Thermochemie von Komplexverbindungen", Akademie-Verlag, Berlin (1956), p. 178.
12) K. B. Yatsimirskii, "Thermochemie von Komplexverbindungen", Akademie-Verlag, Berlin (1956), p. 45.

On the basis of these values, it is found that the thermodynamic stability of these complexes in the solid state decreases in the following order:

$$\begin{array}{ccccc} [Co(NH_3)_5Cl]Cl_2 & > & [Co(NH_3)_5Cl](NO_3)_2 & > & [Co(NH_3)_5Cl]Br_2 \\ \vee & & \vee & & \\ [Co(NH_3)_5NO_3]Cl_2 & > & [Co(NH_3)_5NO_3](NO_3)_2 & & \vee \\ \wedge & & \vee & & \\ [Co(NH_3)_5Br]Cl_2 & > & [Co(NH_3)_5Br](NO_3)_2 & > & [Co(NH_3)_5Br]Br_2 \end{array}$$

The levels of the standard free energy of formation for these complexes are diagrammatized in Fig. 5. From these figures it is found that the decrease of the thermodynamic stability of these monoacidopentamminecobalt(III) complexes is far less for the case when Cl^- in the inner sphere is replaced by NO_3^- or Br^- than for the case when Cl^- in the outer sphere is replaced by NO_3^- or Br^-. This fact might be partly interpreted by the increase of the radius of the anion in the outer sphere in the order, $Cl^- < NO_3^- < Br^-$.

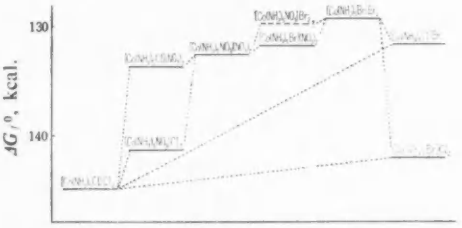

Fig. 5. The levels of the standard free energy of formation for several monoacidopentamminecobalt(III) complexes in the solid state.

Thermodynamic Stability of Monoacidopentamminecobalt(III) Ions. — From the standard free energies of formation of nitratopentamminecobalt(III) and bromopentamminecobalt(III) ions obtained above, and those of chloropentamminecobalt(III) ion[1], nitropentamminecobalt(III) ion[13], sulfatopentamminecobalt(III) ion[6], aquopentamminecobalt(III) ion[1] and hexamminecobalt(III) ion[13], the free energy change for the following substitution reactions are calculated:

$$[Co(NH_3)_5OH_2]^{2+} + NO_2^- = [Co(NH_3)_5NO_2]^{2+} + H_2O(l) \qquad \Delta G^0_{298} = -52590 \text{ cal.}$$

$$[Co(NH_3)_5OH_2]^{3+} + SO_4^{--} = [Co(NH_3)_5SO_4]^+ + H_2O(l) \qquad -6750$$

$$[Co(NH_3)_5OH_2]^{3+} + NH_3\ (aq.) = [Co(NH_3)_5NH_3]^{3+} + H_2O(l) \qquad -320$$

$$[Co(NH_3)_5OH_2]^{3+} + Br^- = [Co(NH_3)_5Br]^{2+} + H_2O(l) \qquad 1040$$

$$[Co(NH_3)_5OH_2]^{3+} + NO_3^- = [Co(NH_3)_5NO_3]^{2+} + H_2O(l) \qquad 1780$$

$$[Co(NH_3)_5OH_2]^{3+} + Cl^- = [Co(NH_3)_5Cl]^{2+} + H_2O(l) \qquad 3825$$

From these values it is concluded that the thermodynamic stability decreases in the order:

$$[Co(NH_3)_5NO_2]^{2+} > [Co(NH_3)_5SO_4]^+ > [Co(NH_3)_6]^{3+} > [Co(NH_3)_5OH_2]^{3+} > [Co(NH_3)_5Br]^{2+} > [Co(NO_3)_5NO_3]^{2+} > [Co(NH_3)_5Cl]^{2+}$$

This order is in good agreement with the spectrochemical series[14] with the exception of $[Co(NH_3)_5SO_4]^+$ and $[Co(NH_3)_5Br]^{2+}$.

Summary

1. By measuring the solubility and the dissociation pressure of aquopentamminecobalt(III) nitrate, the standard free energy of formation of the salt and that of nitratopentamminecobalt(III) nitrate produced by the decomposition of the former in the solid state were determined.

2. In the same way the standard free energy of formation of aquopentamminecobalt(III) bromide and that of bromopentamminecobalt(III) bromide were determined.

3. On the basis of these results, the thermodynamic stabilities of three aquopentamminecobalt(III) complexes, several monoacidopentamminecobalt(III) complexes and their ions were determined.

Department of Chemistry
Faculty of Science
Kanazawa University
Kanazawa

13) A. B. Lamb and A. T. Larson, *J. Am. Chem. Soc.*, **42**, 2038 (1920).

14) Y. Shimura and R. Tsuchida, This Bulletin, **29**, 311 (1956).

Rotatory Dispersion of Metallic Co-ordination Compounds. II. Absorption Spectra and Rotatory Dispersion of Cobalt(III) Complexes of EDTA

By Jinsai HIDAKA, Yoichi SHIMURA and Ryutaro TSUCHIDA

(Received November 25, 1959)

It is well known that rotatory dispersion is closely related to the absorption band, and there are many reports[1] concerning the rotatory dispersion of some metallic complex ions but very few on the relation between the partial "inversive dispersion" and the absorption band. In the former paper of this series[2], anomalous rotatory dispersion in the visible and ultraviolet region has been measured for the cobalt(III) ethylenediamine complexes, analyzed in partial "inversive dispersion" and discussed in relation to their absorption band. Furthermore, a possibility of determining the absolute configuration of the complex ion has been suggested from the viewpoint of the inversive dispersion curve in the wavelength region of the first absorption band.

In the present paper, the anomalous rotatory dispersion of D-$Na_2[Co(edta)NO_2]\cdot 3H_2O$, D-$K[Co(edta)]\cdot 3H_2O$ and D-$K_2[Co(edta)Cl]\cdot 3H_2O$, which were recently resolved by Dwyer et al.[3,4], and D-*cis*-$[Co\,en_2(NO_2)_2]I$ will be studied in the visible and ultraviolet region in the same way as was done in the former report[2].

Experimental

Measurements.—The rotatory dispersion measurements were carried out with a Rudolph photoelectric spectropolarimeter, Model 200S-80. The measurements were made in the region from 700 mμ (42.8×10^{13}/sec.) to 365 mμ (82×10^{13}/sec.) using mainly the lines of the mercury spectrum. A xenon or a tungsten lamp was also used when necessary. The measurements of D-$[Co(edta)NO_2]^{2-}$ and D-$[Co(edta)]^-$ were made in aqueous solutions of $1/5\times10^{-2}$ F, $1/10^{-2}$ F, $1/2\times10^{-2}$ F, and $1/4\times10^{-2}$ F. The solvent employed for D-$[Co(edta)Cl]^{2-}$ was hydrochloric acid (1 : 1) because this complex ion is not so stable in an aqueous solution that it undergoes aquotization rapidly. The concentration of the solution was $1/5\times10^{-2}$ F or $1/10^{-2}$ F, and the measurements were made as rapidly as possible after preparation of the solution to reduce the reaction of the complex ion with weter to the minimum. The concentration of D-*cis*-$[Co\,en_2(NO_2)_2]^+$ was $1/10^{-2}$ F, $1/3\times10^{-3}$ F and $1/6\times10^{-3}$ F in aqueous solutions. The absorption measurements were made by a Beckman DU spectrophotometer. All measurements were made at room temperature.

Material.—Potassium-(ethylenediaminetetraacetato) cobalt(III) trihydrate, $K[Co(edta)]\cdot 3H_2O$, was prepared in violet crystals and resolved by the method of Dwyer et al[3]. Optically active complex ions, D-$[Co(edta)]^-$, were precipitated as a more sparingly soluble salt with D-$[Co\,en_3]^{3+}$.[5] The preparation and resolution of disodium nitro-(ethylenediaminetetraacetato) cobalt(III) trihydrate, $Na_2[Co(edta)NO_2]\cdot 3H_2O$, and dipotassium chloro-(ethylenediaminetetraacetato) cobalt(III) trihydrate, $K_2[Co(edta)Cl]\cdot 3H_2O$, were also made by the direction of Dwyer et al.[4] The D-isomer of both the complex ions was precipitated as a more sparingly soluble salt with L-*cis*-$[Co\,en_2(NO_2)_2]^+$. *cis*-Dinitro-bis-(ethylenediamine) cobalt(III) iodide was prepared and resolved by the method of Werner[6]. The D-isomer was precipitated as a more sparingly soluble salt with *d*-camphorsulphonic acid. These optically active complex ions gave positive value of optical rotation at green lines of a mercury spectrum, and were denoted as a D-isomer.

Results and Discussion

The rotatory dispersion and the absorption curve of D-$Na_2[Co(edta)NO_2]\cdot 3H_2O$, D-$K[Co(edta)]\cdot 3H_2O$, D-$K_2[Co(edta)Cl]\cdot 3H_2O$ are shown in Figs. 1~3. The structures of these complex ions were well established by Dwyer[1] and other workers[7]. The observed curves were analyzed on the basis of the following consideration. It is assumed that the observed curve is the superposition of the partial inversive dispersion[8] and the tail of a total dispersion which has its inversion center in the far ultraviolet

1) W. Kuhn and K. Bein, *Z. physik. Chem.*, **B24**, 355 (1943); W. Kuhn and K. Bein, *Z. anorg. allg. Chem.*, **216**, 321 (1934); J.-P. Mathieu, *J. chim. phys.*, **33**, 78 (1936); J.-P. Mathieu, *Bull. soc. chim. France*, [5] **3**, 476 (1936); R. Tsuchida, *J. Chem. Soc. Japan (Nippon Kagaku Zasshi)*, **58**, 621 (1937); M. Kobayashi, ibid., **64**, 684 (1943).

2) J. Hidaka, S. Yamada and R. Tsuchida, This Bulletin, **31**, 921 (1958).

3) F. P. Dwyer, E. C. Gyarfas and D. P. Mellor, *J. Phys. Chem.*, **59**, 296 (1955).

4) F. P. Dwyer and F. L. Garvan, *J. Am. Chem. Soc.*, **80**, 4480 (1958).

5) A. Werner, *Ber.*, **45**, 121 (1912).

6) A. Werner, *Ber.*, **44**, 2450 (1911).

7) D. H. Bush and J. C. Bailar, Jr., *J. Am. Chem. Soc.*, **75**, 4576 (1953); G. Schwarzenbach, *Helv. Chim. Acta*, **32**, 839 (1949); M. L. Morris and D. H. Bush, *J. Am. Chem. Soc.*, **78**, 5178 (1956).

8) J.-P. Mathieu, *Compt. rend.*, **199**, 278 (1934); J.-P. Mathieu, ibid., **201**, 1183 (1935); J.-P. Mathieu, *Bull. soc. chim. France*, [5] **3**, 476 (1936),

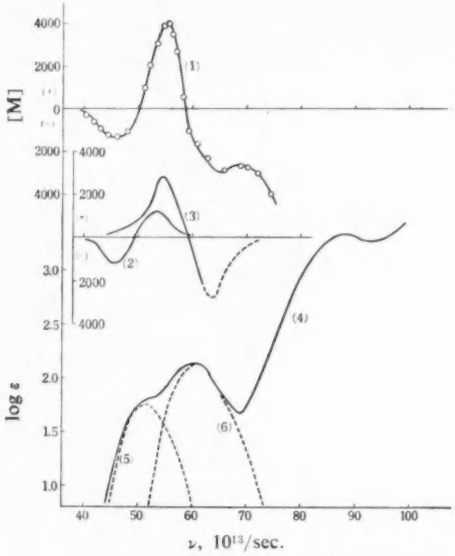

Fig. 1. Rotatory dispersion and absorption of D-$Na_2[Co(edta)NO_2]\cdot 3H_2O$: 1, rotatory dispersion curve; 2—3, curve analyses of the rotatory dispersion curve; 4, absorption curve; 5—6, curve analyses of the first absorption band.

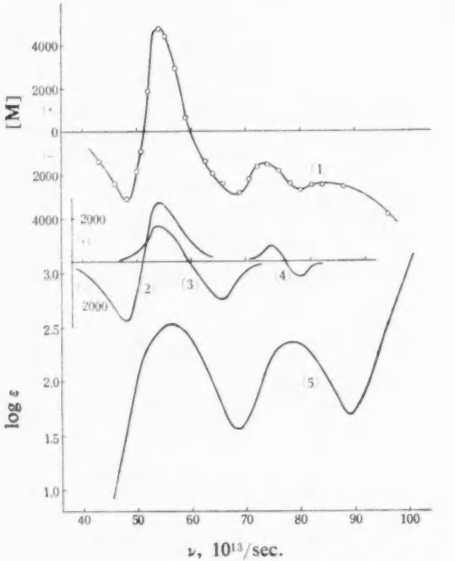

Fig. 2. Rotatory dispersion and absorption of D-$K[Co(edta)]\cdot 3H_2O$: 1, rotatory dispersion curve; 2—4, curve analyses of the rotatory dispersion curve; 5, absorption curve.

region. For the analysis, the method of successive approximation was employed.

D-$Na_2[Co(edta)NO_2]\cdot 3H_2O$. As is seen in Fig. 1, the observed curve indicates that total the dispersion curve is apparently displaced to the negative side on the whole. In the analysis of the curve, therefore it is assumed that the observed curve is the superposition of the partial dispersion in the visible region and the negative tail of a total dispersion concerned in the far ultraviolet region. The shape of the rotatory dispersion curve suggests that an overlapping of two inversive dispersions occurred in its first absorption band. As a result of tentative curve analysis, it was found that two inversive dispersions overlapped with each other in the visible region. The sign of the Cotton effect concerned in the first inversive dispersion is negative. Thus the molar rotation changes from negative (long wavelength side) to positive values (short wavelength side) at about 49 ($\times 10^{13}$/sec.). On the other hand, the second inversive dispersion appears at about 59 ($\times 10^{13}$/sec.) and shows a positive Cotton effect. The magnituds of these two partial dispersions is found to be of the same order. The two inversive dispersions may be regarded as corresponding to the absorption band in these wavelength regions. As is shown in Fig. 1, the first absorption band of $[Co(edta)NO_2]^{2-}$ distinctly splits into two components. The Ia-component is at 60.4 ($\times 10^{13}$/sec.) in the shorter wavelength as compared with the first band of $[Co(edta)]^-$, and the sub-component, Ib, is at 51.4 ($\times 10^{13}$/sec.) in the long wavelength side of the first band of $[Co(edta)]^-$[9]. It has been reported that the center of the inversive rotatory dispersion was almost always in the longer wavelength region in comparison with the position of the absorption maximum[10]. In this respect, the result of the present measurements is in good agreement.

D-$K[Co(edta)]\cdot 3H_2O$. The rotatory dispersion curve of D-$[Co(edta)]^-$ is shown in Fig. 2. The total dispersion curve is apparently displaced to the negative side. This complex ion also shows two inversive dispersions in the region of the first absorption band. The one, with its center at about 51.5 ($\times 10^{13}$/sec.), has a negative Cotton effect and the other, with its center at 61.0 ($\times 10^{13}$/sec.), a positive Cotton effect. As is seen in Fig. 2, the first absorption band of this complex does not split. Judging from the symmetry of the complex ion, however, it is expected that its first absorption band splits into two component

9) Y. Shimura and R. Tsuchida, This Bulletin, **29**, 643 (1956).
10) Y. Shimura, ibid., **31**, 315 (1957).

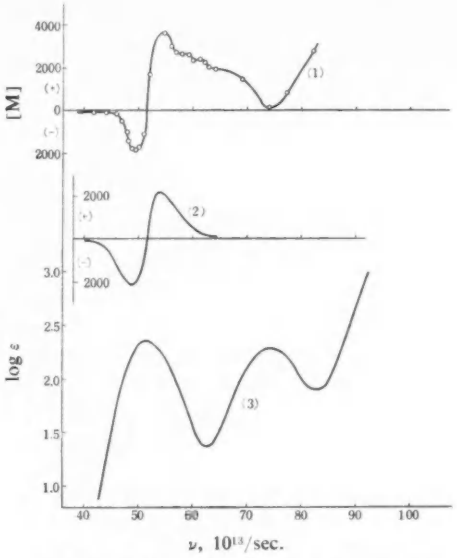

Fig. 3. Rotatory dispersion and absorption of D-K_2[Co(edta)Cl]·$3H_2O$: 1, rotatory dispersion curve; 2, curve analyses of the rotatory dispersion curve; 3, absorption curve; first band, ν_{max}=ca. 52.0 ($\log \varepsilon_{max}$=2.35); second band, ca. 74.0 (2.28).

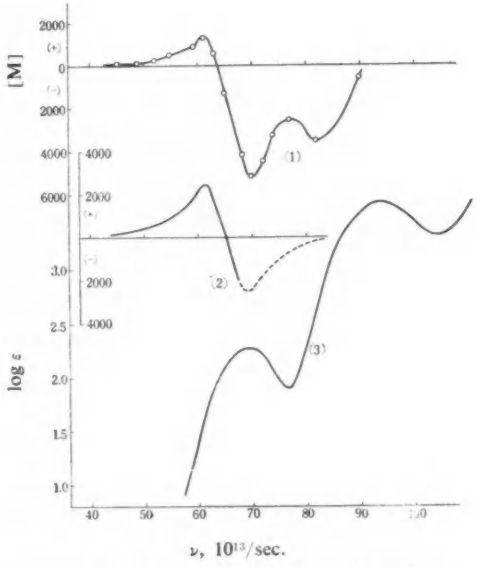

Fig. 4. Rotatory dispersion and absorption of D-*cis*-[Co $en_2(NO_2)_2$]I: 1, rotatory dispersion curve; 2, curve analyses of the rotatory dispersion curve; 3, absorption curve.

absorptions, Ia and Ib. It is considered, therefore, that the two inversive dispersions obtained above probably correspond to the two components of the first absorption band. The optical activity is due to the arrangement of the groups about the central cobalt atom, so the rotatory dispersion curve of complexes of similar configuration should have the same chracteristic. Therefore, the similarity of the rotatory dispersion curve of D-[Co(edta)-NO_2]$^{2-}$ and D-[Co(edta)]$^-$ complexes, in the region of the first absorption band, shows that the two complex ions have a similar configuration. There is another small inversive dispersion with its center at about 77 ($\times 10^{13}$/sec.), which probably belongs to the second absorption band.

D-K_2[Co(edta)Cl]·$3H_2O$. Contrary to the preceding two complexes, the observed curve is apparently displaced to the positive side by the tail of total dispersion from the far ultraviolet side. The result of the measurement and the analysis is shown in Fig. 3. According to the analysis, the inversive dispersion of the first absorption band occurred at 51.8 ($\times 10^{13}$/sec.), which has a negative Cotton effect. In the shorter wavelength side of the first absorption band at about 57~63 ($\times 10^{13}$/sec.), there is a small hump in the rotatory dispersion curve. This fact shows that the first absorption band has a sub-component in this region, although no evidence is observed in the absorption curve. Because this complex is not so stable toward aquotization in solutions, it was not possible to measure the rotation in the region of a wavelength shorter than 82.5 ($\times 10^{13}$/sec.). However, as regards the behavior of the short wavelength end of the observed curve, it may be considered that an inversive dispersion which belongs to the second absorption band also contributes to the observed rotatory dispersion curve. From the results mentioned above for the cobalt(III) complexes of EDTA, it will easily be understood that the analysis of the rotatory dispersion curve is very useful for the study of the absorption bands, especially for the study of their splitting and overlapping.

D-*cis*-[Co $en_2(NO_2)_2$]I. In the region of the first absorption band, as is shown in Fig. 4, there is an inversive dispersion with its center at about 65.5 ($\times 10^{13}$/sec.), which has a positive Cotton effect, and this result coincides with Methieu's[11]. The behavior of the dispersion curve, that is that the observed curve has apparently one inversive dispersion in the region of the first band, resembles that of D-*cis*-[Coen_2Cl NO_2]$^+$ [2].

11) J.-P. Mathieu, *Bull. soc. chim. France*, [5] 3, 487 (1936).

This fact is considered as follows. The two components of the first absorption band, which have the positive sign of the Cotton effect, are so close together that a complete overlapping of two inversive dispersions occurred. In the shorter wavelength region, the observed value of the molar rotation is smaller. Judging from the position of the absorption maximum, it may be suggested that there begins in this region an inversive dispersion which belongs to the nitro-specific absorption band too. Similarly, on the observed curve of D-$[Co(edta)NO_2]^{2-}$, the increase of molar rotation for the negative side in the shorter wavelength end may be regarded as originating from the nitro-specific absorption band.

Summary

The rotatory dispersion measurements have been made for D-$Na_2[Co(edta)NO_2]\cdot 3H_2O$, D-$K[Co(edta)]\cdot 3H_2O$, D-$K_2[Co(edta)Cl]\cdot 3H_2O$ and D-*cis*-$[Co\,en_2(NO_2)_2]I$. On the basis of these measurements, the relation of the splitting of the first absorption band with the so-called anomalous rotatory dispersion has been discussed. In the anomalous rotatory dispersion of D-$[Co(edta)NO_2]^{2-}$, there appear two inversive dispersions due to the component absorption, Ia and Ib, of the split first absorption band. Similarly considered, it has been shown that the first absorption band of $[Co(edta)]^-$ or $[Co(edta)Cl]^{2-}$ may have two component absorptions in accordance with the behavior of its rotatory dispersion curve.

The present authors wish to thank the Ministry of Education for a grant.

Department of Chemistry
Faculty of Science
Osaka University
Kita-ku, Osaka

Ultraviolet Absorption Spectra of Aqueous Solutions and Single Crystals of Thioacetamide and Thiourea

By Haruo Hosoya, Jiro Tanaka and Saburo Nagakura

(Received December 15, 1959)

In a series of previous papers by Nagakura and Tanaka[1-4], electronic absorption spectra of various molecules, in which electron donating and accepting groups are connected with each other directly or through a bridge of conjugated double bonds, were discussed from both experimental and theoretical points of view. In these studies, special attention was paid to absorption bands which can be ascribed to neither of the component groups but to the interaction between the electron donating and accepting groups within a molecule. Since the transition corresponding to this kind of absorption band is apparently accompanied by a great amount of electron transfer from the electron donor to the acceptor, it may be called an intramolecular charge-transfer absorption by analogy with intermolecular cases developed by Mulliken[5]. From both experimental results of polarized ultraviolet absorption spectra and theoretical studies based on the LCMO treatment, it was actually shown that the intramolecular charge-transfer absorption can be found with formamide ($O{=}CH{-}NH_2$), acrolein ($H_2C{=}CH{-}CH{=}O$), nitramide ($H_2N{-}NO_2$), nitrobenzene ($C_6H_5{-}NO_2$), benzoic acid ($C_6H_5{-}COOH$), *p*-nitroaniline ($O_2N{-}C_6H_4{-}NH_2$) and other similar molecules. For example, the strong 370 mμ band of *p*-nitroaniline could reasonably be interpreted as an intramolecular charge-transfer absorption, in view of the fact that the direction of the transition moment associated with the band is parallel to the molecular axis connecting the two nitrogen atoms. A similar interpretation was applied to the 237 mμ band of aniline by Longuet-Higgins and Murrell[6].

1) S. Nagakura and J. Tanaka, *J. Chem. Phys.*, **22**, 236 (1954).
2) S. Nagakura, ibid., **23**, 1441 (1955); *Molecular Physics*, to be published.
3) J. Tanaka, S. Nagakura and M. Kobayashi, *J. Chem. Phys.*, **24**, 311 (1956); J. Tanaka and S. Nagakura, ibid., **24**, 1274 (1956).
4) J. Tanaka, *J. Chem. Soc. Japan, Pure Chem. Sec.* (*Nippon Kagaku Zasshi*), **78**, 1636 (1957); **79**, 1373 (1958).
5) R. S. Mulliken, *J. Phys. Chem.*, **56**, 801 (1952) and other papers.
6) H. C. Longuet-Higgins and J. N. Murrell, *Proc. Phys. Soc.*, **A68**, 601 (1955); J. N. Murrell, ibid., **A68**, 969 (1955).

In the present paper, electronic absorption spectra of thioacetamide ($S{=}C\langle^{CH_3}_{NH_2}$) and thiourea ($S{=}C\langle^{NH_2}_{NH_2}$) are studied as a subject of much interest from the aspect of intramolecular charge-transfer absorption. In these molecules, the thiocarbonyl (C=S) and amino (NH_2) groups are electron acceptor and donor, respectively, and the appearance of the intramolecular charge-transfer absorption may be expected. Especially thiourea seems to be most suitable for studying the effect of so-called cross-conjugation upon the charge-transfer absorption. This is because this molecule shows absorption bands at relatively longer wavelengths than the similar compounds, say urea ($O{=}C\langle^{NH_2}_{NH_2}$), do. By the way, the absorption bands of urea appear at wavelengths below 190 mμ and therefore are difficult to be measured with spectrophotometric instruments usually available at present.

Katagiri et al. measured absorption spectra of thioacetamide and thiourea in ethereal solution and pointed out that the weak band of thioacetamide at 318 mμ is conceivably ascribed to the $n\rightarrow\pi^*$ transition[7]. However, the assignment of the $\pi\rightarrow\pi^*$ transition bands of these two molecules has never been made. In the present paper, it is undertaken to obtain a definite conclusion on the assignment of the absorption bands by measuring the polarized ultraviolet absorption with their crystals and, moreover, by combining the experimental results with theoretical consideration based on the semi-empirical molecular orbital method including configuration interaction.

As is well known, thioacetone ($(H_3C)_2C{=}S$) can not exist as a stable monomer but usually as a trimer[8]. Therefore, it is difficult to obtain peak wavelengths of the absorption spectrum pertinent to the C=S bond, which is one of the important and basic data indispensable for the present study. In order to remove this difficulty, we have undertaken to measure the absorption spectrum of the conjugate acid of thioacetamide ($S{=}C\langle^{\overset{+}{N}H_3}_{CH_3}$) which is isoelectronic with thioacetone. In this connection, the equilibrium between thioacetamide and a proton is studied in detail and its equilibrium constant is obtained by means of the spectrophotometric method.

7) S. Katagiri, Y. Amako and H. Azumi, Presented at the Symposium on Structural Chemistry, Kyoto, October, 1958.
8) E. Baumann and E. Fromm, *Ber.*, **22**, 2593 (1889).
9) A. Bernthsen, *Ann.*, **192**, 47 (1878).
10) A. Hantzsch, ibid., **296**, 93 (1897).

Experimental

Materials.—Commercial thioacetamide of G.R. grade was purified by repeating recrystallization from ethyl ether, m. p. 109.5~110.5°C (uncorrected). The reported value is 107.5~108.5°C[9]. After the purification it was subjected to spectrophotometric measurements as soon as possible, because it has a tendency to decompose easily. Commercial thiourea of G.R. grade was recrystallized from ethanol, m. p. 177~178.5°C (uncorrected). The reported value is 180°C[10]. Hydrochloric acid and sulfuric acid, which are both of G.R. grade, were used as solvents without further purification.

Measurement. — *Ultraviolet Absorption Spectra of Solutions.* — A Cary recording spectrophotometer model 14 M was used for the ultraviolet absorption measurements of solutions. Measurements were usually carried out at room temperature (20~25°C), the quartz cell with a stopper of 1 cm. light path being used. If necessary, however, the temperature of the absorption cell was kept constant by circulating water of a desired constant temperature through the cell jacket.

Ultraviolet Absorption Spectra of Crystals. — An ultraviolet microscope equipped with a Hitachi model EPU monochromator and a polarizer of Rochon prism type was used for the measurement of polarized ultraviolet absorption in the wavelength region of 220~650 mμ[11]. Crystalline axes and planes were identified by the aid of X-ray rotation photographs and of optical examination with a polarizing microscope.

The single crystal of thioacetamide suitable for the measurement of polarized ultraviolet absorption was prepared by sublimation. The crystal showed a well developed (001) cleavage plane and was about 1×2 mm. in size and about 1~2 μ in thickness. The single crystal of thiourea was prepared directly on a quartz plate by dipping it into the ethanol solution and by evaporating the solvent slowly. Two kinds of crystals were obtained, one of which was hexagonal and the other rectangular. The latter was used for the spectroscopic measurement. Its developed plane was shown to be (110) by X-ray rotation photographs.

Experimental Results

Absorption Spectra of Thioacetamide in Aqueous and Hydrochloric Acid Solutions. — The results obtained with the aqueous and hydrochloric acid solutions of thioacetamide are summarized in Table I and Figs. 1 and 2. The ultraviolet absorption spectrum of thioacetamide in aqueous solution apparently consists of three bands. Two of them, which appear at 261 and 210 mμ, are fairly strong and may reasonably be attributed to allowed $\pi\rightarrow\pi^*$ transitions. On the other hand, the longest wavelength band at 318 mμ, whose molar extinction coefficient is only 60, may be regarded as an $n\rightarrow\pi^*$ transition band.

11) For the detail of the instrument, see Ref. 4.

Table I. Absorption spectra of thioacetamide and thiourea in aqueous solutions

a) Thioacetamide

λ_{max} Obs.	λ_{max} Calc.	log ε_{max}* Obs.	f Obs.	f Calc.	Direction of transition moment (Calc.)	Assignment
210 mμ (5.90 eV)	167 mμ (7.44 eV)	3.66	~0.13	0.198	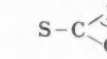	$E_1 \rightarrow E_3$
261 (4.75)	260 (4.77)	4.08	0.216	0.515	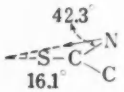	$E_1 \rightarrow E_2$
318 shoulder (3.90)	—	1.8	—	—	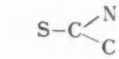	$n \rightarrow \pi^*$

b) Thiourea

195 mμ (6.36 eV)	212 mμ (5.84 eV)	4.11	>0.3	0.600	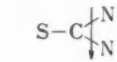	$W_1 \rightarrow W_4$
236 (5.25)	225 (5.51)	4.08	0.227	0.529	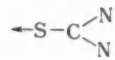	$W_1 \rightarrow W_2$
?	136 (9.11)	?	?	0.025	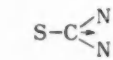	$W_1 \rightarrow W_3$

* ε_{max} is the molar extinction coefficient at the absorption peak.

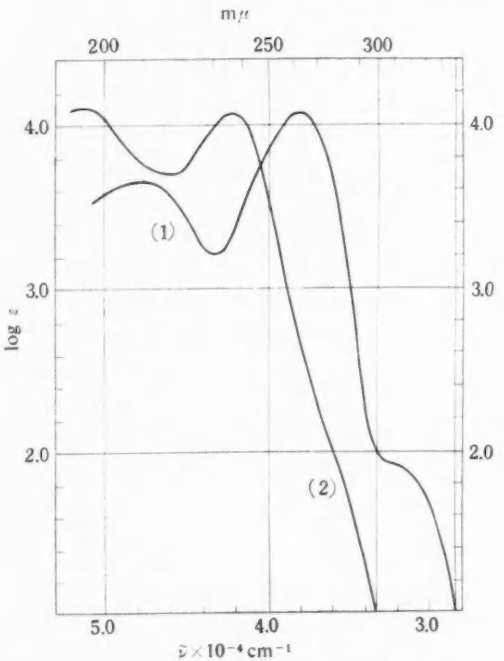

Fig. 1. Ultraviolet absorption spectra of thioacetamide (1) and thiourea (2) in aqueous solutions.

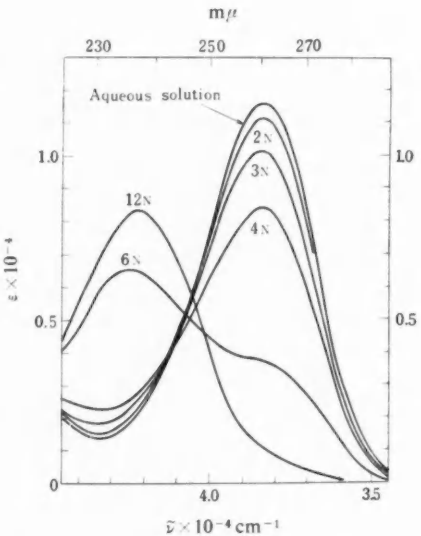

Fig. 2. Ultraviolet absorption spectra of thioacetamide in hydrochloric acid solutions with various acid concentrations.

The absorption spectrum of thioacetamide in hydrochloric acid solution changes considerably from that in aqueous solution. As is seen from Fig. 2, with the increasing concentration of hydrochloric acid, the 261 mμ band gradually decreases its intensity and a new band appears at 237 mμ[12]. Further, an isobestic point can be observed at 245 mμ, though the crossing of absorption curves is not always complete for the solutions of the higher concentrations of hydrochloric acid*. This fact conclusively indicates the existence of an equilibrium between thioacetamide and its conjugate acid. Concerning the mechanism of this equilibrium, there are two possible alternatives which are different from each other in the position where a proton is attached to the parent thioacetamide molecule. They are represented by the following equations:

$$H_2N\text{-}\overset{S}{\overset{\|}{C}}\text{-}CH_3 + H_3O^+ = H_3\overset{+}{N}\text{-}\overset{S}{\overset{\|}{C}}\text{-}CH_3 + H_2O$$

$$H_2N\text{-}\overset{S}{\overset{\|}{C}}\text{-}CH_3 + H_3O^+ = H_2N\text{-}\overset{+SH}{\overset{|}{C}}\text{-}CH_3 + H_2O$$

Here the former equilibrium is adopted as the more probable one. Some details on this point will be discussed in some later parts of the present paper.

From the experimental results regarding the absorption spectrum of thioacetamide in hydrochloric acid solutions of various concentrations, the basicity constant (pK_B) of thioacetamide can be obtained by the aid of the following equations:

$$K_B = (\overset{+}{H_2N}CSCH_3)/(H_2NCSCH_3)(H^+)$$
$$= (\varepsilon - \varepsilon_B)/(\varepsilon_{HB^+} - \varepsilon)(H^+)$$
$$pK_B = \log\{(\varepsilon_{HB^+} - \varepsilon)/(\varepsilon - \varepsilon_B)\} + pH$$

Quantities (H_2NCSCH_3), ($\overset{+}{H_3N}CSCH_3$) and (H^+) are activities of thioacetamide, its conjugate acid and a proton, respectively. Activity coefficients of thioacetamide and its cation are assumed to be equal to unity because of their low concentrations. The activity of the proton can be evaluated by combining the concentration of the solution determined by titration with the value of activity coefficient taken from the literature[13]. Quantities ε, ε_B and ε_{HB^+} represent the apparent molar extinction coefficient of thioacetamide in dilute hydrochloric acid solution, in aqueous solution and in concentrated hydrochloric acid solution, respectively. The values of the above-mentioned quantities actually used for the evaluation of pK_B are listed in Table II, together with the calculated pK_B value.

The average value of pK_B is obtained to be 1.2 at 24.5°C. Concerning the evaluation of this value, there are some ambiguities on the adoption of activity coefficients and on the medium effect upon the absorption spectrum of thioacetamide in concentrated hydrochloric acid. However, the pK_B value of thioacetamide evaluated here seems to be reasonable compared with the value of thiourea quoted in the literature[14].

Polarized Ultraviolet Absorption Spectra of Thioacetamide Crystal.—According to the structural analysis data of thioacetamide crystal by Truter[15], the molecules lie on the (001) plane as is schematically shown in Fig. 3. The polarized ultraviolet absorption spectra of thioacetamide parallel to *a* and *b* axes are shown in Fig. 3. From this figure it is easily seen that the 261 mμ band has stronger intensity in the direction of *b*-axis than in the direction of *a*-axis, and that the reverse is the case for the 210 mμ band, though the dichroism is not so conspicuous for this band as for the 261 mμ band. For these two bands, unfortunately, it is

Table II. Evaluation of the pK_B value of thioacetamide

Concentration of HCl (N)	$(\varepsilon-\varepsilon_B)/(\varepsilon_{HB^+}-\varepsilon)$				(H^+)	pK_B
	260 mμ	270 mμ	280 mμ	Average		
3	0.156	0.157	0.146	0.153	3.665	1.38
4	0.406	0.393	0.372	0.390	7.104	1.26
6	2.90	2.45	2.68	2.68	22.41	0.92

Average pK_B value: 1.19.

* This may be due to the medium effect of the acid.

12) The band corresponding to the 210 mμ band of thioacetamide can not be observed in hydrochloric acid solution, because hydrochloric acid is not transparent in the wavelength region below 220 mμ. However, the spectrum in concentrated sulfuric acid solution which is transparent until 200 mμ shows only one absorption band at 240 mμ, namely the one corresponding to the 237 mμ band in hydrochloric acid solution. This seems to support the opinion that the 210 mμ band of thioacetamide disappears in strongly acidic solution.

13) H. S. Harned and R. W. Ehlers, *J. Am. Chem. Soc.*, 55, 2179 (1933); G. Åkerlöf and J. W. Teare, ibid., 59, 1855 (1937).

14) pK_B=1.0 for thiourea: "Handbook of Chemistry (Kagakubinran)", edited by the Chemical Society of Japan, Maruzen, Tokyo (1958), p. 871.

15) Private communication from Dr. M. R. Truter.

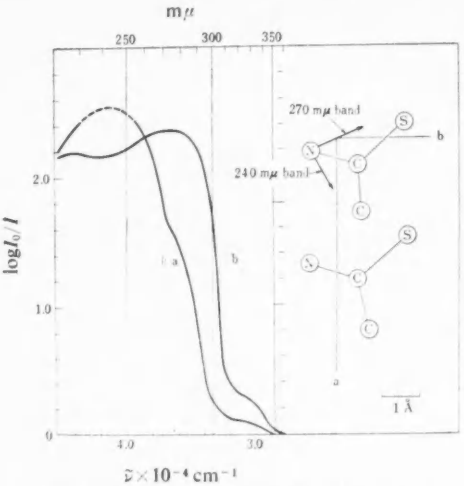

Fig. 3. The polarized ultraviolet absorption spectrum of thioacetamide and the projection of the molecules to the (001) plane. Arrows show the observed directions of transition moments.

difficult to determine exactly the direction of the transition momont from the combination of these spectral data with the crystal analysis result. This is because they overlap with each other and it is difficult to obtain the accurate value of oscillator strength for each band separately. However, it is well accepted that the transition moment of the 261 mμ band is directed very closely to the line connecting the nitrogen and the sulfur atom, thus the absorption intensity being greater in the b-axis spectrum than in the *a*-axis spectrum, while the transition momen of the 210 mμ band is approximately parallel to the line joining the nitrogen atom to the methyl carbon atom, thus the absorption intensity being a little stronger in the *a*-axis apectrum than in the *b*-axis spectrum.

A weak absorption band probably due to $n \rightarrow \pi^*$ transition appears in the 320~340 mμ region and its intensity is much stronger in the direction of *b*-axis than in the direction of *a*-axis. Concerning this weak band, however, one must be careful in determining the direction of the transition moment from the observed absorption intensity ratio, because weak forbidden bands often appear strongly in crystals by borrowing intenisty from allowed transition bands situated nearby[16]. Therefore it seems most likely that the weak band appearing at 320~340 mμ may not exhibit the dichroic property intrinsic to itself but rather the dichroic property characteristic of the 261 mμ band. In fact, the intensity ratio (about 5/1 = I_b/I_a) measured with the weak band is completely consistent with the above-mentioned direction of transition moment of the 261 mμ band.

Absorption Spectra of Thiourea in Aqueous Solution.—As is seen from Table I and Fig. 1, absorption bands of thiourea have a conspicuous tendency to appear at shorter wavelengths compared with the corresponding band of thioacetamide. The same tendency seems to be found also in the case of comparing the absorption spectrum of urea with that of acetamide, though a definite conclusion can not be obtained for the case of these two molecules because of some difficulties from the experimental point of view. Another characteristic of the absorption spectrum of thiourea is the fact that the longest wavelength band of thioacetamide, which is probably associated with $n \rightarrow \pi^*$ transition, disappears.

Polarized Absorption Spectra of Thiourea Crystal.—According to the X-ray crystal analysis study by Wyckoff and Corey and by Kunchur and Truter[17], the molecules of thiourea lie on the (110) plane as is shown in Fig. 4. The polarized ultraviolet absorption spectra of thiourea measured by the use of the incident radiation polarized parallel and perpendicular to the *c*-axis of the crystal are shown in Fig. 4. From this figure it is easily

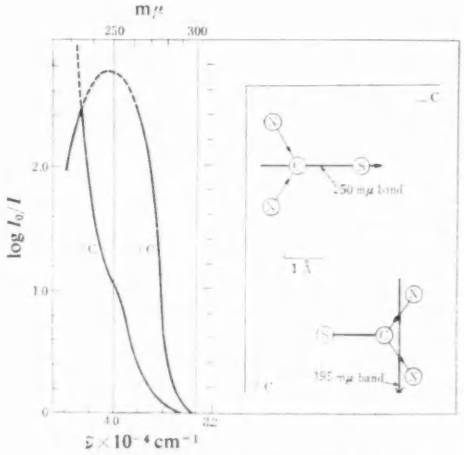

Fig. 4. The polarized ultraviolet absorption spectrum of thiourea and the projection of the molecules to the (110) plane. Arrows show the observed direction of transition moments.

16) D. S. McClure and O. Schnepp, *J. Chem. Phys.*, **23**, 1375 (1955).

17) R. W. G. Wyckoff and R. B. Corey, *Z. Krist.*, **81**, 386 (1932). N. R. Kunchur and M. R. Truter, *J. Chem. Soc.*, **1958**, 2551.

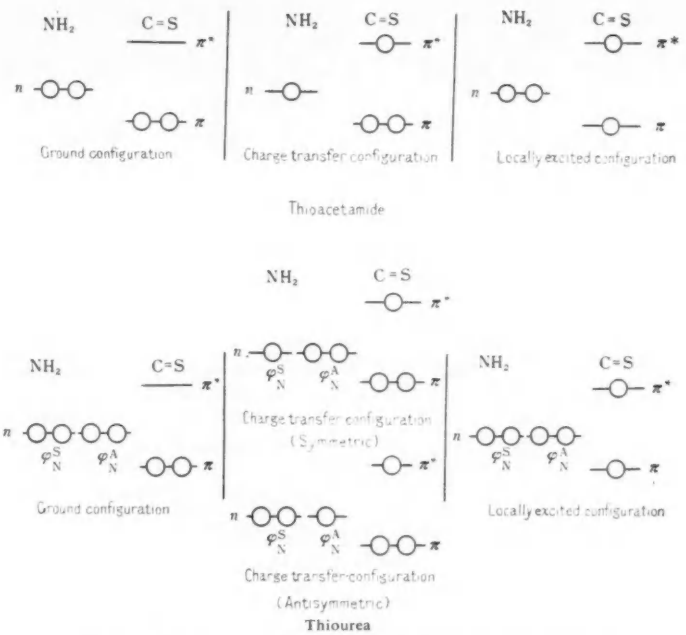

Fig. 5. Electron configurations for thioacetamide and thiourea.

seen that the observed intensity of the longer wavelength band is overwhelmingly great in the direction perpendicular to the *c*-axis compared with that in the direction parallel to the same axis, while the reverse is the case for the shorter wavelength band. This means that the transition moment of the longer wavelength band is evidently perpendicular to the *c*-axis, namely parallel to the C=S bond axis. On the other hand, the transition moment of the shorter wavelength band is determined to be perpendicular to the C=S bond axis.

Theoretical

In the present calculation, only π-electrons are taken into account and moreover the approximation of zero-differential overlap is adopted. In actual calculations, four and six π-electrons are taken for thioacetamide and thiourea, respectively. Now let us explain the actual calculation procedure in some detail, initially taking thioacetamide as an example.

Following Longuet-Higgins and Murrell's procedure[6], three electron configurations are constructed for this molecule in terms of π-electron molecular orbitals (φ_1, φ_2) of the electron accepting groups (C=S) and the nonbonding $2p$ atomiic orbital (χ_N) on the nitrogen atom of the electron donating group (NH_2)[18]. These configurations (a), (b) and (c) corresponding to ground, charge-transfer and locally excited configurations, respectively, are schematically shown in Fig. 5. As is well known, the wave functions for these configurations are written as follows:

$$\psi_G = 1/\sqrt{4!}\ \sum(-1)^p \mathrm{P}\varphi_1(1)\alpha(1)\varphi_1(2)\beta(2) \times \chi_N(3)\alpha(3)\chi_N(4)\beta(4) \quad (1)$$

$$\psi_{CT} = 1/\sqrt{4!}\ \sum(-1)^p \mathrm{P}\varphi_1(1)\alpha(1)\varphi_1(2)\beta(2) \times \chi_N(3)\alpha(3)\varphi_2(4)\beta(4) \quad (2)$$

$$\psi_{LE} = 1/\sqrt{4!}\ \sum(-1)^p \mathrm{P}\varphi_1(1)\alpha(1)\varphi_2(2)\beta(2) \times \chi_N(3)\alpha(3)\chi_N(4)\beta(4) \quad (3)$$

Here, $\sum(-1)^p\mathrm{P}$ is the usual antisymmetrizing summation over all permutations of the electrons. The wave functions φ_1 and φ_2 in Eqs. 1—3 can be determined following the procedure described in the Appendix.

Next one must take into account configuration interaction in terms of the three electron configurations mentioned above. According to this procedure, the energy levels of the molecule turn out to be obtained as solutions of the following secular equation:

18) According to the X-ray crystal analysis data of thioacetamide, hydrogen atoms of amino group are almost coplanar with heavy atoms.[15] This means that the nonbonding electrons of nitrogen may reasonably be assumed to belong to the pure $2p\pi$ atomic orbital.

$$\begin{vmatrix} H_G-E & H_{G\cdot LE} & H_{G\cdot CT} \\ H_{G\cdot LE} & H_{LE}-E & H_{LE\cdot CT} \\ H_{G\cdot CT} & H_{LE\cdot CT} & H_{CT}-E \end{vmatrix} = 0 \qquad (4)$$

where, $H_G = \int \psi_G H \psi_G d\tau$, $H_{G\cdot LE} = \int \psi_G H \psi_{LE} d\tau$, etc.

Suppose the energy of the ground configuration is taken as a standard. The value of H_{CT}, the energy of the charge-transfer configuration, can be evaluated by the following equation:[20]

$$H_{CT} = I_N - A_{C=S} - \{d^2_{11}(CC \mid NN) + d^2_{12}(SS \mid NN)\} \qquad (5)$$

where I_N and $A_{C=S}$ are the ionization potential of the nonbonding electron of the amino nitrogen atom and the electron affinity of the C=S group, respectively. The former is set equal to the ionization potential of ammonia which is determined as 10.15 eV by Watanabe from the photoionization experiment.[19] The quantities d_{11} and d_{12} are coefficients of atomic orbitals in φ_1 or φ_2 molecular orbital and are evaluated to be 0.6902 and 0.7236 (see Appendix), respectively. Two center Coulomb integrals (CC | NN) and (SS | NN) are calculated with the aid of uniformly charged sphere approximation, by taking the C–N and C–S bond distances as 1.324 and 1.713 Å, respectively, and further by taking ∠SCN as 121.6°[15]. The value of $A_{C=S}$ is assumed to be −0.32 eV which seems to be reasonable compared with that of the C=O bond, −1.20 eV.[2]

The energy value of the locally excited configuration, H_{LE}, is set equal to the observed excitation energy corresponding to the $\pi \rightarrow \pi^*$ transition pertinent to the C=S group. It is natural to take this value from the experimental result on the absorption spectrum of thioacetone. Unfortunately, however, this expectation can not be satisfied, because thioacetone usually exists as trimer like $Me_2C\langle^{S\,C\,Me_2}_{S\,C\,Me_2}\rangle^{S}_{S}$[18]. Then in the present calculation this value is taken to be 5.24 eV from the experimental result of the absorption spectrum of thioacetamide in hydrochloric acid solution. As mentioned above, thioacetamide in this condition exhibits the peak absorption at 237 mμ. This absorption band is conceivably ascribed to the protonated thioacetamide represented by $R\rangle^{S}_{}C{-}\overset{+}{N}H_3$. Since in this protonated cation the resonance effect of the amino group can be neglected to the first approximation, the 237 mμ band may be regarded as due to the $\pi \rightarrow \pi^*$ transition pertinent to the C=S bond. The present consideration on this point is consistent with the observation by Katagiri et al.[7] that thiocamphor shows a peak absorption at 242 mμ (5.12 eV).

Following the procedure developed by Longuet-Higgins and Murrell,[9] and also by Pople,[20] values of $H_{G\cdot CT}$, $H_{G\cdot LE}$ and $H_{CT\cdot LE}$ can easily be evaluated as follows:

$$H_{G\cdot CT} = \sqrt{2}\, d_{12}\beta_{CN} = 1.414 \times 0.7236 \times (-2.1) = -2.15 \text{ eV}$$

$$H_{G\cdot LE} = 0$$

$$H_{CT\cdot LE} = -d_{11}\beta_{CN} = -0.6902 \times (-2.1) = 1.45 \text{ eV}$$

Here β_{CN} is the core resonance integral between the π-electron orbital of carbon and the nonbonding orbital of nitrogen. In the present calculation β_{CN} is assumed to be an appropriate value of −2.1 eV.

By inserting the energy integral values into Eq. 4 and by solving it, the three energy levels of thioacetamide can be determined. Further, wave functions corresponding to these energy levels can easily be evaluated following the usual procedure in the variation method. The results are shown in Table III. Here values in parentheses are squares of coefficients of corresponding component wave functions. In view of the fact that these values represent magnitudes of contributions of electron configurations to a certain state of the molecule, it may be said that the lowest state (E_1) is principally composed of the ground configuration and the contribution of the charge-transfer configuration to that state is only 17%.[21] On the other hand, in the E_2 state contributions of the charge-transfer and locally excited configurations are almost equal and amount to 43%.

From the energy values for the states of thioacetamide given in Table III, excitation energies corresponding to $E_1 \rightarrow E_2$ and $E_1 \rightarrow E_3$ transitions can be calculated to be 4.77 eV and 7.44 eV, respectively. Values of the transition moments Q_{1i}'s and oscillator strength f_{1i}'s associated with these transitions are calculated by the following equations[22]:

$$Q_{1i} = \int \Psi_1 e r \Psi_i d\tau \qquad i = 2, 3 \qquad (6)$$

$$f_{1i} = 4.704 \times 10^{-7} \tilde{\nu}_{1i} Q^2_{1i} \qquad (7)$$

where $\tilde{\nu}_{1i}$ is the wave number (cm^{-1}) of the absorption peak under consideration and Q_{1i} is represented in Debye units. The calculated

19) K. Watanabe, *J. Chem. Phys.*, **26**, 542 (1957).

20) J. A. Pople, *Proc. Phys. Soc.*, **A68**, 81 (1955).

21) This apparently corresponds to the fact that the electronic structure of thioacetamide can be represented by a resonance hybrid between the following two structures:

$$H_3C\rangle^{S}_{}C{-}NH_2 \longleftrightarrow H_3C\rangle^{S}_{}C{=}\overset{+}{N}H_2$$

22) R. S. Mulliken, *J. Chem. Phys.*, **7**, 14 (1939); J. R. Platt and H. B. Klevens, *Rev. Modern Phys.*, **16**, 182 (1944).

TABLE III. ENERGY LEVELS AND WAVE FUNCTIONS FOR THIOACETAMIDE

Energy level	Symmetry	Wave function
$E_1=-0.9929$ eV	A'	$\Psi_1=0.9036\,\phi_G-0.0971\,\phi_{LE}+0.4173\,\phi_{CT}$ (0.8165 0.0094 0.1741)
$E_2=3.7811$ eV	A'	$\Psi_2=-0.3740\,\phi_G-0.6538\,\phi_{LE}+0.6578\,\phi_{CT}$ (0.1399 0.4275 0.4327)
$E_3=6.4519$ eV	A'	$\Psi_3=-0.2090\,\phi_G+0.7503\,\phi_{LE}-0.6271\,\phi_{CT}$ (0.0437 0.5630 0.3933)

TABLE IV. ENERGY LEVELS AND WAVE FUNCTIONS FOR THIOUREA

Energy level	Symmetry	Wave function
$W_1=-1.7653$ eV	A_1	$\Phi_1=0.8555\,\phi_G-0.1454\,\phi_{LE}+0.4968\,\phi^S{}_{CT}$ (0.7319 0.0211 0.2468)
$W_2=3.7397$ eV	A_1	$\Phi_2=-0.4328\,\phi_G-0.7275\,\phi_{LE}+0.5324\,\phi^S{}_{CT}$ (0.1873 0.5293 0.2835)
$W_3=7.3357$ eV	A_1	$\Phi_3=-0.2840\,\phi_G+0.6705\,\phi_{LE}+0.6854\,\phi^S{}_{CT}$ (0.0807 0.4496 0.4698)
$W_4=4.0700$ eV	B_1	$\Phi_4=\phi^A{}_{CT}$

values of f_{1i}'s are listed in Table I in comparison with the observed valuse which are obtained from absorption curves with the aid of the following equation:

$$f_{1i}^{obs}=4.32\times10^{-9}\int\varepsilon d\bar{\nu} \qquad (8)$$

where ε denotes the molar extinction coefficient. Directions of transition moments can also be evaluated readily from magnitudes of their components parallel and perpendicular to the C-S bond axis in the molecular plane. Consequently it is found that directions of transition moments associated with transitions $E_1\rightarrow E_2$ and $E_1\rightarrow E_3$ are inclined by 16° to the C-S bond and by 46° to the N-C bond, respectively. These theoretical results are schematically shown in Table I.

The calculation of π-electron structure is carried out also with thiourea by the same method as described in the case of thioacetamide. Therefore, it seems tedious to describe repeatedly the details of the calculation procedure. However, it may be necessary to add some note on the fact that in the case of thiourea two group orbitals, whose wave functions are represented by $\varphi^S{}_N=(\chi_{1N}+\chi_{2N})/\sqrt{2}$ and $\varphi^A{}_N=(\chi_{1N}-\chi_{2N})/\sqrt{2}$, can be obtained from the two nonbonding orbitals belonging to the amino groups. Consequently, in this case two charge-transfer configurations must be taken into account. Suppose that the wave functions of these two charge-transfer configurations and of the ground and locally excited configurations can be designated by $\psi^S{}_{CT}$ and $\psi^A{}_{CT}$[23], ϕ_G and and ϕ_{LE}, respectively (see Fig. 5). Among these wave functions, only $\psi^A{}_{CT}$ is antisymmetric with respect to the symmetry plane perpendicular to the molecular plane and including the C-S bond axis, while $\psi^S{}_{CT}$, ϕ_G and ϕ_{LE} are all symmetric with the same symmetry plane. Therefore it is readily concluded that the electron configuration represented by $\psi^A{}_{CT}$ can not mix with the other configurations. On the other hand, three configurations represented by ϕ_G, $\psi^S{}_{CT}$ and ϕ_{LE} interact with one another. The configuration interaction in terms of these three configurations finally results in three new states. The energy values and wave functions of these new states are given in Table IV[24].

From the energy values given in Table IV, excitation energies corresponding to $W_1\rightarrow W_2$, $W_1\rightarrow W_4$ and $W_1\rightarrow W_3$ are evaluated to be 5.51, 5.84 and 9.11 eV., respectively. It is inferred from this that the observed two absorption bands (236 and 195 mμ) in near ultraviolet region may reasonably be ascribed to the $W_1\rightarrow W_2$ and $W_1\rightarrow W_4$ transitions. The directions of transition moments for these two transitions

23) $\psi^S{}_{CT}=1/\sqrt{6!}\sum(-1)^p p\phi_1(1)\alpha(1)\phi_1(2)\beta(2)\phi^S{}_N(3)\alpha(3)\phi_2(4)\beta(4)\phi^A{}_N(5)\alpha(5)\phi^A{}_N(6)\beta(6)$
$\psi^A{}_{CT}=1/\sqrt{6!}\sum(-1)^p p\phi_1(1)\alpha(1)\phi_1(2)\beta(2)\phi^S{}_N(3)\alpha(3)\phi^S{}_N(4)\beta(4)\phi^A{}_N(5)\alpha(5)\phi_2(6)\beta(6)$

24) The values of matrix elements used for the evaluation of energy levels of thiourea are as follows:
$H_G=0$
$H^S{}_{CT}-H^A{}_{CT}=4.07$ eV.
$H_{LE}=5.24$ eV.
$H_{G\text{-}CT}=2d_{12}\beta_{CN}=2\times0.7236\times(-2.1)=-3.04$ eV.
$H_{G\text{-}LE}=0$
$H_{LE\text{-}CT}=-\sqrt{2}\,d_{11}\beta_{CN}=-1.414\times0.6902\times(-2.1)=2.05$ eV.
The values of I_N and A_{C-S} necessary for the evaluation of $H^S{}_{CT}$ and $H^A{}_{CT}$ are the same as those employed in the case of thioacetamide (see Eq. 5). The values of (NN | CC) and (NN | SS), however, are newly calculated for thiourea by the method as described in the case of thioacetamide, by the use of the C-N and S-N distances determined by X-ray crystal analysis ($d_{C-N}=1.35$ Å, $d_{C-S}=1.64$ Å, ∠NCS=126°; see Ref. 16 for these data).

can easily be found from the symmetry properties of the upper and lower states for each transition. That is to say, the direction of transition moment for the $W_1 \rightarrow W_2$ transition is expected to be exactly parallel to the C=S bond axis, while that for the $W_1 \rightarrow W_4$ transition is perpendicular to the same axis. Combining this theoretical expectation with the experimental results regarding polarized ultraviolet absorption, it is possible to determine clearly the assignment of these two absorption bands. This point will be explained in the next chapter.

Discussion

Assignment of Absorption Bands of Thioacetamide. — Experimental and theoretical results concerning the absorption spectra of thioacetamide are summarized in Table I and Figs. 1 and 3. From these results it is seen that the directions of transition moments determined theoretically for $E_1 \rightarrow E_2$ and $E_1 \rightarrow E_3$ transitions, whose excitation energies are calculated to be 4.77 eV. (260 mμ) and 7.44 eV. (167 mμ), respectively, are approximately equal to the directions of transition moments observed with the 261 mμ and 210 mμ bands, respectively. This fact gives a powerful support for the assignment that the 261 mμ and 210 mμ bands ought to be ascribed to the transitions $E_1 \rightarrow E_2$ and $E_1 \rightarrow E_3$, respectively. According to the above assignment, the agreement between the theoretical and experimental excitation energies is satisfactory for the 261 mμ band, but some discrepancy is seen for the 210 mμ band. A principal reason for this discrepancy is thought to be the neglect of electron configurations with higher energies, say configurations including two electron jumps. Although there is the above-mentioned difficulty from the quantitative point of view, the assignment of the two absorption bands of thioacetamide may be thought to be finally determined by the present experimental and theoretical studies.

Concerning the assignment of the weak band at 318 mμ, much can not be said. As pointed out by Katagiri et al.[7], however, this band is tentatively due to an $n \rightarrow \pi^*$ transition, namely due to the excitation of a nonbonding electron of the sulfur atom to the excited π-electron orbital of the C=S bond.

Assignment of Absorption Spectrum of Thiourea. — The results regarding the absorption spectrum of thiourea are given in Table I and Figs. 1 and 4. This molecule shows fairly strong absorption bands at 236 and 195 mμ. Calculated excitation energies for the $W_1 \rightarrow W_2$ and $W_1 \rightarrow W_4$ transitions are 5.51 (225 mμ) and 5.84 eV. (212 mμ), respectively. In this case, it is dangerous to determine the assignment of these two bands from the theoretical excitation energies alone, because the energy difference between W_2 and W_4 states is only 0.33 eV. and there may be some possibility that energy levels of these two states are reversed with each other by changing to only a small extent some parameters adopted in the present calculation. Fortunately, however, this difficulty is completely removed by considering the result of the polarized ultraviolet absorption measurement on the single crystal.

As is seen from Fig. 4, experimental results on the polarized ultraviolet absorption spectrum shows that the directions of transition moments of the longer and shorter wavelength bands are parallel and perpendicular to the C=S bond axis, respectively. Theoretical consideration in

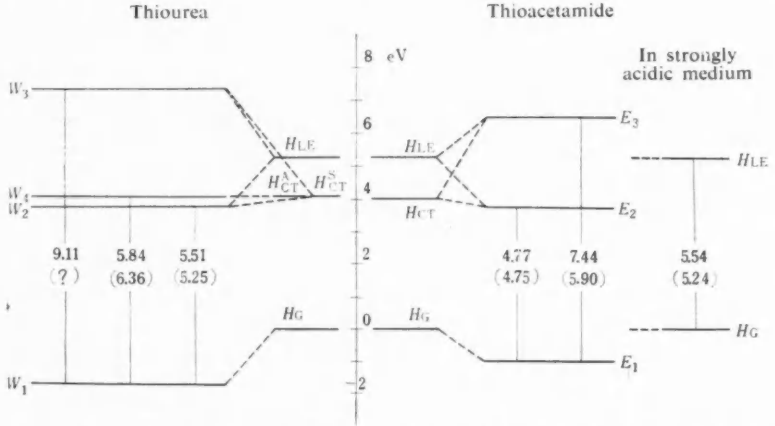

Fig. 6. Energy level diagrams for thioacetamide and thiourea, showing the relation between observed (in parentheses) and calculated transition energies.

the preceding chapter concludes that the transition moments associated with $W_1 \rightarrow W_2$ and $W_1 \rightarrow W_3$ ought to have directions exactly parallel and perpendicular to the C=S bond axis, respectively. These facts lead to the conclusion that the 236 mμ and 195 mμ bands correspond to the $W_1 \rightarrow W_2$ and $W_1 \rightarrow W_4$ transitions, respectively.

Of these two absorption bands, the shorter wavelength (195 mμ) band may be called a typical intramolecular charge-transfer band, because the upper state (W_4) of the corresponding transition is completely constructed from the charge-transfer configuration. This charge-transfer configuration includes electron transfer from the orbital represented by an antisymmetric combination of the nonbonding electron orbitals of the two nitrogen atoms to the φ_2 orbital pertinent to the C=S bond. From the resonance viewpoint, this means that the upper state of the 195 mμ band can be represented approximately by the resonance hybrid between the following two structures:

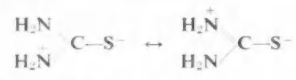

On the other hand, the 236 mμ band exhibits strongly the character of the locally (C=S) excited band, because in the excited state corresponding to this band the contribution of the locally excited configuration is great and amounts to 53%. In this sense, the 236 mμ band of thiourea may be regarded as the shifted one of the 237 mμ band pertinent to the C=O bond.

The relation between the energy state and the ultraviolet absorption spectrum described hitherto on thioacetamide and thiourea are schematically shown in Fig. 6.

Absorption Spectrum of Thioacetamide in Hydrochloric Acid Solution.—The fact that the 261 mμ and 210 mμ bands ($E_1 \rightarrow E_2$ and $E_1 \rightarrow E_3$ transitions, respectively) of thioacetamide disappear and a new band appears at 237 mμ in concentrated hydrochloric acid solution (240 mμ in concentrated sulfuric acid solution) seems to give an important information regarding the position of the proton attached to the parent molecule. Concerning the position of the proton, there are conceivably two alternatives, namely the nitrogen atom of the amino group and the sulfur atom of the thiocarbonyl group. In the latter case, it may be expected that the electron affinity of the C=S group increases considerably and the energy of the charge-transfer configuration given by Eq. 5 apparently decreases. From this it may be predicted that the 261 mμ band of thioacetamide will shift toward longer wavelengths if the proton be attached to the sulfur atom. The experimental result is completely reverse to this prediction. This seems to support the other possibility, namely the fact that proton is attached to the nitrogen atom. This conclusion is in agreement with the result obtained from the absorption measurement in the infrared region[25].

Appendix

The Molecular Orbital Functions Pertinent to the C=S Bond. — π-Electron orbitals of the C=S bond are represented by the linear combination of the $2p$ atomic orbital of carbon (χ_C) and the $3p$ atomic orbital of sulfur (χ_S):

$$\varphi_1 = d_{11}\chi_C + d_{12}\chi_S \tag{9}$$

$$\varphi_2 = d_{12}\chi_C - d_{11}\chi_S \tag{10}$$

The problem is to calculate the values of coefficients d_{11} and d_{12}. The calculation is carried out by the aid of the combination of Roothaan's LCAO SCF method[26] with Pariser and Parr's approximation[27]. The values of energy integrals actually adopted to the calculation are as follows:

$$\alpha_C = -I_C - \int \chi_C U_S \chi_C d\tau = -11.54 - 7.76 = -19.30\,\text{eV}. \tag{12}$$

$$\alpha_S = -I_S - \int \chi_S U_C \chi_S d\tau = -12.50 - 7.65 = -20.15\,\text{eV}. \tag{11}$$

$$\beta_{CS} = -2.0\,\text{eV}. \quad \text{(assumed value)}$$

$$(CC|CC) = \int \chi_C(1)\chi_C(2)\frac{e^2}{r_{12}}\chi_C(1)\chi_C(2)d\tau = 11.54 - 0.46 = 11.08\,\text{eV}.$$

$$(CC|SS) = \int \chi_C(1)\chi_S(2)\frac{e^2}{r_{12}}\chi_C(1)\chi_S(2)d\tau = 7.37\,\text{eV}.$$

$$(SS|SS) = \int \chi_S(1)\chi_S(2)\frac{e^2}{r_{12}}\chi_S(1)\chi_S(2)d\tau = 12.50 - 2.70 = 9.80\,\text{eV}.$$

Here U and α represent core potential and core Coulomb integral concerning atoms each of which is referred to by a suffix, respectively. β_{CS} is the core resonance integral between the χ_C and χ_S orbitals. I_C and I_S are the ionization potential of the $2p$ electron of carbon and of the $3p$ electron of sulfur, respectively. These values are taken from Pritchard and Skinner's table[28]. Integrals $\int \chi_C U_S \chi_C d\tau$ and $\int \chi_S U_C \chi_S d\tau$ are assumed to be equal to electrostatic attraction between two spherically charged ($-e/2$ each) tangent balls on one atom and the opposite charge ($+e$) on the other

25) E. Spinner, *Spectrochim. Acta*, **12**, 95 (1959).
26) C. C. J. Roothaan, *Rev. Modern Phys.*, **23**, 69 (1951).
27) R. Pariser and R. G. Parr, *J. Chem. Phys.*, **21**, 466, 767 (1953).
28) H. O. Pritchard and H. A. Skinner, *Chem. Revs.*, **55**, 745 (1955).

atom. Following Pariser and Parr's procedure[27], one center Coulomb repulsion integral, (CC | CC) or (SS | SS) is set equal to the difference between the ionization potential and the electron affinity. These two quantities are taken from Pritchard and Skinner's table. The two center Coulomb repulsion integral (CC | SS) is evaluated under the uniformly charged sphere approximation[29], taking the C=S bond distance as 1.71 Å, the value obtained by Truter from the X-ray analysis data on thioacetamide[15].

In order to obtain more accurate values for the core Coulomb integrals, the polarization effect of the σ-electrons of the C=S orbital upon them is taken into account. According to Moffit's method[30], the corrected ionization potentials can be obtained by the following equation[31]:

$$I'_C = -11.54 - 0.1436(11.08 - 7.37) = -12.08 \text{ eV}.$$

$$I'_S = -12.50 + 0.1436(9.80 - 7.37) = -12.15 \text{ eV}.$$

Substituting these values for I_C and I_S in Eqs. 11 and 12, the corrected core Coulomb integrals become as follows:

$$\alpha'_C = -19.84 \text{ eV}. \qquad \alpha'_S = -19.80 \text{ eV}.$$

By using these integral values, the iterative procedure following Roothaan's method is continued until self-consistent results are obtained with d_{11}, d_{12} and orbital energies (ε_1, ε_2). The final results thus obtained are as follows[32]:

$$d_{11} = 0.6902 \qquad d^2_{11} = 0.4764$$

$$d_{12} = 0.7236 \qquad d^2_{12} = 0.5236$$

$$\varepsilon_1 = -12.946 \text{ eV}. \qquad \varepsilon_2 = -1.566 \text{ eV}.$$

$$\varphi_1 = 0.6902\chi_C + 0.7236\chi_S$$

$$\varphi_2 = 0.7236\chi_C - 0.6902\chi_S$$

Further the excitation energy ΔE corresponding to the $\varepsilon_1 \to \varepsilon_2$ transition can be calculated by the following equations:

$$\Delta E = \varepsilon_2 - \varepsilon_1 - (11 \mid 12) + 2(12 \mid 12) = 5.54 \text{ eV}.$$

$$(11 \mid 22) = d^2_{11}d^2_{12}\{(CC \mid CC) + (SS \mid SS)\} + (d^4_{11} + d^4_{12})(CC \mid SS)$$

$$(12 \mid 12) = d^2_{11}d^2_{12}\{(CC \mid CC) + (SS \mid SS) + 2(CC \mid SS)\}$$

The calculated value, 5.54 eV., may be said to be in fairly good agreement with the observed one, 5.24 eV.

29) R. G. Parr, *J. Chem. Phys.*, **20**, 1499 (1952).

30) W. Moffitt, *Proc. Roy. Soc.* (*London*), **A202**, 534 (1950).

31) In this calculation the following energy values are used:

$I^\sigma_S = 20.0$ eV. $\qquad A^\sigma_S = 4.0$ eV.

$I^\sigma_C = 15.42$ eV. $\qquad A^\sigma_C = 3.32$ eV.

$\beta^\sigma_{CS} = -2.0$ eV.

where I and A represent ionization potential and electron affinity, respectively, and the superscript σ means that the corresponding quantity is concerned with σ-electrons. The quantities on carbon are taken from Pritchard and Skinner's table[28] and those on sulfur are roughly estimated from corresponding values for oxygen which are also obtained from the table.

32) Katagiri et al. calculated independently the wave functions and orbital energies of the C=S bond and obtained the following results:

$\psi_1 = 0.6330\chi_C + 0.7741\chi_S$

$\psi_2 = 0.7741\chi_C - 0.6330\chi_S$

$\varepsilon_1 = -11.98$ eV $\qquad \varepsilon_2 = -1.90$ eV

S. Katagiri, Y. Amako and H. Azumi, Presented at the Symposium on Electronic States, Tokyo, September, 1959.

Summary

Ultraviolet absorption spectra of thioacetamide and thiourea are measured under various conditions. In aqueous solution, three bands (210, 261 and 318 mμ) for thioacetamide and two bands (195 and 236 mμ) for thiourea are observed. Further, polarized ultraviolet absorption spectra are measured with their crystals. On the basis of the results regarding the polarized ultraviolet absorption spectra, the directions of transition moments can be determined as follows: 1) the directions of transition moments of the 261 and 210 mμ bands of thioacetamide are approximately parallel to the axis connecting the nitrogen and sulfur atoms and connecting the nitrogen and methyl carbon atoms, respectively, 2) the directions of transition moments of the 236 and 195 mμ bands of thiourea are parallel and perpendicular to the C=S axis, respectively. From the combination of the experimental results concerning the directions of transition moments with theoretical consideration based on semi-empirical LCAO treatment including configuration interaction, the assignment of the four absorption bands under consideration are finally determined. One of the noticeable conclusions is that the 195 mμ band of thiourea can be regarded as a typical intramolecular charge-transfer absorption.

It is shown that in the hydrochloric acid solution of thioacetamide the 261 mμ band decreases its intensity and a new band appears at 237 mμ. By measuring the dependence of intensities of these two bands upon the acid strength of the solution, it is concluded that the 237 mμ band is due to the conjugate acid of thioacetamide. The pK_B value of thioacetamide is determined spectrophotometrically to be 1.2 at 24.5°C. From the comparison of the wavelength of the peak absorption of thioacetamide with that of its conjugate acid, it is seen that the proton is conceivably attached to the amino group.

The authors wish to express their sincere thanks to Dr. M. R. Truter for her kindness in giving valuable information on the X-ray crystal analysis data of thioacetamide prior to publication. Their thanks are also due to Dr. T. Sakurai in our Institute for his kind cooperation in identifying the crystal axis of thiourea.

The Institute for Solid State Physics
The University of Tokyo
Shinryudo-cho, Minatoku
Tokyo

SHORT COMMUNICATIONS

The Crystal Structure of Tetra-thiourea-palladium(II) Chloride, $[Pd(SCN_2H_4)_4]Cl_2$

By Shun'ichiro Ooi, Tsuyoshi Kawase, Kazumi Nakatsu and Hisao Kuroya

(Received April 11, 1960)

It is well known that thiourea is capable of forming a number of coordination compounds with metallic ions. Recently, we reexamined the preparation methods of some of them, the chemical analyses being carried out carefully, and obtained quite well-formed crystals of the palladium(II) complex salt, $Pd(SCN_2H_4)_4Cl_2$. We have therefore, attempted to investigate the crystal structure of this compound. There are only a few structural studies[1-4] of the thiourea coordination compounds.

The crystal was prepared by the method of Kurnakow[5]. The products are monoclinic, showing the predominant (100) face. The crystallographic data are: $a=16.89$, $b=11.18$ $c=8.89$ Å, $\beta=91.5$, $Z=4$, $\rho_{obs}=1.92$ and $\rho_{calc}=1.91$ g./cm^3. Space group $C2/c$ or Cc was given by the observation of the systematically absent reflections. However, the method of Howells

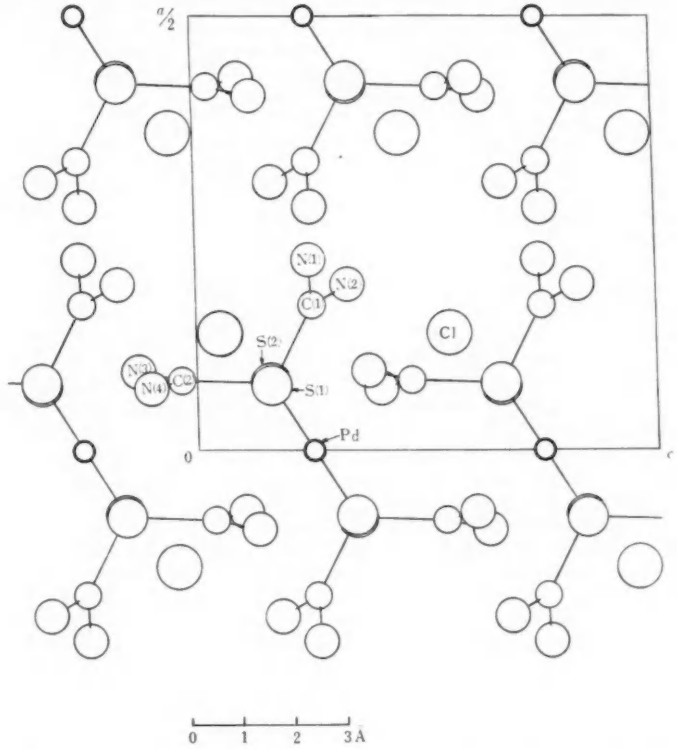

Fig. 1. Projection of the structure upon a plane normal to the *b*-axis.

1) M. Nardelli, L. Cavalca and A. Braibanti, *Gazz. chim. ital.*, **86**, 1037 (1956).
2) M. Nardelli, L. Cavalca and A. Braibanti, ibid., **87**, 137 (1957).
3) C. B. Knobler, Y. Okaya and R. Pepinsky, *Z. Krist.*, **111**, 385 (1959).
4) M. Nardelli and G. Fava, *Acta Cryst.*, **12**, 727 (1959).
5) Kurnakow, *J. prakt. Chem.*, [2] **50**, 496 (1894).

TABLE I. ATOMIC COORDINATES

	x/a	*y/b*	*z/c*
Pd	0	0.324	0.250
S (1)	0.073	0.482	0.158
S (2)	0.079	0.167	0.155
Cl	0.135	0.182	0.050
N (1)	0.220	0.561	0.242
N (2)	0.189	0.380	0.328
N (3)	0.092	0.078	−0.136
N (4)	0.071	0.288	−0.105
C (1)	0.167	0.476	0.247
C (2)	0.081	0.183	−0.037

et al.[6], applied to (*hk*0) reflections, was indicative of the presence of a center of symmetry, which was, in turn, favorite to $C2/c$. The structure analysis was carried out by using (*h*0*l*) and (*hk*0) data obtained from Weissenberg photographs which were taken with Cu$K\alpha$ radiation. From Patterson projections on (010) and (001), the positions of palladium, chlorine and sulfur atoms could be deduced. A usual Fourier method was, then, applied to further analysis. Atomic coordinates listed in Table I gave the reliability index $R=0.18$ and 0.16 for (*h*0*l*) and (*hk*0), respectively.

In Fig. 1, the structure projected on (010) is shown. The crystal is essentially ionic and consisted of $[Pd(SCN_2H_4)_4]^{2+}$ and Cl^-. A palladium atom is surrounded by four sulfur atoms in an approximately rectangular configuration with 3.00 and 3.15 Å for the lengths of shorter sides, and 3.50 Å for the longer ones. A complex ion has a two-fold rotation axis bisecting the two shorter sides and passing through the palladium atom. All S—C bonds projected on the plane formed with 4S's and Pd, are parallel to the shorter sides. Bond distances and angles found in a complex ion are: Pd—S=2.33 and 2.35 Å, ∠S—Pd—S=82°, 85° and 97°, ∠Pd—S—C=106 and 107°, S—C=1.72 and 1.75 Å, C—N=1.32, 1.37 and 1.47 Å, ∠S—C—N=120, 121, 123 and 126° and ∠N—C—N 117°. No significant discrepancies could be found in the dimensions between the thiourea molecule reported by Kunchur and Truter[7] on the thiourea crystal and the one in the present work. The bond angles formed at S's can be compared with those in $Cu(SCN_2H_4)_2Cl_2$[5] and in $Pb(SCN_2H_4)_2Cl_2$[4].

Institute of Polytechnics
Osaka City University
Osaka, Japan

6) E. R. Howells, D. C. Phillips and D. Rogers, *Acta Cryst.*, 3, 210 (1950).
7) N. R. Kunchur and M. Truter, *J. Chem. Soc.*, **1958**, 2551.

The Structure and a Novel Type Rearrangement of a Ketol Produced by the Robinson Annelation Reaction

By Takeshi MATSUMOTO and Akira SUZUKI

(Received May 17, 1960)

In the course of a study directed to the synthesis of a certain diterpenoid skeleton[1], the authors condensed ethyl 1, 2, 3, 4-tetrahydro-2-oxo-5-methoxy-1-naphthyl acetate[2] with methyl vinyl ketone, expecting the formation of either ketol I or its dehydration product II. However, the obtained ketol [m. p. 134~135°C; ν_{max}^{Nujol} 3380 (OH), 1733 and 1185 (ester), and 1700 cm^{-1} (ketone); λ_{max}^{MeOH} 271 (ε 1410) and 278 mμ (ε 1310); Found: C, 68.44; H, 7.10. Calcd. for $C_{16}H_{24}O_5$: C, 68.65; H, 7.28%] was actually a bridged ring compound III. Moreover, attempted acetylation of III with isopropenyl acetate in the presence of *p*-toluenesulfonic acid resulted in a remarkable change in the carbon skeleton of compound III, a spirocyclic acetate IV [m. p. 97.5~98.5°C; ν_{max}^{Nuj} 1730 (ester) and 1715 cm^{-1} (ketone); Found: C, 67.10; H, 6.94. Calcd. for $C_{21}H_{26}O_6$: C, 67.36; H, 7.00%] being produced. The formation of a similar bridged ring ketol system through the Robinson annelation reaction was first disclosed only quite recently by W. S. Johnson and his co-workers[3]. Conversion of the skeletons III to IV seems, so far as the authors are aware, to have never been described in the literature.

The structures of both compounds III and IV were determined by the NMR spectra[4]. The spectrum of ketol III showed one sharp maximum at high applied magnetic field characteristic of proton resonance for the $-C-CH_3$ group (203 c. p. s., standard, benzene; observed relative peak area, 3.4) and is completely accounted for in terms of structure III. Further, presence of an intramolecular hydrogen bond, as indicated by the infrared spectrum (ν_{max} 3430 cm^{-1}, in 0.0046 M solution in tetrachloroethylene) clearly defines the conformation of the ketol as V. In the NMR spectrum of acetate IV, presence of a $-\underset{|}{C}-CH_3$ group and

1) T. Matsumoto and A. Suzuki, This Bulletin, **32**, 1283 (1959); **33**, 33 (1960).
2) T. Matsumoto and A. Suzuki, to be published.
3) W. S. Johnson, J. J. Korst, R. A. Clement and J. Dutta, *J. Am. Chem. Soc.*, **82**, 614 (1960).
4) Taken on a Varian 40 MC instrument in $CDCl_3$ solution.

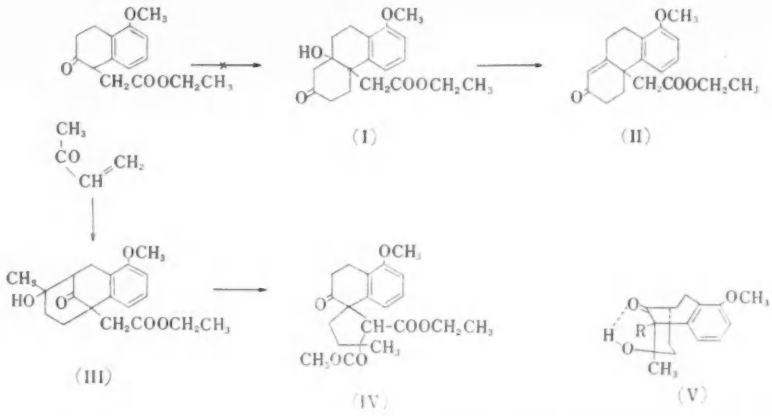

absence of the $-\overset{|}{C}-CH_2-CO_2-$ group are indicated respectively by the appearance of a sharp peak at 190 c. p. s. (relative peak area, 3.1) and by the disappearance of the singlet peak at 151 c. p. s. (relative peak area, 1.7) of III. The only one structure consistent with the observed findings is expressed by formula IV. The resonance line due to $-\overset{|}{C}-CH_3$ group of the acetate is shifted to the lower magnetic field by 13 c. p. s. as compared with that of the ketol. This shift might be an indication of the *cis* location of the methyl and ethoxycarbonyl groups.

Chemistry Department
Faculty of Science
Hokkaido University
Sapporo

The Existence of Acid Centers of a Lewis Type on Silica-Alumina Surface

By Michio OKUDA and Taro TACHIBANA

(Received May 10, 1960)

Recently, attention has been paid to the nature of acid centers on silica-alumina surface[1]. In order to study this problem spectroscopically, we have measured electronic spectra of some reagents adsorbed from their cyclohexane solutions on silica-alumina according to a procedure described by Robin[2].

A sample of silica-alumina was kindly supplied by Professor Shiba of Tokyo Institute of Technology and stated to contain approximately 13% alumina and no ferric ion. This sample was used as an adsorbent without further heat treatment (SA-1), or after heat treatment for 3 hr. at 110°C (SA-2), for 3 hr. at 430°C (SA-3) in dry air.

By using benzeneazodiphenylamine (pK_a: 1.52) as Walling's acid-base indicator, it was found that the adsorbent shows surface acidity. As is clearly seen from Fig. 1, benzeneazodiphenylamine adsorbed exhibits the two absorption bands at 440 mμ and 538 mμ, which are evidently associated with the free base of the dye and its conjugated acid respectively. The latter specimen is produced by the reaction of the free base with a proton of protonic acid or aluminum atom as Lewis acid. The heat treatment of adsorbents increases the intensity of the acid band, indicating the increase of the amount of acid centers on the silica-alumina surface.

To obtain some information on whether or not these acid centers involve those of a Lewis type, *p*-phenylenediamine, which is a typical electron donor and is suitable for detecting electron accepting ability of the opponent entity, was adsorbed on silica-alumina adsorbents and its absorption spectrum was examined. The absorption spectrum of *p*-phenylenediamine adsorbed showed two characteristic bands at 324 mμ and 468 mμ, as shown in Fig. 2. The former band was identified with that of *p*-phenylenediamine in alcohol (λ_{max}: 312 mμ)[3] and the latter band with that of its semiquinone

1) J. E. Mapes and R. P. Eischens, *J. Phys. Chem.*, **58**, 1059 (1954); E. I. Kotov, *Optika i Spektroskopiya*, **3**, 115 (1957).

2) M. Robin, *J. Chem. Educ.*, **33**, 526 (1956).

3) L. C. Anderson and J. W. Steedly, Jr., *J. Am. Chem. Soc.*, **76**, 5144 (1954).

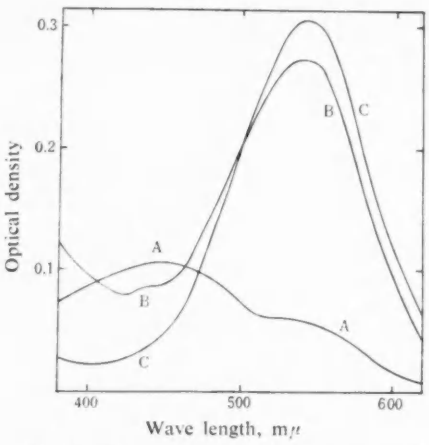

Fig. 1. Absorption spectra of benzeneazodiphenylamine adsorbed on silica-alumina (A, SA-1; B, SA-2; C, SA-3).

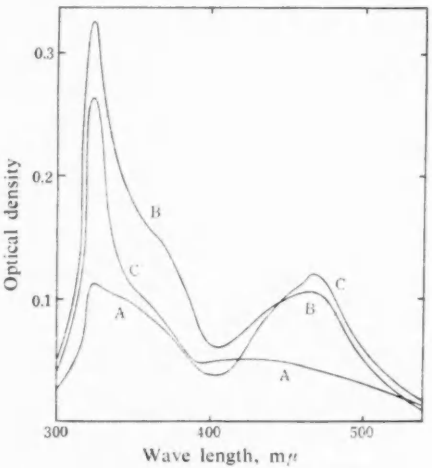

Fig. 2. Absorption spectra of *p*-phenylenediamine adsorbed on silica alumina (A, SA-1; B, SA-2; C, SA-3.)

cation radical $(NH_2C_6H_4NH_2)^+$ in water (λ_{max}: 462 mμ)[4]. Fig. 2 shows also that the intensity of absorption band of semiquinone increases with the increasing temperatures of heat treatment of adsorbent. The existence of semiquinone radicals on the adsorbent was also confirmed by the appearence of electron spin resonance spectrum. On the other hand, semiquinone radical could not be observed with the absorption spectrum of *p*-phenylenediamine adsorbed on a silica gel sample containing protonic acid.

The present results lead us to consider that the vacant 3*p* orbital of the aluminum atom on silica-alumina surface accepts one electron from the highest occupied π orbital of the *p*-phenylenediamine molecule adsorbed and, therefore, aluminum atoms react with a base as Lewis acid centers, the structure of which has been proposed by Mills et al.[5]. It was also shown that the amount of Lewis acid centers increases with the temperature of heat treatment of the silica-alumina sample. The method of electronic spectra studied by us has given a more direct evidence for the existence of Lewis acid centers on silica-alumina sample than that obtained by other methods hitherto reported[1].

Chemical Laboratory
Ochanomizu University
Bunkyo-ku, Tokyo

4) L. Michaelis, M. P. Schubert and S. Granick, ibid., **61**, 1981 (1939).

5) T. H. Milliken, Jr., G. H. Mills and A. G. Oblad, *Disc. Faraday Soc.*, No. 8, 279 (1950).

---

*Ein Beitrag zur Entwicklung der Harztüpfelmethode mittels Zentrifugierens der fein zerriebenen Ionenaustauscherteilchen**,[1]

Von Masatoshi FUJIMOTO

(Eingegangen am 6. Mai, 1960)

Beim Zentrifugieren einer mit einem Farbreaktionssystem berührenden, wäßrigen Suspension der fein zerriebenen Ionenaustauscherteilchen lassen sich die an den Austauscher stark adsorbierten, stark sich färbenden Bestandteile der genannten Reaktion an die Spitze des Zentrifugenröhrchens schnell und dicht ausammeln. Durch raffinierte Anwendung dieser Erscheinung auf die Harztüpfelmethode[2] wurde es bei der vorliegenden Arbeit eine Reihe von schnellen und wesentlich empfindlichen Nachweismethoden neu festgestellt.

Die wesentlich größere Ausdehnung der Oberfläche an den fein geteilten Harzteilchen

* Mikroanalyse mit Hilfe von Ionenaustauscherharzen. XVI.

1) XV. Mitteilung: M. Fujimoto, *Naturwissenschaften*, **47**, Heft 11, im Druck (1960).

2) In bezug auf die Einzelheiten der Harztüpfelmethode, vgl. M. Fujimoto, *Chemist-Analyst*, **49**, 4 (1960). Vgl. auch hierzu die in 1954–1957 in diesem Bulletin vom Verfasser nacheinander mitgeteilten Veröffentlichungen.

im Vergleich mit der an der gleichen Menge der Harzkugeln mit größerem Durchmesser ist an der hier vorgeschlagenen Methode besonders günstig, denn ein einziger Nachteil der empfindlichsten Harztüpfelmethode, d. h., die langsame Diffusion der gewöhnlich größeren, sich färbenden Ionen in die größeren Harzkugeln mit nur beschränktem Flächeninhalt**, kann erfolgreich beseitigt werden.

Ausführung: (*1*) *Darstellung der Harzsuspension mit beinahe gleicher Korngröße.*—0.5 bzw. 1 g völlig gereinigten, farblosen Ionenaustauscherharzes wird in einem Achatmörser mit geringer Menge entionisierten Wassers etwa 15 Min völlig zerrieben. Das Harz geht in eine weiße und zähe Paste über. Danach wird dieser Harzschleim mit entionisiertem Wasser zur Suspension umgeschüttelt. Diese wird durch wiederholtes Zentrifugieren unter bestimmtem Bereich der Drehungsanzahl, 0～1000, 1000～2000 Drgg. pro Min, u. s. w., und jedesmaliges Auswaschen mit entionisiertem Wasser raffiniert, um die Korngröße der Harzteilchen möglichst gleichmäßig regulieren zu lassen. Die hier erhaltenen Harzteilchen werden mit entionisiertem Wasser zur bestgeeigneten Konzentration verdünnt.

(*2*) *Anreicherung der mit den sich färbenden Reaktionsprodukten beladenen Harzteilchen durch Zentrifugieren.*—In einem Spitzröhrchen (Abb. 1) wird ein Tropfen der Probelösung (od. der

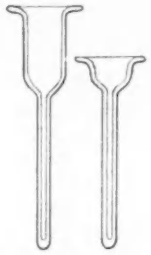

Abb. 1. Mikrospitzröhrchen (1/2 nat. Gr.)

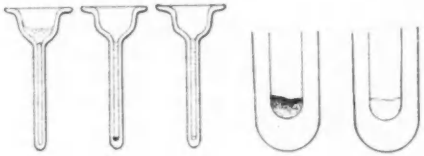

a b c b' c'

Abb. 2. Die Zustände der Harzteilchen im Mikrospitzröhrchen.
a: Die in dem Gemische der Probe- und Reagens-lösungen schwebenden Harzteilchen.
b: Die an die Spitze abgeschleuderten Harzteilchen beim Nachweise.
c: Diegleichen Harzteilchen beim Blindversuche.
b' und c': Die zehnfach vergrößerten Bilder der Spitzen an b und c.

TABELLE I. VERGLEICHUNG DER BEI DEN VERSCHIEDENEN NACHWEISMETHODEN ERHALTENEN EMPFINDLICHKEITEN

	Ionen	Kobalt(II)	Kupfer(II)
	Reagens	1 M NH_4NCS	0.001proz. PAN****
	Harzart	stark basisches Harz in Chloridform	stark saures Harz in H- od. NH_4-Form
Erfassungsgrenze* bei	gewöhnlicher Tüpfelmethode	0.5 γg[a] (0.30)	0.004 γg[c] (2.40)
	Harztüpfelmethode**	0.16 γg[b] (0.80)	0.0016 γg[c] (2.80)
	vorliegendem Verfahren***	0.023 γg (1.64)	0.00008 γg (4.10)

* Die einklammerten Werte sind die pE. G. entsprechenden Nachweises, worunter man die negativen gemeinen Logarithmen der auf Mikrogramme ausgedrückten Erfassungsgrenze, d. h., $-\log_{10}$ (E. G. in γg) versteht.

** Die hier gegebenen Erfassungsgrenzen wurden erst 10 bis 20 Min nach der Mischung erlangt.

*** Die hier beobachteten Erfassungsgrenzen wurden schon 1 bis 3 Min nach der Mischung erlangt.

**** 1-(2-Pyridylazo)-2-naphthol.

a) F. Feigl, „Spot Tests in Inorganic Analysis", 5. Aufl., Elsevier Publishing Co., Amsterdam (1958), S. 146ff.
b) M. Fujimoto, Dieses Bulletin, **27**, 48 (1954).
c) M. Fujimoto und T. Iwamoto, unveröffentlichte Resultate.

** Dieser Nachteil wurde dadurch teilweise verbessert, daß man die fein zerriebenen Harzteilchen als Träger der stark sich färbenden Bestandteile an die Grenzfläche zweier flüssigen Phasen ansammeln läßt[1].

Reagenslösung) mit einem Tropfen der Harzsuspension versetzt. Sodann wird ein Tropfen der Reagenslösung (od. der Probelösung) hinzugefügt, wobei die Harzteilchen eine Weile in der ganzen Lösung schweben und sogleich die in der Lösung vorhandenen, stark sich färbenden Ionen adsorbieren (Abb. 2a). Nach 1 bzw. 3 Min langem Stehen wird das Gemisch etwa 1 Min zentrifugiert. Es ist dabei empfehlenswert, daß man dies unter einer Anzahl der Drehung wesentlich größer als die bei der Reinigung der Harzsuspension abschleudern läßt, um die gefärbten Harzteilchen an die Spitze der Kapillare möglichst scharf, dicht und schnell ansammeln zu lassen. Das 1 Min lange Abschleudern unter höchstens 3000 Drgg. pro Min ist zur Abtrennung des Harzteilchens genügend. Die Farbe der auf solche Weise an die Spitze angesammelten Harzteilchen ist mit einer Lupe (20 mal) leicht zu erkennen.

Weil die kleineren Harzteilchen, die die sich färbenden Bestandteile schneller als die größeren Teilchen anreichern können, sich in der Kapillare langsamer als die größeren fallen, färbt sich die dabei an der Spitze gebildete Harzschicht von unten nach oben allmählich stärker (Abb. 2b'), und infolgedessen wird die Nachweisempfindlichkeit bedeutend erhöht.

Zwei sinnfällige Beispiele für die Erhöhung der Empfindlichkeit des Nachweises mittels oben vorgeschlagenen Verfahrens, sogenannter „Harz-zentrifugierenmethode", stehen in Tabelle I, in der das Erfassungsgrenze beim vorliegenden Verfahren mit dem bei der gewöhnlichen Tüpfelmethode sowie der Harztüpfelmethode verglichen wird.

Die obenerwähnte Methode ist nicht nur der gewöhnlichen Tüpfelmethode sondern auch der Harztüpfelmethode daran weit überlegen, daß man durch einfaches Zentrifugieren der gereinigten Harzsuspension eine wesentlich verbesserte Empfindlichkeit schnell und sicher gewinnen kann. Die große Austauschgeschwindigkeit beim kleinsten Harzteilchen ermöglicht den schnellen und empfindlichsten Nachweis gegen größere Menge der hoch verdünnten Probelösung. Überdies sei es möglich, durch Vergleichung der an der gleichen Menge der Harzteilchen entstehenden Farben mit den einer Reihe von Standards entschieden kleine Stoffmenge ziemlich genau zu bestimmen, worüber der Verfasser zur Zeit einige Versuche durchführt.

Laboratorium der analytischen Chemie
Chemisches Institut der
wissenschaftlichen Fakultät
Universität zu Tokyo
Hongo, Tokyo